The development of a Holocene cryptotephra framework in northwestern North America

by

Lauren J. Davies

A thesis submitted in partial fulfillment of the requirements for the degree of

Doctor of Philosophy

Department of Earth and Atmospheric Sciences
University of Alberta

Abstract

This thesis contributes to the development of a cryptotephra framework in northwestern North America, providing the initial data for the construction of a regional cryptotephra framework where key cryptotephra layers (those which are widely distributed, easily correlated, and have well constrained chronological control) are identified for use as chronostratigraphic tools. Three aims are outlined: addressing geographical gaps for cryptotephra records in northwestern Canada; defining regionally significant cryptotephra beds that can be used to improve local and regional s chronologies; and demonstrating the potential for cryptotephra as isochrons in the area.

Previous knowledge of cryptotephra in the area and any tephra with potential to be transported and preserved distally is summarised, including reference geochemical major element glass datasets and Bayesian age modelling of quality-assessed bounding dates. Previously published data is reviewed and supplemented using new data produced at the University of Alberta. This represents an important summary and evaluation of tephra data for nineteen beds from Alaska and the Yukon.

A new cryptotephra record covering ~10,400 cal yr BP is presented from a soligenic peatland in north-central Yukon. Seventy-five tephra peaks are identified during the Holocene, and detailed discussion, including modelled ages and geochemical major element glass datasets, is given for fifty-two samples representing sixty-four geochemical populations. A total of thirty-four tephra identified have a combination of significant glass concentrations, distinctive geochemical data, useful stratigraphic positions/timings, and potential correlation to other known records over a wide area. These beds are important contributions to the regional tephrostratigraphy.

Chronological data for three methods commonly used to date peatland archives (^{14}C, ^{210}Pb and cryptotephra) are compared at six sites in northern and central Alberta. Consistent offsets between ^{14}C and ^{210}Pb dates are identified at five of these sites before the 1960s. Historical cryptotephra, reported here for the first time in Alberta, are used as an independent check of these methods. They also contribute complementary data to ecological interpretations of changes in peat accumulation rate (e.g. local fires, permafrost development, water availability) that are included as boundaries in the final age-depth models. Bayesian modelling of the resulting data using the P_Sequence function of OxCal v4.2 produces improved age models at four of the sites.

All data are synthesised in Chapter 5 and a comparative cryptotephra stratigraphy is produced using the records published across North America. Appendices are included here in the text; supplementary Tables and Figures are deposited as digital files through Dataverse.

Preface

Chapter 2 of this thesis has been published as "Davies, L.J., Jensen, B.J.L., Froese, D.G., Wallace, K.L., 2016. Late Pleistocene and Holocene tephrostratigraphy of interior Alaska and Yukon: Key beds and chronologies over the past 30,000 years. Invited review, *Quaternary Science Reviews*, 146: 28-53". I was responsible for the literature review, data analysis, producing Bayesian age-depth models, and lead authorship of the manuscript. D.G. Froese was the supervisory author and was involved with concept formation and manuscript composition. Tephra data from the reference collection at the University of Alberta was produced by B.J.L. Jensen, who also contributed to manuscript composition. K.L. Wallace provided reference material for analysis at the University of Alberta and geochemical data produced at the Alaska Volcano Observatory. All co-authors read and provided comments on the manuscript.

Chapter 3 of this thesis is in preparation for publication in Quaternary Science Reviews. I was responsible for sample preparation and laboratory analyses, data analysis, and lead authorship of the manuscript. D.G. Froese read and provided comments on the manuscript

Chapter 4 of this thesis is accepted for publication pending minor revisions with Quaternary Geochronology as "Davies, L.J., Froese, D.G., Appleby, P.G., Jensen, B.J.L., Magnan, G., Mullan-Bordreau, G., Noernberg, T., Shotyk, W., van Bellen, S., Zaccone, C. High-resolution Bayesian age modelling of peat bogs from northern Alberta, Canada, using pre- and post-bomb ^{14}C, ^{210}Pb and tephrochronology". This work is part of a larger international research collaboration led by W. Shotyk from the Department of Renewable Resources at the University of Alberta. I was responsible for evaluating the chronological data, creating and testing multiple iterations of Bayesian age-depth models, analysing the final research data, and lead authorship of the manuscript. D.G. Froese was involved with concept formation, ^{14}C dating and manuscript writing. Core collection and processing were undertaken by T. Noerenberg. Data for environmental histories were supplied by G. Magnan, G. Mullan-Bordreau, S. van Bellen and C. Zaccone. Data for ^{210}Pb age models were provided by P.G. Appleby and reference tephra data were provided by B.J.L. Jensen. All co-authors read and provided comments on the manuscript.

The introductory statements in Chapter 1 and concluding analysis in Chapter 5 are my own original work.

This thesis is dedicated to my family -

without them I wouldn't be where, or who, I am today.

Acknowledgements

In September 2011 I was hiking in the Peak District, a well-earned break after finishing my MSc project, and at the top of an inland cliff my phone gained signal for long enough to receive an email with details of a cryptotephra project in Edmonton, Alberta. I could never have imagined what that would lead to.

Since that time, and going forward from here, I feel inexpressibly grateful for the support and guidance from my supervisor. Thank you, Duane, for your patience, for the multitude of opportunities you've provided me with, and for helping me learn to see beyond the fine details. I am also indebted with thanks to Britta – although we haven't geographically overlapped for a large part of my time here in Edmonton, we may have discussed data and distal tephra records enough for a lifetime of work already. Thank you for always understanding my frustrations, and for helping me develop from a geographer to something approaching more of an earth scientist!

Further thanks to the members of my supervisory committee, and those involved in both my candidacy exam and final defence: Thomas Stachel, Alex Wolfe, David Olefeldt, Siwan Davies, Alwynne Beaudoin and Charlie Schweger. I deeply appreciate you taking the time to be involved in and support my development as a graduate student. This project has overlapped several subject areas and taken me beyond my comfort zone, and I value the opinions and insights provided to keep me focused and prepared for the challenges I've come across.

This research was made possible through funding for fieldwork costs in 2013 awarded by the Geological Society of America (GSA) and Canadian Circumpolar Institute (CCI), and long-term grants from the Natural Science and Engineering Research Council and Canada Research Chairs program to Duane Froese. Thanks also to the University of Alberta, Nature and Environment Research Council (NERC), National Science Foundation (NSF), Quaternary Research Association (QRA), International Quaternary Association (INQUA), American Geophysical Union (AGU), Canadian Quaternary Association (CANQUA) and GSA for numerous grants and awards that have allowed me to travel and participate in conferences, workshops and courses across North America and the UK. These have been integral to my development as a researcher and I am deeply grateful for the experiences.

This whole body of work could not have been completed without help at every stage – thanks to all of those involved with core collection from the DHP174 site: Alberto Reyes and Joel Pumple initially in 2012 and Sasiri Bandara, Matt Mahony, Trevor Porter and Ann Hammad subsequently in 2013. Thanks to Sasiri Bandara and Kasia Staniszewska for their help and assistance in the lab with core subsampling and sample processing. Although it was not originally planned as part of my thesis, I'm very grateful for the opportunity to collaborating with many researchers studying peat bogs in northern and central Alberta – many thanks for the insights and discussion (and data!) provided by Bill Shotyk, Peter Appleby, Tommy Noernberg, Simon van Bellen, Gabriel Magnan, Claudio Zaccone, Gillian Mullan-Bordreau and members of the SWAMP lab.

I would like to acknowledge the support and input of the scientists who have provided tephra from their studies over many years to develop the University of Alberta tephra database. Specific thanks in relation to my work are addressed to Kristi Wallace and Vera Ponomareva, and thanks for proximal samples and data provided by Tom Ager, Judith Fierstein, Eric Carson, John Fournelle, Game McGimsey and Katherine Mulliken. Special thanks to Andrew Locock for his support in the production of EPMA data (no matter how many new issues the JEOL presented).

Quite generally, I would like to recognise both the cryptotephra community and the UK Quaternary community– thank you to all of those who I've spoken to either by email and skype or at conferences and workshops, and for the opportunities made available for students. Interacting with such a welcoming and supportive group of people is a large part of why I enjoy this work! Through my MSc at Royal Holloway and events hosted and supported by the QRA, INQUA and INTAV, I've met so many inspirational people who are passionate about what they do. Specific thanks to Christine Lane, Siwan Davies, Peter Abbott, John Lowe, Nick Pearce, David Lowe and John Westgate. Further thanks to those who have personally tutored and mentored me over the years and encouraged me to grow as a researcher and academic – Nick Middleton, David Banister, Elizabeth Baigent, Abi Stone, Simon Blockley, and all the way back to Mr Griffiths, Mrs Davidson and Mr Bennett at Colchester County High School. The confidence and skills you have taught me have proven invaluable and taken me far.

The Earth and Atmospheric Sciences department has been a great environment both for work and socialising, with fantastic faculty, staff and students. Thanks to Mark Labbe and Martin von Dollen for all of their help in the Thin Section lab and for their conversation, which kept me going while I was polishing pucks. Thanks to the multiple iterations of the Froese and Reyes lab groups over the years – Matt, Joel, Amanda, Robin and Trevor, Sasiri, Kasia, Hector, Joe, Sophie, and Martin – and to the old (and not so old) guard – Britta, Berto, Shawna, Janina, Carolyn, Danielle, Pedro, Leanne, Yannick, Reed, Ricky, Faye, Kurt, Alex, Devon, Andy. You've all helped make the best (and sometimes haziest) memories I have of Edmonton and you're what I'll miss the most without a doubt. Particular thanks to my housemates over the years – Mandy, Merilie, Tyler, Marika (plus Morgan and Shade!) for your patience with my endless plans, Netflix binging, and for always sharing good food, drink, and company. Don't think for a moment that living in different countries will mean that you're free of me!

To my friends across the pond – my Colchester girls, Stu, Jas, the Woodstock crew and Quatskis - thank you for not forgetting me, for the endless calls and messages it's taken to keep in touch, and for making me feel like I'm home again as soon as I touch down. Hannah and Alex, I feel you've both borne the brunt of my late-night messaging and anxieties – thank you for your limitless patience and wise, kind words.

Last but definitely not least, thanks to my family – living so far away for all this time has presented many challenges but I'm glad I've been able to share a little corner of Canada with you. Thank you for always believing in me – everything I've achieved wouldn't have been possible without your love and support. I promise, this time I'm really coming home!

Table of Contents

LIST OF TABLES

LIST OF FIGURES

CHAPTER 1: INTRODUCTION

We study palaeo-environmental records for a number of reasons, but three broad aims can be defined: understanding how Earth's systems and environments have changed in the past, delimiting the possible range of outcomes, and identifying the causes and consequences of these changes. These questions are addressed on any conceivable spatial and temporal scale, but significant value can be added where chronostratigraphic links that connect records together exist. This allows direct tie-points between a range of archives and proxy records as well as increased precision for comparing the timing of events (e.g. leads and lags within a system).

As volcanic ash from a single eruption has the same age wherever it occurs, far-travelled deposits from explosive eruptions – tephra – can be used as isochrons where it is possible to characterise a primary airfall event. Characterisation and correlation is possible using major element geochemical analyses of glass shards as each eruption, volcano and source region can have a unique fingerprint for identification. Once identified, tephra layers can be used to link and synchronize depositional records, and to transfer relative or numerical ages to the sequences using lithostratigraphic and compositional data associated with the ash layers (e.g. Sarna-Wojcicki, 2000; Alloway et al., 2007; Lowe et al., 2016). Regional tephra frameworks vary in their spatial and temporal coverage but are built using sites, ideally, with records of multiple tephra falls, and increase both our understanding of tephra transportation and deposition and the potential for the use of tephra as chronostratigraphic tools in further research (e.g. Haflidason et al., 2000; Turney et al., 2004; Lowe et al., 2008; Swindles et al., 2011; Lawson et al., 2012; Narcisi et al., 2012; Davies et al., 2014; Lowe et al., 2015; Plunkett et al., 2015; Ponomareva et al., 2017).

Within North America, there is a rich history of both volcanic activity and tephra research, with a focus on proximal deposits and currently active areas including Alaska, the Aleutian Arc, the Wrangells and the Cascades. Initial identifications of visible tephra beds from these source areas in peatlands was undertaken by the mid 20th century (e.g. Hansen, 1949; Fryxell, 1965; Westgate et al., 1969) but work by Westgate et al. (1970), Zoltai (1989), and others during the 1970s and 1980s brought increased attention to the potential use of tephra deposits for correlating sedimentary records within continental western Canada. Since then, numerous visible tephra have been identified throughout western Canada (including, but not limited to: Clague et al.,

1995; Fraser and Burn, 1997; Beierle and Smith, 1998; Westgate et al., 2001; Froese et al., 2002, 2006; Yu et al., 2003; Livingston et al., 2009; Jensen and Beaudoin, 2016).

Few investigations, however, consider the potential for cryptotephra layers (which are not visible to the naked eye), with exceptions being recent studies from Alaska (e.g. de Fontaine et al., 2007; Payne et al., 2008; Monteath et al., 2017) and northern BC (Lakeman et al., 2008). The discovery of ultra-distal cryptotephra traced from western sources to the east coast, Greenland, and beyond in to Europe (Pyne-O'Donnell et al., 2012, 2016; Jensen et al., 2014; Mackay et al., 2016) indicates the potential for a tephra framework across the continent, and beyond. However, the majority of Canada does not have any reported cryptotephra records - there are over 4000 km between visible deposits at western sites and ultra-distal east coast cryptotephra.

In this thesis, I test the potential for development of a cryptotephra framework in northwestern North America. The work outlined here will provide the initial data for the construction of a regional cryptotephra framework, where key tephra layers (those which are widely distributed, easily identified and correlated, and have well constrained chronological control) can be identified for use in future chronological work.

Palaeo-records representing the Holocene and up to the modern day are used as these are typically higher resolution than older records and they allow the overlap of multiple chronological techniques. While the potential for long, continuous, high resolution records that can be utilised to produce quantitative estimates of past climatic fluctuations exists within the Arctic and Subarctic, these records present many challenges given their varying degrees of chronological uncertainty and temporal resolution (e.g. Kaufman et al., 2004; McKay and Kaufman, 2014; Sundqvist et al., 2014; Briner et al., 2016). The identification of well constrained cryptotephra isochrons would provide a fast and relatively inexpensive method to precisely date palaeo-records in a wide range of depositional settings and allow accurate correlations of proxy records both between sites and with long regional and global records such as those preserved in ice cores, marine sediments, and loess-palaeosol sequences.

Western Canada has good potential for cryptotephra deposition as it lies downwind of the numerous active volcanoes of the Aleutian Arc, Alaskan Peninsula and Wrangell volcanic fields. Visible tephra from the Cascade volcanic region have been recorded as far north as central

Alberta but have not been reported beyond this. Additional potential active sources further afield include the volcanoes of Kamchatka and Japan.

The aims and objectives of this thesis are defined as follows:

- Address geographical gaps for cryptotephra records in northwestern Canada
    - Review current knowledge
    - Produce new record
- Define regionally significant cryptotephra beds present that can be used to improve local and regional scale chronologies
    - Age modelling
    - Geochemical characterisation
    - Update geographical distributions
- Demonstrate the potential for cryptotephra as isochrons in the area
    - Key distal correlations
    - Direct application for modern eruptions
    - Comparison to current proximal and ultra-distal records

These aims and objectives are addressed through three papers: Chapter 2 is a review of the current knowledge regarding distal tephra upwind of northwestern North America; Chapter 3 is a Holocene cryptotephra record from Yukon Territory that significantly expands the number of beds previously found within Canada, and Chapter 4 is an in-depth comparison of dating techniques using peat cores from Fort McMurray and demonstrates a potential use of modern cryptotephra in the region. These papers lay out the groundwork for a cryptotephra-framework in northwestern North America, summarised in Chapter 5 along with suggestions for future research directions.

1.1 Detailed Chapter Summaries

A version of this chapter has been published as:

Davies, L.J., Jensen, B.J.L., Froese, D.G., Wallace, K.L., 2016. Late Pleistocene and Holocene tephrostratigraphy of interior Alaska and Yukon: Key beds and chronologies over the past 30,000 years. Invited review, *Quaternary Science Reviews*, 146: 28-53.

> *The Aleutian Arc-Alaska Peninsula and Wrangell volcanic field are the main source areas for tephra deposits found across Alaska and northern Canada, and increasingly, tephra from these eruptions have been found further afield in North America, Greenland, and Europe. However, there have been no broad scale reviews of the Late Pleistocene and Holocene tephrostratigraphy for this region since the 1980s, and this lack of data is hindering progress in identifying these tephra both locally and regionally. To address this*

gap and the variable quality of associated geochemical and chronological data, we undertake a detailed review of the latest Pleistocene to Holocene tephra found in interior Alaska and Yukon. This paper discusses nineteen tephra that have distributions beyond southwest Alaska and that have the potential to become, or already are, important regional markers. This includes three 'modern' events from the 20th century, ten with limited data availability but potentially broad distributions, and six that are widely reported in interior Alaska and Yukon. Each tephra is assessed in terms of chronology, geochemistry and distribution, with new Bayesian age estimates and geochemical data when possible. This includes new major-element geochemical data for Crater Peak 1992, Redoubt 1989–90, and two andesitic tephra from St Michael Island (Tephra D), as well as revised age estimates for Dawson tephra, Oshetna, Hayes set H, Aniakchak CFE II, and the White River Ashes, northern and eastern lobes.

Chapter 3

A version of this paper is in preparation for submission to Quaternary Science Reviews.

A cryptotephra record is presented for the Holocene from a soligenic peatland in the north-central Yukon, Canada (DHP174). This site records continuous accumulation since 10,400 cal yr BP, and at least 75 identifiable cryptotephra layers are identified with 1cm resolution analyses. From these, a distal tephrostratigraphy is defined using 28 peaks representing 34 eruptions with distinct geochemical populations (each with >10 EPMA analyses presented here). Major element geochemical characterisation indicates that these layers are primarily produced from the Aleutians and south-eastern Alaska, not surprisingly given the location and predominant wind direction. Two ultra-distal tephra in the early Holocene are correlated with large caldera forming eruptions from Kamchatka (KO) and the Kurile Islands (TR(Zv)). No influence is seen from any active volcanic sources to the south. This work demonstrates that cryptotephra in northwestern North America, while rarely employed in research today, have significant potential to support a wide range of research projects. This record is presented as a key contribution to the development of a regional tephrostratigraphic framework within North America by providing a thorough characterisation of 34 Holocene cryptotephra transported in to northwestern Canada from western sources.

Chapter 4

A version of this chapter has been accepted pending minor revisions by Quaternary Geochronology in February 2017:

Davies, LJ, Froese, DF, Appleby, PG, Jensen, BJL, Magnan, G, Mullan-Bordreau, G, Noernberg, T, Shotyk, W, van Bellen, S, Zaccone. High-resolution Bayesian age modelling of peat bog profiles from northern Alberta, Canada, using pre- and post-bomb ^{14}C, ^{210}Pb and tephrochronology.

High-resolution studies of peat profiles are frequently undertaken to investigate natural and anthropogenic disturbances over time. However, overlapping profiles of the most commonly applied age-dating techniques, including ^{14}C and ^{210}Pb, often show significant offsets (>decadal) and biases that can be difficult to resolve. Here we investigate variations in the chronometers and individual site histories from six ombrotrophic peat bogs in central and northern Alberta. Dates produced using pre- and post-bomb ^{14}C, ^{210}Pb (corroborated with ^{137}Cs and ^{241}Am), and cryptotephra peaks, are compared and then integrated using OxCal's P_Sequence function to produce a single Bayesian age model. Environmental histories for each site obtained using physical and chemical characteristics of the peat cores, e.g. macrofossils, humification, ash content, and dry density, provide important constraints for the models by highlighting periods with significant changes in accumulation rate, e.g. fire events, permafrost development, and prolonged surficial drying. Despite variable environmental histories, it is possible to produce high-resolution age-depth models for each core sequence. Consistent offsets between ^{14}C and ^{210}Pb dates pre-1960s are seen at five of the six sites, but tephra-corrected ^{210}Pb data can be used to produce more coherent models at three of these sites. Processes such as permafrost development and thaw, surficial drying and local fires can disrupt the normal processes by which chronological markers and environmental records are incorporated in the peat record. In consequence, applying standard dating methodologies to these records will result in even greater uncertainties and discrepancies between the different dating tools. These results show that using any single method to accurately date peat profiles where accumulation has not been uniform over time may be unreliable, but a comprehensive multi-method investigation paired with the application of Bayesian statistics can produce more robust chronologies. New cryptotephra data for the Alberta region are also reported here, including the historical Novarupta-Katmai 1912 eruption, White River Ash (East), and glass from Mt. St. Helens, Mt. Churchill, and probable Aleutian sources.

1.2 References

Alloway, B.V., Larsen, G., Lowe, D.J., Shane, P.A.R., Westgate, J.A., 2007. Quaternary Stratigraphy - Tephrochronology, in: Elias, S.A. (Ed.), Encyclopedia of Quaternary Science. Elsevier, pp. 2869–2898. https://doi.org/10.1016/B0-44-452747-8/00075-2

Beierle, B., Smith, D.G., 1998. Severe drought in the early Holocene (10,000-6800 BP) interpreted from lake sediment cores, southwestern Alberta, Canada. Palaeogeogr. Palaeoclimatol. Palaeoecol. 140, 75–83. https://doi.org/10.1016/S0031-0182(98)00044-3

Clague, J.J., Evans, S.G., Rampton, V.N., Woodsworth, G.J., 1995. Improved age estimates for the White River and Bridge River tephras, western Canada. Can. J. Earth Sci. 32, 1172–1179. https://doi.org/10.1139/e95-096

Davies, S.M., Abbott, P.M., Meara, R.H., Pearce, N.J.G., Austin, W.E.N., Chapman, M.R., Svensson, A., Bigler, M., Rasmussen, T.L., Rasmussen, S.O., Farmer, E.J., 2014. A North

Atlantic tephrostratigraphical framework for 130-60 ka b2k: New tephra discoveries, marine-based correlations, and future challenges. Quat. Sci. Rev. 106, 101–121. https://doi.org/10.1016/j.quascirev.2014.03.024

de Fontaine, C.S., Kaufman, D.S., Scott Anderson, R., Werner, A., Waythomas, C.F., Brown, T.A., 2007. Late Quaternary distal tephra-fall deposits in lacustrine sediments, Kenai Peninsula, Alaska. Quat. Res. 68, 64–78. https://doi.org/10.1016/j.yqres.2007.03.006

Fraser, T.A., Burn, C.R., 1997. On the nature and origin of 'muck' deposits in the Klondike area, Yukon Territory. Can. J. Earth Sci. 34, 1333–1344. https://doi.org/10.1139/e17-106

Froese, D., Westgate, J., Preece, S., Storer, J., 2002. Age and significance of the Late Pleistocene Dawson tephra in eastern Beringia. Quat. Sci. Rev. 21, 2137–2142. https://doi.org/10.1016/S0277-3791(02)00038-0

Froese, D.G., Zazula, G.D., Reyes, A. V., 2006. Seasonality of the late Pleistocene Dawson tephra and exceptional preservation of a buried riparian surface in central Yukon Territory, Canada. Quat. Sci. Rev. 25, 1542–1551. https://doi.org/10.1016/j.quascirev.2006.01.028

Fryxell, R., 1965. Mazama and Glacier Peak Volcanic Ash Layers: Relative Ages. Science 147, 1288–1290. https://doi.org/10.1126/science.147.3663.1288

Haflidason, H., Eiriksson, J., Van Kreveld, S., 2000. The tephrochronology of Iceland and the North Atlantic region during the middle and Late Quaternary: A review. J. Quat. Sci. 15, 3–22. https://doi.org/10.1002/(SICI)1099-1417(200001)15:1<3::AID-JQS530>3.0.CO;2-W

Hansen, H.P., 1949. Postglacial Forests in South Central Alberta, Canada. Am. J. Bot. 36, 54–65.

Jensen, B.J.L., Beaudoin, A.B., 2016. Geochemical characterization of tephra deposits at archaeological and palaeoenvironmental sites across south-central Alberta and southwest Saskatchewan, in: Woywitka, R. (Ed.), Back on the Horse: Recent Developments in Archaeological and Palaeontological Research in Alberta. Archaeological Survey of Alberta, Edmonton, Alberta, pp. 154–160.

Jensen, B.J.L., Pyne-O'Donnell, S., Plunkett, G., Froese, D.G., Hughes, P.D.M., Sigl, M., McConnell, J.R., Amesbury, M.J., Blackwell, P.G., van den Bogaard, C., Buck, C.E., Charman, D.J., Clague, J.J., Hall, V.A., Koch, J., Mackay, H., Mallon, G., McColl, L., Pilcher, J.R., 2014. Transatlantic distribution of the Alaskan White River Ash. Geology 42, 875–878. https://doi.org/10.1130/G35945.1

Kaufman, D.S., Ager, T.A., Anderson, N.J., Anderson, P.M., Andrews, J.T., Bartlein, P.J., Brubaker, L.B., Coats, L.L., Cwynar, L.C., Duvall, M.L., Dyke, A.S., Edwards, M.E., Eisner, W.R., Gajewski, K., Geirsdóttir, A., Hu, F.S., Jennings, A.E., Kaplan, M.R., Kerwin, M.W., Lozhkin, A. V., MacDonald, G.M., Miller, G.H., Mock, C.J., Oswald, W.W., Otto-Bliesner, B.L., Porinchu, D.F., Rühland, K., Smol, J.P., Steig, E.J., Wolfe, B.B., 2004. Holocene thermal maximum in the western Arctic (0-180°W). Quat. Sci. Rev. 23, 529–560. https://doi.org/10.1016/j.quascirev.2003.09.007

Lakeman, T.R., Clague, J.J., Menounos, B., Osborn, G.D., Jensen, B.J.L., Froese, D.G., 2008. Holocene tephras in lake cores from northern British Columbia, Canada. Can. J. Earth Sci. 45, 935–947. https://doi.org/10.1139/E08-035

Lawson, I.T., Swindles, G.T., Plunkett, G., Greenberg, D., 2012. The spatial distribution of Holocene cryptotephras in north-west Europe since 7 ka: Implications for understanding ash fall events from Icelandic eruptions. Quat. Sci. Rev. 41, 57–66. https://doi.org/10.1016/j.quascirev.2012.02.018

Livingston, J.M., Smith, D.G., Froese, D.G., Hugenholtz, C.H., 2009. Floodplain stratigraphy of the ice jam dominated middle Yukon River: a new approach to long-term flood frequency. Hydrol. Process. 23, 357–371. https://doi.org/10.1002/hyp.7106

Lowe, D.J., Alloway, B., 2014. Tephrochronology, in: Rink, W.J., Thompson, J. (Eds.), Encyclopedia of Scientific Dating Methods. Springer Netherlands, Dordrecht, p. 26. https://doi.org/10.1007/978-94-007-6326-5_19-2

Lowe, D.J., Shane, P.A.R., Alloway, B. V., Newnham, R.M., 2008. Fingerprints and age models for widespread New Zealand tephra marker beds erupted since 30,000 years ago: a framework for NZ-INTIMATE. Quat. Sci. Rev. 27, 95–126. https://doi.org/10.1016/j.quascirev.2007.01.013

Lowe, J.J., Ramsey, C.B., Housley, R.A., Lane, C.S., Tomlinson, E.L., Stringer, C., Davies, W., Barton, N., Pollard, M., Gamble, C., Menzies, M., Rohling, E., Roberts, A., Blockley, S., Cullen, V., Grant, K., Lewis, M., MacLeod, A., White, D., Albert, P., Hardiman, M., Lee, S., Oh, A., Satow, C., Cross, J.K., Law, C.B., Todman, A., Bourne, A., Matthews, I., Müller, W., Smith, V., Wulf, S., Anghelinu, M., Antl-Weiser, W., Bar-Yosef, O., Boric, D., Boscato, P., Ronchitelli, A., Chabai, V., Veselsky, A., Uthmeier, T., Farrand, W., Gjipali, I., Ruka, R., Güleç, E., Karavanic, I., Karkanas, P., King, T., Komšo, D., Koumouzelis, M., Kyparissi, N., Lengyel, G., Mester, Z., Neruda, P., Panagopoulou, E., Shalamanov-Korobar, L., Tolevski, I., Sirakov, N., Guadelli, A., Guadelli, J.L., Ferrier, C., Skrdla, P., Slimak, L., Soler, N., Soler, J., Soressi, M., Tushabramishvilii, N., Zilhão, J., Angelucci, D., Albert, P., Bramham Law, C., Cullen, V.L., Lincoln, P., Staff, R., Flower, K., Aouadi-Abdeljaouad, N., Belhouchet, L., Barker, G., Bouzouggar, A., Van Peer, P., Kindermann, K., Gerken, K., Niemann, H., Tipping, R., Saville, A., Ward, T., Clausen, I., Weber, M.J., Kaiser, K., Torksdorf, J.F., Turner, F., Veil, S., Nygaard, N., Pyne-O'Donnell, S.D.F., Masojc, M., Nalepka, D., Jurochnik, A., Kabacinski, J., Antoine, P., Olive, M., Christensen, M., Bodu, P., Debout, G., Orliac, M., De Bie, M., Van Gils, M., Paulissen, E., Brou, L., Leesch, D., Hadorn, P., Thew, N., Riede, F., Heinen, M., Joris, O., Richter, J., Uthmeier, T., Knipping, M., Stika, H.P., Friedrich, M., Conard, N., Malina, M., Kind, C.J., Beutelspacher, T., Mortensen, M.F., Burdukiewicz, J.M., Szynkiewicz, A., Poltowicz-Bobak, M., Bobak, D., Wisniewski, A., Przezdziecki, M., Valde-Nowak, P., Muzyczuk, A., Bramham Law, C., Cullen, V.L., Davies, L., Lincoln, P., MacLeod, A., Morgan, P., Aydar, E., çubukçu, E., Brown, R., Coltelli, M., Castro, D. Lo, Cioni, R., DeRosa, R., Donato, P., Roberto, A. Di,

Gertisser, R., Giordano, G., Branney, M., Jordan, N., Keller, J., Kinvig, H., Gottsman, J., Blundy, J., Marani, M., Orsi, G., Civetta, L., Arienzo, I., Carandente, A., Rosi, M., Zanchetta, G., Seghedi, I., Szakacs, A., Sulpizio, R., Thordarson, T., Trincardi, F., Vigliotti, L., Asioli, A., Piva, A., Andric, M., Brauer, A., de Klerk, P., Filippi, M.L., Finsinger, W., Galovic, L., Jones, T., Lotter, A., Müller, U., Pross, J., Mangerud, J., Lohne, Pyne-O'Donnell, S., Markovic, S., Pini, R., Ravazzi, C., Riede, F., TheuerKauf, M., Tzedakis, C., Margari, V., Veres, D., Wastegård, S., Ortiz, J.E., Torres, T., Díaz-Bautista, A., Moreno, A., Valero-Garcés, B., Lowick, S., Ottolini, L., 2015. The RESET project: Constructing a European tephra lattice for refined synchronisation of environmental and archaeological events during the last c. 100 ka. Quat. Sci. Rev. 118, 1–17. https://doi.org/10.1016/j.quascirev.2015.04.006

Mackay, H., Hughes, P.D.M., Jensen, B.J.L., Langdon, P.G., Pyne-O'Donnell, S.D.F., Plunkett, G., Froese, D.G., Coulter, S.E., Gardner, J.E., 2016. A mid to late Holocene cryptotephra framework from eastern North America. Quat. Sci. Rev. 132, 101–113. https://doi.org/10.1016/j.quascirev.2015.11.011

Monteath, A.J., van Hardenbroek, M., Davies, L.J., Froese, D.G., Langdon, P.G., Xu, X., Edwards, M.E., 2017. Chronology and glass chemistry of tephra and cryptotephra horizons from lake sediments in northern Alaska, USA. Quat. Res. 88, 169–178. https://doi.org/10.1017/qua.2017.38

Narcisi, B., Petit, J.R., Delmonte, B., Scarchilli, C., Stenni, B., 2012. A 16,000-yr tephra framework for the Antarctic ice sheet: A contribution from the new Talos Dome core. Quat. Sci. Rev. 49, 52–63. https://doi.org/10.1016/j.quascirev.2012.06.011

Payne, R., Blackford, J., van der Plicht, J., 2008. Using cryptotephras to extend regional tephrochronologies: An example from southeast Alaska and implications for hazard assessment. Quat. Res. 69, 42–55. https://doi.org/10.1016/j.yqres.2007.10.007

Plunkett, G., Coulter, S.E., Ponomareva, V. V., Blaauw, M., Klimaschewski, A., Hammarlund, D., 2015. Distal tephrochronology in volcanic regions: Challenges and insights from Kamchatkan lake sediments. Glob. Planet. Change 134, 26–40. https://doi.org/10.1016/j.gloplacha.2015.04.006

Ponomareva, V., Portnyagin, M., Pendea, I.F., Zelenin, E., Bourgeois, J., Pinegina, T., Kozhurin, A., 2017. A full holocene tephrochronology for the Kamchatsky Peninsula region: Applications from Kamchatka to North America. Quat. Sci. Rev. 168, 101–122. https://doi.org/10.1016/j.quascirev.2017.04.031

Pyne-O'Donnell, S.D.F., Cwynar, L.C., Jensen, B.J.L., Vincent, J.H., Kuehn, S.C., Spear, R., Froese, D.G., 2016. West Coast volcanic ashes provide a new continental-scale Lateglacial isochron. Quat. Sci. Rev. 142, 16–25. https://doi.org/10.1016/j.quascirev.2016.04.014

Pyne-O'Donnell, S.D.F., Hughes, P.D.M., Froese, D.G., Jensen, B.J.L., Kuehn, S.C., Mallon, G., Amesbury, M.J., Charman, D.J., Daley, T.J., Loader, N.J., Mauquoy, D., Street-Perrott, F.A., Woodman-Ralph, J., 2012. High-precision ultra-distal Holocene tephrochronology in North America. Quat. Sci. Rev. 52, 6–11. https://doi.org/10.1016/j.quascirev.2012.07.024

Sarna-Wojcicki, A., 2000. Tephrochronology, in: Noller, J.S., Sowers, J.M., Lettis, W.R. (Eds.), Quaternary Geochronology; Methods and Applications. American Geophysical Union, Washington, DC, pp. 357–377. https://doi.org/10.1029/RF004p0357

Swindles, G.T., Lawson, I.T., Savov, I.P., Connor, C.B., Plunkett, G., 2011. A 7000 yr perspective on volcanic ash clouds affecting northern Europe. Geology 39, 887–890. https://doi.org/10.1130/G32146.1

Turney, C.S.M., Lowe, J.J., Davies, S.M., Hall, V., Lowe, D.J., Wastegård, S., Hoek, W.Z., Alloway, B., 2004. Tephrochronology of Last Termination sequences in Europe: A protocol for improved analytical precision and robust correlation procedures (a joint SCOTAV-INTIMATE proposal). J. Quat. Sci. 19, 111–120. https://doi.org/10.1002/jqs.822

Westgate, J.A., Preece, S.J., Froese, D.G., Walter, R.C., Sandhu, A.S., Schweger, C.E., 2001. Dating Early and Middle (Reid) Pleistocene Glaciations in Central Yukon by Tephrochronology. Quat. Res. 56, 335–348. https://doi.org/10.1006/qres.2001.2274

Westgate, J.A., Smith, D., Nichols, H., 1969. Late Quaternary pyroclastic layers in the Edmonton area, Alberta., in: Pawluk, S. (Ed.), Proceedings of Symposium on Pedology and Quaternary Research, Geology Department Contract. Edmonton, Alberta, pp. 180–186.

Westgate, J.A., Smith, D., Tomlinson, M., 1970. Late Quaternary tephra layers in southwestern Canada, in: Smith, R.A., Smith, J.W. (Eds.), Early Man and Environments in Northwest North America. Calgary, Alberta, pp. 13–34.

Yu, Z., Vitt, D.H., Campbell, I.D., Apps, M.J., 2003. Understanding Holocene peat accumulation pattern of continental fens in western Canada. Can. J. Bot. 81, 267–282. https://doi.org/10.1139/b03-016

Zoltai, S.C., 1989. Late Quaternary volcanic ash in the peatlands of central Alberta. Can. J. Earth Sci. 26, 207–214. https://doi.org/10.1139/e89-017

CHAPTER 2: LATE PLEISTOCENE AND HOLOCENE TEPHROSTRATIGRAPHY OF INTERIOR ALASKA AND YUKON: KEY BEDS AND CHRONOLOGIES OVER THE PAST 30,000 YEARS

2.1 Introduction

Volcanic ash deposits (tephra) are a key chronostratigraphic component of late Quaternary palaeoenvironmental reconstructions, as seen, for example, in the North Atlantic region (e.g. Abbott and Davies, 2012; Blockley et al., 2014; Davies et al., 2014). This is largely because individual tephra deposits allow a level of precision and accuracy in dating and correlation that is unachievable through other means (e.g. Lane et al., 2013). Methods such as radiocarbon dating have been used to construct chronologies, but have accompanying errors that can limit the comparison of widely distributed palaeoenvironmental records. Radiocarbon dating can also be affected by issues of sample selection, taphonomy, contamination, and stratigraphic integrity (e.g. Olsson, 1974; Lowe and Walker, 2000; Nilsson et al., 2001; Oswald et al., 2005; Brock et al., 2010). In particular, high latitude regions with an abundance of 'old' carbon on the landscape, because of slow rates of decomposition, are particularly susceptible to producing complicated radiocarbon chronologies (e.g. Karrow and Anderson, 1975; Nelson et al., 1988; Abbott and Stafford, 1996; Zimov et al., 1997; Kennedy et al., 2010; Reyes and Cooke, 2011). The development of detailed tephrostratigraphic frameworks can help overcome barriers in interpretation that are created by the inherent uncertainty in age models that constrain many depositional records and their associated palaeoenvironmental data.

The use of tephra deposits as a tool for stratigraphy and chronology has been enhanced in recent decades (e.g. Braitseva et al., 1997; Davies et al., 2012; Kaufman et al., 2012; Lowe et al., 2013; Moriwaki et al., 2016). In practice, tephrostratigraphy and -chronology relates to the use of visible (macro) beds, or non-visible, microscopic deposits known as 'cryptotephra'. In northwestern North America the majority of tephrostratigraphic studies have been limited to areas where visible tephra are present (e.g. Péwé, 1975; Miller and Smith, 1987; Westgate et al., 1970; Beget et al., 1991; Clague et al., 1995; Foit et al., 2004; Kuehn et al., 2009a; Jensen et al., 2011; Preece et al., 2011a), and only a few studies have identified cryptotephra (e.g. Zoltai, 1989; de Fontaine et al., 2007; Lakeman et al., 2008; Payne et al., 2008). Additionally, while detailed Plio-Pleistocene syntheses of tephra in the Yukon and Alaska exist (e.g. Preece et al.,

1999; 2011b; Jensen et al., 2008; 2016; Péwé et al., 2009), Holocene syntheses are largely missing. There are a number of individual records for specific volcanic sources from proximal settings (e.g. Stelling et al., 2005; Larsen et al., 2007; Schiff et al., 2008, 2010), or study areas focused in southwest Alaska and the eastern Aleutian arc (e.g. Riehle, 1985; Miller and Smith, 1987; Riehle et al., 1999; Carson et al., 2002; Fierstein, 2007; de Fontaine et al., 2007; Kaufman et al., 2012;). However, there are no broad overviews of Holocene and latest Pleistocene tephra extending to distal sites.

The Late Quaternary tephra record of northwestern North America is increasingly important not just for researchers within western North America, but also further afield. On modern timescales, the distribution of volcanic ash is of significant interest for local hazard assessment and also at a regional level for aviation safety (e.g. Casadevall, 1994; Bull et al., 2011). Cryptotephra play an important role in developing tephrostratigraphic frameworks and understanding eruptive histories because they can greatly expand the known distribution of previously identified tephra (e.g. Turney et al., 1997; Davies et al., 2001) and result in the discovery of new eruptions (Wastegård, 2002; Davies et al., 2003; Pyne-O'Donnell, 2007; MacLeod et al., 2015). Cryptotephra studies also have great potential for chronological applications such as linking and comparing disparate palaeoenvironmental records if the tephra is well characterised and dated (e.g. Lowe et al., 2007; Lowe et al., 2012; Lane et al., 2013; Streeter and Dugmore, 2014). The recent discovery of Pacific northwest tephra more than 5000 km from their source in eastern Canada (Pyne-O'Donnell et al., 2012), Europe (Jensen et al., 2014a) and the eastern United States (Jensen et al., 2014b; Mackay et al., 2016; Pyne-O'Donnell et al., 2016), demonstrates the excellent potential for developing a cryptotephra framework across northern North America.

In order to more fully utilise the currently available Alaska eruption records, a baseline of well-characterised and dated tephra - the foundations of a regional tephrostratigraphy– is required. The aim of this review is to provide an assessment of available tephra data for this region as a starting point to achieve this goal. This review is restricted to tephra from the latest Pleistocene and Holocene as sedimentary records from this time period are commonly studied, but tephra records younger than the Dawson tephra (~30,000 cal yr BP) are not always well documented. This paper focuses on tephra found within eastern Beringia, the unglaciated region of Alaska and Yukon, and reassesses their geographical distribution, geochemical characterisation and age estimates, to update the regional tephrostratigraphy.

2.1.1. Regional setting

The study region for this review is limited to the interior of Alaska and Yukon (Fig. 1) for several reasons - this area preserves late Pleistocene sedimentary records that normally would have been removed by glaciation elsewhere, and captures the distal record of large magnitude eruptions from sources in the Wrangell volcanic field (WVF) and Aleutian Arc-Alaska Peninsula (AAAP). By choosing this more distal area we are attempting to reduce the "background noise" created by the large number of small eruptions that have deposited hundreds of tephra in locations proximal to the source volcanoes. Tephra found in the interior are the most likely to be significant for both a regional tephrostratigraphy, and one that may be applied more broadly across North America. The northern limit of the North American Cordillera is a significant topographic barrier within the region and the prevailing winds that flow around it create a natural break in the landscape. These conditions have restricted the distribution of visible tephra in the area, for example tephra from the Cascades or southern volcanic sources that are found in central and southern Canada (e.g. Zoltai, 1989; Westgate et al., 1969; Lakeman et al., 2008) have not been reported in this region. Hence, this study area can be thought of as preserving tephra from Alaska, and potentially sources further upwind, such as Kamchatka.

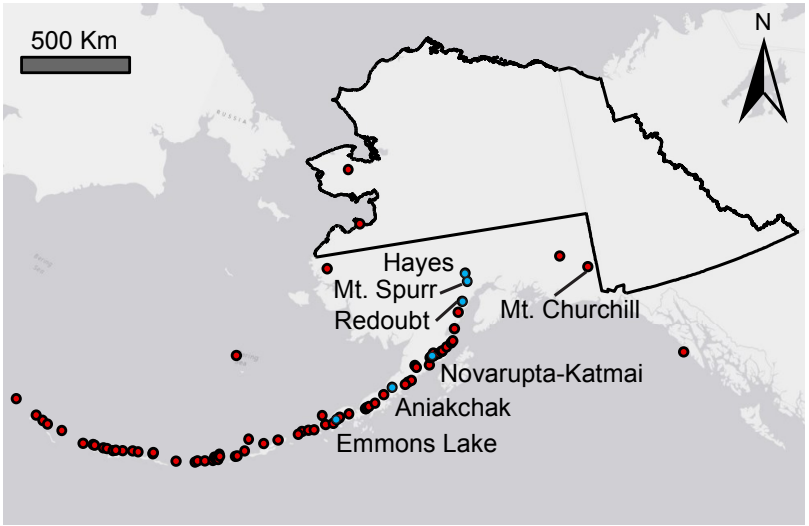

Figure 2.1 Location map showing study area outlined in black. Circle symbols mark volcanoes known to be active during the Holocene, blue stars are volcanoes which produced tephra referred to within this study (Alaska Volcano Observatory, 2014).

The Alaska Volcano Observatory reference library (Alaska Volcano Observatory, 2014) documents the long-term activity of volcanoes in the area. Of Alaska's 130 volcanoes and

volcanic fields, 96 have been active either historically or within the Holocene (Miller et al., 1998). From historical observations since ~ 1760 CE more than 50 volcanoes have been active, and the eruption database currently catalogues 177 tephra plumes and falls from 27 volcanoes (Alaska Volcano Observatory, 2014). These eruption records give us an indication of the high level of volcanic activity and tephra production occurring, but not necessarily how many tephra have been preserved distally. The transport distances of the eruptive ejecta are related to factors such as the height of the eruption column, duration of the event, and prevailing winds at the time of the eruption (e.g. Turner and Hurst, 2001; Watt et al., 2009; Bull et al., 2011). As many of the eruptions documented were relatively small events with limited transport potential, the actual number of tephra preserved distally will be significantly less even before factoring in additional issues influencing the preservation and taphonomy of tephra layers within sedimentary records (e.g. Dugmore et al., 1996; Beierle and Bond, 2002; Davies et al., 2007; Payne and Gehrels, 2010; Pyne-O'Donnell, 2010; Watson et al., 2015).

The Kamchatka Peninsula can also be considered here as a potential source of distal cryptotephra in this region given the large number of active volcanoes present and their favourable position in terms of prevailing wind direction. However, while Yalcin et al. (2003) report finding shards from the Ksudach 1907 eruption in the Eclipse ice core (see section 3 for details), there have been no published occurrences of visible deposits of Kamchatkan tephra within eastern Beringia.

2.2 Materials and Methods

We reviewed the literature to assess which tephra have been identified within the study area and collated available information on those tephra, particularly with respect to stratigraphy, glass geochemistry, and chronological control. One additional radiocarbon date and new electron probe microanalysis (EPMA) data produced at the University of Alberta, Edmonton, have been included here. The datasets used within this review are detailed in the Supplementary Data (Tables S2.1–S2.7).

A full characterisation of tephra deposits also describes attributes such as glass morphology, mineralogy, and trace-element composition of whole rock or glass samples. These can be particularly useful, or even necessary, for distinguishing between different tephra or identifying complex volcanic histories (e.g. Westgate et al., 2008, 2013; Preece et al., 2011a, b, 2014; Smith et al., 2011). However, when working with distal samples, and cryptotephra in particular, these

observations are not always possible (e.g. if only the glass fraction is deposited) or undertaken (e.g. if EPMA data appear sufficient for a project, or if the required analytical equipment is not available). For this study we focus on assessing the attributes most commonly utilised in tephra studies: major-element glass geochemistry, chronology and stratigraphy. Additional information on glass morphology, mineralogy and trace element geochemistry that is available is summarised in Table S2.1.

Tephra identified within the study area are split into three categories for discussion: modern tephra (occurring within the period of historical observations), tephra with limited characterisation (for example, those which have been reported from a single site or have only approximate chronologies), and widely reported tephra (identified at multiple sites, and with numerous reported age estimates). Unless stated otherwise, tephra are discussed from oldest to youngest within each section.

2.2.1. Age modelling

Tephra can be dated in a number of ways, either directly using methods such as fission track or Ar-Ar dating of glass or associated minerals, or indirectly by dating the surrounding sediments that preserve the tephra. Indirect dating is commonly undertaken using high-precision radiocarbon dating or using layer counting if the record is incremental, such as ice cores or varved lake deposits (e.g. Lowe, 2011; Lowe and Alloway, 2015). Within this study, the term 'date' is used to refer to an indirect and/or unmodelled date produced from material associated with a tephra, and the term 'age' refers to either a direct date, a date representing a maximum or minimum chronological limit, or a modelled outcome combining one or more dates associated with a tephra to estimate the time of deposition. Modelled ages are reported in the appropriate model output (e.g. cal yr BP, BC/AD); dates are reported in the format they were originally published.

Within the study area, and for the time frame under consideration, almost all tephra are dated indirectly using radiocarbon. Only 6 of the 216 dates reviewed within this study are produced using other methods: dates for the Dawson tephra include one fission-track (Naeser et al., 1982) and two optically stimulated luminescence (OSL; Demuro et al, 2008) dates, and the White River Ash east (WRAe) and Aniakchak have associated ice-core ages from Greenland (Pearce et al., 2004; Coulter et al., 2012; Jensen et al., 2014a). All dates reviewed here are detailed in the

Supplementary Data (Tables S5–S6). The new date included here was obtained from material pre-treated at the University of Alberta following Olssen (1986) and analysed at the University of California Irvine Keck Carbon Cycle AMS Facility, California.

Radiocarbon dating is one of the most common techniques applied when indirectly dating tephra from the late Quaternary, but it is the application of Bayesian modelling that allows the construction of precise and reliable age estimates and chronologies using multiple bracketing dates (Blockley et al., 2008). These techniques have been widely adopted in a variety of studies (e.g. Demuro et al. 2008; Kuehn et al., 2009a; Lohne et al., 2013; Lowe et al., 2013; Smith et al., 2013), and are particularly useful where tephra are not preserved within annually resolved records (e.g. Wohlfarth et al., 2006; Matthews et al., 2011; Bronk-Ramsey et al., 2015).

The widely reported tephra discussed here are well documented in the literature, but many have discrepancies in reported ages either within or between different study sites that have yet to be resolved. Averages of dates or the results from just one study are often taken as the accepted age estimate in subsequent publications. This study uses Bayesian modelling of reported ages to produce robust estimates of the eruption age for each tephra (e.g. Buck et al., 2003*;* Blockley et al., 2008), with the intention of producing comparable, statistically reliable, and consistent age estimates between sites.

The large numbers of radiocarbon dates that can be associated with a particular eruption create a challenge in determining which age best estimates the timing of tephra deposition. Several strategies have been proposed, ranging from those that are purely statistical (e.g. Wilson and Ward, 1981; Christen, 1994; Lowe et al., 1998; Egan et al., 2015), to those that first filter the dataset for the reliability of the dates (e.g. Kuehn et al., 2009a; Reyes and Cooke, 2011) prior to any modelling. When discussing the treatment of outliers Bronk Ramsey (2009b) recommends manual elimination of dates because it clarifies which dates are used to support the analysis, although statistical methods can also be used to support these manual decisions. In this paper we have compiled all dates associated with each tephra occurrence before manually eliminating dates based on criteria similar to those used in Kuehn et al. (2009a). Radiocarbon dates were excluded based on: (1) the problematic nature of the material dated (e.g. bulk sediments, aquatic macrofossils, gastropod and mollusc shells); (2) unclear stratigraphic relations to the tephra layer; and, (3) distances deemed too far from the tephra within the sequence to be relevant

(including modelled ages based on such dates). Any dates where information regarding any of these criteria could not be found were also excluded. Where dates were highlighted in their original publication as being problematic, but with no clear indication of what dates were in question, all dates were included in the model and OxCal's agreement indices were used to further assess the sequence.

The remaining dates that were deemed robust were used as input for a Bayesian model utilising the *Tau_Boundary* function in OxCal v4.2 (Bronk Ramsey, 2009a), with IntCal13 (Reimer et al., 2013) used for calibrations, where necessary, to model best age estimates for the eruptions.

2.2.2. EPMA major-element geochemistry

It is widely recognised that EPMA major-element data collected from individual glass shards (and mineral assemblages, when present) is the first step in characterising (or 'fingerprinting') tephra (e.g. Smith & Westgate, 1968; Westgate & Gorton, 1981; Froggatt, 1992; Lowe, 2011). New data are reported here from glass shards analysed on a JEOL 8900 Superprobe at the University of Alberta by wavelength dispersive spectrometry (WDS) following established protocols (e.g. Jensen et al., 2008; Table 2.1).

Tephra layer	**Lab #**[1]	**Sample location**
Dawson	UA 1000	Sulphur Creek, Klondike Goldfields
Tephra II	UA 2660	Zagoskin Lake, St Michael Island
Tephra II	UA 2661	Puyuk Lake, St Michael Island
HH7	UA 1451, 1877, 1901, 1902, 1903, 1915	Halfway House, W of Fairbanks
Hayes set H, unit F2	AT 2561	Hayes River section
Aniakchak CFE II	UA 1602	Zagoskin Lake, St Michael Island
WRAn	UA 1046	40-mile
WRAe	UA 1119	N. Klondike Highway, 20km N of Carmacks
Ksudach 1907	UA 1497, 1498	Kamchatka
Katmai 1912	UA 1364	Kodiak Island, station 07JANV-2
Redoubt 1989-1990	UA 2754	Seismic station RDN, Alaska
Crater Peak 1992	UA 2619	Anchorage, Alaska

Table 2.1: Details of tephra layers with major element glass composition data published within this study. Names from the original publications are kept here – for correlations refer to Table 2.5. [1] UA = University of Alberta Tephrochronology Lab #; AT = Alaska Tephra Laboratory and Data Center identification #.

Samples containing glass were wet sieved using distilled water and subjected to density separation using either the heavy liquid Lithium Heteropolytungstate (LST) or Tetrabromoethane

(TBE). The 75–150μm fraction of each sample between 2.0–2.42gcm^{-3} was mounted in an epoxy puck and polished to expose glass surfaces before being carbon coated prior to EPMA.

A standard suite of ten elements (Si, Ti, Al, Fe, Mn, Mg, Ca, Na, K, Cl) were measured using a 10 μm beam with 15 keV accelerating voltage and 6 nA beam current in order to minimize alkali migration during analyses. Two secondary standards of known composition were run concurrently with all tephra samples: either UA 5831 or ID 3506, both Lipari rhyolite obsidians that have been shown to be indistinguishable in major element composition (Kuehn et al., 2009b), and a reference sample of Old Crow tephra, a well-characterized, secondarily hydrated tephra bed (e.g. Kuehn et al., 2011). Additionally, previously unpublished average data (Wallace and McGimsey) for Black Peak Tephra and the late glacial Aniakchak caldera-forming eruption (CFE I) are included here for comparison. These analyses were completed on a JEOL 8900 electron microprobe equipped with 5 wavelength x-ray spectrometers at the USGS, Menlo Park, CA. Analytical conditions were 15 kV accelerating voltage, 5 nA beam current, and 5 μm beam diameter; further details are included in Table S2.4. All results are normalized to 100% and presented as weight percent (wt%) oxides. New major- and minor-element geochemical data and associated standard measurements, as well as averaged geochemical data from the published literature are reported in the Supplementary Data (Tables S2.2–S2.3).

While EPMA is essential for characterising tephra, particularly for cryptotephra where glass shards may be the only physical evidence of the eruption, published data are not always comparable given variations in how analyses are undertaken and data are reported (e.g. Froggatt, 1992; Hunt and Hill, 1996; Kuehn et al, 2011). A key consideration is the analysis of both appropriate calibration standards as well as secondary glass standards in order to enable inter-lab comparisons. Procedures may also vary in terms of the elements (Mn, Cl, P, and F are commonly excluded) and the number of data points analysed. This can affect the comparability of datasets - Cl can be relatively diagnostic for identifying some AAAP and WVF tephra and/or sources. For example, tephra from Hayes volcano tend to have distinctively high Cl, generally between 0.30–0.50 wt%. In this review, we highlight published data that report on analytical methods and secondary standards, use individual analyses or averaged data, and those that provide glass versus whole rock analyses. Representative individual glass shard analyses and concurrently analysed secondary standard data have been included where possible in the Supplementary Data, as well as all average EPMA populations referred to from previous work (Tables S2.2–S2.4).

2.3 Modern Eruptions

Five eruptions that occurred during historical times that are of interest to this review are as follows: Ksudach 1907; Novarupta-Katmai 1912; Hekla 1947; Redoubt 1989–1990; and Crater Peak 1992. The Novarupta-Katmai eruption of June 1912 (Hildreth and Fierstein, 2012), which has been found as a cryptotephra in Greenland ice cores (Coulter et al., 2012), the eruption of Redoubt from December 1989–April 1990 (Scott and McGimsey, 1994), and the Crater Peak eruption of June–September 1992 (McGimsey et al., 2001) were large eruptions that likely deposited ash within the study area (Fig. 2.2). These would be expected to be present as a near surface cryptotephra although they have not been reported to date.

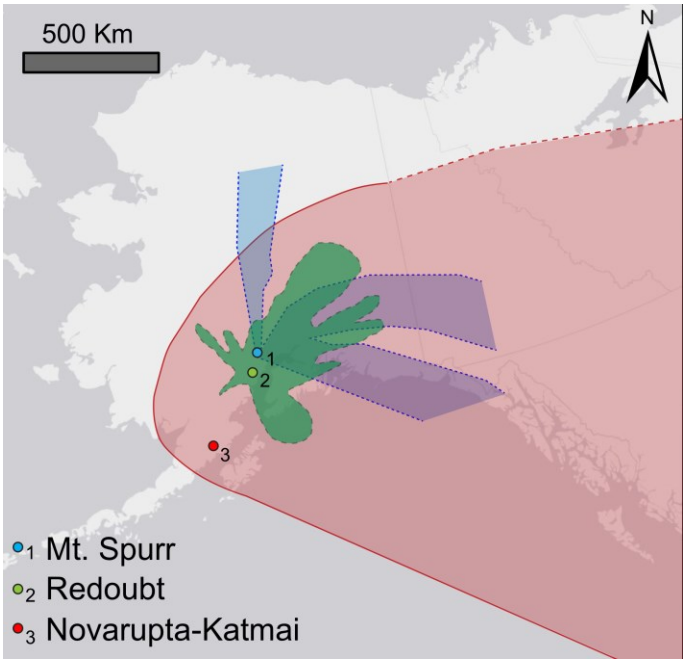

Figure 2.2 Location map showing approximate areas of tephra deposition from ash plumes generated from Novarupta-Katmai 1912 (red solid plume; Hildreth and Fierstein, 2012), Redoubt 1989–1990 (green horizontally-dashed plume; Scott and McGimsey, 1994), and Crater Peak 1992 (blue diagonally-dashed plume; McGimsey et al., 2001).

Yalcin et al. (2003) report four cryptotephra within an ice core from the Eclipse Icefield, St Elias Mountains: Novarupta-Katmai 1912 and Redoubt 1989–1990 from Alaska, Ksudach 1907 from Kamchatka, and Hekla 1947 from Iceland. Many of these cryptotephra have low numbers of shards analysed for geochemistry (fewer than 15 shards) giving limited scope for comparison; this is unfortunately common for analyses of cryptotephra preserved within ice cores. Additionally, the geochemical data were collected via energy dispersive spectroscopy (EDS) on a scanning electron microscope (SEM), which only produces semi-quantitative results.

Given that some of the eruptions they discuss have heterogeneous glass populations, averaged geochemical data values are not a reliable method of correlation. Data plots are preferable for exploring within-sample variation, and those included in Yalcin et al. (2003) only show average points for the reference samples, masking the known varied geochemical signatures of Katmai 1912 and Ksudach 1907, and fail to demonstrate a convincing correlation in the datasets. Figure 2.3 compares the average SEM-EDS results published for the four Eclipse events with major-element geochemical data for reference material generated at the University of Alberta (Table 2.2).

Tephra	UA#	SiO_2	TiO_2	Al_2O_3	FeO_t	MnO	MgO	CaO	Na_2O	K_2O	Cl	Total	H_2O_d	n
Novarupta-Katmai 1912	1364	76.65	0.27	12.64	1.69	0.06	0.27	1.32	3.93	2.99	0.19	100	1.67	113
		(2.81)	(0.17)	(0.91)	(0.82)	(0.03)	(0.27)	(0.86)	(0.21)	(0.27)	(0.03)	--	(1.03)	
Redoubt 1989-90	2754	77.87	0.29	12.25	0.98	0.04	0.15	0.89	3.84	3.61	0.09	100	2.24	24
		(0.83)	(0.06)	(0.60)	(0.13)	(0.02)	(0.06)	(0.25)	(0.28)	(0.33)	(0.04)	--	(0.63)	
Crater Peak 1992	2619	63.30	0.84	15.99	6.37	0.18	1.96	4.91	4.63	1.63	0.25	100	3.03	36
		(0.51)	(0.06)	(0.36)	(0.21)	(0.04)	(0.16)	(0.24)	(0.17)	(0.09)	(0.04)	--	(0.72)	

Table 2.2: Average major element glass composition of Novarupta-Katmai 1912, Redoubt 1989–1990, and Crater Peak 1992. Samples are from proximal sites within Alaska as detailed in Table 1. (#) = standard deviation; FeOt = total iron oxide as FeO; H_2Od = water by difference.

Average geochemical data presented for the Eclipse event samples have large standard deviations, particularly for SiO_2 and Fe_2O_3 for Eclipse event 31, suggested to correlate with Hekla 1947. Eclipse event 44 has no overlap with Ksudach 1907 EPMA data; Eclipse event 5 has almost no overlap with the SiO_2 range of Redoubt 1990; and Eclipse event 41 and Katmai 1912 reference data display a significant offset from one another with the alkalis. The reference data Yalcin et al. (2003) include is also unsuitable for comparison. Hekla 1947 data from Thorarinsson (1954) are most likely bulk analyses obtained using XRF as these data were published before EPMA techniques were first applied to tephra (Smith and Westgate, 1968).

The discovery of a tephra such as Hekla 1947 at this site requires particularly strong supporting evidence given that the transport pathway would be against dominant wind patterns and because it has not been discovered elsewhere west of Greenland and the North Atlantic. Additionally, comparisons of major- and minor-element geochemical data between rhyolitic AAAP and Icelandic tephra show significant overlap (Blockley et al., 2015).

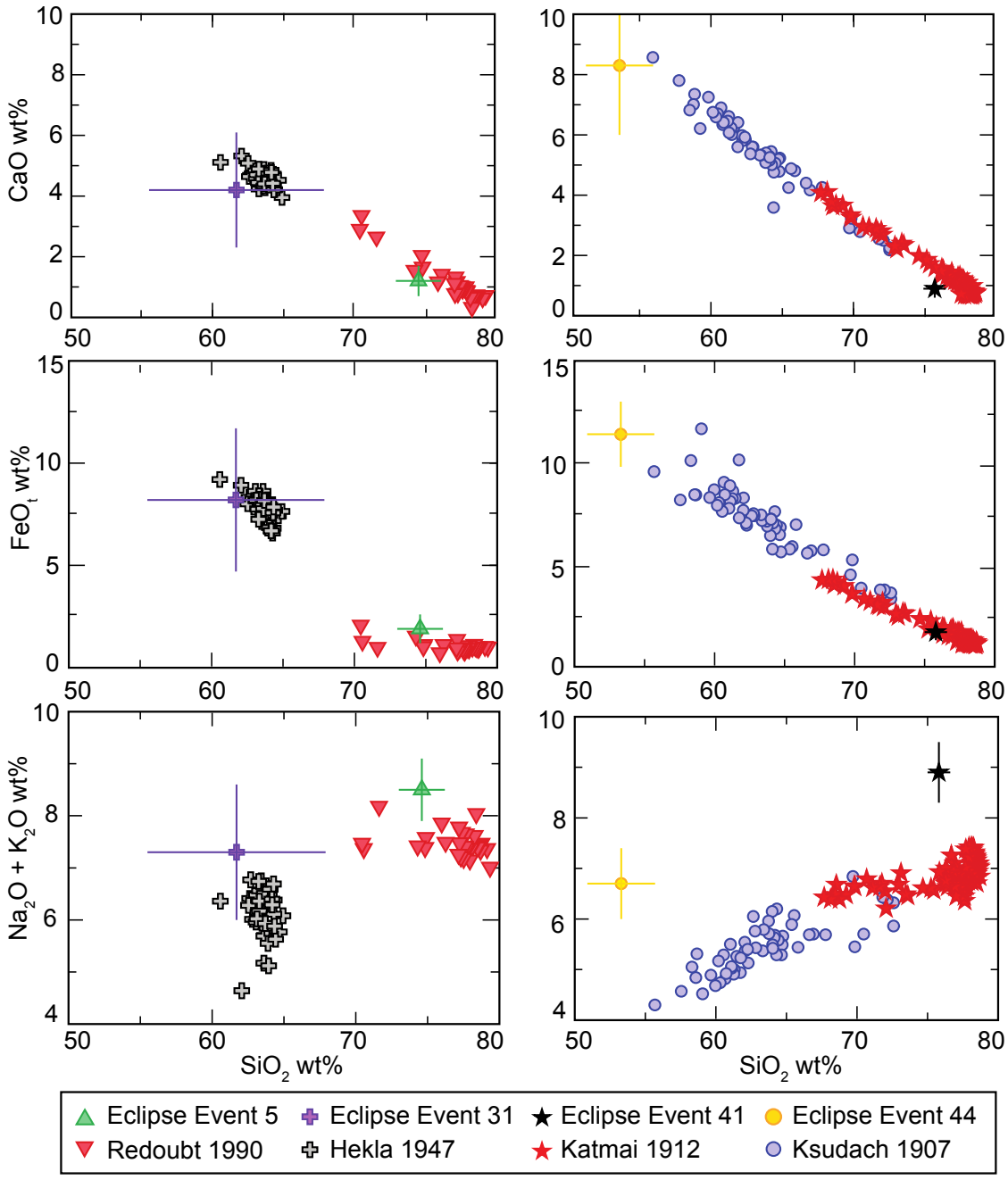

Figure 2.3 Major-element glass geochemical plots comparing averages and standard deviations for data published for Eclipse Event samples (Yalcin et al., 2003) with reference material from proximal sites within Alaska as detailed in Table 2.1. In the legend, each Eclipse Event is paired with the eruption Yalcin et al. (2003) suggest it correlates to.

In summary, while there is significant potential for the preservation of distal tephra from historical eruptions in eastern Beringia there are no published records confirming the presence of these tephra. Nonetheless, because Katmai has been reported in Greenland, and the distribution maps of Redoubt 1989–1990 and Crater Peak 1992 cover interior Alaska, major-element geochemical data are included here for future studies that may find these as cryptotephra in the area (Fig. 2.4; Table 2.2).

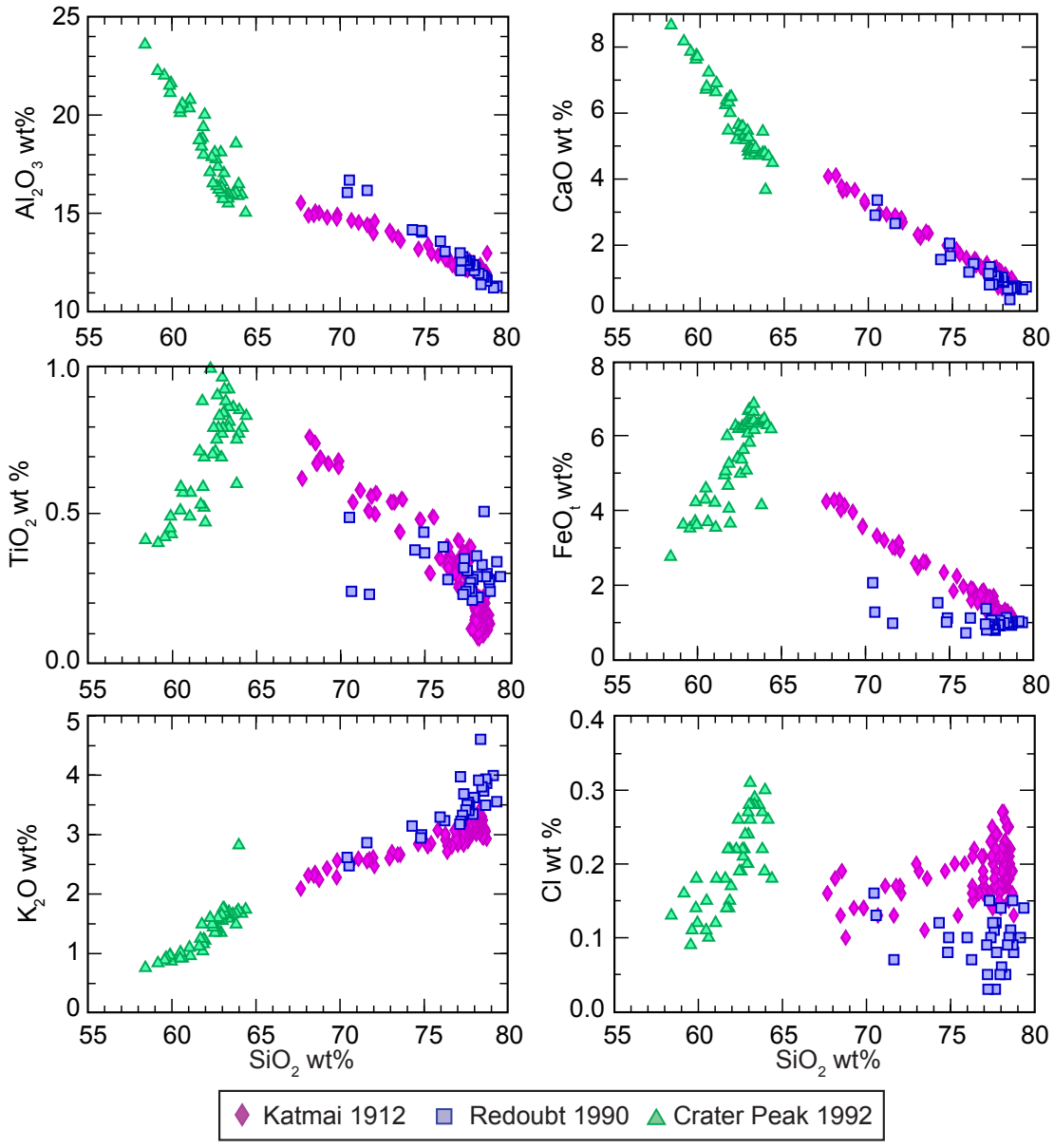

Figure 2.4 Major-element glass geochemical plots of Novarupta-Katmai 1912, Redoubt 1989–90, and Crater Peak 1992. Samples are from proximal sites within Alaska as detailed in Table 2.1.

2.4 Tephra with Limited Characterisation

This section discusses tephra that have been reported within the study area but only at one site, or in a localised area with limited chronological information. Ten tephra reported from Alaska are reviewed - four visible and six cryptotephra (Fig. 2.5; Table 2.3). Where dates have been published with the tephra we include modelled age estimates but with the caveat that without multiple constraining dates, these estimates represent a first approximation.

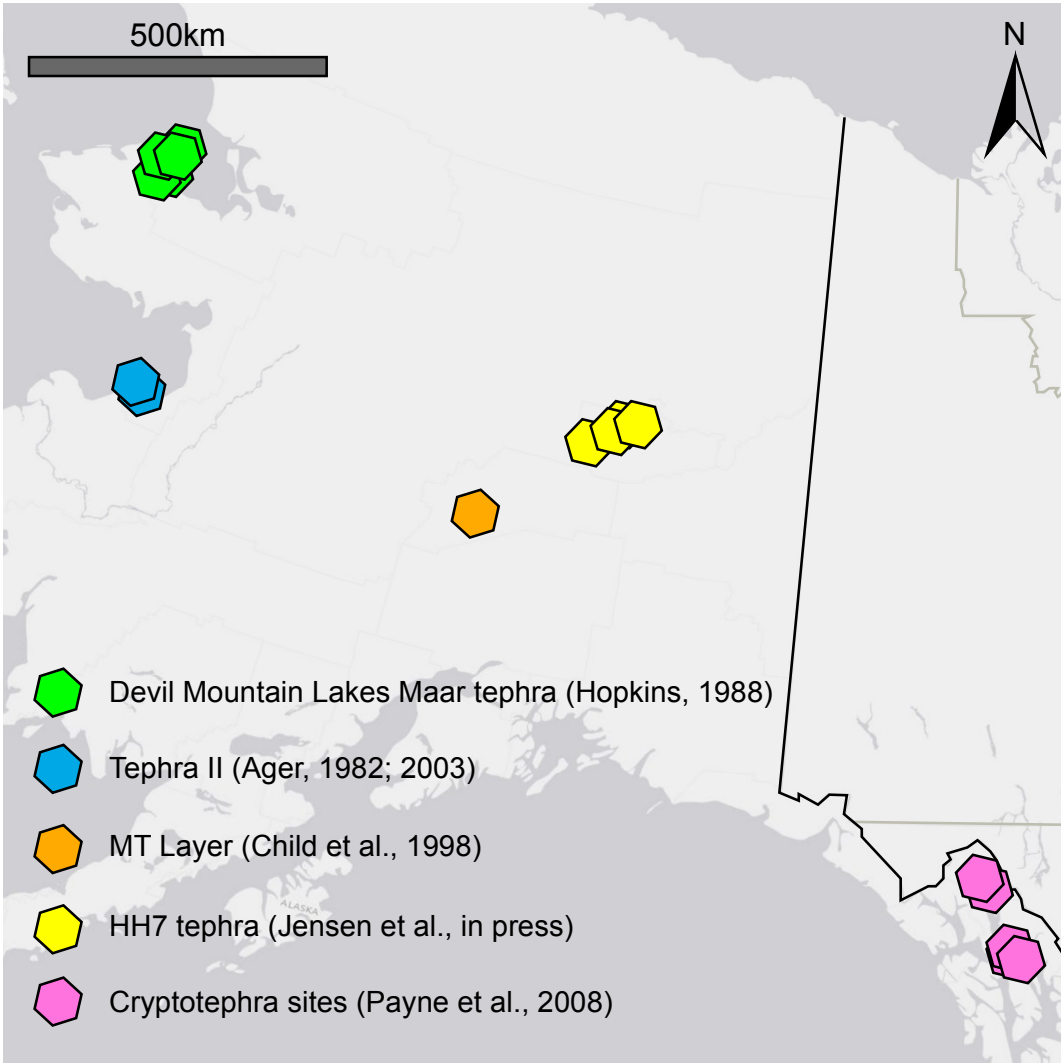

Figure 2.5 Location map showing sites where reported tephra have limited characterisation (i.e. are present only at one site or in a localized area).

Tephra	Location	Lab #[1]	Age estimate		IUGS (glass)	SiO_2	TiO_2	Al_2O_3	FeO_t	MnO	MgO	CaO	Na_2O	K_2O	Cl	Total	H_2O_d	n	Publication
HH7 pop. 1	Halfway House, 50km W of Fairbanks	UA 1451, 1877, 1901-1903, 1915	75cm above Dawson tephra	<29,055-29,470 cal yr BP[2]	Rhyolite	78.57	0.12	12.41	0.87	0.06	0.18	1.03	3.27	3.28	0.20	100	6.29	81	Jensen et al. (2016)
						(0.47)	(0.04)	(0.37)	(0.09)	(0.03)	(0.05)	(0.11)	(0.24)	(0.32)	(0.04)	--	(1.05)		
HH7 pop. 2					Rhyolite	76.79	0.14	13.47	1.04	0.06	0.28	1.68	3.83	2.56	0.15	100	4.59	25	
						(0.34)	(0.04)	(0.19)	(0.09)	(0.03)	(0.05)	(0.13)	(0.16)	(0.14)	(0.04)	--	(1.9)		
Chatanika	Chatanika River, 40km N of Fairbanks	UT 2178	14,510±450–14,760±850 ^{14}C yr BP[3]	16,595-19710 cal yr BP	Rhyolite	76.67	0.13	13.47	0.99	0.05	0.29	1.54	3.78	2.90	0.19	100	6.37	23	Péwé (1975)
						(0.72)	(0.04)	(0.67)	(0.15)	(0.03)	(0.13)	(0.31)	(0.32)	(0.52)	(0.08)	--	(1.81)		
Zagoskin Lake – II	Zagoskin Lake, St Michael Island	UA 2660	<14,970±170 ^{14}C yr BP[4]	<17,990-18,400 cal yr BP	Andesite	61.49	1.25	16.18	7.17	0.21	2.09	5.23	4.47	1.82	0.11	100	2.31	31	*This paper*; Ager (1982); Ager (2003)
						(0.78)	(0.05)	(0.35)	(0.34)	(0.03)	(0.24)	(0.38)	(0.17)	(0.12)	(0.01)	--	(0.78)		
Puyuk Lake – II	Puyuk Lake, St Michael Island	UA 2661	<15,610±220 ^{14}C yr BP[4]	<18,420-19,130 cal yr BP	Andesite	61.36	1.29	16.2	7.25	0.21	2.12	5.28	4.43	1.79	0.1	100	1.67	35	
						(1.08)	(0.07)	(0.37)	(0.41)	(0.04)	(0.27)	(0.39)	(0.15)	(0.16)	(0.02)	--	(1.03)		
Tephra D*	Arolik Lake, Ahklun Mountains	UA 1781	--	15,505±312 cal yr BP[5]	Andesite	61.34	1.24	16.38	7.1	0.18	2.28	5.18	4.47	1.75	0.12	100	1.86	16	Kaufman et al. (2012)
						(0.56)	(0.06)	(0.25)	(0.26)	(0.04)	(0.14)	(0.27)	(0.45)	(0.09)	(0.03)	--	(0.86)		
MT Layer (WL4C2)	Wonder Lake, Denali National Park	ACT 1080	<10,060±70 ^{14}C yr BP[6]	11,400-11,760 cal yr BP	Andesite	61.14	1.18	16.76	7.01	--	2.29	5.11	4.59	1.8	0.1	100	1.91	18	Child et al. (1998)
						(0.61)	(0.17)	(0.80)	(0.55)	--	(0.29)	(0.35)	(0.29)	(0.20)	(0.02)	--	(1.13)		
MT Layer (WL11B1 –74-75)		ACT 2079			Andesite	60.61	1.44	16.34	7.56	--	2.5	5.28	4.38	1.79	0.11	100	1.8	27	
						(0.56)	(0.23)	(0.71)	(0.32)	--	(0.13)	(0.24)	(0.20)	(0.15)	(0.02)	--	(2.12)		
MT Layer (WL 17A2-59)		ACT 2083			Andesite	60.72	1.54	16.71	7.31	--	2.28	4.84	4.74	1.77	0.09	100	2.37	20	
						(1.02)	(0.34)	(1.02)	(0.72)	--	(0.37)	(0.59)	(0.36)	(0.22)	(0.03)	--	(2.77)		
Crater Peak reference	Skilak Lake, Kenai Peninsula	SK-7-3-9	300±50[7]	--	Andesite	59.16	1.17	16.08	8.52	--	2.81	8.52	4.26	1.67	0.13	100	2.21	7	Beget et al. (1994)
						(1.35)	(0.08)	(0.13)	(0.67)	--	(0.33)	(0.67)	(0.15)	(0.14)	(0.06)	--	(1.09)		

Table 2.3: Average major element glass composition of tephra with limited characterisation, with reference material for proposed correlatives included for comparison where relevant. (#) = standard deviation; FeOt = total iron oxide as FeO; H_2O_d = water by difference. 1 UA = University of Alberta Tephrochronology Lab #; UT = University of Toronto Tephrochronology Lab #; ACT = Alaska Center for Tephrochronology Lab #. 2 Age estimate for Dawson, section 5.1. 3 Dates from Péwé (1975). 4 Bulk sediment dates believed to be contaminated with old carbon. 5 Average age from Kaufman et al. (2012). 6 One date provided from Child et al. (1998). 7 Age estimated in Beget et al. (1994) from sedimentation rate estimates and interpolation between historic tephras at the top of the cores and the 500-year-old Augustine tephra B found lower in the core.

Tephra	Location	Lab #[1]	Age estimate		IUGS (glass)	SiO_2	TiO_2	Al_2O_3	FeO_t	MnO	MgO	CaO	Na_2O	K_2O	Cl	Total	H_2O_d	n	Publication
MTR 190	Mt. Riley, SE Alaska panhandle	--	--	8660 cal yr BP[8]	Rhyolite	77.61	0.12	12.9	1.10	0.06	0.21	1.07	3.63	3.31	--	100	3.00	2	Payne et al. (2008)
						(2.22)	(0.01)	(1.25)	(0.11)	(0.04)	(0.12)	(0.42)	(0.03)	(0.26)	--	--	(0.90)		
MTR 146		--	--	6300 cal yr BP[8]	Rhyolite	75.89	0.21	13.69	1.41	0.05	0.33	1.67	3.61	3.15	--	100	2.92	18	
						(1.32)	(0.09)	(0.91)	(0.32)	(0.03)	(0.11)	(0.26)	(0.24)	(0.53)	--	--	(2.30)		
ECR 162	Eaglecrest Bog, SE Alaska panhandle	--	4485±30 ^{14}C yr BP	5030-5300 cal yr BP	Rhyolite	72.33	0.52	14.88	2.5	0.17	0.53	1.76	4.17	3.14	--	100	4.12	21	
						(0.38)	(0.08)	(0.17)	(0.09)	(0.03)	(0.04)	(0.10)	(0.31)	(0.08)	--	--	(1.19)		
ECR 100		--	--	2840 cal yr BP[8]	Rhyolite	78.77	0.41	11.65	1.51	0.06	0.25	1.63	3.71	2.1	--	100	4.79	2	
						(0.50)	(0.10)	(0.19)	(0.21)	(0.01)	(0.06)	(0.18)	(0.55)	(0.17)	--	--	(0.74)		
CHP 184	Chilkoot Pond, SE Alaska panhandle	--	>468±55 ^{14}C yr BP	410-570 cal yr BP	Rhyolite	75.64	0.15	14.03	1.22	0.05	0.25	1.60	3.62	3.45	--	100	2.61	12	
						(0.87)	(0.04)	(0.39)	(0.19)	(0.04)	(0.09)	(0.19)	(0.32)	(0.15)	--	--	(1.26)		
Lena	SE Alaska panhandle	CHP 33[9]	257±22 ^{14}C yr BP	285-310 cal yr BP	Rhyolite	75.24	0.18	14.21	1.39	0.05	0.33	1.78	3.51	3.32	--	100	4.57	29	
						(0.91)	(0.06)	(0.42)	(0.23)	(0.04)	(0.10)	(0.21)	(0.61)	(0.19)	--	--	(1.25)		

Table 2.3: Average major element glass composition of tephra with limited characterisation, with reference material for proposed correlatives included for comparison where relevant. (#) = standard deviation; FeOt = total iron oxide as FeO; H_2O_d = water by difference. 1 UA = University of Alberta Tephrochronology Lab #; UT = University of Toronto Tephrochronology Lab #; ACT = Alaska Center for Tephrochronology Lab #. 8 Ages interpolated from age-depth models produced for each core. 9 Date produced from one site (Chilkoot Pond), stratigraphically correlated with other Lena tephra but not geochemically analysed.

2.4.1. Devil Mountain Lakes Maar tephra

The oldest of the visible tephra discussed here is the Devil Mountain Lakes Maar tephra, northern Seward Peninsula (Fig. 2.5). The tephra is estimated to cover an area of ~ 2500 km^2 (Höfle et al. 2000), and has maximum age constraints produced from radiocarbon dating of a buried land-surface beneath the tephra deposit (Table S2.5). The area is described as containing four maar lakes, the shield volcano Devil Mountain, and multiple associated cinder cones and other volcanic structures (Goetchaus and Birks, 2001). Despite this being a complicated volcanic landscape, the tephra is identified as the product of one complex eruptive episode of the youngest of the maar vents by Begét et al. (1996). This interpretation is based on the existence of a single tephra at numerous sites around the maar, the similarity of the radiocarbon dates produced from beneath the tephra, and the absence of any significant stratigraphic breaks in either the distal ash or the proximal sequence. Höfle et al. (2000) report the plume direction to the north and west as indicated by the thickest cover of tephra, which is greater than 1 m at many sites. The tephra is described as having a texture of sandy loam to gravel sized pumice, although it is not specified if this variation occurs at one location or with varying distance from the source (Höfle and Ping, 1996). While there are no published geochemical data associated with this tephra, it is reported as basaltic (Begét and Mann, 1992).

Eighteen published dates were deemed robust (Table S2.5) and used as input for a Bayesian *Tau_Boundary* model that produced an age estimate of 20,115–20,740 cal yr BP (Fig. 2.6a). One date from Spiker et al. (1978; W-2806) is reported in Hopkins (1988) as overlying the tephra. This date provides an additional constraint on the model although it is unclear how it relates to the tephra stratigraphically. Its inclusion does not significantly affect the modelled age range, causing less than 10 years variation.

2.4.2. HH7 tephra

The HH7 tephra (Fig. 5) was first identified at Halfway House, a late-middle Pleistocene to Holocene loess deposit approximately 50 km west of Fairbanks, Alaska, and is also present at several other sites in and around Fairbanks (Jensen et al., 2016). HH7 is generally found within a few metres of the surface in loess deposits as a semi-continuous bed that is rarely more than 1 cm thick. Its presence across this area suggests that this tephra is widely dispersed. Glass from the HH7 tephra is rhyolitic and bimodal with two main geochemical populations ranging from 76

to 77.5 and 78 to 80 SiO_2 wt% (Jensen et al., 2016; Table 2.3). Glass morphology is predominantly thick-walled pumice and shards often contain microlites and phenocrysts (Table S1).

There are no radiocarbon dates directly associated with HH7, but it is present at the Gold Hill III locality (details in Preece et al., 1999 and Evans et al., 2011) ~75 cm above Dawson tephra (ca. 30 cal ka BP, discussed in detail in section 5.1). It is also below a magnetic susceptibility high at Halfway House and Gold Hill IV that most likely represents the last glacial maximum, which in the central Alaska Range is estimated around 16 ka (Dortch et al., 2010; Jensen et al., 2016). Based on striking similarity in stratigraphic context and glass morphology and mineralogy, the HH7 may correlate to the Chatanika tephra, first described by Péwé (1975). The little remaining material from the original sample of Chatanika tephra, however, has precluded fully testing this correlation. There are two radiocarbon dates bracketing the Chatanika tephra from a ground squirrel nest ~2 m below the tephra and on coprolites extracted from another nest ~1.5 m above the tephra (Péwé 1975; Table S2.5). Figure 2.6b shows a modeled eruption age estimate of 16,595–19,710 cal yr BP for the Chatanika tephra based on these two dates. Although this range is broad, it is consistent with HH7 stratigraphy.

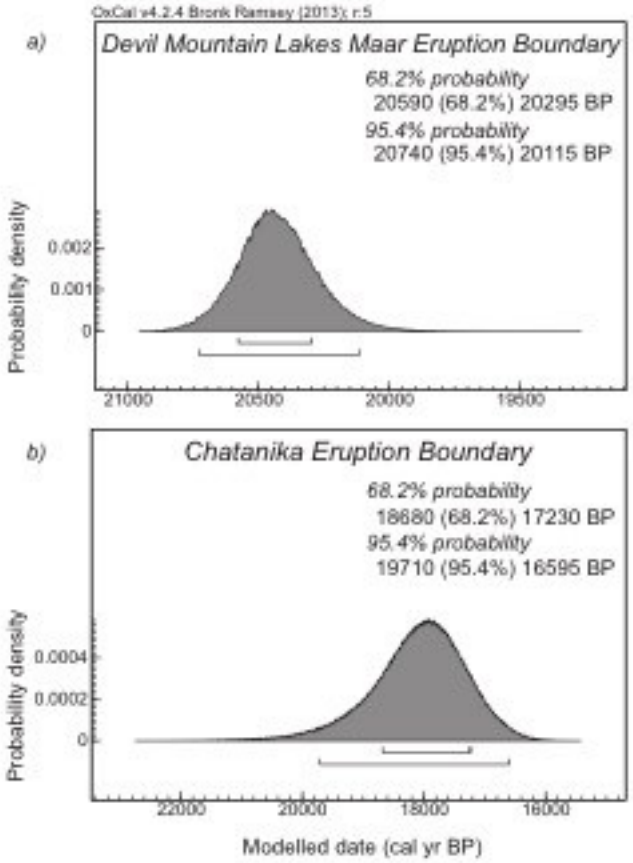

Figure 2.6 Bayesian *Tau_Boundary* probability density function plots derived using OxCal v4.2.4 and IntCal13 for the ages of a) the Devil Mountain Lakes Maar eruption; b) the Chatanika eruption.

2.4.3. Tephra II, Zagoskin and Puyuk Lake (Tephra D)

Ager (1982, 2003) reports a 5 cm thick grey tephra near the base of cores taken from Puyak and Zagoskin Lakes on St Michael Island (Fig. 2.5) in western Alaska. Although no geochemical data were published with the original reports, they were analysed but did not match any known tephra at the time (Ager, 2003; pers. comm.). The original samples from both locations have been analysed here and new data are shown in Figure 2.7 and Table 2.3, along with analyses for a younger tephra from Zagoskin Lake that is correlated to the mid-late Holocene caldera-forming eruption (CFE II) of Aniakchak volcano (Riehle et al., 1987; UA 1602 – see Table 4 for details). The basal tephra present in both Zagoskin and Puyak lakes are correlative, have a glass morphology predominantly comprised of highly vesicular pumice shards, and are andesitic in composition. They also correlate with Tephra D from the Ahklun Mountains (Kaufman et al., 2012), and hence shall be referred to as such (Fig. 7). This indicates Tephra D is distributed well beyond southwestern Alaska. The zones outlined on Figure 7 show the geochemical range of major element data produced from whole rock samples of Aniakchak CFE I and II (Bacon et al., 2014). Although these data are not directly comparable to EPMA glass data due to the incorporation of minerals, it does show that the relations between Tephra D and Aniakchak CFE II glass data (UA 1602) mirror that between the whole rock CFE I and II data for multiple elements. The offset seen for wt% FeOt and SiO_2 are as expected given from the presence of common phenocryst phases (e.g. plagioclase). This suggests that Tephra D may also be sourced from Aniakchak.

Tephra D is given a maximum age of 15,610±220 ^{14}C yr BP at Puyuk Lake, and a minimum age of 14,970±170 ^{14}C yr BP at Zagoskin Lake, although these radiocarbon dates are likely to be older than expected as they are bulk sediment dates (Ager, 2003; pers. comm.) Tephra D has a mean age of 15,505±312 cal yr BP from two sites (Kaufman et al., 2012) and this is believed to be a more reliable estimate for the tephra as the constraining dates are produced from plant macrofossils. These ages do not support a correlation between Tephra D and Aniakchak CFE I, which has a suggested maximum age from VanderHoek and Myron (2004) of 9470±40 ^{14}C yr BP. The apparent geochemical associations do, however, suggest that Tephra D may originate from an earlier eruption of Aniakchak that has not been reported from the proximal records. This is potentially due to glacial erosion of pre-Holocene deposits surrounding the Aniakchak volcano.

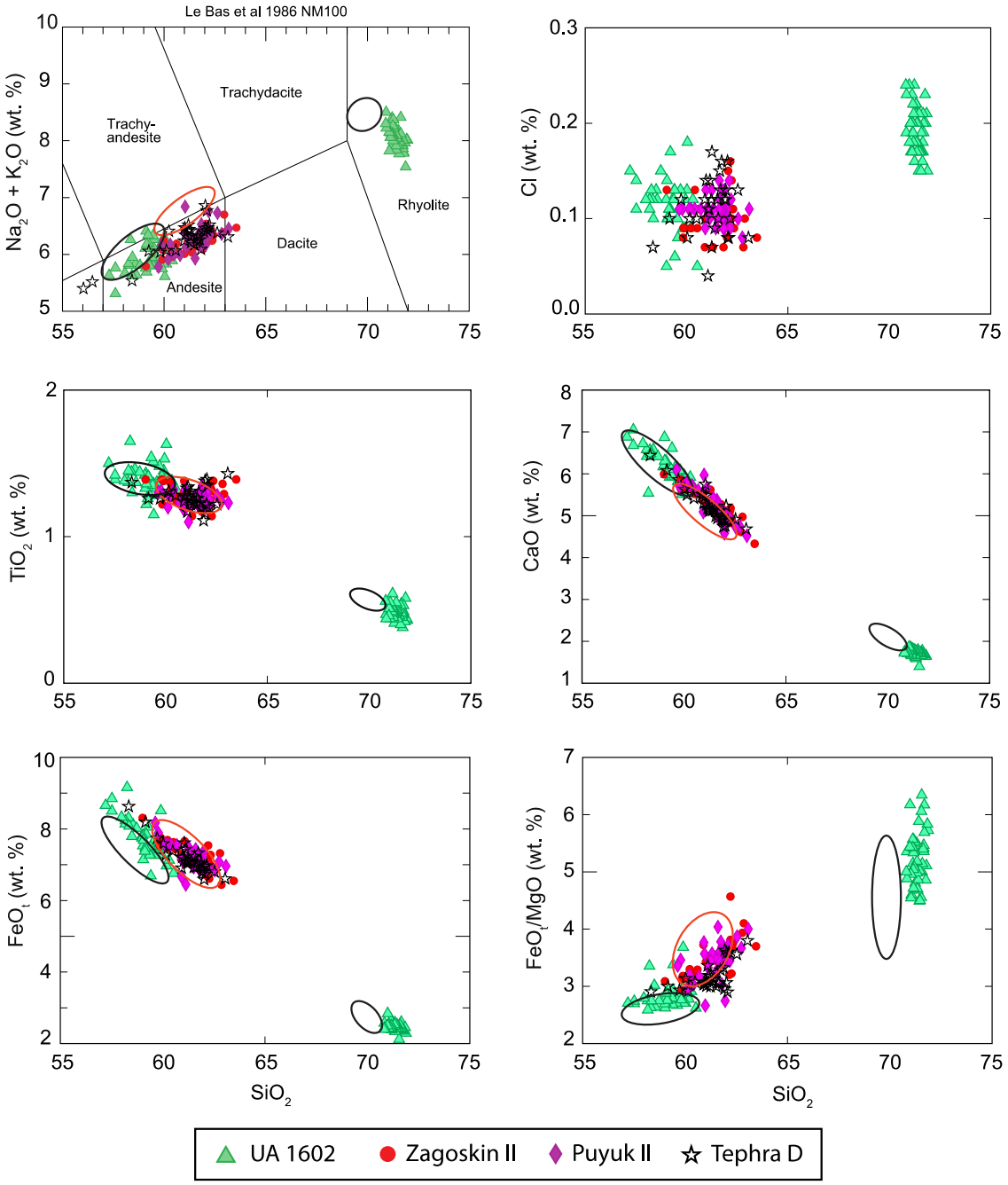

Figure 2.7 Major-element glass geochemical plots of Tephra II samples from Zagoskin and Puyuk lakes, St Michael Island. Data for Aniakchak CFE II (Zagoskin Lake; UA 1602) and Tephra D from Kaufman et al. (2012) are included for comparison. Fields indicate compositional ranges describing whole rock geochemical data of Aniakchak CFE I (orange dashed line) and bimodal Aniakchak CFE II products (black solid line) from Bacon et al., (2014).

2.4.4. MT Layer, Wonder Lake

Child et al. (1998) report a 4–6 cm thick mafic tephra from Wonder Lake (Fig. 2.5), central Alaska, described as a dense, chocolate brown, silt-sized deposit that is best preserved in the shallow ends of the lake and largely absent in the deeper central basin. It is suggested that the ash-fall occurred in winter and that the uneven preservation is a result of the lake surface being at least partially frozen over. Average major-element geochemical data are published for samples from three coring locations (WL 8, 11, and 17; Table 2.3), and it was tentatively correlated to tephra from Crater Peak, located ~250km south of the lake. However, the data averages are also similar to Tephra D and Aniakchak (Fig. 2.8), and hence the correlation based on averages alone is not clear.

A maximum age of 10,060±70 ^{14}C yr BP was published from a wood fragment preserved within clay underlying the tephra in one core (WL 18; Child et al., 1998), and no further dates were produced from the other coring locations. A tephra of this age or geochemical signature has not been reported at any other sites in the area or proximally at Mt. Spurr, but given the geochemical similarities with Aniakchak CFE I this is a possible correlation. The maximum age constraints for the MT Layer and Aniakchak CFE I (<9470±40 ^{14}C yr BP; VanderHoek and Myron, 2004) are similar, although neither tephra is well constrained.

2.4.5. Cryptotephra records

Payne et al. (2008) report six new rhyolitic cryptotephra from peatland sites (Point Lena, Spaulding Meadows, Eaglecrest Bog, Mount Riley, and Chilkoot Pond) in south-eastern Alaska (Fig. 2.5). Technically this is outside of the study area of this review, but these layers are included given the paucity of cryptotephra reported elsewhere in Alaska and Yukon. An additional bed correlated with the WRAe (Lena 100) is discussed in section 5.5.2. Glass shard concentrations are not reported, but it is indicated that the identified beds were associated with "maximum glass concentrations" in the cores. They include major-element geochemical data collected by EPMA for six new tephra, but do not publish secondary standard data that was measured throughout the run using an andradite garnet sample. The ages of the cryptotephra were estimated from radiocarbon dating of both plant macrofossils and bulk peat samples (Table 2.3).

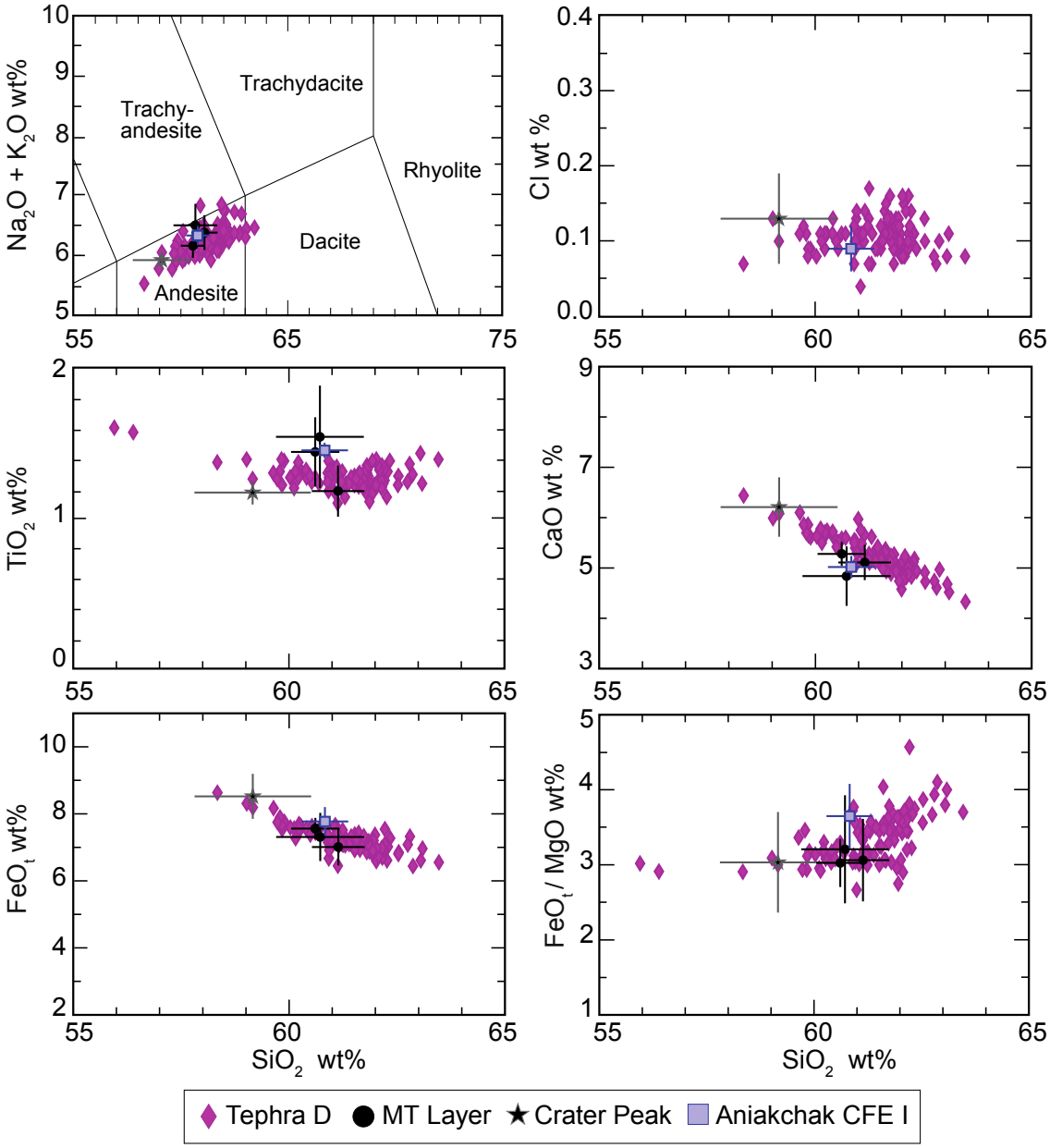

Figure 2.8 Average major-element glass geochemical plots of MT Layer samples from Wonder lakes (Child et al., 1998). Average data for Crater Peak (Beget et al., 1994) and Aniakchak CFE I (Wallace and McGimsey, unpublished), and point data for Tephra D (this paper; Kaufman et al., 2012) are included for comparison.

Three tephra were directly radiocarbon dated, while the remaining three have ages determined from age-depth models using linear interpolation between ages calibrated with OxCal v.3.10 (Bronk Ramsey, 2005). The geochemistry of these beds is reported as similar to several volcanic centres in the area (Mt. Churchill, Aniakchak, Augustine, and Redoubt), but the age estimates do not match previously reported eruptions (Table 2.3).

Three of the cryptotephra are reported with geochemistry similar to Mt. Churchill: Lena, CHP 184, and MTR 146. The Lena tephra is reported at all five sites, occurring within the top 25–40 cm of the core sequences and dated to ~300 cal yr BP at Chilkoot Pond. CHP 184 is present at only Chilkoot Pond but is reported as having uncertain age control due to unusual peat accumulation patterns. It is unknown if it dates to ~500 cal yr BP, as suggested from the radiocarbon minimum age, or is significantly older because this depth of peat typically represents several thousand years at their other sites. MTR 146 has an interpolated age of ~6300 cal yr BP and is a separate event reported only from Mt Riley - this represents an older eruption, likely from Mt. Churchill.

Two tentative correlations with Augustine and Redoubt are made for ECR 100 (2840 cal yr BP) and MTR 190 (8660 cal yr BP) respectively based on major-element geochemistry, but only two points comprise each data set. While this allows a general comparison with other datasets to be made, it results in low confidence for correlation.

The final cryptotephra, ECR 162, is reported only at Eaglecrest Ridge, and is the most geochemically distinct of those reported. It has an age estimate of 5030–5300 cal yr BP, which is similar to that reported for caldera formation at Black Peak (Miller and Smith, 1987), but the geochemistry is significantly different (Fig. 2.9). Payne et al. (2008) suggested that Aniakchak is a more likely correlative, although there are no known eruptions from that time. ECR 162 geochemistry is similar to Aniakchak CFE II (Fig. 2.9), but has higher SiO_2 and K_2O wt%, and lower Na_2O and Al_2O_3 wt%. ECR 162 also does not correlate with other tephra reported in Kaufman et al. (2012) that predate Aniakchak CFE II, including the 4.7 ka and 5.8 ka tephra from Lone Spruce, and the 5.3 ka tephra from Sunday Pond (Fig. 2.9). As the data compared in Figure 9 are produced from different labs, there are no published secondary standard data associated with the ECR 162 analyses, and a reference sample of Aniakchak tephra was not analysed concurrently, it is not possible to conclude if these differences are an artefact of

different analytical conditions. Therefore, there is insufficient evidence to confidently correlate ECR 162 with any particular source or eruption characterised to date.

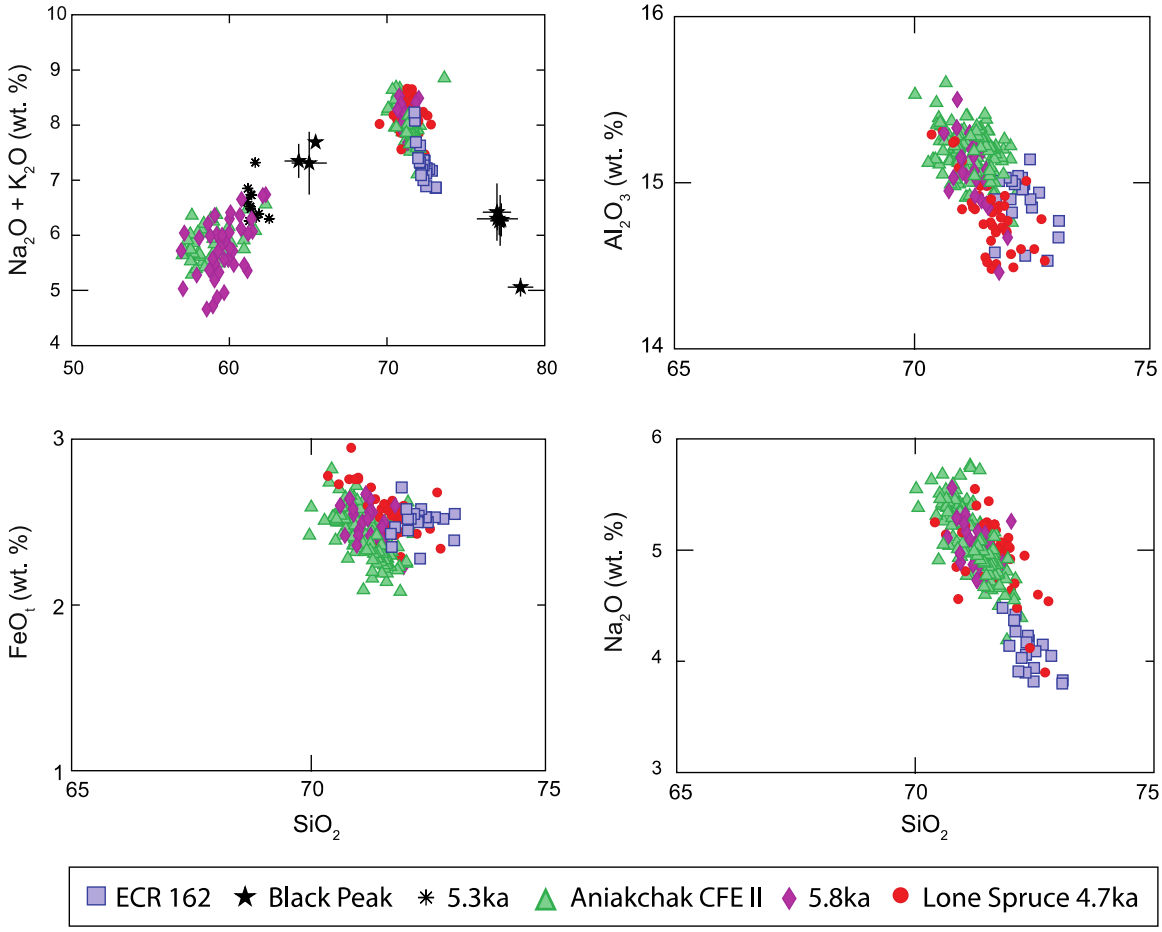

Figure 2.9 Major element glass geochemical plots of ECR 162 tephra (Payne et al., 2008) with reference material from Black Peak (Wallace and McGimsey, unpublished), Aniakchak CFE II, and the 4.7ka, 5.3ka, and 5.8ka tephra (Kaufman et al., 2012) for comparison.

2.5 Widely Distributed and Well-Characterised Tephra

Within the study area, there are six tephra (or tephra sets) that have correlations within and beyond eastern Beringia (Fig. 2.10; Table 2.4). Each tephra is considered in turn, with a focus on its geographic distribution, geochemical characteristics, and best age estimate.

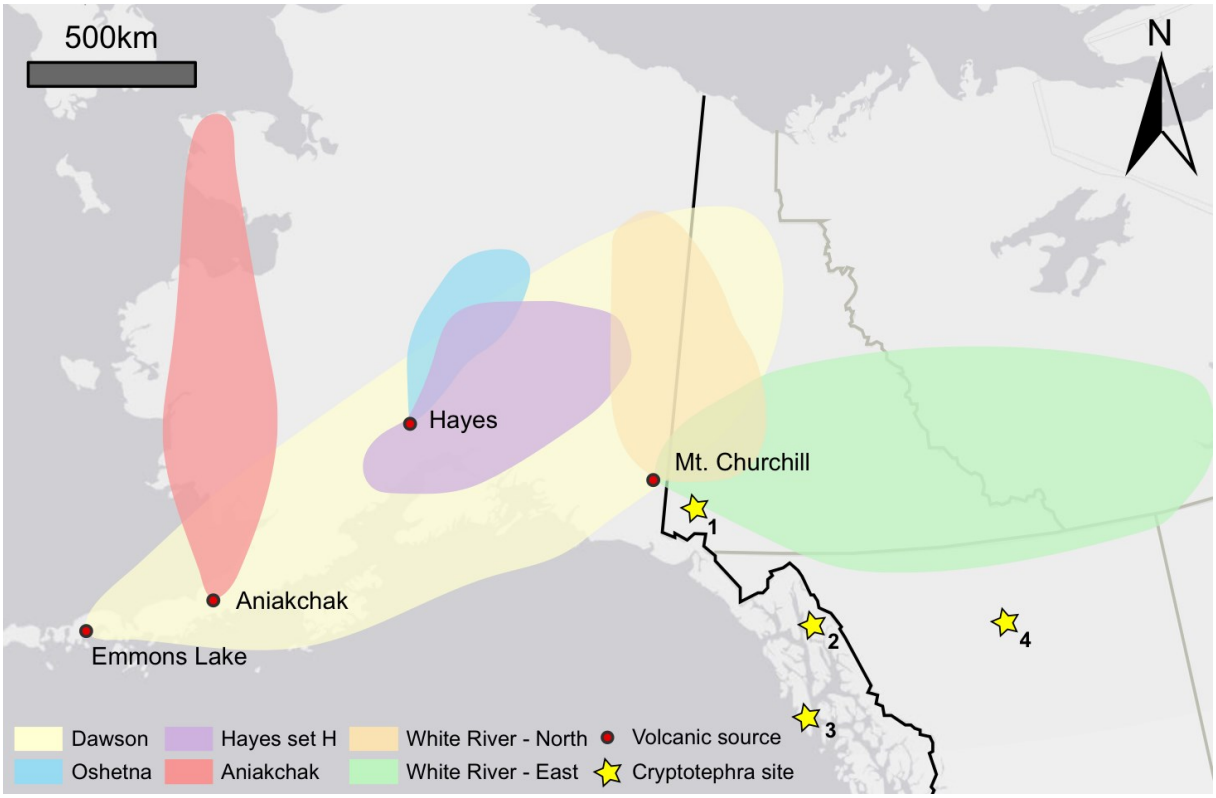

Figure 2.10 Location map showing approximate geographical distributions for tephra layers which are widely distributed within the study area. Volcanic sources attributed to each tephra layer are labelled with circle symbols.

Tephra	Location	Lab #	Age estimate	IUGS (glass)	SiO_2	TiO_2	Al_2O_3	FeO_t	MnO	MgO	CaO	Na_2O	K_2O	Cl	Total	H_2O_d	n	Reference
Dawson	Klondike Goldfields, Yukon Territory	UA 1000	29,055-29,470 cal BP	Rhyolite	74.21	0.27	13.67	2.04	0.07	0.22	1.26	4.43	3.63	0.22	100	2.14	439	Preece et al. (2011a,b)
					(0.27)	(0.08)	(0.15)	(0.09)	(0.04)	(0.03)	(0.07)	(0.18)	(0.11)	(0.03)	--	(1.48)		
Oshetna (SP16B-67 popn. 1)	Wonder Lake, Denali National Park	ACT 1082	6785-6880 cal BP[a] 6555-6895 cal BP[b]	Rhyolite	72.54	0.49	14.35	2.31	--	0.71	2.41	4.19	2.77	0.21	100	4.84	17	Child et al. (1998)
					(0.46)	(0.11)	(0.34)	(0.25)	--	(0.13)	(0.28)	(0.25)	(0.08)	(0.04)	--	(2.39)		
Oshetna (SP16B-67 popn. 2)				Rhyodacite	69.77	0.54	15.85	2.88	--	0.91	3.1	4.29	2.45	0.22	100	3.24	9	Child et al. (1998)
					(0.66)	(0.15)	(0.93)	(0.51)	--	(0.23)	(0.43)	(0.32)	(0.23)	(0.04)	--	(2.23)		
Oshetna (WL8B1-36)		ACT 1076		Rhyodacite	72.71	0.39	14.91	2.19	--	0.64	2.26	4.05	2.66	0.2	100	4.2	17	Child et al. (1998)
					(1.93)	(0.12)	(1.43)	(0.75)	--	(0.57)	(0.54)	(0.68)	(0.37)	(0.07)	--	(2.95)		
Oshetna (WL9B2-31)		ACT 1073		Rhyolite	72.81	0.32	14.85	2.17	--	0.56	2.35	4.06	2.82	0.2	100	3.21	8	Child et al. (1998)
					(0.37)	(0.15)	(0.38)	(0.46)	--	(0.24)	(0.08)	(0.38)	(0.28)	(0.09)	--	(1.17)		
Oshetna (WL11A2-20)		ACT 1078		Rhyolite	72.4	0.41	14.62	2.36	--	0.63	2.26	4.38	2.73	0.21	100	1.62	10	Child et al. (1998)
					(0.6)	(0.06)	(0.34)	(0.25)	--	(0.07)	(0.13)	(0.15)	(0.06)	(0.05)	--	(0.24)		
Ref. Oshetna	Suisitna Valley	nd		Rhyodacite	72.55	0.43	14.63	2.29	--	0.66	2.31	4.2	2.72	0.21	100	2.21	22	Beget, unpublished
					(1.00)	(0.10)	(0.70)	(0.42)	--	(0.26)	(0.32)	(0.36)	(0.17)	(0.05)	--	(1.09)		
Hayes set H - tephra F2	Hayes River Valley	AT 2561	3910-4205 cal BP	Rhyolite	74.14	0.21	14.49	1.51	0.09	0.47	2.12	3.93	2.66	0.33	100	2.76	29	Wallace et al. (2014)
					(0.46)	(0.05)	(0.20)	(0.10)	(0.04)	(0.04)	(0.11)	(0.17)	(0.08)	(0.04)	--	(1.39)		
Aniakchak CFE II (pop. 1)	Zagoskin Lake, St Michael Island	UA 1602	3570-3605 cal BP[a] 3390-3550 cal BP[b]	Andesite	59.21	1.35	16.63	7.51	0.22	2.76	6.20	4.42	1.59	0.12	100	2.60	16	Kaufman et al. (2012)
					(1.77)	(0.09)	(0.23)	(0.97)	(0.03)	(0.39)	(0.81)	(0.39)	(0.21)	(0.04)	--	(1.4)		
Aniakchak CFE II (pop. 2)	Zagoskin Lake, St Michael Island	UA 1602		Rhyolite	71.15	0.49	15.24	2.48	0.14	0.51	1.75	5.13	2.95	0.19	100	2.32	43	Kaufman et al. (2012)
					(0.27)	(0.04)	(0.14)	(0.10)	(0.03)	(0.03)	(0.09)	(0.28)	(0.10)	(0.03)	--	(1.92)		
WRAn	40-mile, Yukon Territory	UA 1046	1605-1805 cal BP	Rhyolite	73.02	0.22	14.83	1.72	0.06	0.37	2.17	4.19	3.09	0.33	100.00	2.17	32	This study
					(1.35)	(0.07)	(0.62)	(0.32)	(0.02)	(0.11)	(0.36)	(0.37)	(0.15)	(0.05)	--	(0.92)		
WRAe	N. Klondike Highway, 20km N of Carmacks	UA 1119	1100-1110 cal BP[a] 1095-1170 cal BP[b]	Rhyolite	73.65	0.19	14.34	1.60	0.07	0.38	1.91	4.31	3.21	0.34	100	2.91	79	Jensen et al. (2014a)
					(0.97)	(0.12)	(0.63)	(0.33)	(0.20)	(0.22)	(0.30)	(0.31)	(0.36)	(0.08)	--	(1.73)		

Table 2.4: Description of well-characterised tephra, with reference material for proposed correlatives included for comparison where relevant: age estimate, location, and average major element glass composition. (#) = standard deviation; FeOt = total iron oxide as FeO; H2Od = water by difference. a Including, and b excluding, dates associated directly with the tephra model boundary (i.e. from within the tephra; ice core ages)

2.5.1. Dawson tephra

The oldest tephra discussed here is the Dawson tephra, an important chronostratigraphic marker bed that has been widely documented in the Yukon (e.g. Naeser et al., 1982; Westgate et al., 2000; Froese et al., 2002, 2006; Sanborn et al. 2006; Demuro et al., 2008). The Dawson tephra represents the most prominent tephra in the Klondike, Yukon Territory (Froese et al., 2002), and while it is generally poorly represented in Alaska, it has been reported in marine cores from the Gulf of Alaska (Begét et al., 2004, 2005; Jensen et al., 2013) and is present as a thin and discontinuous layer at Halfway House and Gold Hill, near Fairbanks (Jensen et al., 2016). Emmons Lake Volcanic Center has been identified as its source, and the eruption is one of at least two rhyolitic caldera-forming eruptions in the late Quaternary, with an estimated eruptive volume of >50 km^3 (Mangan et al., 2003). Figure 2.10 shows its probable minimum distribution.

Dawson tephra glass is rhyolitic with an average SiO_2 content of ~74 wt%; glass morphology consists mainly of thin, bubble-wall shards with a minor mineral component (Table S2.1). Major element data for this well characterised tephra are summarised in Table 2.4 (and detailed in Table S2.2). Within the Klondike region the primary thickness was estimated as more than 15 cm (Westgate et al., 2000; Froese et al., 2002) based on a wide range of documented thicknesses (15–>100 cm; Fig. 2.11). Froese et al. (2006) suggest that it was deposited during late winter or spring based on its interbedding with surface icings preserved at a site in the Klondike, Yukon and further suggest this may have lessened its environmental impact by falling on snow.

Figure 2.11 Image of DT at Sulphur Creek, Klondike Goldfields, Yukon Territory.

A fission-track date of less than 52 ka represents the first age associated with the Dawson tephra (Naeser et al., 1982); since then a total of twenty independent radiocarbon and luminescence dates have been published bracketing the eruption. Of these dates, thirteen were used in our Bayesian model (Tables S2.5–S2.6). Dawson tephra is unique here, having been dated by methods other than ^{14}C (Naeser et al., 1982; Demuro et al., 2008). Our Bayesian *Tau_Boundary* model combines the ^{14}C, OSL and fission-track dates to give an age estimate of 29,055–29,470 cal yr BP (Fig. 2.12a) for the eruption, which is in agreement with the ages suggested by Froese et al. (2006), but is slightly younger than the Bayesian estimate of Demuro et al. (2008).

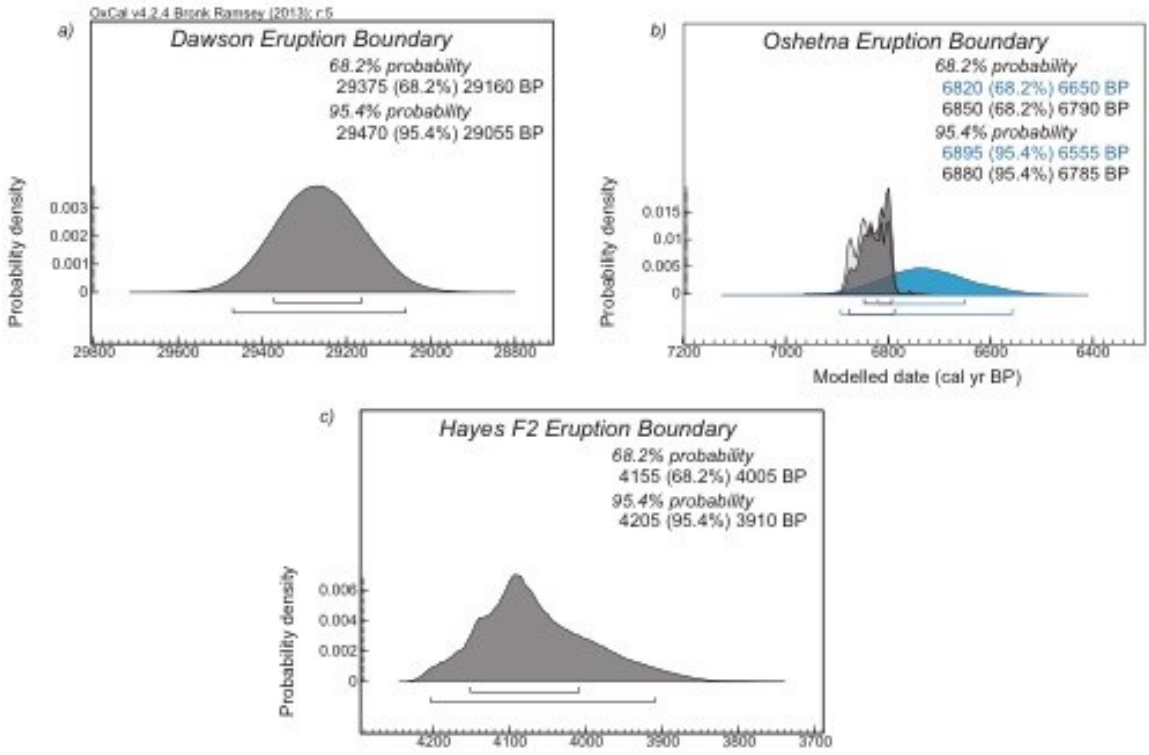

Figure 2.12 Bayesian *Tau_Boundary* probability density function plot derived using OxCal v4.2.4 and IntCal13 for the ages of a) the Dawson tephra; b) the Oshetna tephra using all dates (black) and excluding the ^{14}C date reported from within the tephra (blue); c) Hayes F2 tephra.

2.5.2. Oshetna tephra

The Oshetna tephra has been reported at several sites within central Alaska, particularly in association with archaeological sites in the Susitna valley (e.g. Dixon, 1985). While its source was not identified, it has recently been suggested that it may originate from the Hayes volcano (Wallace et al., 2014). Figure 2.10 shows reported locations nominally attributed to the Oshetna

tephra (based mostly on stratigraphic context) with a likely minimum distribution using Hayes as a source. The actual distribution may be more complicated - Oshetna tephra geochemistry has not been fully characterised in the literature due to low glass-shard content. Mulliken (2016) identifies at least four geochemical groups in EPMA glass data from previously defined Oshetna tephra deposits in the middle Susitna River Valley, with average values ranging from 64 to 76 SiO_2 wt%. It is therefore unclear if the Oshetna tephra actually represents one single eruption.

Most papers reporting the Oshetna tephra are archaeological or palynological records that generally correlate tephra at their sites to Oshetna by stratigraphy and not geochemistry. Without the geochemical data, it is unclear if these tephra actually represent the same deposit. Overall there is a lack of published data on the Oshetna tephra, limited to average major-element geochemical data for five Oshetna tephra samples in Child et al. (1998) (Table 2.4). These data are produced from four samples from Wonder Lake cores (FT-2, the middle of the three identified tephra), and one reference sample from the Susitna valley (Begét, unpublished). There is coherence between the sample averages (excluding pop. 2 of ACT 1082), although the glass hydration values and standard deviations are high. ACT 1078 has a particularly high SiO_2 wt% standard deviation; these data would be better compared using plots of individual point data rather than the averages.

Nine of the seventeen radiocarbon dates published in association with the Oshetna tephra meet our model criteria (Table S2.5). Eight of these bracket the deposits, with a single date produced from within a tephra layer (Lynch et al., 2002). Our Bayesian *Tau_Boundary* model produces an age estimate of 6785–6880 cal yr BP that fits closely with previously published ages, however if the date from within the tephra is not included then the range tends towards a slightly younger estimate of 6555–6895 cal yr BP (Fig. 2.12b).

2.5.3. Hayes Tephra Set H

Hayes volcano is the northern-most active volcano in the Alaskan Peninsula, although the limited exposure of volcanic deposits at the source has led to little being known about the volcano's eruptive history. The best understood eruptive period of Hayes is defined by Hayes tephra set H, a middle Holocene set of seven to eight tephra layers originally described by Riehle (1985) at a proximal locality known as site 23. Tephra comprising set H have been reported as widely dispersed in southern and central Alaska (Fig. 2.10). In addition to set H, Hayes is considered the

source for the late-middle Holocene Devil tephra and Watana tephra layers of the middle Susitna valley (Dilley, 1988; Dixon and Smith, 1990; Mulliken, 2016). As previously mentioned, it has been argued recently that the Oshetna tephra may also originate from Hayes (Wallace et al., 2014).

Set H is thought to represent a complicated eruptive period of Hayes volcano that displays variations in glass geochemistry and dispersal patterns through the set. This is likely the result of a series of eruptions occurring over a span of several hundred years. Previous publications uniquely named each distal tephra attributed to Hayes: the Jarvis Ash Bed (Péwé, 1975), Tangle Lakes ash (Begét et al., 1991), and Cantwell Ash Bed (Bowers, 1979), each with overlapping geochemical and chronological information. Begét et al. (1991) argued that these tephra were actually representative of a single event, with major element geochemistry within error, and suggested that it may be correlated to either unit C, D, or E of Riehle et al. (1990) at site 23. Riehle (1994) concluded that the glass geochemistry of this unified Jarvis Creek Ash (as named in Begét et al., 1991) and unit G at site 23 were correlative and proposed that the group of beds should be referred to informally as Hayes tephra set H. Riehle (1994) also proposed that the formal stratigraphic name of the Jarvis Ash Bed should be limited to Hayes set H tephra located in the formal Holocene loess unit of interior Alaska known as Engineer Loess.

This complicated scenario was recently addressed by Wallace et al. (2014) who documented a single proximal stratigraphic sequence of eight tephra layers in the Hayes River valley that broadly correlate to set H. The Jarvis Creek Ash (Beget et al., 1991)/unit G (Riehle, 1994) is identified as correlating to the 40 cm thick tephra F (Wallace et al., 2014); geochemical analyses for tephra F2 are summarised in Table 4 (and detailed in Table S2.2). Only tephra F2 has been correlated with deposits in our study area, although a slightly earlier event in set H named tephra H by Wallace et al. (2014) has been identified in the Kenai Peninsula (Combellick and Pinney, 1995). New results from Mulliken (2016) also suggest the Watana tephra, found in the middle Susitna River Valley, correlates to set H (most likely the F2 and H tephra).

In terms of chronology, seventeen publications report a total of forty-six radiocarbon dates relating to set H (Table S2.5), however many were measured using bulk sediment or aquatic macrofossils and only fifteen dates were included in our Bayesian model. This model is interpreted as estimating the eruption date of unit G/tephra F rather than the entire set H, as this

specific event appears to have the greatest distribution. A Bayesian *Tau_Boundary* model estimate for unit G/tephra F is 3910–4205 cal yr BP (Fig. 2.12c), which is consistent with estimates for set H (~3700–4200 cal yr BP).

2.5.4. Aniakchak caldera-forming eruption II (CFE II)

Aniakchak is one of the most active volcanic sites observed in the eastern Aleutian-Arc with more than forty estimated explosive eruptions during the Holocene, including two caldera-forming events (Riehle et al., 1999; Neal et al., 2001; Bacon et al., 2014). The majority of the resulting deposits lie north and northeast of the vent, following prevailing winds (Neal et al., 2001). The late Holocene caldera-forming event (CFE II) has an estimated eruptive volume of >50 km^3 and produced the most widely dispersed tephra layer associated with Aniakchak to date (Miller and Smith, 1987). Aniakchak CFE II has been reported north of the volcano up to west-central Alaska as a visible tephra, as a cryptotephra in the Prospector-Russell Col ice core, St Elias Mountains (Dunning, 2011; Zdanowicz et al., 2014), and as far afield as Newfoundland (Pyne-O'Donnell et al., 2012) and Greenland (Pearce et al., 2004; Denton and Pearce, 2008; Coulter et al., 2012). Figure 2.10 shows the distribution of the visible Aniakchak CFE II deposits as it has been reported in the study area.

Visible deposits of the Aniakchak CFE II have bimodal rhyolitic-andesitic geochemistry (71–72 and 57–61 SiO_2 wt%; Table 4), while distal records beyond Alaska appear to only contain the rhyolitic population (e.g. Pyne-O'Donnell et al., 2012). Variation in the distal geochemistry has been observed, and is likely related to a change in wind-direction during the eruption (e.g. Jensen et al., 2011) and/or because the more mafic shards are denser and therefore fall out before being transported long distances (e.g. Lane et al., 2012). Trace element characterisation has been used to support distal correlations (Pearce et al., 2004), and to distinguish between different eruptions of Aniakchak volcano (Kaufman et al., 2012).

Given its extensive range and occurrence in Holocene sediments, there are forty-seven radiocarbon dates associated with deposits of the Aniakchak CFE II tephra. Of these, only nineteen dates from overlying, intercalated and underlying dates were included in our Bayesian model (Tables S2.5–S2.6). To test for agreement in age between terrestrial records and the Greenland ice core occurrences, our model was run with and without the Greenland ice core ages.

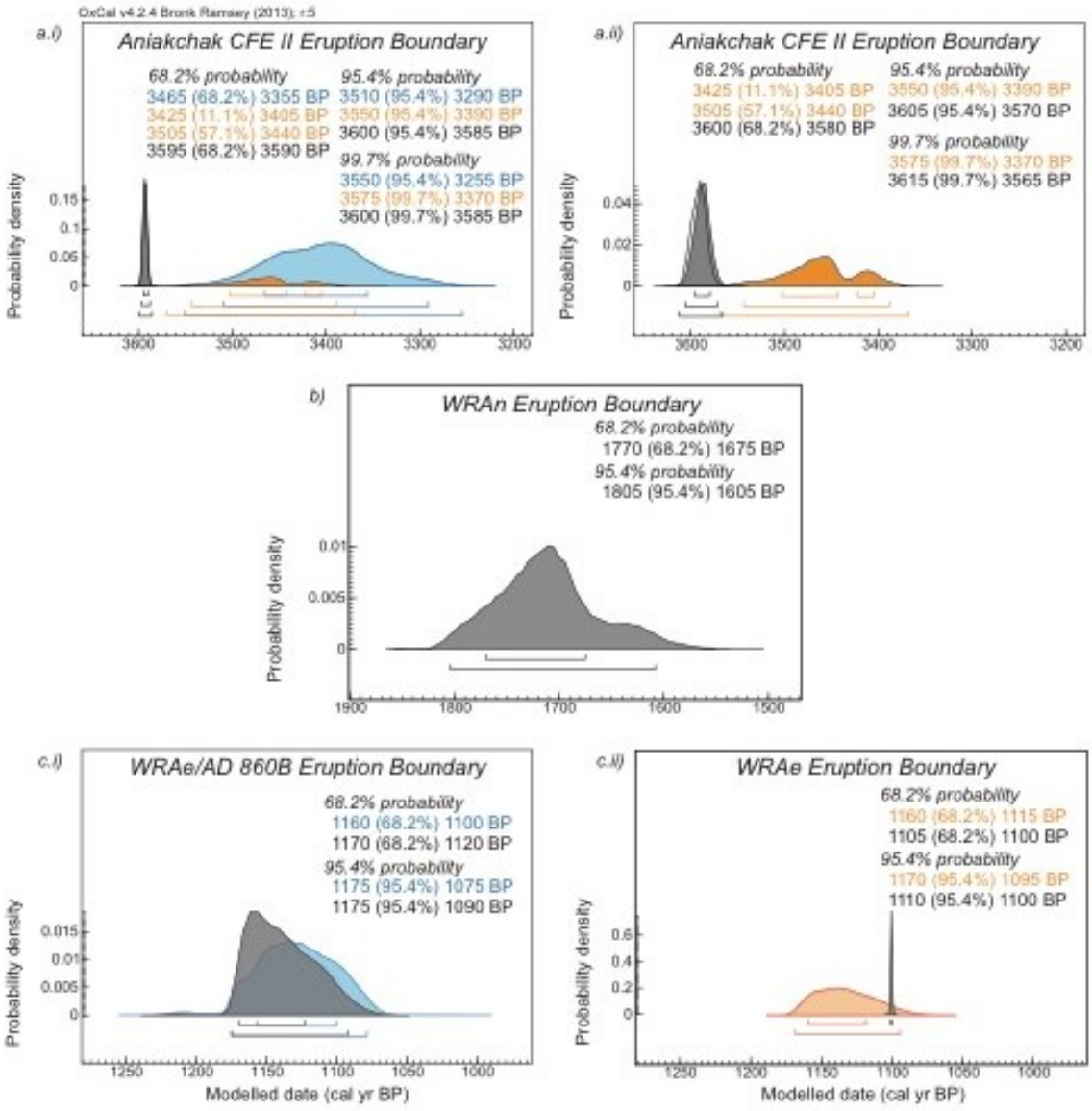

Figure 2.13 Bayesian *Tau_Boundary* probability density function plots derived using OxCal v4.2.4 and IntCal13 for the age of:

a) The Aniakchak CFE II eruption. i) Using all ^{14}C dates (blue), adding one 14C date associated with the eruption boundary (orange), associating the Greenland ice-core ages with the boundary (black); ii) With one ^{14}C date associated with the eruption boundary (orange), associating the Greenland ice-core ages with increased error ranges with the boundary (black).

b) The WRAn eruption.

c) The WRAe eruption. i) Using all ^{14}C dates associated with WRAe (black), using all ^{14}C dates associated with AD 860B (blue); ii) Using all ^{14}C dates combined (orange); also including Greenland ice-core ages (black).

The two Bayesian age estimates are 3585–3600 cal yr BP including the Greenland ice core ages, and 3290–3510 cal yr BP without (black and blue outlines respectively, Fig. 2.13a.i). Including Greenland ice core ages reduces the error associated with the model age estimate due to their low associated errors, and makes the final age slightly older; but even at the 99.7% probability these ages do not overlap. The ice core age model is also irreconcilable with a date from 0 to 5 mm below the tephra (Blackford et al., 2014). If this date is instead associated with the tephra boundary, this produces good model agreement indices (AI; orange outline on Fig. 2.13a.i) but there is still no overlap with the ice core ages. In order to achieve an overlap the ranges associated with the ice core ages must be increased from 4–5 years to 20 years (Fig. 2.13a.ii) and even then this is only just within range. Hence, Greenland ice core ages (Pearce et al., 2004; Coulter et al., 2012) for the Aniakchak CFE II tephra appear to predate other published radiocarbon ages by at least 50–60 years.

2.5.5. White River Ashes

The White River Ash (WRA), as formally defined by Péwé (1975), actually consists of two geochemically similar late Holocene tephra that originated in the Wrangell volcanic field, but are separated by ~500 years and have different plume trajectories. Figure 10 maps the current known visible distribution of the northern and eastern White River Ashes (WRAn, WRAe). The WRAe is one of the only cryptotephra to have been identified in the study area (Payne et al., 2008; Addison et al., 2010; Dunning, 2011), and forms a very prominent visible deposit through much of south and central Yukon into the Northwest Territories (e.g. Lerbekmo 2008). WRAn has not been identified yet as a cryptotephra, but found as a visible unit through eastern Alaska and western Yukon, roughly centred along the Yukon-Alaska border (e.g. Lerbekmo and Campbell, 1969, Péwé 1975). While their source has been debated in the literature (Lerbekmo and Campbell, 1969; McGimsey et al., 1992; Richter et al., 1995; Lerbekmo, 2008), Preece et al. (2014) conclude that they are both the products of Mt. Churchill. When originally defined by Péwé (1975), the two tephra were considered lobes of similar age that had differing geographical distributions. Although they have since been identified as being distinct units, both tephra maintain their formal name, the White River Ash, albeit with a qualifier attached to distinguish the two units. We recommend that any new tephra identified from Mt. Churchill should be referred to using the source rather than WRA to avoid confusion.

Major and trace element glass geochemistry for both deposits has been well characterised in the literature (Jensen et al., 2014a; Preece et al., 2014; Table 4; Tables S1–S2). The WRAn has a greater SiO_2 wt% range (72–78%) compared to the WRAe (73–76%), but there is considerable overlap for other oxides. Recent work by Preece et al. (2014) that examined proximal deposits on and near Mt. Churchill shows geochemical sub-units within the WRA beds, potentially identifies other eruptions, and generally indicates a greater complexity to Mt. Churchill's eruptive history. The proximal deposits of WRAn show that it was the product of an event where the tephra either became increasingly silicic tephra toward the end of the one eruption, or is the product of two closely spaced eruptions tapping the same magma chamber.

At a proximal site approximately 100 km southeast of Mt. Churchill (location 12, SW Yukon; Preece et al., 2014), there is a 10 cm deposit of peat between WRAe and a second, younger, eruption. It is unclear, with insufficient age control and geochemical data, if this young unit may be related to the Lena tephra of Payne et al. (2008). These eruptions are not discussed here for age-modelling, however, as they have not been reported at any other sites.

2.5.5.1. WRAn

WRAn is the oldest of the pair, and is primarily reported along the Alaska/Yukon border. Within the literature, seventeen dates have been published, and three are excluded from our age model (Table S5).

The accepted dates bracket the eruption, and give a Bayesian age estimate of 1605–1805 cal yr BP (Figure 13b). This is slightly younger than previous reports such as Leberkmo et al. (1975) and Jensen and Froese (2006), but is in agreement with individual radiocarbon dates.

2.5.5.2. WRAe

WRAe is the most widely distributed of the two deposits, having been correlated across to eastern Canada (Pyne-O'Donnell et al., 2012), the northeastern Unites States (MacKay et al., 2016), Greenland and Europe (Jensen et al., 2014a). It should be noted that within northwestern North America it had significant effects on the lives and migration patterns of the ancestral Athapaskan people of the area (e.g. Moodie et al. 1992; Mullen, 2012). The estimated eruptive volume is ~50 km^3 (Leberkmo, 2008), with visible layers greater than 2.5cm thick recorded more than 600 km from source (Richter et al., 1995).

Dates associated with WRAe come from North America and Europe (where it was previously recognised as AD860B; Table S2.5–S2.6). Within North America, thirty-one published dates are associated the WRAe, ten of which were excluded from our age model. Several of these dates are produced from buried stumps, killed by the ashfall, allowing a high level of confidence when dating the eruption. This is demonstrated by the high precision dates reported from a spruce tree (Jensen et al., 2014a) that give a ^{14}C wiggle-matched age of 833–850 CE. Within Europe, five dates have been published in association with AD860B (Pilcher et al., 1995; Balascio et al., 2011), and the most commonly used age is 776–887 CE produced by high precision ^{14}C wiggle matching of the humine fraction of peat samples (Pilcher et al., 1996). This layer was also correlated with glass found in Greenland Ice Cores (NGRIP; Coulter et al., 2012) and given a Greenland Ice Core Chronology (GICC05) age of 846–847 CE (Vinther et al., 2006).

Our model was run iteratively to test for differences in the dates from North America versus Europe (Fig. 2.13c). The combined dates from both North America and Europe are within agreement (Fig. 2.13c.i), although the combination of both sets of dates (Fig. 2.13c.ii) produces a slightly smaller age range (1095–1170 cal yr BP) than either of the models ran alone. The addition of the GICC05 age (Fig. 2.13c.ii), as expected, reduces the range significantly as the associated error of 1 year dominates the model. The radiocarbon dates and GICC05 ages are in agreement at the 95.4% probability range, although the GICC05 date is ~10 years younger than the modelled radiocarbon dates at the 68.2% probability range.

2.6 Discussion

In this paper we have summarised the available data for nineteen distal tephra beds that are either found or likely to be found within the study area of interior Alaska and Yukon. We now assess the potential of these beds for distal correlation, including potential distributions and challenges, before discussing issues related specifically to the datasets.

2.6.1. Modern eruptions

Three modern eruptions, Novarupta-Katmai 1912 (Hildreth and Fierstein, 2012), Redoubt 1989–1990 (Scott & McGimsey, 1994), and Crater Peak 1992 (McGimsey et al., 2001), have plume trajectories indicating they are likely to be found as cryptotephra in the study area, but at present these beds have not been reported in the study area, though Katmai 1912 is found in NGRIP (Coulter et al., 2012).

The four cryptotephra reported from the Eclipse Icefield, St Elias Mountains (Ksudach 1907, Novarupta-Katmai 1912, Hekla 1947, 1989 Redoubt 1989–1990; Yalcin et al., 2003) have limited support for their identification, particularly Hekla 1947 and Ksudach 1907. It is more likely that Redoubt 1989–1990 and Novarupta-Katmai 1912 are present, but the unsuitable nature of the reference data used for comparison and the use of SEM data, which are not fully quantitative, suggest these records should be re-examined before any further conclusions are made.

2.6.2. Tephra with limited characterisation

2.6.2.1. Reported visible tephra

The Devil Mountain Lakes tephra is a locally erupted basaltic deposit produced from the youngest of the Quaternary maars in the region. It is unlikely to have been dispersed much further than the peninsula or recorded in distal records, even though this phreatomagmatic eruption was extremely explosive due to magma-permafrost interactions (Hopkins, 1988; Begét et al., 1996). The remaining poorly constrained tephra all have appreciably more potential for being found and correlated elsewhere.

HH7 tephra is reported in and around the Fairbanks region. It is consistently present as a visible bed in loess deposits that post-date DT, but is likely still MIS 2 in age. The Chatanika tephra, deposited ~16,600–19,700 cal yr BP, is of similar age, geochemistry and morphology. These tephra may correlate, but if not, they represent two closely spaced eruptions, likely from the same source, that are both important regional markers for this timeframe.

The tephra reported from two lakes on St Michael Island by Ager (1982, 2003) correlate with Tephra D of Kaufman et al. (2012) from the Ahklun Mountains. It is likely that the published maximum age for Tephra D from St Michael Island (<15,610 ^{14}C yr B.P) is unreliable as it is produced from underlying bulk sediment samples. Additional samples dated elsewhere that were in context with the well-dated Aniakchak CFE II tephra are 2000–4000 years older than expected due to either a loss of stratigraphic integrity (e.g. Beierle and Bond, 2002), or reworking of old carbon (Ager, 1982). Instead, the age of 15,505±312 cal yr BP associated with Tephra D from Kaufman et al (2012) is recommended as the most accurate at this point.

Tephra D is potentially derived from Aniakchak volcano, although proximal late glacial records lack sufficient chronological control and published glass geochemical data to support this supposition. It is possible that any proximal records would have been buried or eroded by either of the subsequent caldera forming eruptions or the numerous smaller events that have occurred in the Holocene. Regardless, given its wide distribution this tephra has significant potential for correlation within western Alaska.

The estimated maximum age for the MT Layer reported by Child et al. (1998) does not match previously reported eruptions from Mt. Spurr. This absence may reflect a lack of proximal preservation in the areas that have been studied near the vent. It is also possible that this tephra may be a late glacial product from Aniakchak as the average data from Aniakchak CFE I (Fig. 8; Table S4) show greater similarity than the reference material for Crater Peak used by Child et al. (1998). Chronologically they are also similar, with maximum age constraints of ~10,500–11,500 cal yr BP. However, this cannot be fully tested without the original individual glass analyses from Child et al. (1998) and a comprehensive glass geochemical dataset from Aniakchak CFE I. This tephra has good potential for being recorded within central and northern Alaska given the reported thickness of the deposit at Wonder Lake.

2.6.2.2. Reported cryptotephra

Payne et al. (2008) report seven cryptotephra from southeast Alaska: WRAe, and six previously unreported beds. Two of these unknowns are geochemically similar to Mt. Churchill and are discussed below with the WRA (section 6.3.5). Dates and ages discussed here are reproduced from Payne et al. (2008).

Tephra ECR 162 has a modelled age of 5030–5300 cal yr BP and a reported eruption from the adjacent Black Peak volcano (Miller and Smith, 1987) fits well with the age estimate, but is an unlikely source given the significant geochemical differences. The original data used for comparison from Riehle et al., (1999) is average glass major-element data with relatively few shards analysed (n=3, 4) and high standard deviations (4 and 13 SiO_2 wt%, respectively). However, the glass geochemical data for Black Peak included here (Wallace & McGimsey, unpublished) are sufficient to exclude it as a potential source (Fig. 9). Aniakchak is suggested in the original report as a likely source although there are currently no reported eruptions at that time and the EPMA data for ECR 162 are offset from previous distal analyses of Holocene

tephra from Aniakchak (Fig. 9). However, as no associated secondary standard data were published with Payne et al's (2008) dataset and reference material for Aniakchak tephra or other potential correlatives were not ran concurrently, it is not possible to exclude Aniakchak as a source.

Payne et al. (2008) do not attribute any of their cryptotephra to the Mt Edgecumbe Volcanic Field (MEVF) due to low glass geochemical similarity coefficients (SC<0.85) despite this vent being the closest source to their sites. Addison et al. (2010) report a cryptotephra (Unit A of EW0408) found in three marine cores from basins adjacent to the MEVF that have similarity coefficients of 0.90 when compared to ECR 162. Their core chronology also suggests a modelled age of ~5300 cal yr BP for the cryptotephra, but their glass geochemistry overlaps more strongly with mid Holocene rhyolites from MEVF (SC>0.96) (Riehle and Brew, 1984). Current data for the MEVF, therefore, does not suggest a correlation is likely.

Two tentative correlations between ECR 100 (~2840 cal yr BP) and Augustine volcano, and MTR 190 (~8660 cal yr BP) with Redoubt, are suggested by Payne et al. (2008). However, both of these cryptotephra have only two data points, and for MTR 190 these points were produced at different labs (Bergen and Edinburgh) and are not similar, and thus provide insufficient evidence to support a correlation. Furthermore, is unclear what the cryptotephra shard concentrations were for these layers, and if they are significantly above background.

2.6.3. Widely distributed and well characterised tephra

2.6.3.1. Dawson tephra

The distribution of Dawson tephra shown in Figure 10 represents a simple model of ash dispersal from Emmons Lake Volcanic Center to the prominent sites in the Klondike area of central Yukon. However, while Dawson tephra is found commonly in the Yukon, it has rarely been found in the interior of Alaska. Explanations for this have included invoking a more complicated plume trajectory based on satellite data of modern plume movement (e.g. Begét et al., 2004, 2005), or a paucity of late MIS-2 records around the Fairbanks area (e.g. Muhs et al., 2003; Froese et al., 2006). However, recent work has shown that MIS 2 sediments are present, and that Dawson tephra can be found in locations around Fairbanks, but generally as a thin, poorly preserved layer (Jensen et al., 2016). It is also found as a thick deposit in the Gulf of Alaska

(Begét et al., 2004; Jensen et al., 2013), supporting Begét's hypothesis that complicated plume dynamics are a more likely cause for its limited distribution in the central interior of Alaska.

2.6.3.2. Oshetna

Identification of the Oshetna tephra is more complicated than previously published literature has suggested and there are significant ambiguities in its chronology and geochemical characterisation (Mulliken, 2016). The Oshetna tephra may represent multiple eruptions, phases of a complex eruption similar in style to the well-known Hayes Tephra set H, or one large eruption from a heterogeneous magma chamber, producing a range of glass populations as seen with Novarupta-Katmai 1912 (Hildreth and Fierstein, 2012).

It is advised, therefore, to regard the identification and use of Oshetna tephra with caution until additional data can better clarify the situation. The *Tau_Boundary* age estimate of 6555–6895 cal yr BP (produced without including the date from within the tephra layer) is a broad enough interval that it could represent multiple events over decades or centuries.

2.6.3.3. Hayes set H

Two of the set H tephra appear to be relatively far travelled and therefore good candidates for correlation elsewhere in the study area. Wallace et al. (2014) identified tephra units F and H from a proximal section that appear to correlate with distal records. Based on that work, tephra F correlates to what is considered the 'classic' Hayes tephra, the most widely distributed unit found broadly to the northeast of the volcano, also known as the Jarvis Ash/unit G of (Riehle, 1994). Tephra H has been described in the Kenai Peninsula (Combellick and Pinney, 1995), and the middle Susitna River Valley (Mulliken, 2016) where it has been correlated with what was previously identified as the oxidised phase of the Watana tephra. There is no evidence that any of the other set H tephra are found beyond the proximal deposits.

While there is significant overlap in glass major-element geochemistry among some proximal set H deposits (Units B, D, E, F1 and F2 of Wallace et al. (2014); Figure 2.14), Tephra F and H can be distinguished from each other most easily using differences in their wt% SiO_2, Cl, and Al_2O_3. Wallace et al. (2014) suggest that more work on tephra in the proximal region is needed to fully characterize the eruptive history of Hayes volcano, including a determination of whether or not Oshetna also represents an eruption from this active Holocene volcano.

Collectively, these new data and previous evidence show that only one event of the set (unit G/tephra F) is present in the study area as a visible bed, and it is geochemically distinguishable from the other units. Therefore, to simplify the complicated nomenclature that exists, we suggest that Péwé's (1975) formal stratigraphic name of the Jarvis Ash Bed should take precedent when discussing this particular distal unit in Hayes set H, alternatively described as unit G, tephra F, Tangles Lakes tephra, Jarvis Creek Ash, and Cantwell tephra.

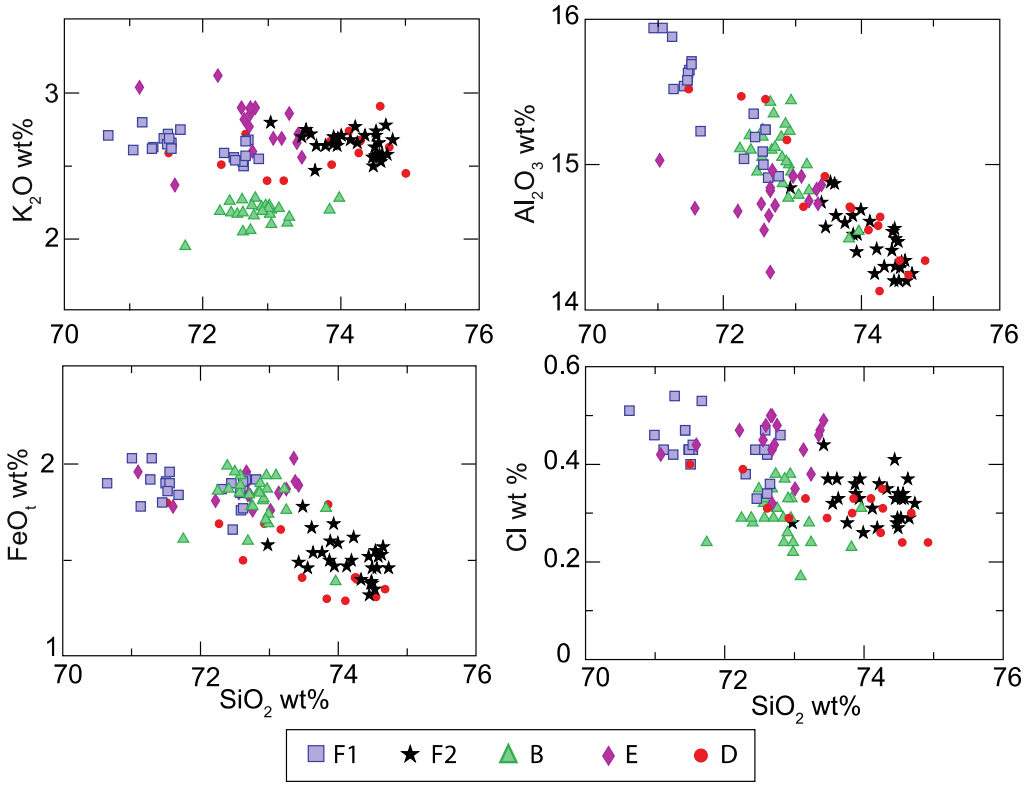

Figure 2.14 Major element geochemical plots comparing five proximal units of the Hayes set H tephra (data from Wallace et al., 2014).

2.6.3.4. Aniakchak

Aniakchak volcano has been very active throughout the Holocene, with two caldera forming events and dozens of smaller explosive eruptions identified from proximal stratigraphic and geochemical evidence (Neal et al., 2001; Bacon et al., 2014). Although these tephra have yet to be reported within the study area of this report, there is potential for long-distance transport and deposition. Here we discuss complexities of Aniakchak tephra to improve their potential for

correlation if found in distal records, and illustrate how distal records can provide new perspectives on complex and incomplete proximal deposits.

It has been shown here that the dates reported from Greenland ice cores (Pearce et al., 2004; Coulter et al., 2012) for Aniakchak CFE II are irreconcilable with the radiocarbon dates. Given the confidence placed in the geochemical correlation of these samples it is most likely that this chronological difference is a result of an offset which is not fully accounted for by low counting errors associated with the ice core ages (±2 years at this depth for GICC05). Our model suggests an offset of at least 20–75 years to allow overlap with the Bayesian modelled 68.2% and 95.4% ranges. This is similar to the conclusion of other recent papers investigating synchronicity of the GICC05 (Vinther et al., 2006) and IntCal (Reimer et al., 2009, 2013) timescales which suggest Holocene GICC05 ages are 7–70 years too old depending on the time period considered (Lohne et al., 2013; Muscheler et al., 2014; Baillie and McAneney, 2015; Torbenson et al., 2015; Adolphi and Muscheler, 2016)

Beyond the most commonly recognised mid-late Holocene Aniakchak CFE II tephra, three additional tephra with geochemical data similar or indistinguishable from Aniakchak CFE II have been reported distally from the vent, with modelled ages of 400, 3100, and 5800 cal yr BP (Kaufman et al., 2012). Trace-element geochemistry indicates that the 5800 cal yr BP event is a separate event, but the 400 and 3100 cal yr BP events are indistinguishable from CFE II by either their major or trace element geochemistry. This similarity has made it difficult to determine whether these events represent reworked deposits or separate eruptions (Kaufman et al., 2012). Their discovery at other locations, or a proximal site where additional analyses may aid discrimination between the tephra (e.g. mineralogy), would lend support to the argument for multiple events. For example, recent work examining cryptotephra in marine sediments in the Chukchi Sea claims to re-create this stratigraphy, which combined with evidence of a 400 cal yr BP eruption at Aniakchak, suggests all three may represent separate events (Browne et al., 2003; Bacon et al., 2014; Ponomareva et al., 2014).

In addition to these three tephra, there are multiple samples that show a strong similarity to either the dominant rhyolite glass population of the Ankaichak CFE II (e.g. Lone Spruce, 4.1 ka; Kaufman et al., 2012), or the minor basaltic to andesitic population (Bacon et al., 2014). It is not clear, given the lack of proximal glass geochemical data from Aniakchak, if these events are also

sourced from this volcano or a related nearby peak (e.g. Veniaminof, Black Peak). Whole rock data for the early Holocene CFE I eruption indicates that the tephra geochemistry varies noticeably (particularly for K_2O, Zr, and other incompatible-element concentrations; Bacon et al., 2014), such that distal tephra may be equally distinctive. As mentioned previously, both Tephra D and the MT Layer major-element geochemical data show strong similarities with Aniakchak geochemistry and may represent late glacial activity (potentially Aniakchak CFE I for the MT Layer) that has not been reported or fully characterised from proximal records.

2.6.3.5. White River Ashes/Mt. Churchill

While the WRA have been used regionally as distinct marker beds, particularly WRAe, it can be difficult to identify which bed is present at a site without a clear stratigraphy and/or if only glass is preserved. Further complexity in proximal deposits is reported by Preece et al. (2014) where both ilmenite and glass geochemical data identify distinct compositional subunits in WRAe and WRAn tephra that are interpreted to be the result of multiple magma bodies or layers within the Mt. Churchill magmatic system. This is more pronounced for the WRAn than WRAe, and while it may be reflected somewhat by the larger SiO_2 wt% range in WRAn, is unlikely to be observed more distally without trace-element or ilmenite analyses.

Growing evidence suggests that Mt. Churchill has been a more active source than previously realised. Payne et al. (2008) report two additional 'White River-like' cryptotephra at 257±22 cal yr BP (the Lena tephra, replicated at five sites in the area) and ~6300 cal yr BP (an interpolated age; found only at one site). A younger tephra reported at proximal site 12 of Preece et al. (2014), which is separated from WRAe tephra by 10 cm of peat, was previously interpreted by Leberkmo et al. (1975) as reworked WRAe. However, further work shows identifiable differences in its geochemistry, suggesting it may represent a younger eruption (Preece et al., 2014). Although geochemical comparisons of this tephra with the Lena tephra of Payne et al. (2008) are inconclusive, they have similar ages, and therefore may represent the same event or another younger period of activity. Preliminary cryptotephra data presented from a soligenic peatland site in central Yukon Territory increases the potential number of Mt. Churchill eruptions to at least half a dozen throughout the Holocene (Davies and Froese, 2015) suggesting that Mt. Churchill produced far more than the two well-documented WRA tephra.

2.6.4. Datasets

Table 5 summarises the data for nineteen tephra (or sets) identified over the past 30,000 years. While each tephra has been discussed in turn, we will now address broader issues dealing with how these tephra are characterised and reported.

Tephra	Location[a]	Lab #[b]	Age estimate	IUGS (glass)	Reference[c]
Dawson	Klondike Goldfields, Yukon Territory	UA 1000	29055-29470 cal BP	Rhyolite	Preece et al. (2011)
Devil Mountain Lakes Maar	Northern Seward Peninsula	nd	20115-20740 cal BP	Basalt	Hopkins (1988); Beget et al. (1991); Hofle et al. (2000).
HH7	Halfway House, W of Fairbanks	UA 1451, 1877, 1901, 1902, 1903, 1915	<29055-29470 cal BP	Rhyolite	Jensen et al. (2016); Péwé (1975)
			16595-19710 cal BP[d]		
Tephra D (Tephra II)	Zagoskin & Puyak Lake, St Michael Island	UA 2660, 2661	15505±312 cal BP	Andesite	This paper; Ager (1982), (2003); Kaufman et al., (2012)
	Arolik & Nimgun Lake, Ahklun Mountains	UA 1781			
MT Layer	Wonder Lake, Denali National Park	ACT 1080, 2079, 2083	<10060±70 ^{14}C yr BP[f]	Andesite	Child et al. (1998)
			(11400-11760 cal BP)		
MTR 190	Mt. Riley, SE Alaska panhandle	nd	8660 cal Bp[e]	Rhyolite	Payne et al. (2008)
MTR 146	Mt. Riley, SE Alaska panhandle	nd	6300 cal Bp[e]	Rhyolite	Payne et al. (2008)
Oshetna	Denali National Park; Suisitna Valley	ACT 1082, 1076, 1073, 1078	6785-6880 cal BP[g]	Rhyodacite	Child et al. (1998)
			6555-6895 cal BP[h]		
ECR 162	Eaglecrest Bog, SE Alaska panhandle	nd	4485±30 ^{14}C yr BP[e]	Rhyolite	Payne et al. (2008)
			5030-5300 cal BP[e]		
Jarvis Ash (Hayes set H, unit G/tephra F2)	Hayes River proximal sequence	ACT 2561	3910-4205 cal BP	Rhyolite	Riehle et al. (1990); Wallace et al. (2014)
Aniakchak CFE II	Zagoskin Lake, St Michael Island	UA 1602	3570-3605 cal BP[g]	Andesite/ Rhyolite	Riehle et al. (1987); Kaufman et al. (2012)
			3390-3550 cal BP[h]		
ECR 100	Eaglecrest Bog, SE Alaska panhandle	nd	2840 cal BP[e]	Rhyolite	Payne et al. (2008)
WRAn	40-mile, Yukon Territory	UA 1046	1605-1805 cal BP	Rhyolite	Leberkmo et al. (1975); Preece et al. (2014)
WRAe (AD860B)	N. Klondike Highway, 20km N of Carmacks	UA 1119	1100-1110 cal BP[g]	Rhyolite	Leberkmo et al. (1975); Preece et al. (2014); Jensen et al. (2014a)
			1095-1170 cal BP[h]		
CHP 184	Chilkoot Pond, SE Alaska panhandle	nd	>468±55 ^{14}C yr BP[e]	Rhyolite	Payne et al. (2008)
Lena	SE Alaska panhandle	CHP 33[i]	257±22 ^{14}C yr BP[e]	Rhyolite	Payne et al. (2008)
			285-310 cal BP[e]		
Novarupta-Katmai 1912	Kodiak Island, station 07JANV-2	UA 1364	---	Rhyodacite	Hildreth and Fierstein (2012)
Redoubt 1989-90	Seismic station RDN, Alaska	UA 2754	---	Rhyolite	Scott & McGimsey (1994)
Crater Peak 1992	Anchorage, Alaska	UA 2619	---	Andesite	McGimsey et al. (2001)

Table 2.5: Summary of the characterisation of all tephra described within this study in chronological order (oldest to youngest). Correlations to previously named tephra are shown in brackets where relevant. a The location provided is either a type site/source of reference material with a published dataset, or the prominent area the tephra has been reported from. b ACT = Alaska Center for Tephrochronology; UA = Univ. of Alberta. c For tephra with multiple references, those with detailed datasets, key information, or new sites have been included. d Date modelled for the Chatanika tephra. e Dates from Payne et al. (2008). f Maximum date from Child et al. (1998). g Including dates associated directly with the tephra model boundary (i.e. from within the tephra; ice core ages). h Excluding dates associated directly with the tephra model boundary (i.e. from within the tephra; ice core ages). i Date produced from one site (Chilkoot Pond), stratigraphically correlated with other Lena tephra but not geochemically analysed.

2.6.4.1. Published datasets

Developments in radiocarbon dating, Bayesian modelling, and key correlation tools (e.g. the standardisation of EPMA) allow a re-evaluation of the published literature to extract the most reliable data for the eruptions that are available. For radiocarbon data, most published dates are presented as both raw (uncalibrated) and calibrated dates with details of the calibration set used. The description of the material analysed, however, is often poor or absent, and we exclude a number of dates because they do not meet our model criteria. This is particularly true for older studies using radiometric dates where it is assumed that bulk material analyses were used for peat or lake sediments. Ideally, published dates should have associated details of the material analysed (e.g. bulk material, woody macrofossil, leaf fragment, etc.), its stratigraphic relationship with the tephra, and information regarding the analyses (e.g. the laboratory and protocol used). Where one or more of these details is lacking, the dates are not included in our models.

For glass geochemical analyses the situation is more variable. Due to significant differences in data produced between labs, recommendations for standardisation of EPMA have been published (e.g. Froggatt, 1992; Kuehn et al., 2011). These address reporting of analytical conditions, as well as data from calibration and secondary standards. Recognition of the Wrangell-sourced WRAe in European records (Jensen et al., 2014), and the debate over the identification of the Aniakchak CFE II tephra in Greenland (Pearce et al., 2004), highlight the importance of including complete geochemical datasets in publications in order to facilitate useful comparisons. Many papers published after the protocol recommendations were established do conform to this style of reporting, however a large amount of the data discussed here unfortunately pre-dates this. A good example for best practices is followed by Wallace et al. (2014): the supplementary data includes full details of the methodology, the standards analysed, and the geochemical data of all analyses (including those which were discarded).

Records of other tephra characteristics (e.g. glass morphology, mineralogy, trace element geochemistry) within the study area are inconsistent, with tephra commonly having either all attributes described or none (Table S1). Understandably, this relates largely to whether the tephra has a well-defined proximal and/or prominent site (i.e. where thick visible deposits occur, preserving both glass and mineral components): while widely documented tephra such as Dawson, Hayes set H, Aniakchak, the WRAs, and modern eruptions are well described, other

sparsely reported tephra such as Oshetna and those with limited known field sites (e.g. MT Layer, Tephra D) have very little. This is inevitable if the tephra is not well represented in the field (e.g. has only the glass component), but there are significant opportunities identified here from distal records to fill gaps in our understanding with the discovery of new sites or reanalysis of older samples. This includes, for example, improving our characterisation of a tephra such as Oshetna, which is found and utilised in a range of studies (e.g. archaeological, palaeoenvironmental), but has many unknowns surrounding its eruption and deposition. Also, a focus on records covering a specific age range, such as the late glacial and early Holocene – a time of dramatic climatic changes that has more widespread tephra preserved than has previously been highlighted (e.g. HH7, Chatanika, Tephra D, MT Layer).

2.6.4.2. Age modelling

A number of dates from the literature were excluded based on our model criteria; statistics regarding the dates included in our Bayesian model are summarised in the Supplementary Data. Only about half of the published dates met our data quality requirements and are included in the age models, and of these ages, most (83 of 120) were maximum dates, predating the given eruption. There is a general lack of material post-dating the eruptions, and only one of the tephra beds has dated material from within the tephra layer itself. Maximum dates are generally preferred and can give very accurate age estimates, particularly if the material dated was killed by the ashfall. Due to potential delays in organic development and accumulation following an ashfall, depending on the concentration/thickness of the tephra, dating of overlying material is generally not preferred for assessing eruption age. However, any model indirectly constraining a tephra age benefits from a more balanced representation of dates in order to fully constrain the age ranges produced and reduce associated errors. The most extreme example of this is the Devil Mountain tephra where the input dates are all maximum ages, which is not ideal for Bayesian modelling. This is demonstrated by the large tail that can be seen to the right-hand side of the probability density plot (Fig. 6a).

A total of eight dates for three different eruptions were removed from the models after they produced irreconcilably low agreement indices in the first model run. In the case of the WRAe, Payne et al. (2008) report that some dates are out of sequence or likely to have been contaminated which is supported by our model. In another case, Fraser and Burn (1997) do not

discuss why their grass-bed radiocarbon date below Dawson tephra disagrees with other dates and it is therefore difficult to justify rejecting it from our model dataset. Overall, it appears that the *Tau_Boundary* function does not handle dates that are very close or immediately predating the eruption very well, as is seen with Blackford et al.'s (2014) date for 0–5 mm below the Aniakchak CFE II eruption. Our modelled ages are generally similar to previously published age estimates, not unexpected given the inclusion of the same raw dates, but this is not always the case. The model age of Dawson tephra differs from that of Demuro et al. (2008), likely the result of different model structures (*Tau_Boundary* vs Phase model) and calibration data sets (IntCal13 of Reimer et al. (2013) and Cariaco Basin of Hughen et al. (2006)).

Tephra ages can appear to have lower associated errors and narrower ranges than are realistic when there are limited published associated dates, or dates produced from only a few locations. Oshetna tephra, for example, has high agreement indices for the modelled age and fits well with previously published dates. However, this apparent precision could be a consequence of including only nine dates within the model, and may mask additional complexity that has not yet been fully appreciated. Additionally, if the date produced from within Oshetna tephra is excluded, the age range produced is significantly wider. The *Tau_Boundary* function is heavily influenced by the association of dates with the boundary itself, rather than just pre and post dating it. The inclusion of dates from more distal locations and the comparison of multiple model runs can help investigate this potential bias. It is important to acknowledge that wider age ranges, higher associated errors, or lower agreement indices are a function of the quality of dataset used.

The *Tau_Boundary* function models a single eruptive event with the assumption that dates cluster closely to the event boundary. While this is applicable in most cases, datasets such as Hayes set H which are composed of deposits of multiple closely space eruptions, show that our errors are significantly increased. In this situation the modelled age represents a broad range, possible for multiple eruptions, and provides little improvement from previously published estimates. Unless further consideration of the original datasets can shed more light on their records, or new analyses can produce additional dates that are tied to specific eruptions, the *Tau_Boundary* function does not offer any improvement on previous attempts at age modelling.

2.7 Summary

The development of a robust tephrostratigraphic framework for northwestern North America, and its application to the developing North American cryptotephra framework, is dependent on the reliable characterisation and dating of distal tephra beds. In this review we have identified nineteen tephra which are preserved distally from SW Alaska, and summarised all available geochemical and chronological data in order to address the absence of an accessible, high quality synthesis of the tephra found in interior Alaska and Yukon.

Three modern eruptions have plume trajectories that indicate they are likely to be found as near surface cryptotephra in the study area: Novarupta–Katmai 1912, Redoubt 1989–90, and Crater Peak 1992. Major element geochemical data for each of these tephra are published here to facilitate future correlations. The previous identification of Ksudach 1907 and Hekla 1947 (Yalcin et al., 2003) is shown to require further work, as current data are insufficient to support these correlations.

Summaries of ten tephra - four visible and six cryptotephra - with limited data previously reported are discussed and updated where possible. The Devil Mountain Lakes tephra is unlikely to have a significant distribution outside of the Seward Peninsula. Tephra D, now known to be present on St Michael Island, and the MT Layer represent late glacial and early Holocene mafic-intermediate tephra that have conceivably broad distributions. Reports of cryptotephra are sparse in the study area, but the six new tephra detailed in Payne et al. (2008) demonstrate the potential for future studies here.

The six remaining tephra reviewed here are widely reported in interior Alaska, Yukon, and further afield, representing the most well documented tephra erupted from the AAAP and WVF during the Holocene. The collective dataset of major element geochemical data and ages shown here is a baseline for robust correlations. However, our understanding of these beds can still be improved, as shown here by the revised age estimates produced for Dawson tephra and WRAn, the limited characterisation of Oshetna tephra, and the offset demonstrated between ages for Aniakchak CFE II from Greenland ice cores and radiocarbon dates from Alaska.

Volcanoes in Alaska are challenging to characterise proximally given the large number of active volcanoes, their remote locations, and the removal and/or burial of proximal sediments by glaciation or subsequent eruptions. Distal tephra records complement proximal studies, and are a

key source of information for large events that may be unknown from the proximal record. This is particularly relevant for late glacial and early Holocene tephra, which are more likely to have been removed or subsequently buried but are well-preserved in distal records e.g. HH7 in loess, Tephra D, the MT Layer, and Oshetna, in lake sediments.

If new distal tephra can be attributed confidently to a specific source this has obvious benefits, but it is not necessary for the development of a robust regional tephrostratigraphy. There is a minimum level of evidence required to confidently assign a correlation – and this is not always met when published datasets are too sparse (e.g. ECR 100 and MTR 190, Payne et al., 2008) or the proximal data is not well-characterised. Studies of older distal tephra in the region have focused on comprehensively reporting both well-defined isochrons and unprovenanced beds (e.g. (Preece et al., 1999, 2011b, Jensen et al., 2008, 2013).

Here we have demonstrated that a rich record of distal tephra is preserved across Alaska, Yukon, and further afield as cryptotephra horizons, and this framework is now available for further testing, revision, and development. We predict this record will be an important dataset to facilitate improved understanding of northern volcanic hazards and allow further development of tephra from the WVF and AAAP to date and correlate palaeoenvironmental records from this remarkable area.

2.8 References

Abbott, M.B., Stafford, T.W., Jr., 1996. Radiocarbon Geochemistry of Modern and Ancient Arctic Lake Systems, Baffin Island, Canada. Quaternary Research 45, 300–311. doi:10.1006/qres.1996.0031

Abbott, P.M., Davies, S.M., 2012. Volcanism and the Greenland ice-cores: the tephra record. Earth Science Reviews 115, 173–191. doi:10.1016/j.earscirev.2012.09.001

Addison, J.A., Begét, J.E., Ager, T.A., Finney, B.P., 2010. Marine tephrochronology of the Mt. Edgecumbe Volcanic Field, Southeast Alaska, USA. Quaternary Research 73, 277-292. doi:10.1016/j.yqres.2009.10.007

Adolphi, F., Muscheler, R., 2016. Synchronizing the Greenland ice core and radiocarbon timescales over the Holocene - Bayesian wiggle-matching of cosmogenic radionuclide records. Climate of the Past 12, 15–30. doi:10.5194/cp-12-15-2016

Ager, T.A., 1982. Vegetational history of western Alaska during the Wisconsin glacial interval and the Holocene, in: Hopkins, D.M., Matthews, Jr. V.J., Schweger, C.E., Young, S.B.

(Eds.), Paleoecology of Beringia. Academic Press, New York, pp. 75–93. doi:10.1016/B978-0-12-355860-2.50012-0

Ager, T.A., 2003. Late Quaternary vegetation and climate history of the central Bering land bridge from St. Michael Island, western Alaska. Quaternary Research 60, 19–32. doi:10.1016/S0033-5894(03)00068-1

Alaska Volcano Observatory, 2014. Alaska Volcano Observatory Online Library. Available at: http://www.avo.alaska.edu/downloads/. [Accessed 30 September 15].

Bacon, C.R., Neal, C.A., Miller, T.P., McGimsey, R.G., Nye, C.J., 2014. Postglacial eruptive history, geochemistry, and recent seismicity of Aniakchak volcano, Alaska Peninsula. Professional Paper 1810. US Geological Survey, Washington, DC. doi:10.3133/pp1810

Baillie, M.G.L., McAneney, J., 2015. Tree ring effects and ice core acidities clarify the volcanic record of the first millennium. Climate of the Past 11, 105–114. doi:10.5194/cp-11-105-2015

Balascio, N.L., Wickler, S., Narmo, L.E., Bradley, R.S., 2011. Distal cryptotephra found in a Viking boathouse: the potential for tephrochronology in reconstructing the Iron Age in Norway. Journal of Archaeological Science 38, 934–941. doi:10.1016/j.jas.2010.11.023

Beget, J.E., Mann, D., 1992. "Caldera" formation by unusually large phreatomagmatic eruptions through permafrost in arctic Alaska. Abstracts [Fall Meeting, 1992], Eos Trans. AGU, 73(43), 636, doi:10.1029/91EO10347.

Beget, J.E., Reger, R.D., Pinney, D., Gillispie, T., Campbell, K., 1991. Correlation of the Holocene Jarvis Creek, Tangle Lakes, Cantwell, and Hayes Tephras in South-Central and Central Alaska. Quaternary Research 35, 174–189. doi:10.1016/0033-5894(91)90065-D

Beget, J.E., Stihler, S.D., Stone, D.B., 1994. A 500-year-long record of tephra falls from Redoubt Volcano and other volcanoes in upper Cook Inlet, Alaska. Journal of Volcanology and Geothermal Research 62, 55–67. doi:10.1016/0377-0273(94)90028-0

Begét, J.E., Hopkins, D.M., Charron, S.D., 1996. The largest known maars on Earth, Seward Peninsula, northwest Alaska. Arctic 49, 62–69. doi:10.2307/40511986

Begét, J.E., Pedersen, T.F., Muhs, D., 2004. Terrestrial–marine correlation of the 24 kyr BP Dawson tephra: implications for dispersal and preservation of Alaskan tephra deposits. American Geophysical Union Annual Fall Meeting, San Francisco, CA, Fall Meeting Supplement 85, Abstract V21C-02.

Begét, J. E., Pederson, T., Muhs, D., 2005. Terrestrial-marine correlation of the Daswon tephra, in: Alloway, B.V., Froese, D.G., Westgate, J.A (Eds.), Proceedings of the International Field Conference and Workshop on Tephrochronology & Volcanism: Dawson City, Yukon Territory, Canada July 31st – August 8th, 2005. Institute of Geological & Nuclear Sciences science report 2005/22. 55.

Beierle, B., Bond, J., 2002. Density-induced settling of tephra through organic lake sediments. Journal of Paleolimnology 28, 433–440. doi:10.1023/A:1021675501346

Blackford, J.J., Payne, R.J., Heggen, M.P., la Riva Caballero, de, A., van der Plicht, J., 2014. Age and impacts of the caldera-forming Aniakchak II eruption in western Alaska. Quaternary Research 82, 85–95. doi:10.1016/j.yqres.2014.04.013

Blockley, S.P.E., Ramsey, C.B., Lane, C.S., Lotter, A.F., 2008. Improved age modelling approaches as exemplified by the revised chronology for the Central European varved lake Soppensee. Quaternary Science Reviews 27, 61–71. doi:10.1016/j.quascirev.2007.01.018

Blockley, S.P.E., Bourne, A.J., Brauer, A., Davies, S.M., Hardiman, M., Harding, P.R., Lane, C.S., MacLeod, A., Matthews, I.P., Pyne-O'Donnell, S.D.F., Rasmussen, S.O., Wulf, S., Zanchetta, G., 2014. Tephrochronology and the extended intimate (integration of ice-core, marine and terrestrial records) event stratigraphy 8–128 ka b2k. Quaternary Science Reviews 106, 88–100. doi:10.1016/j.quascirev.2014.11.002

Blockley, S.P.E., Edwards, K.J., Schofield, J.E., Pyne-O'Donnell, S.D.F., Jensen, B.J.L., Matthews, I.P., Cook, G.T., Wallace, K.L., Froese, D.G., 2015. First evidence of cryptotephra in palaeoenvironmental records associated with Norse occupation sites in Greenland. Quaternary Geochronology 27, 145–157. doi:10.1016/j.quageo.2015.02.023

Bowers, P.M., 1979. The Cantwell ash bed, a Holocene tephra in the central Alaska Range, in: Alaska Division of Geological & Geophysical Surveys, Short Notes on Alaskan Geology - 1978: Alaska Division of Geological & Geophysical Surveys Geologic Report 61E, p. 19-24. doi:10.14509/412

Braitseva, O.A., Ponomareva, V.V., Sulerzhitsky, L., Melekestsev, I., Bailey, J., 1997. Holocene key-marker tephra layers in Kamchatka, Russia. Quaternary Research 47, 125–139. doi:10.1006/qres.1996.1876

Brock, F., Froese, D.G., Roberts, R.G., 2010. Low temperature (LT) combustion of sediments does not necessarily provide accurate radiocarbon ages for site chronology. Quaternary Geochronology 5, 625–630. doi:10.1016/j.quageo.2010.06.003

Bronk Ramsey, C. (2005) OxCal program v.3.10. Oxford University.

Bronk Ramsey, C., 2009a. Bayesian analysis of radiocarbon dates. Radiocarbon 51, 337–360.

Bronk Ramsey, C., 2009b. Dealing with outliers and offsets in radiocarbon dating. Radiocarbon 51, 1023–1045.

Bronk Ramsey, C., Albert, P.G., Blockley, S.P.E., Hardiman, M., Housley, R.A., Lane, C.S., Lee, S., Matthews, I.P., Smith, V.C., Lowe, J.J., 2015. Improved age estimates for key Late Quaternary European tephra horizons in the RESET lattice. Quaternary Science Reviews 118, 18–32. doi:10.1016/j.quascirev.2014.11.007

Browne, B.L., Gardner, J.E., Neal, C.A., Nicholson, R., 2003. The ~400 yr B.P. caldera-forming eruption Half Cone Volcano, Aniakchak Caldera, Alaska - Abstract, in: Alaska Geological Society Geology Symposium abstract volume. Alaska Geological Society, p. 27.

Buck, C.E., Higham, T.F.G., Lowe, D.J., 2003. Bayesian tools for tephrochronology. The Holocene 13, 639–647. doi:10.1191/0959683603hl652ft

Bull, K.F., Cameron, C.E., Coombs, M.L., Diefenbach, A.K., Lopez, T., McNutt, S.R., Neal, C.A., Payne, A.L., Power, J.A., Schneider, D.J., Scott, W.E., Snedigar, S., Thompson, G., Wallace, K.L., Waythomas, C.F., Webley, P.W., Werner, C.A., 2011. The 2009 eruption of Redoubt Volcano, Alaska, Alaska Division of Geological and Geophysical Surveys Report of Investigation. doi:10.14509/23123

Carson, E.C., Fournelle, J.H., Miller, T.P., Mickelson, D.M., 2002. Holocene tephrochronology of the Cold Bay area, southwest Alaska Peninsula. Quaternary Science Reviews 21, 2213–2228. doi:10.1016/S0277-3791(02)00023-9

Casadevall, T.J., 1994. The 1989–1990 eruption of Redoubt Volcano, Alaska: impacts on aircraft operations. Journal of Volcanology and Geothermal Research 62, 301–316. doi:10.1016/0377-0273(94)90038-8

Child, J.K., Beget, J.E., Werner, A., 1998. Three Holocene Tephras Identified in Lacustrine Sediment Cores from the Wonder Lake Area, Denali National Park and Preserve, Alaska, U.S.A. Arctic and Alpine Research 30, 89–95. doi:10.2307/1551749

Christen, J.A., 1994. Bayesian interpretation of ^{14}C results. PhD thesis, University of Nottingham.

Clague, J.J., Evans, S.G., Rampton, V.N., Woodsworth, G.J., 1995. Improved age estimates for the White River and Bridge River tephras, western Canada. Canadian Journal of Earth Sciences 32, 1172–1179. doi:10.1139/e95-096

Combellick, R.A., Pinney, D.S., 1995. Radiocarbon age of probable Hayes tephra, Kenai Peninsula, Alaska, in: Combellick, R.A., Tannian, F. (Eds.), Short Notes on Alaskan Geology. Alaska Division of Geological and Geophysical Surveys. Professional Report 117, 1-9.

Coulter, S.E., Pilcher, J.R., Plunkett, G., Baillie, M., Hall, V.A., Steffensen, J.P., Vinther, B.M., Clausen, H.B., Johnsen, S.J., 2012. Holocene tephras highlight complexity of volcanic signals in Greenland ice cores. Journal of Geophysical Research 117, D21303. doi:10.1029/2012JD017698

Davies, LJ, Froese, D.F.G., 2015. Major North American cryptotephra: Characterising key beds from the Holocene of northwestern North America. XIX INQUA Congress, Nagoya, Japan.

Davies, S.M., Turney, C.S.M., Lowe, J.J., 2001. Identification and significance of a visible, basalt-rich Vedde Ash layer in a Late-glacial sequence on the Isle of Skye, Inner Hebrides,

Scotland. Journal of Quaternary Science 16, 99–104. doi:10.1002/jqs.611

Davies, S.M., Wastegård, S., Wohlfarth, B., 2003. Extending the limits of the Borrobol Tephra to Scandinavia and detection of new early Holocene tephras. Quaternary Research 59, 345–352. doi:10.1016/S0033-5894(03)00035-8

Davies, S.M., Elmquist, M., Bergman, J., Wohlfarth, B., Hammarlund, D., 2007. Cryptotephra sedimentation processes within two lacustrine sequences from west central Sweden. The Holocene 17, 319–330. doi:10.1177/0959683607076443

Davies, S.M., Abbott, P.M., Pearce, N.J.G., Wastegård, S., Blockley, S.P.E., 2012. Integrating the INTIMATE records using tephrochronology: rising to the challenge. Quaternary Science Reviews 36, 11–27. doi:10.1016/j.quascirev.2011.04.005

Davies, S.M., Abbott, P.M., Meara, R.H., Pearce, N.J.G., Austin, W.E.N., Chapman, M.R., Svensson, A., Bigler, M., Rasmussen, T.L., Rasmussen, S.O., Farmer, E.J., 2014. A North Atlantic tephrostratigraphical framework for 130–60 ka b2k: new tephra discoveries, marine-based correlations, and future challenges. Quaternary Science Reviews 106, 101–121. doi:10.1016/j.quascirev.2014.03.024

Davies, S.M., 2015. Cryptotephras: the revolution in correlation and precision dating. Journal of Quaternary Science 30, 114–130. doi:10.1002/jqs.2766

de Fontaine, C.S., Kaufman, D.S., Anderson, R.S., Werner, A., Waythomas, C.F., Brown, T.A., 2007. Late Quaternary distal tephra-fall deposits in lacustrine sediments, Kenai Peninsula, Alaska. Quaternary Research 68, 64–78. doi:10.1016/j.yqres.2007.03.006

Demuro, M., Roberts, R.G., Froese, D.G., Arnold, L.J., Brock, F., Ramsey, C.B., 2008. Optically stimulated luminescence dating of single and multiple grains of quartz from perennially frozen loess in western Yukon Territory, Canada: Comparison with radiocarbon chronologies for the late Pleistocene Dawson tephra. Quaternary Geochronology 3, 346–364. doi:10.1016/j.quageo.2007.12.003

Denton, J.S., Pearce, N.J.G., 2008. Comment on "A synchronized dating of three Greenland ice cores throughout the Holocene" by B. M. Vinther et al.: No Minoan tephra in the 1642 B.C. layer of the GRIP ice core. Journal of Geophysical Research 113, D04303–7. doi:10.1029/2007JD008970

Dilley, T.E., 1988, Holocene tephra stratigraphy and pedogenesis in the middle Susitna River valley, Alaska: Fairbanks, University of Alaska, unpub. M.S. thesis, p. 97.

Dixon, E.J., 1985. Cultural chronology of central interior Alaska. Arctic Anthropology 22, 47-66. doi:10.2307/40316079

Dixon, E. J., Smith, G. S., 1990. A regional application of tephrochronology in Alaska. In: Lasca, N. P., Donahue, J. (Eds.), *Archaeological Geology of North America*. Centennial Special Volume 4. Boulder, Colo.: Geological Society of America, 383-398.

Dortch, J. M., Owen, L. A., Caffee, M. W., Li, D., Lowell, T. V., 2010. Beryllium-10 surface exposure dating of glacial successions in the Central Alaska Range. Journal of Quaternary Science 25, 1259–1269. doi:10.1002/jqs.1406

Dugmore, A.J., Newton, A.J., Edwards, K.J., Larsen, G., Blackford, J.J., Cook, G.T., 1996. Long-distance marker horizons from small-scale eruptions: British tephra deposits from the AD 1510 eruption of Hekla, Iceland. Journal of Quaternary Science 11, 511–516. doi:10.1002/(SICI)1099-1417(199611/12)11:6<511::AID-JQS284>3.0.CO;2-C

Dunning, H., 2011. Extending the applications of tephrochronology in Northwestern North America. *Msc Thesis*, University of Alberta.

Egan, J., Staff, R., Blackford, J., 2015. A revised age estimate of the Holocene Plinian eruption of Mount Mazama, Oregon using Bayesian statistical modelling. The Holocene 25, 1054–1067. doi:10.1177/0959683615576230

Evans, M.E., Jensen, B.J.L., Kravchinsky, V.A., Froese, D.G., 2011. The Kamikatsura event in the Gold Hill loess, Alaska. Geophysical Research Letters 38, L13302. doi:10.1029/2011GL047793

Fierstein, J., 2007. Explosive eruptive record in the Katmai region, Alaska Peninsula: an overview. Bulletin of Volcanology 69, 469–509. doi:10.1007/s00445-006-0097-y

Foit, F.F., Jr, Gavin, D.G., Hu, F.S., 2004. The tephra stratigraphy of two lakes in south-central British Columbia, Canada and its implications for mid-late Holocene volcanic activity at Glacier Peak and Mount St. Helens, Washington, USA. Canadian Journal of Earth Sciences 41, 1401–1410. doi:10.1139/e04-081

Fraser, T.A., Burn, C.R., 1997. On the nature and origin of “muck” deposits in the Klondike area, Yukon Territory. Canadian Journal of Earth Sciences 34, 1333–1344. doi:10.1139/e17-106

Froese, D.G., Westgate, J., Preece, S., Storer, J., 2002. Age and significance of the Late Pleistocene Dawson tephra in eastern Beringia. Quaternary Science Reviews 21, 2137–2142. doi:10.1016/S0277-3791(02)00038-0

Froese, D.G., Zazula, G.D., Reyes, A.V., 2006. Seasonality of the late Pleistocene Dawson tephra and exceptional preservation of a buried riparian surface in central Yukon Territory, Canada. Quaternary Science Reviews 25, 1542–1551. doi:10.1016/j.quascirev.2006.01.028

Froggatt, P.C., 1992. Standardization of the chemical analysis of tephra deposits. Report of the ICCT Working Group. Quaternary International 13-14, 93–96. doi:10.1016/1040-6182(92)90014-S

Goetcheus, V.G., Birks, H.H., 2001. Full-glacial upland tundra vegetation preserved under tephra in the Beringia National Park, Seward Peninsula, Alaska. Quaternary Science Reviews 20, 135–147. doi:10.1016/S0277-3791(00)00127-X

Hildreth, W., Fierstein, J., 2012. The Novarupta-Katmai Eruption of 1912: Largest Eruption of the Twentieth Century: Centennial Perspectives. U.S. Geological Survey Professional Paper 1791, p. 259.

Höfle, C., Ping, C.L., 1996. Properties and soil development of late-Pleistocene paleosols from Seward Peninsula, northwest Alaska. Geoderma 71, 219–243. doi:10.1016/0016-7061(96)00007-9

Höfle, C., Edwards, M.E., Hopkins, D.M., Mann, D.H., Ping, C.-L., 2000. The Full-Glacial Environment of the Northern Seward Peninsula, Alaska, Reconstructed from the 21,500-Year-Old Kitluk Paleosol. Quaternary Research 53, 143–153. doi:10.1006/qres.1999.2097

Hopkins, D.M., 1988. The Espenberg maars: a record of explosive volcanic activity in the Devil Mountain-Cape Espenberg area, Seward Peninsula, Alaska, in: Schaaf, J. (Ed.), The Bering Land Bridge National Preserve: An Archeological Survey. National Park Service, Alaska Region Research/Management Report AR-14, Anchorage. p. 262-321.

Hughen, K., Southon, J., Lehman, S., Bertrand, C., Turnbull, J., 2006. Marine-derived 14C calibration and activity record for the past 50,000 years updated from the Cariaco Basin. Quaternary Science Reviews 25, 3216–3227. doi:10.1016/j.quascirev.2006.03.014

Hunt, J.B., Hill, P.G., 1996. An inter-laboratory comparison of the electron probe microanalysis of glass geochemistry. Quaternary International 34-36, 229–241. doi:10.1016/1040-6182(95)00088-7

Jensen, B.J.L., Froese, D.G., 2006. Characterization and revised distribution of the White River Ash in Yukon Territory and eastern Alaska, in: Program and Abstracts, 36th International Arctic Workshop, March 16–19, 2006: Boulder, Colorado. Institute of Arctic and Alpine Research, University of Colorado.

Jensen, B.J.L., Froese, D.G., Preece, S.J., Westgate, J.A., Stachel, T., 2008. An extensive middle to late Pleistocene tephrochronologic record from east-central Alaska. Quaternary Science Reviews 27, 411–427. doi:10.1016/j.quascirev.2007.10.010

Jensen, B.J.L., Preece, S.J., Lamothe, M., Pearce, N.J.G., Froese, D.G., Westgate, J.A., Schaefer, J., Beget, J.E., 2011. The variegated (VT) tephra: A new regional marker for middle to late marine isotope stage 5 across Yukon and Alaska. Quaternary International 1–12. doi:10.1016/j.quaint.2011.06.028

Jensen, B.J.L., Reyes, A.V., Froese, D.G. (2013) Marine tephrostratigraphy in the Gulf of Alaska and comparison to terrestrial records from eastern Beringia, in: Program and Abstracts, CANQUA-CGRG biannual meeting, August 18-21, 2013: University of Alberta, Edmonton.

Jensen, B.J.L., Pyne-O'Donnell, S.D.F., Plunkett, G., Froese, D.G., Hughes, P.D.M., Sigl, M., McConnell, J.R., Amesbury, M.J., Blackwell, P.G., van den Bogaard, C., Buck, C.E., Charman, D.J., Clague, J.J., Hall, V.A., Koch, J., Mackay, H., Mallon, G., McColl, L.,

Pilcher, J.R., 2014a. Transatlantic distribution of the Alaskan White River Ash. Geology 42, 875–878. doi:10.1130/G35945.1

Jensen, B.J.L., Mackay, H., Pyne-O'Donnell, S.D.F., Plunkett, G., Hughes, P.D.M., Froese, D.G., Booth, R., 2014b. Exceptionally Long Distance Transport of Volcanic Ash: Implications for Stratigraphy, Hazards and the Sourcing of Distal Tephra Deposits. American Geophysical Union Fall Meeting, Dec 15-19, San Francisco.

Jensen, B.J.L., Evans, M.E., Froese, D.G., Kravchinsky, V.A., 2016. 150,000 years of loess accumulation in central Alaska. Quaternary Science Reviews 135, 1–23. doi:10.1016/j.quascirev.2016.01.001

Karrow, P.F., Anderson, T.W., 1975. Palynological study of lake sediment profiles from southwestern New Brunswick: Discussion. Canadian Journal of Earth Sciences 12, 1808–1812. doi:10.1139/e75-161

Kaufman, D.S., Jensen, B.J.L., Reyes, A.V., Schiff, C.J., Froese, D.G., Pearce, N.J.G., 2012. Late Quaternary tephrostratigraphy, Ahklun Mountains, SW Alaska. Journal of Quaternary Science 27, 344–359. doi:10.1002/jqs.1552

Kennedy, K.E., Froese, D.G., Zazula, G.D., Lauriol, B., 2010. Last Glacial Maximum age for the northwest Laurentide maximum from the Eagle River spillway and delta complex, northern Yukon. Quaternary Science Reviews 29, 1288–1300. doi:10.1016/j.quascirev.2010.02.015

Kuehn, S.C., Froese, D.G., Carrara, P.E., Foit, F.F., Jr, Pearce, N.J.G., Rotheisler, P., 2009a. Major- and trace-element characterization, expanded distribution, and a new chronology for the latest Pleistocene Glacier Peak tephras in western North America. Quaternary Research 71, 201–216. doi:10.1016/j.yqres.2008.11.003

Kuehn, S.C., Froese, D.G., Pearce, N.J.G., Foit, F.F., 2009b. ID3506, a New/Old Lipari Obsidian Standard for Characterization of Natural Glasses and Tephrochronology: Eos Transactions of the AGU, Fall Meet. Suppl., Abstract V31E-2010.

Kuehn, S.C., Froese, D.G., Shane, P.A.R., INTAV Intercomparison Participants, 2011. The INTAV intercomparison of electron-beam microanalysis of glass by tephrochronology laboratories: Results and recommendations. Quaternary International 1–29. doi:10.1016/j.quaint.2011.08.022

Lakeman, T.R., Clague, J.J., Menounos, B., Osborn, G.D., Jensen, B.J.L., Froese, D.G., 2008. Holocene tephras in lake cores from northern British Columbia, Canada. Canadian Journal of Earth Sciences 45, 935–947. doi:10.1139/E08-035

Lane, C.S., Blockley, S.P.E., Mangerud, J., Smith, V.C., Lohne, Ø.S., Tomlinson, E.L., Matthews, I.P., Lotter, A.F., 2012. Was the 12.1ka Icelandic Vedde Ash one of a kind? Quaternary Science Reviews 33, 87–99. doi:10.1016/j.quascirev.2011.11.011

Lane, C.S., Brauer, A., Blockley, S.P.E., Dulski, P., 2013. Volcanic ash reveals time-

transgressive abrupt climate change during the Younger Dryas. Geology 41, 1251–1254. doi:10.1130/G34867.1

Larsen, J.F., Neal, C., Schaefer, J., Beget, J.E., Nye, C.J., 2007. Late Pleistocene and Holocene Caldera-Forming Eruptions of Okmok Caldera, Aleutian Islands, Alaska, in: Eichelberger, J., Gordeev, E., Izbekov, P., Kasahara, M., Lees, J., (Eds.), Volcanism and Subduction: The Kamchatka Region, Geophysical Monograph Series 172. American Geophysical Union, Washington, D. C. doi:10.1029/172GM24

Lerbekmo, J.F., 2008. The White River Ash: Largest Holocene Plinian tephra. Canadian Journal of Earth Sciences 45, 693–700, doi:10.1139/E08-023.

Lerbekmo, J.F., Campbell, F.A., 1969. Distribution, composition, and the source of the White River Ash, Yukon Territory. Canadian Journal of Earth Sciences 6, 109–116. doi:10.1139/e69 -011 .

Lerbekmo, J.F., Westgate, J.A., Smith, D.G.W., Denton, G.H., 1975. New data on the character and history of the White River volcanic eruption, Alaska, in: Suggate, R.P., Cresswell, M.M., (Eds.), Quaternary studies. Wellington, Royal Society of New Zealand, p. 203–209.

Lohne, Ø.S., Mangerud, J., Birks, H.H., 2013. Precise 14C ages of the Vedde and Saksunarvatn ashes and the Younger Dryas boundaries from western Norway and their comparison with the Greenland Ice Core (GICC05) chronology. Journal of Quaternary Science 28, 490–500. doi:10.1002/jqs.2640

Lowe, D.J., 2011. Tephrochronology and its application: A review. Quaternary Geochronology 6, 107–153. doi:10.1016/j.quageo.2010.08.003

Lowe, D.J., Alloway, B., 2015. Tephrochronology, in: Rink, W.J., Thompson, J.W. (Eds.), Encyclopedia of Scientific Dating Methods, Encyclopedia of Earth Sciences Series. Springer Netherlands, Dordrecht, pp. 783–799. doi:10.1007/978-94-007-6304-3_19

Lowe, D.J., McFadgen, B.G., Higham, T.F.G., Hogg, A.G., Froggatt, P.C., Nairn, I.A., 1998. Radiocarbon age of the Kaharoa Tephra, a key marker for late- Holocene stratigraphy and archaeology in New Zealand. The Holocene 8, 487–495. doi:10.1191/095968398667037879

Lowe, D.J., Blaauw, M., Hogg, A.G., 2013. Ages of 24 widespread tephras erupted since 30,000 years ago in New Zealand, with re-evaluation of the timing and palaeoclimatic implications of the Lateglacial cool episode recorded at Kaipo bog. Quaternary Science Reviews 74, 170–194. doi:10.1016/j.quascirev.2012.11.022

Lowe, J.J., Walker, M.J.C., 2000. Radiocarbon dating the last glacial-interglacial transition (ca. 14-9 ^{14}C ka BP) in terrestrial and marine records: The need for new quality assurance protocols. Radiocarbon 42, 53–68.

Lowe, J.J., Blockley, S., Trincardi, F., Asioli, A., Cattaneo, A., Matthews, I.P., Pollard, M., Wulf, S., 2007. Age modelling of late Quaternary marine sequences in the Adriatic: Towards

improved precision and accuracy using volcanic event stratigraphy. Continental Shelf Research 27, 560–582. doi:10.1016/j.csr.2005.12.017

Lowe, J.J., Barton, N., Blockley, S., Ramsey, C.B., Cullen, V.L., Davies, W., Gamble, C., Grant, K., Hardiman, M., Housley, R., Lane, C.S., Lee, S., Lewis, M., MacLeod, A., Menzies, M., Müller, W., Pollard, M., Price, C., Roberts, A.P., Rohling, E.J., Satow, C., Smith, V.C., Stringer, C.B., Tomlinson, E.L., White, D., Albert, P., Arienzo, I., Barker, G., Borić, D., Carandente, A., Civetta, L., Ferrier, C., Guadelli, J.-L., Karkanas, P., Koumouzelis, M., Müller, U.C., Orsi, G., Pross, J., Rosi, M., Shalamanov-Korobar, L., Sirakov, N., Tzedakis, P.C., 2012. Volcanic ash layers illuminate the resilience of Neanderthals and early modern humans to natural hazards. Proceedings of the National Academy of Sciences 109, 13532–13537. doi:10.1073/pnas.1204579109

Lynch, J.A., Clark, J.S., Bigelow, N.H., Edwards, M.E., Finney, B.P., 2002. Geographic and temporal variations in fire history in boreal ecosystems of Alaska. Journal of Geophysical Research 108, 8152–17. doi:10.1029/2001JD000332

Macáas, J.L., Sheridan, M.F., 1995. Products of the 1907 eruption of Shtyubel' Volcano, Ksudach Caldera, Kamchatka, Russia. Geological Society of America Bulletin 107, 969–0986. doi:10.1130/0016-7606(1995)107<0969:POTEOS>2.3.CO;2

Mackay, H., Hughes, P.D.M., Jensen, B.J.L., Langdon, P.G., Pyne-O'Donnell, S.D.F., Plunkett, G., Froese, D.G., Coulter, S., Gardner, J.E., 2016. A mid to late Holocene cryptotephra framework from eastern North America. Quaternary Science Reviews 132, 101–113. doi:10.1016/j.quascirev.2015.11.011

MacLeod, A., Matthews, I.P., Lowe, J.J., Palmer, A.P., Albert, P.G., 2015. A second tephra isochron for the Younger Dryas period in northern Europe: The Abernethy Tephra. Quaternary Geochronology 28, 1–11. doi:10.1016/j.quageo.2015.03.010

Mangan, M.T., Waythomas, C.F., Miller, T.P., Trusdell, F.A., 2003. Emmons Lake Volcanic Center, Alaska Peninsula: source of the Late Wisconsin Dawson tephra, Yukon Territory, Canada. Can. J. Earth Sci. 40, 925–936. doi:10.1139/e03-026

Matthews, I.P., Birks, H.H., Bourne, A.J., Brooks, S.J., Lowe, J.J., MacLeod, A., Pyne-O'Donnell, S.D.F., 2011. New age estimates and climatostratigraphic correlations for the Borrobol and Penifiler Tephras: evidence from Abernethy Forest, Scotland. Journal of Quaternary Science 26, 247–252. doi:10.1002/jqs.1498

McGimsey, R.G., Richter, D.H., duBois, G.D., Miller, T.P., 1992. A Postulated New Source for the White River Ash, Alaska, in: Bradley, D.C., Ford, A.B., (Eds.), U.S. Geological Survey Bulletin B 1999, 212-218.

McGimsey, RG, Neal, CA, Riley, CM (2001) Areal Distribution, Thickness, Mass, Volume, and Grain Size of Tephra-Fall Deposits from the 1992 Eruptions of Crater Peak Vent, Mt. Spurr Volcano, Alaska. USGS Open-File Report 01–370, p. 32.

Miller, T.P., Smith, R.L., 1987. Late Quaternary caldera-forming eruptions in the eastern Aleutian arc, Alaska. Geology 15, 434–438. doi:10.1130/0091-7613(1987)15<434:LQCEIT>2.0.CO;2

Miller, T.P., McGimsey, R.G., Richter, D.H., Riehle, J.R., Nye, C.J., Yount, M.E., Dumoulin, J.A., 1998. Catalog of the historically active volcanoes of Alaska, U.S. Geological Survey Open-File Report OF 98-0582, p. 104.

Moodie, D.W., Catchpole, A.J.W., Abel, K., 1992. Northern Athapaskan Oral Traditions and the White River Volcano. Ethnohistory 39, 148. doi:10.2307/482391

Moriwaki, H., Nakamura, N., Nagasako, T., Lowe, D.J., Sangawa, T., 2016. The role of tephras in developing a high-precision chronostratigraphy for palaeoenvironmental reconstruction and archaeology in southern Kyushu, Japan, since 30,000 cal. BP: An integration. Quaternary International 397, 79–92. doi:10.1016/j.quaint.2015.05.069

Muhs, D.R., Ager, T.A., Been, J., Bradbury, J.P., Dean, W.E., 2003. A late quaternary record of eolian silt deposition in a maar lake, St. Michael Island, western Alaska. Quaternary Research 60, 110–122. doi:10.1016/S0033-5894(03)00062-0

Mullen, P.O., 2012. An archaeological test of the effects of the White River Ash eruptions: Arctic Anthropology 49, 35–44, doi:10.1353 /arc.2012.0013.

Mulliken, K., 2016. Holocene volcanism and human occupation in the middle Susitna River Valley, Alaska. *Msc Thesis*, University of Alaska Fairbanks.

Muscheler, R., Adolphi, F., Knudsen, M.F., 2014. Assessing the differences between the IntCal and Greenland ice-core time scales for the last 14,000 years via the common cosmogenic radionuclide variations. Quaternary Science Reviews 106, 81–87. doi:10.1016/j.quascirev.2014.08.017

Naeser, N.D., Westgate, J.A., Hughes, O.L., Péwé, T.L., 1982. Fission-track ages of late Cenozoic distal tephra beds in the Yukon Territory and Alaska. Canadian Journal of Earth Sciences 19, 2167–2178. doi:10.1139/e82-191

Neal, C., McGimsey, R.G., Miller, T.P., Riehle, J.P., Waythomas, C.F., 2001. Preliminary volcano-hazard assessment for Aniakchak Volcano, Alaska. U.S. Geological Survey Open-File Report OF 00-0519, p. 35.

Nelson, R.E., Carter, L.D., Robinson, S.W., 1988. Anomalous radiocarbon ages from a Holocene detrital organic lens in Alaska and their implications for radiocarbon dating and paleoenvironmental reconstructions in the arctic. Quaternary Research 29, 66–71. doi:10.1016/0033-5894(88)90072-5

Nilsson, M., Klarqvist, M., Bohlin, E., Possnert, G., 2001. Variation in 14C age of macrofossils and different fractions of minute peat samples dated by AMS. The Holocene 11, 579–586. doi:10.1191/095968301680223521

Olsson, I.U., 1974. Some problems in connection with the evaluation of C 14dates. Geologiska Föreningen i Stockholm Förhandlingar 96, 311–320. doi:10.1080/11035897409454285

Olsson I (1986) Radiometric Methods, in: Berglund B (Ed) Handbook of Holocene palaeoecolgy and palaeohydrology. John Wiley and Sons, Chichester, 273-312.

Oswald, W.W., Anderson, P.M., Brown, T.A., Brubaker, L.B., Hu, F.S., Lozhkin, A.V., Tinner, W., Kaltenrieder, P., 2005. Effects of sample mass and macrofossil type on radiocarbon dating of arctic and boreal lake sediments. The Holocene 15, 758–767. doi:10.1191/0959683605hl849rr

Payne, R., Gehrels, M.J., 2010. The formation of tephra layers in peatlands: An experimental approach. Catena 81, 12–23. doi:10.1016/j.catena.2009.12.001

Payne, R., Blackford, J., van der Plicht, J., 2008. Using cryptotephras to extend regional tephrochronologies: An example from southeast Alaska and implications for hazard assessment. Quaternary Research 69, 42–55. doi:10.1016/j.yqres.2007.10.007

Pearce, N.J.G., Westgate, J.A., Preece, S.J., Eastwood, W.J., Perkins, W.T., 2004. Identification of Aniakchak (Alaska) tephra in Greenland ice core challenges the 1645 BC date for Minoan eruption of Santorini. Geochemistry, Geophysics, Geosystems 5, Q03005. doi:10.1029/2003GC000672

Péwé, T.L., 1975. Quaternary Geology of Alaska. U.S. Geological Survey Professional Paper 835.

Péwé, T.L., Westgate, J.A., Preece, S.J., Brown, P.M., Leavitt, S.W., 2009. Late Pliocene Dawson Cut Forest Bed and new tephrochronological findings in the Gold Hill Loess, east-central Alaska. Geological Society of America Bulletin 121, 294–320. doi:10.1130/B26323.1

Pilcher, J.R., Hall, V.A., McCormac, F.G., 1995. Dates of Holocene Icelandic volcanic eruptions from tephra layers in Irish peats. The Holocene 5, 103–110. doi:10.1177/095968369500500111

Pilcher, J.R., Hall, V.A., McCormac, F.G., 1996. An outline tephrochronology for the Holocene of the north of Ireland. Journal of Quaternary Science 11, 485–494. doi:10.1002/(SICI)1099-1417(199611/12)11:6<485::AID-JQS266>3.3.CO;2-K

Ponomareva, V.V., Polyak, L., Portnyagin, M., Abbott, P., Davies, S., 2014. A Holocene cryptotephra record from the Chukchi margin: the first tephrostratigraphic study in the Arctic Ocean. Presented at the PAST Gateways International Conference and Workshop, Trieste, Italy.

Preece, S.J., Westgate, J.A., Stemper, B.A., Péwé, T.L., 1999. Tephrochronology of late Cenozoic loess at Fairbanks, central Alaska. Geological Society of America Bulletin 111, 71–90. doi:10.1130/0016-7606(1999)111<0071:TOLCLA>2.3.CO;2

Preece, S.J., Pearce, N.J.G., Westgate, J.A., Froese, D.G., Jensen, B.J.L., Perkins, W.T., 2011a. Old Crow tephra across eastern Beringia: a single cataclysmic eruption at the close of Marine Isotope Stage 6. Quaternary Science Reviews 30, 2069–2090. doi:10.1016/j.quascirev.2010.04.020

Preece, S.J., Westgate, J.A., Froese, D.G., Pearce, N.J.G., Perkins, W.T., Fisher, T., 2011b. A catalogue of late Cenozoic tephra beds in the Klondike goldfields and adjacent areas, Yukon Territory 11Yukon Geological Survey Contribution 010. Can. J. Earth Sci. 48, 1386–1418. doi:10.1139/e10-110

Preece, S.J., McGimsey, R.G., Westgate, J.A., Pearce, N., Hart, W.K., Perkins, W.T., 2014. Chemical complexity and source of the White River Ash, Alaska and Yukon. Geosphere 10, 1020–1024. doi:10.1130/GES00953.1

Pyne-O'Donnell, S.D.F., 2007. Three new distal tephras in sediments spanning the Last Glacial–Interglacial Transition in Scotland. Journal of Quaternary Science 22, 559–570. doi:10.1002/jqs.1066

Pyne-O'Donnell, S.D.F., 2010. The taphonomy of Last Glacial-Interglacial Transition (LGIT) distal volcanic ash in small Scottish lakes. Boreas 40, 131–145. doi:10.1111/j.1502-3885.2010.00154.x

Pyne-O'Donnell, S.D.F., Hughes, P., Froese, D.G., Jensen, B.J.L., Kuehn, S.C., Mallon, G., Amesbury, M.J., Charman, D.J., Daley, T.J., Loader, N.J., Mauquoy, D., Street-Perrott, F.A., Woodman-Ralph, J., 2012. High-precision ultra-distal Holocene tephrochronology in North America. Quaternary Science Reviews 52, 6–11. doi:10.1016/j.quascirev.2012.07.024

Pyne-O'Donnell, S.D.F., Cwynar, L.C., Jensen, B.J.L., Vincent, J.H., Kuehn, S.C., Spear, R., Froese, D.G., 2016. West Coast volcanic ashes provide a new continental-scale Lateglacial isochron. Quaternary Science Reviews 142, 16–25. doi:10.1016/j.quascirev.2016.04.014

Reimer, P.J., Baillie, M.G.L., Bard, E., Bayliss, A., Beck, J.W., Blackwell, P.G., Bronk Ramsey, C., Buck, C.E., Burr, G.S., Edwards, R.L., Friedrich, M., Grootes, P.M., Guilderson, T.P., Hajdas, I., Heaton, T.J., Hogg, A.G., Hughen, K.A., Kaiser, K.F., Kromer, B., McCormac, F.G., Manning, S.W., Reimer, R.W., Richards, D.A., Southon, J.R., Talamo, S., Turney, C.S.M., Plicht, J.v.d., 2009. IntCal09 and Marine09 radiocarbon age calibration curves, 0–50,000 years cal BP. Radiocarbon 51, 1111-1150.

Reimer P.J., Bard, E., Bayliss, A., Beck, J.W., Blackwell, P.G., Ramsey, C.B., Buck, C.E., Cheng, H., Edwards, R.L., Friedrich, M., Grootes, P.M., Guilderson, T.P., Haflidason, H., Hajdas, I., Hatté, C., Heaton, T.J., Hoffmann, D.L., Hogg, A.G., Hughen, K.A., Kaiser, K.F., Kromer, B., Manning, S.W., Niu, M., Reimer, R.W., Richards, D.A., Scott, E.M., Southon, J.R., Staff, R.A., Turney, C.S.M., Plicht, J.v.d., 2013. IntCal13 and Marine13 radiocarbon age calibration curves 0-50,000 years cal BP: Radiocarbon 55, 1869–87.

Reyes, A.V., Cooke, C.A., 2011. Northern peatland initiation lagged abrupt increases in

deglacial atmospheric CH4. Proceedings of the National Academy of Sciences 108, 4748–4753. doi:10.1073/pnas.1013270108

Richter, D.H., Preece, S.J., McGimsey, R.G., Westgate, J.A., 1995. Mount Churchill, Alaska: source of the late Holocene White River Ash. Canadian Journal of Earth Sciences 32, 741–748. doi:10.1139/e95-063

Riehle, J.R., 1985. A reconnaissance of the major Holocene tephra deposits in the upper Cook Inlet region, Alaska. Journal of Volcanology and Geothermal Research 26, 37–74. doi:10.1016/0377-0273(85)90046-0

Riehle, J.R., 1994. Heterogeneity, Correlatives, and Proposed Stratigraphic Nomenclature of Hayes Tephra Set H, Alaska. Quaternary Research 41, 285–288. doi:10.1006/qres.1994.1032

Riehle, J.R., Brew, D.A., 1984. Explosive latest Pleistocene(?) and Holocene activity of the Mount Edgecumbe volcanic field, Alaska. In: Reed, K.M., Bartsch-Winkler, S. (Eds.), The United States Geological Survey in Alaska: accomplishments during 1982, 111–115.

Riehle, J.R., Meyer, C.E., Ager, T.A., Kaufman, D.S., Ackerman, R.E., 1987. The Aniakchak tephra deposit, a late Holocene marker horizon in western Alaska, in: Hamilton, T.D., Galloway, J.P. (Eds.) Geologic Studies in Alaska by the U.S. Geological Survey during 1986. U.S. Geological Survey Circular 998.

Riehle, J.R., Bowers, P.M., Ager, T.A., 1990. The Hayes tephra deposits, and upper Holocene marker horizon in south-central Alaska. Quaternary Research 33, 276–290. doi:10.1016/0033-5894(90)90056-Q

Riehle, J. R., Meyer, C. E., Miyaoka, R. T., 1999. Data on Holocene tephra (volcanic ash) deposits in the Alaska Peninsula and lower Cook Inlet region of the Aleutian volcanic arc, Alaska: U.S. Geological Survey Open-File Report OF 99-0135.

Sanborn, P.T., Smith, C.A.S., Froese, D.G., Zazula, G.D., Westgate, J.A., 2006. Full-glacial paleosols in perennially frozen loess sequences, Klondike goldfields, Yukon Territory, Canada. Quaternary Research 66, 147–157. doi:10.1016/j.yqres.2006.02.008

Schiff, C.J., Kaufman, D.S., Wallace, K.L., Werner, A., Ku, T.-L., Brown, T.A., 2008. Modeled tephra ages from lake sediments, base of Redoubt Volcano, Alaska. Quaternary Geochronology 3, 56–67. doi:10.1016/j.quageo.2007.05.001

Schiff, C.J., Kaufman, D.S., Wallace, K.L., Ketterer, M.E., 2010. An improved proximal tephrochronology for Redoubt Volcano, Alaska. Journal of Volcanology and Geothermal Research 193, 203–214. doi:10.1016/j.jvolgeores.2010.03.015

Scott, W.E., McGimsey, R.G., 1994. Character, mass, distribution, and origin of tephra-fall deposits of the 1989–1990 eruption of redoubt volcano, south-central Alaska. Journal of Volcanology and Geothermal Research 62, 251–272. doi:10.1016/0377-0273(94)90036-1

Smith, D.G.W., Westgate, J.A., 1968. Electron probe technique for characterising pyroclastic deposits. Earth and Planetary Science Letters 5, 313–319. doi:10.1016/S0012-821X(68)80058-5

Smith, V.C., Pearce, N.J.G., Matthews, N.E., Westgate, J.A., Petraglia, M.D., Haslam, M., Lane, C.S., Korisettar, R., Pal, J.N., 2011. Geochemical fingerprinting of the widespread Toba tephra using biotite compositions. Quaternary International 246, 97–104. doi:10.1016/j.quaint.2011.05.012

Smith, V.C., Staff, R.A., Blockley, S.P.E., Bronk Ramsey, C., Nakagawa, T., Mark, D.F., Takemura, K., Danhara, T., Suigetsu 2006 project members, 2013. Identification and correlation of visible tephras in the Lake Suigetsu SG06 sedimentary archive, Japan: chronostratigraphic markers for synchronising of east Asian/west Pacific palaeoclimatic records across the last 150 ka. Quaternary Science Reviews 67, 121–137. doi:10.1016/j.quascirev.2013.01.026

Spiker, E., Kelley, L., Rubin, M., 1978. US Geological Survey radiocarbon dates XIII. Radiocarbon 20, 139-156.

Stelling, P., Gardner, J.E., Beget, J.E., 2005. Eruptive history of Fisher Caldera, Alaska, USA. Journal of Volcanology and Geothermal Research 139, 163–183. doi:10.1016/j.jvolgeores.2004.08.006

Streeter, R., Dugmore, A., 2014. Late-Holocene land surface change in a coupled social-ecological system, southern Iceland: a cross-scale tephrochronology approach. Quaternary Science Reviews 86, 99–114. doi:10.1016/j.quascirev.2013.12.016

Thorarinsson, S., (1954) The tephra-fall from Hekla on March 29, 1947, in: The Eruption of Hekla 1947– 48, part 2. Soc. Sci. Islandica, Reykjavik, 1-68.

Torbenson, M.C.A., Plunkett, G., Brown, D.M., Pilcher, J.R., Leuschner, H.H., 2015. Asynchrony in key Holocene chronologies: Evidence from Irish bog pines. Geology 43, 799–802. doi:10.1130/G36914.1

Turner, R., Hurst, T., 2001. Factors influencing volcanic ash dispersal from the 1995 and 1996 eruptions of Mount Ruapehu, New Zealand. Journal of Applied Meteorology 40, 56–69. doi:10.1175/1520-0450(2001)040<0056:FIVADF>2.0.CO;2

Turney, C., Harkness, D.D., Lowe, J.J., 1997. The use of microtephra horizons to correlate Late-glacial lake sediment successions in Scotland. Journal of Quaternary Science 525–531. doi:10.1002/(SICI)1099-1417(199711/12)12:63.3.CO;2-D

VanderHoek, R., Myron, R., 2004. An archaeological overview and assessment of Aniakchak National Monument and Preserve. U.S. National Park Service Research/Resources Management Report AR/CRR-2004-47.

Vinther, B.M., Clausen, H.B., Johnsen, S.J., Rasmussen, S.O., Andersen, K.K., Buchardt, S.L., Dahl-Jensen, D., Seierstad, I.K., Siggaard-Andersen, M.L., Steffensen, J.P., Svensson, A., Olsen, J., Heinemeier, J., 2006. A synchronized dating of three Greenland ice cores throughout the Holocene. Journal of Geophysical Research 111, D13102. doi:10.1029/2005JD006921

Wallace, K.L., Coombs, M.L., Hayden, L.A., Waythomas, C.F., 2014. Significance of a near-source tephra-stratigraphic sequence to the eruptive history of Hayes Volcano, south-central Alaska. U.S. Geological Survey Scientific Investigations Report 2014-5133. doi:10.3133/sir20145133.

Wastegård, S., 2002. Early to middle Holocene silicic tephra horizons from the Katla volcanic system, Iceland: new results from the Faroe Islands. Journal of Quaternary Science 17, 723–730. doi:10.1002/jqs.724

Watson, E.J., Swindles, G., Lawson, I.T., Savov, I.P., 2015. Spatial variability of tephra and carbon accumulation in a Holocene peatland. Quaternary Science Reviews 124, 248–264. doi:10.1016/j.quascirev.2015.07.025

Watt, S.F.L., Pyle, D.M., Mather, T.A., Martin, R.S., Matthews, N.E., 2009. Fallout and distribution of volcanic ash over Argentina following the May 2008 explosive eruption of Chaitén, Chile. Journal of Geophysical Research 114, B04207–11. doi:10.1029/2008JB006219

Westgate, J.A., Gorton, M.P., 1981. Correlation techniques in tephra studies, in: Self, S., Sparks, R.S.J., (Eds.), Tephra Studies. Reidel, Dordrecht, pp. 73-94.

Westgate, J.A., Smith, D., Nichols, H., 1969. Late Quaternary pyroclastic layers in the Edmonton area, Alberta. Geology Department Contract 464, 179-86, University of Alberta.

Westgate, J.A., Smith, D., Tomlinson, M., 1970. Late Quaternary tephra layers in southwestern Canada, in: Smith, R.A., Smith, J.W. (Eds.), Early Man and Environments in Northwest North America. Proceedings of the Second Annual Palaeo-environmental Workshop, University of Calgary Archaeological Association, The Students' Press, Calgary, Alberta, 13–34.

Westgate, J.A., Preece, S.J., Kotler, E., Hall, S., 2000. Dawson tephra: a prominent stratigraphic marker of Late Wisconsinan age in west-central Yukon, Canada. Canadian Journal of Earth Sciences 37, 621–627. doi:10.1139/cjes-37-4-621

Westgate, J.A., Preece, S.J., Froese, D.G., Pearce, N.J.G., Roberts, R.G., Demuro, M., Hart, W.K., Perkins, W., 2008. Changing ideas on the identity and stratigraphic significance of the Sheep Creek tephra beds in Alaska and the Yukon Territory, northwestern North America. Quaternary International 178, 183–209. doi:10.1016/j.quaint.2007.03.009

Westgate, J.A., Pearce, N.J.G., Perkins, W.T., Preece, S.J., CHESNER, C.A., MUHAMMAD, R.F., 2013. Tephrochronology of the Toba tuffs: four primary glass populations define the

75-ka Youngest Toba Tuff, northern Sumatra, Indonesia. Journal of Quaternary Science 28, 772–776. doi:10.1002/jqs.2672

Wilson, S.R., Ward, G.K., 1981. Evaluation and clustering of radiocarbon age determinations: procedures and paradigms. Archaeometry 23, 19–39. doi:10.1111/j.1475-4754.1981.tb00952.x

Wohlfarth, B., Blaauw, M., Davies, S.M., Andersson, M., Wastegård, S., Hormes, A., Possnert, G., 2006. Constraining the age of Lateglacial and early Holocene pollen zones and tephra horizons in southern Sweden with Bayesian probability methods. Journal of Quaternary Science 21, 321–334. doi:10.1002/jqs.996

Yalcin, K., Wake, C.P., Germani, M.S., 2003. A 100-year record of North Pacific volcanism in an ice core from Eclipse Icefield, Yukon Territory, Canada. J. Geophys. Res. 108, 4012–12. doi:10.1029/2002JD002449

Zdanowicz, C., Fisher, D., Bourgeois, J., Demuth, M., Zheng, J., Mayewski, P.A., Kreutz, K., Osterberg, E., Yalcin, K., Wake, C., Steig, E.J., Froese, D.G., Goto-Azuma, K., 2014. Ice Cores from the St. Elias Mountains, Yukon, Canada: Their Significance for Climate, Atmospheric Composition and Volcanism in the North Pacific Region. Arctic 67, 35–24. doi:10.14430/arctic4352

Zimov, S.A., Voropaev, Y.V., Semiletov, I.P., Davidov, S.P., Prosiannikov, S.F., Chapin, F.S., Chapin, M.C., Trumbore, S., Tyler, S., 1997. North Siberian Lakes: A Methane Source Fueled by Pleistocene Carbon. Science 277, 800–802. doi:10.1126/science.277.5327.800

Zoltai, S.C., 1989. Late Quaternary volcanic ash in the peatlands of central Alberta. Canadian Journal of Earth Sciences 26, 207–214. doi:10.1139/e89-017

CHAPTER 3: A HOLOCENE CRYPTOTEPHRA RECORD FROM NORTHWESTERN CANADA WITH MORE THAN 34 DISTAL TEPHRA FALLS SINCE 10,400 CAL YR BP

3.1 Introduction

Distal tephra deposits – volcanic ash preserved as synchronous isochrons within a range of environmental archives – are well established chronological and stratigraphical tools (e.g. Lowe, 2011). The characterisation of visible and crypto- tephra layers establishes their applicability more widely and facilitates their use in palaeo-environmental reconstructions, which benefit from increased chronological control and correlation between records. Cryptotephra, in particular, can help develop records of eruption histories and extend the known limits of ash distribution (Davies, 2015).

Arguably, a thoroughly defined regional tephrostratigraphic framework (e.g. Bronk Ramsey et al., 2015; Lane et al., 2017; Lowe et al., 2013) is the most broadly useful conclusion of descriptive tephra studies, providing a basis for correlations over tens to thousands of kms with applications for a wide range of scientific fields. This outcome, however, is only possible through the careful characterisation of multiple far reaching sites and records, pieced together through time and space. Significant contributions to such a framework can be made through the analysis of high resolution continuous records which can accurately record numerous eruptions.

In North America, there are well-established distal visible tephra records from key source areas including Alaska, the Aleutian Island arc, and the Cascades (e.g. Westgate et al., 1970; Péwé, 1975a, 1975b; Miller and Smith, 1987; Begét et al., 1991; Clague et al., 1995; Preece et al., 1999, 2011b; Kuehn et al., 2009; Péwé et al., 2009; Jensen et al., 2013). Focusing on northern sources, fourteen tephra in the Holocene have been identified as having documented or likely distal transport (Davies et al., 2016) and three of these are recorded as ultra-distal cryptotephra (Pyne-O'Donnell et al., 2012; Mackay et al., 2016). The mid-Holocene caldera forming eruption of Aniakchak (CFE II) and the eastern lobe of the White River Ash (WRAe) have the furthest-travelled distal records to date but represent only a small subset of the eruptions occurring. The importance and persistence of tephra sourced from North America are shown by cryptotephra records published in recent years (e.g. Mackay et al., 2016; Monteath et al., 2017; Pyne-O'Donnell et al., 2016, 2012) and correlations to Greenland and Europe (e.g. Abbott and Davies,

2012; Jensen et al., 2014). However, in continental North America there is a paucity of records between Alaska and sites on the east coast.

Here, we present a Holocene cryptotephra record preserved in a soligenic peatland located at km 174 of the Dempster Highway (hereafter: DHP174) in north-central Yukon, Canada (65.21061N, 138.32208W). The aim of this study is to provide a thorough characterisation of cryptotephra in northwestern North America deposited from western volcanic sources. The Yukon is an important location for late Quaternary records as it was not completely covered by ice during the last glaciation (Duk-Rodkin, 1999) and therefore preserves longer records than can be found in areas to the east and south that were impacted by the Laurentide and Cordilleran ice sheets. Furthermore, the Yukon is downwind of numerous active volcanic sources in Alaska and the Aleutians, and has well documented visible tephra records for the Plio-Pleistocene period (e.g. Jensen et al., 2008; Preece et al., 2011b). This location can therefore provide a more complete reference record for Arctic North America.

3.1.1. Regional setting

DHP174 is located in the northern Ogilvie Mountains of north-central Yukon (Figure 3.1). The site is located within the zone of continuous permafrost and has a subarctic continental climate with large variations in daily and seasonal temperatures. Average daily temperatures in Dawson range from -26°C in January to +16°C in July, with ~325mm annual precipitation focused in the summer months (1981-2010 data; Environment and Climate Change Canada, 2017). During the late Quaternary, the Yukon has been affected by both the Laurentide and Cordilleran ice sheets, as well as local montane glaciers and ice caps. The area cored here, however, was unglaciated throughout (Duk-Rodkin, 1999).

DHP174 is a soligenic peatland formed on a north facing slope at ~720m asl. Water is received directly from precipitation and from percolation through or over the underlying slope. Cores were collected from a relatively horizontal fluvial terrace between the slope and a nearby creek (Figure 3.1) on both the modern peatland surface and an exposed surface of stripped peats ~2m lower where underlying polygonal ice structures are visible. Surface vegetation includes black spruce and birch shrub, Labrador tea, cloudberry, and a range of ericaceous shrubs and lichens.

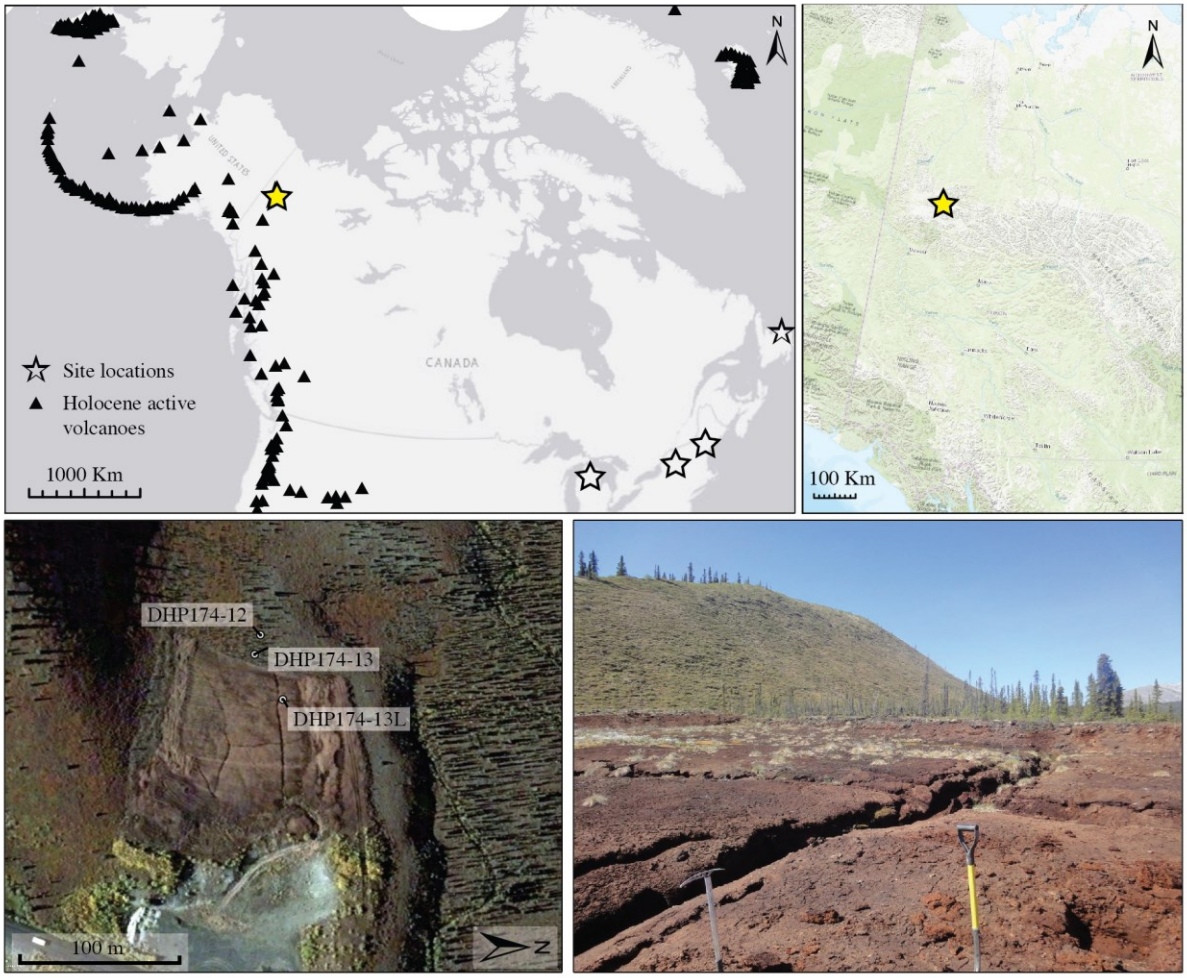

Figure 3.1: Location map showing:

a) the Yukon Territory in Canada. Volcanic sources known to be active in the Holocene marked by black triangles; sites with published cryptotephra records are shown with stars and the DHP174 record is shown with a yellow filled star.

b) DHP174 site location within the Yukon Territory;

c) Coring locations within DHP174 (including from the stripped surface);

d) Photograph of DHP174 coring locations.

3.2 Materials and Methods

3.2.1. Core collection

Cores were collected from DHP174 in the early summer of 2012 and 2013. A shovel was used to sample the thawed material at the time of sampling (16-30 cm depth) and a light, portable drill

(similar to Calmels et al., 2005) was used to extract 10 cm diameter cores from the frozen permafrost. Data are reported here from three cores (Figure 3.1c and 3.2): the upper surface of the peatland was cored in both 2012 (DHP174-12; 3.6m) and 2013 (DHP174-13, 3.85m), and the lower, stripped peatland surface was cored in 2013 only (DHP174-13L, 3.32m). The upper surface cores are composed entirely of peat, predominantly *Sphagnum* sp., while the lower surface core reach silt sediments underlying the peatland. Cores were wrapped in plastic and kept frozen after collection, and transferred for subsampling at the University of Alberta, Edmonton. Depths are reported in cm for individual cores or core composite depths (ccd) for the DHP174 composite profile.

3.2.2. Radiocarbon dating and age modelling

Seventeen macrofossil samples were picked for radiocarbon dating from the three core profiles (Table 3.1; Figure 3.2). Sphagnum remains were preferred where possible as they can provide reliable ^{14}C dates (Nilsson et al., 2001), however samples picked from non-peat core sections at the base of the profile contained other terrestrial plant macrofossils (e.g. twigs, leaves). Samples were pre-treated at the University of Alberta following standard procedures (Reyes et al., 2010) and analysed at the Keck-Carbon Cycle AMS facility (University of California, Irvine).

Sample ID	UCIAMS #	Depth (cm)	Depth (ccd)	Fraction modern	±	14C age (BP)	±
DHP174-12	167484	4	4	1.2080	0.0022	---	---
	167482	14	14	---	---	165	20
	114734	64	64	---	---	2190	25
	122285	136	136	---	---	3520	20
	122290	213	213	---	---	5180	40
	114735	271	271	---	---	6915	20
	114739*	361	361	---	---	7735	30
DHP174-13	142067	22	22	---	---	1165	45
	131059*	130	130	---	---	2810	35
	131060	260	260	---	---	6445	25
	142072	368	368	---	---	8610	30
	131061	385	385	---	---	8670	120
DHP174-13L	131062	25	215	---	---	5380	25
	142071	106	296	---	---	7435	30
	142069	186	376	---	---	8780	70
	142070	214	404	---	---	9290	25
	131063	244	434	---	---	9265	40
	167483	278	468	---	---	12305	30
	131068	331	521	---	---	13040	240

Table 3.1: Summary of ^{14}C dates produced from the three peat cores. Starred (*) dates are interpreted as anomolous. ^{14}C dates were calibrated using Bomb13NH1 (Hua et al., 2013) and IntCal13 (Reimer et al., 2013) calibration curves as appropriate in Oxcal v4.2 (Bronk Ramsey, 2009a). Red dates were not used as they are independent of the tephra record.

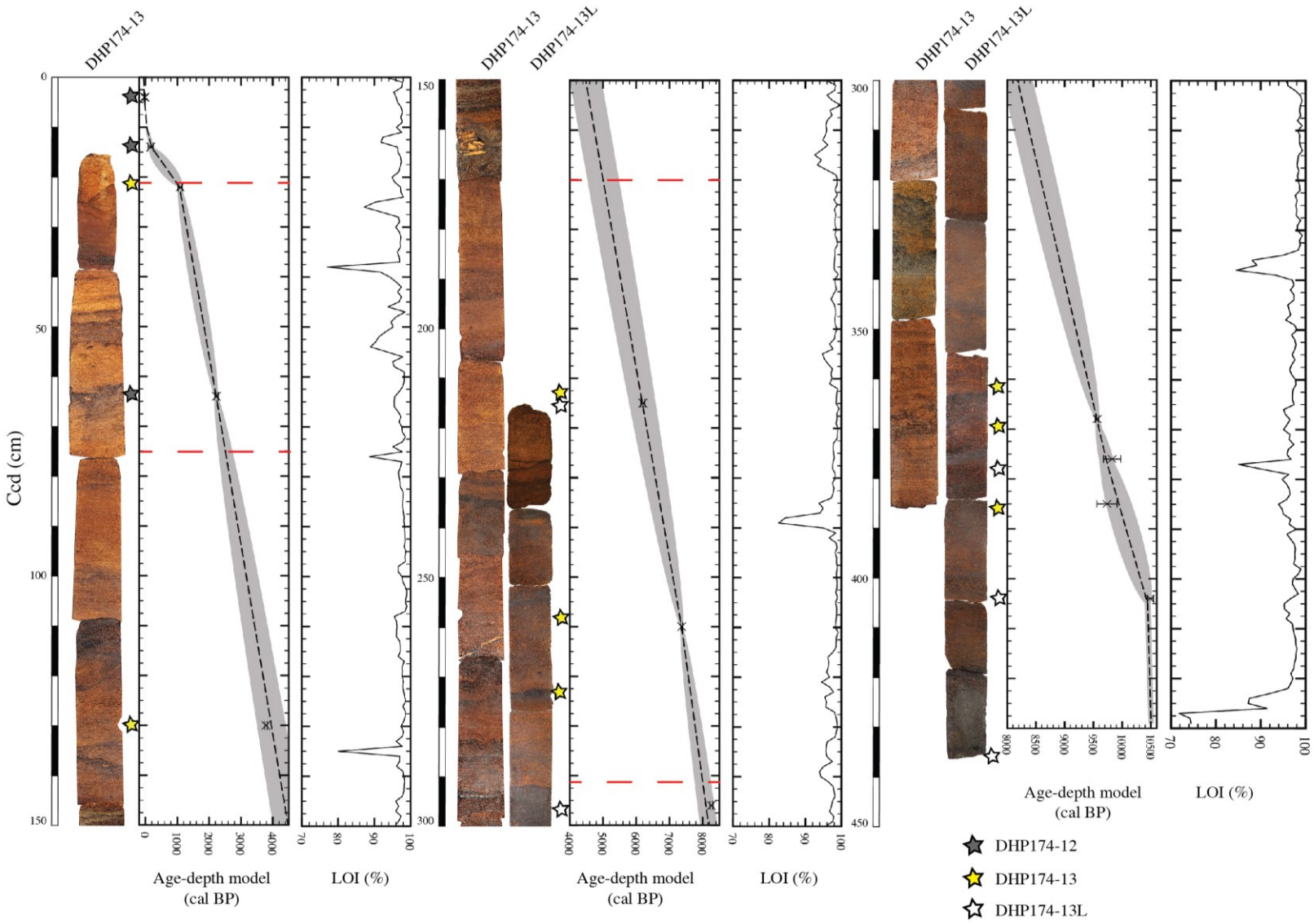

Figure 3.2: DHP174 core stratigraphy including photographs, organic content (% loss on ignition data) ^{14}C sample depths and Bayesian age model results.

Two secondary standards were also pre-treated concurrently (a last interglacial non-finite-age wood, AVR-PAL-07; and a middle Holocene wood, FIRI-F standard) and the resulting ^{14}C values were within expected ranges (Martinez et al., submitted; Table S3.1). The unknown ^{14}C dates were calibrated using Bomb13NH1 (Hua et al., 2013) and IntCal13 (Reimer et al., 2013) calibration curves as appropriate with Oxcal v4.2 (Bronk Ramsey, 2009a). Bayesian age-depth models were constructed using OxCal's Poisson process model (P_Sequence, Bronk Ramsey, 2008). One date (DHP174-13 130cm) was rejected as an outlier.

3.2.3. Cryptotephra analysis

Glass shard concentration profiles were produced using standard methods (Blockley et al., 2005) at 1cm resolution. A composite profile was produced for the three cores as shown in Figure 3.3 and 3.4. Glass was identified in all samples; late Holocene samples with particularly high concentrations were spiked using a known concentration of Lycopodium spores to enable relative estimates of their shard contents. Peaks identified for geochemical analyses were bulk-processed using heavy liquid floatation where glass concentrations were high (i.e. 1000s+ of shards/dry gram; Blockley et al., 2005), or extracted using acid digestion (using concentrated HNO_3 and H_2SO_4 - Dugmore et al., 1995) where concentrations were lower. Acid digestion has been shown to efficiently remove organic peat fibres without chemically altering or degrading the glass shards (Roland et al., 2015) and provides good yields of glass. Samples were mounted in an epoxy puck and polished to expose glass surfaces before being carbon coated prior to electron probe microanalysis (EPMA).

New data are reported here from glass shards analysed on a JEOL 8900 Superprobe or a Cameca SX100 at the University of Alberta by wavelength dispersive spectrometry (WDS) following established protocols (e.g. Jensen et al., 2008). A standard suite of ten elements (Si, Ti, Al, Fe, Mn, Mg, Ca, Na, K, Cl) were measured using a 10 or 5 μm beam (depending on shard size) with 15 keV accelerating voltage and 6 nA beam current to minimize alkali migration during analyses (Spray and Rae, 1995; Morgan and London, 2005). Where intensity data loss does occur, it has been shown that empirical corrections can be applied if the data demonstrate linear variance over time (Nielsen and Sigurdsson, 1981). The 5 μm analyses reported here have both Si and Na corrected for Time Dependent Intensity (TDI) loss (or gain) using a self-calibrated correction with Probe for EPMA software (Donovan et al., 2015).

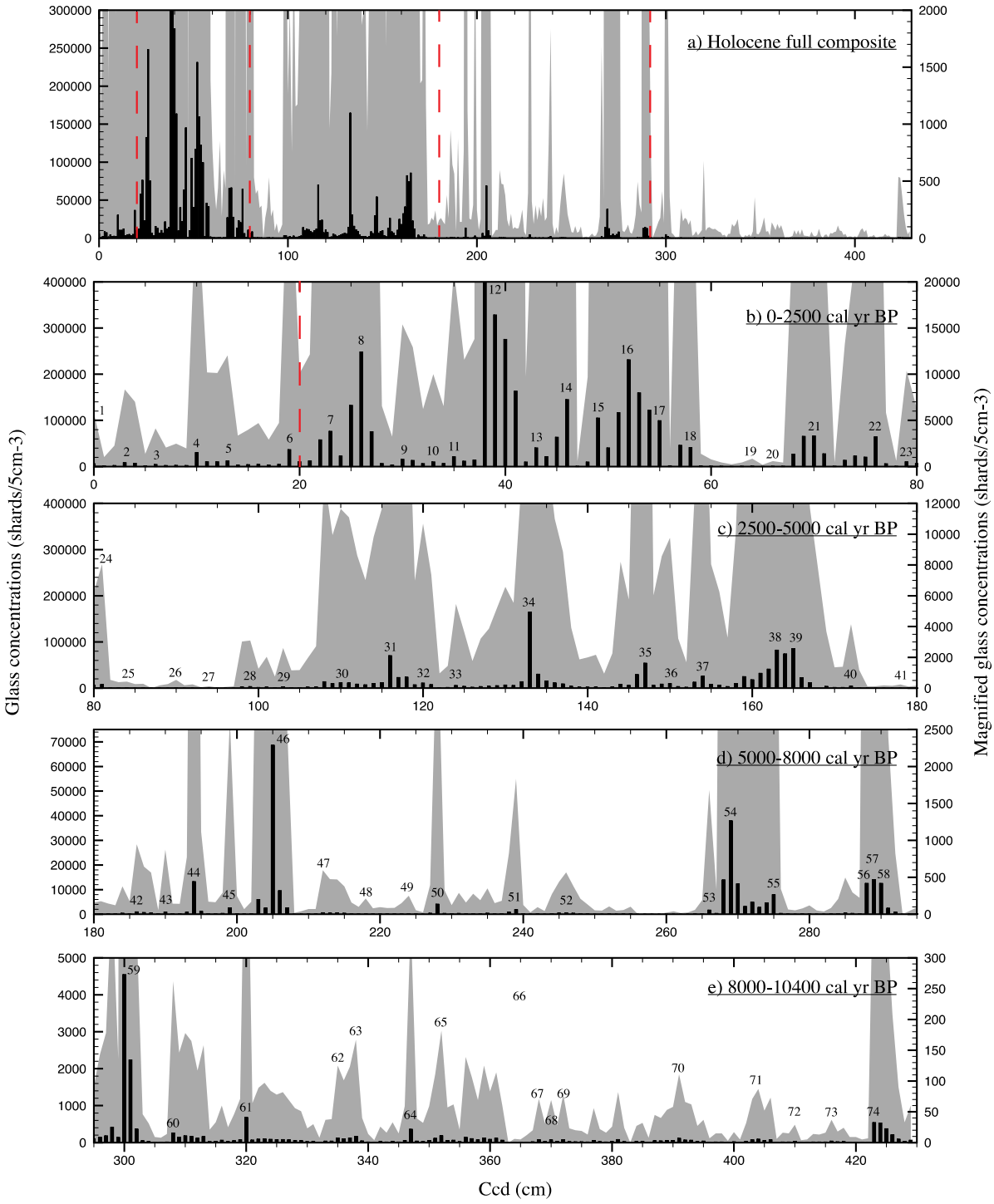

Figure 3.3 Glass shard concentration profiles (shards/5cm^{-3}) for DHP174. Black bars show glass concentrations; grey areas show the same signal, magnified. Results shown are a composite record from the three coring locations. Representations of the time periods used here for discussion are shown. Note the different scales used for each panel due to changes in the magnitude of glass concentrations over time.

Two secondary standards of known composition were run concurrently with all tephra samples: ID 3506, a Lipari rhyolite obsidian, and a reference sample of Old Crow tephra, a well-characterized, secondarily hydrated tephra bed (e.g. Kuehn et al., 2011; Preece et al., 2011a). All results are normalized to 100% and presented as weight percent (wt%) oxides. New major-element geochemical data and associated standard measurements, as well as data for relevant reference material, are reported in the Supplementary Information (Table S3.2). Individual glass shards were analysed with a minimum goal of 30 shards per sample, although this was not always attainable where samples had small, fine grained shards, substantial micro-crystalline contamination, or were glass poor. Additionally, where samples contained wide ranges of geochemical signatures, and 30 analyses were inadequate to represent the populations present, re-analysis was attempted if material was available. Analyses with totals of less than 94% and those where the presence of mineral inclusions were suspected, were discarded. Populations with coherent trends in oxide values were identified where possible using bivariate plots, and glass analyses identified as outliers have been listed separately in the geochemical data (Table S3.2).

3.3 Results

A total of seventy-five cryptotephra peaks have been identified in a composite core sequence compiled from the three coring locations at DHP174. Figure 3.4 details the core correlations using ^{14}C and cryptotephra tie points. There is an observable background signal of glass throughout the cores; peaks in glass concentration chosen for geochemical analysis are shown in Figure 3.3 and numbered from the surface for reference.

3.3.1. Age model and core descriptions

Cores from DHP174 are predominantly organic matter (>95%) with seven short deviations (5-20% non-organic material) from this trend. At 39cm ccd this related to the presence of abundant glass. There are no significant changes in pore ice content with the exception of one small ice lens (5mm) present at 293 ccd. Hence, although DHP174 is a soligenic peatland, accumulated material is predominantly related to peat growth and not colluvial deposition. Peatland initiation began around 10,400 cal yr BP and accumulation rates have been consistent since then (~25 years/cm) up until ~1,000 cal yr BP when either a hiatus or a period of severely decreased accumulation occurred (12-21 ccd, average ~100 years/cm). Modern accumulation rates in the less-compressed mosses are relatively higher, with ~10 years/cm for the last century.

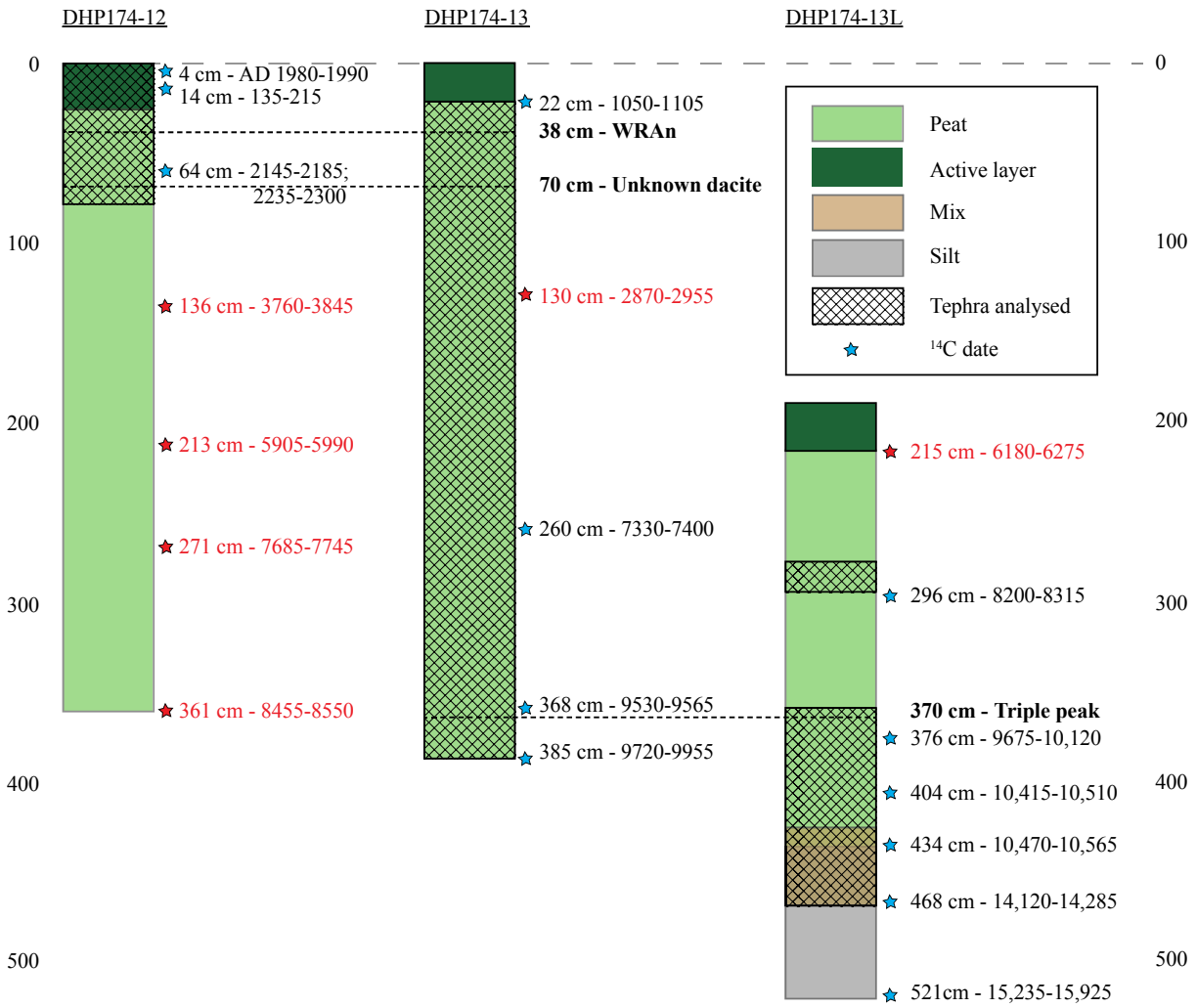

Figure 3.4: DHP174 core stratigraphic logs detailing ^{14}C and cryptotephra sampling and inter-core correlations used for the composite profile. Bold labels refer to tephra correlations between cores. Red ^{14}C dates = anomalous, italic ^{14}C dates are not used in the core chronology as they are independent of the tephra record.

All ^{14}C dates reported here followed their observed stratigraphic order and no age-reversals were present (Table 3.1) although one date (DHP174-13 130 ccd) was identified as an outlier. To further constrain the modern period, the associated age of 1912 for the eruption of Novarupta-Katmai was included at 10 ccd depth. The resulting P_Sequence model for the composite core is shown in Figure 3.2 and mean and one sigma age estimates for cryptotephra at specific depths are listed with their major element geochemical averages. Modelled tephra ages are described as cal yr BP and rounded to five years except for modern eruptions where calendar ages (AD) rounded to one year are used.

ID	Depth (ccd)	UA #	Modelled age (mean cal BP)	1SD	Shards/ 5cm^3		SiO_2	TiO_2	Al_2O_3	FeO	MnO	MgO	CaO	Na_2O	K_2O	Cl	H_2O_d	*n*
DHP-2	3	*2682*	-40	12	8354	a	77.84	0.27	12.38	0.99	0.04	0.17	1.01	3.74	3.49	0.10	2.44	18
			(1990)				(0.65)	(0.04)	(0.39)	(0.15)	(0.03)	(0.09)	(0.22)	(0.19)	(0.19)	(0.04)	(0.56)	
DHP-4	10	*2684*	38	1	30084	-	77.01	0.29	12.57	1.56	0.05	0.24	1.15	3.97	3.00	0.20	3.31	28
			(1912)				(1.05)	(0.11)	(0.42)	(0.34)	(0.03)	(0.11)	(0.36)	(0.18)	(0.17)	(0.02)	(1.1)	
DHP-5	13	*2685*	155	65	12038	a	75.00	0.19	13.90	1.32	0.05	0.30	1.52	3.95	3.51	0.33	2.92	21
			(1795)				(1.12)	(0.05)	(0.56)	(0.19)	(0.04)	(0.1)	(0.29)	(0.17)	(0.16)	(0.03)	(1.18)	
DHP-6	19	*2686*	740	265	36421	a	69.30	0.74	15.06	3.42	0.14	0.76	2.43	4.65	3.34	0.17	2.10	24
		2508					(0.26)	(0.05)	(0.16)	(0.12)	(0.04)	(0.05)	(0.1)	(0.26)	(0.38)	(0.02)	(0.88)	
						b	74.08	0.21	14.33	1.46	0.05	0.35	1.77	4.10	3.35	0.33	2.44	22
							(0.9)	(0.04)	(0.42)	(0.13)	(0.02)	(0.07)	(0.24)	(0.23)	(0.18)	(0.03)	(0.99)	
DHP-7	23	*2509*	1095	85	76117	a	75.86	0.35	12.99	1.94	0.06	0.41	2.20	3.96	1.96	0.31	2.11	42
							(0.28)	(0.04)	(0.19)	(0.07)	(0.03)	(0.03)	(0.09)	(0.16)	(0.11)	(0.03)	(1.19)	
						b	74.44	0.18	14.20	1.40	0.03	0.31	1.74	3.98	3.45	0.32	2.58	22
							(0.78)	(0.04)	(0.36)	(0.18)	(0.03)	(0.08)	(0.19)	(0.16)	(0.21)	(0.04)	(0.98)	
DHP-8	26	*2767, 2510*	1175	130	248063	a	74.00	0.20	14.27	1.45	0.05	0.36	1.79	4.14	3.39	0.36	2.51	28
							(0.64)	(0.04)	(0.31)	(0.16)	(0.03)	(0.06)	(0.17)	(0.12)	(0.15)	(0.04)	(1.06)	
		2510				b	75.90	0.33	12.90	1.96	0.06	0.43	2.19	3.96	1.95	0.31	1.93	13
							(0.29)	(0.05)	(0.12)	(0.1)	(0.03)	(0.03)	(0.07)	(0.16)	(0.06)	(0.05)	(0.61)	
DHP-9	30	*2511*	1285	165	15392	-	73.92	0.22	14.44	1.47	0.04	0.35	1.82	4.05	3.38	0.35	2.18	21
		2768					(0.48)	(0.04)	(0.25)	(0.13)	(0.03)	(0.05)	(0.13)	(0.12)	(0.17)	(0.04)	(1.03)	
DHP-11	35	*2513*	1425	195	21209	-	74.53	0.21	14.09	1.36	0.05	0.30	1.62	4.09	3.41	0.34	2.43	19
		2770					(1.56)	(0.06)	(0.75)	(0.25)	(0.02)	(0.1)	(0.37)	(0.25)	(0.19)	(0.03)	(1.32)	
DHP-12	38	*2514, 2601*	1505	200	2149678	-	76.00	0.20	13.30	1.32	0.05	0.24	1.24	3.88	3.50	0.31	2.27	45
		2771					(0.74)	(0.04)	(0.45)	(0.12)	(0.03)	(0.05)	(0.18)	(0.2)	(0.15)	(0.04)	(1.58)	
DHP-13	43	*2515*	1645	210	40059	-	75.79	0.20	13.45	1.41	0.06	0.24	1.30	3.86	3.40	0.28	0.12	18
							(0.4)	(0.05)	(0.32)	(0.11)	(0.03)	(0.03)	(0.13)	(0.17)	(0.15)	(0.05)	(0.92)	
DHP-14	46	*2516*	1725	205	144840	-	75.57	0.21	13.49	1.45	0.06	0.26	1.34	3.86	3.46	0.30	0.42	17
							(0.5)	(0.05)	(0.29)	(0.1)	(0.03)	(0.03)	(0.17)	(0.15)	(0.12)	(0.03)	(0.87)	
DHP-15	49	*2517*	1810	200	104941	-	76.27	0.18	13.17	1.37	0.05	0.21	1.20	3.77	3.49	0.29	0.57	16
							(0.72)	(0.04)	(0.42)	(0.12)	(0.02)	(0.04)	(0.18)	(0.13)	(0.12)	(0.04)	(0.4)	
DHP-16	52	*2518*	1890	190	231108	-	76.08	0.18	13.27	1.36	0.05	0.23	1.25	3.75	3.56	0.30	1.80	24
		2602					(0.83)	(0.07)	(0.43)	(0.22)	(0.02)	(0.05)	(0.17)	(0.19)	(0.17)	(0.04)	(1.23)	
DHP-17	55	*2362*	1975	170	99118	-	75.99	0.18	13.41	1.31	0.05	0.23	1.25	3.89	3.52	0.32	0.62	30
		2519					(0.72)	(0.05)	(0.42)	(0.17)	(0.02)	(0.05)	(0.17)	(0.19)	(0.17)	(0.03)	(0.58)	
DHP-18	58	*2520*	2055	150	41163	-	75.78	0.17	13.54	1.37	0.06	0.23	1.33	3.82	3.39	0.30	0.84	12
							(0.45)	(0.04)	(0.34)	(0.08)	(0.02)	(0.02)	(0.18)	(0.17)	(0.16)	(0.04)	(0.78)	

Table 3.2: Average major element geochemical data for identifiable populations of analysed tephra samples (n > 10). (#) = standard deviation; FeOt = total iron oxide as FeO; H2Od = water by difference.

ID	Depth (ccd)	UA #	Modelled age (mean cal BP)	1SD	Shards/ 5cm^3		SiO_2	TiO_2	Al_2O_3	FeO	MnO	MgO	CaO	Na_2O	K_2O	Cl	H_2O_d	*n*
DHP-21	70	*2521*	2380	170	65993	a	65.03	1.10	16.13	5.08	0.17	1.47	3.93	4.92	2.06	0.12	1.03	33
		2603					(0.39)	(0.07)	(0.18)	(0.15)	(0.03)	(0.09)	(0.12)	(0.20)	(0.09	(0.02)	(1.84)	
						b	73.69	0.25	14.74	1.73	0.08	0.50	2.29	3.72	2.71	0.38	3.21	38
							(0.75)	(0.05)	(0.25)	(0.18)	(0.03)	(0.06)	(0.18)	(0.18)	(0.13)	(0.05)	(1.14)	
						c	74.44	0.33	13.66	2.25	0.09	0.40	2.24	4.27	2.06	0.25	1.86	10
							(0.31)	(0.04)	(0.16)	(0.12)	(0.03)	(0.03)	(0.08)	(0.11)	(0.1)	(0.02)	(0.61)	
DHP-22	76	*2522*	2540	235	64266	a	75.98	0.19	13.38	1.30	0.05	0.23	1.23	3.81	3.53	0.31	1.53	47
		2607					(0.67)	(0.05)	(0.43)	(0.13)	(0.02)	(0.05)	(0.19)	(0.17)	(0.17)	(0.03)	(1.09)	
DHP-24	81	*2524*	2670	270	8064	-	75.97	0.20	13.35	1.36	0.05	0.24	1.27	3.74	3.53	0.30	1.81	22
		2608					(0.49)	(0.04)	(0.3)	(0.15)	(0.03)	(0.04)	(0.15)	(0.16)	(0.2)	(0.04)	(1.36)	
DHP-25	84	*2527*	2750	290	423	a	75.25	0.18	13.90	1.40	0.05	0.20	1.49	3.94	3.29	0.29	1.11	11
							(1.34)	(0.05)	(0.87)	(0.17)	(0.03)	(0.05)	(0.4)	(0.33)	(0.26)	(0.04)	(1.02)	
DHP-27	94	*2530*	3010	345	130	-	75.84	0.17	13.48	1.40	0.05	0.22	1.34	3.73	3.45	0.31	1.12	15
							(0.67)	(0.04)	(0.4)	(0.15)	(0.03)	(0.05)	(0.2)	(0.21)	(0.25)	(0.05)	(0.95)	
DHP-30	110	*2544*	3430	410	11644	-	76.08	0.16	13.53	1.20	0.05	0.25	1.13	3.88	3.49	0.31	1.51	19
							(0.78)	(0.05)	(0.37)	(0.13)	(0.03)	(0.04)	(0.15)	(0.22)	(0.17)	(0.02)	(0.73)	
DHP-31	116	*2417*	3590	425	69950	-	71.31	0.49	15.13	2.41	0.13	0.49	1.70	5.17	3.12	0.20	1.40	67
		2545					(0.27)	(0.05)	(0.14)	(0.05)	(0.03)	(0.03)	(0.08)	(0.19)	(0.16)	(0.03)	(1.12)	
DHP-32	120	*2546*	3695	435	10687	a	77.47	0.24	12.51	1.44	0.07	0.33	2.04	4.00	1.67	0.23	3.03	9
							(0.5)	(0.04)	(0.4)	(0.11)	(0.02)	(0.03)	(0.14)	(0.24)	(0.13)	(0.04)	(0.95)	
DHP-34	133	*2548*	4035	460	164555	a	74.03	0.22	14.64	1.62	0.08	0.48	2.12	3.85	2.67	0.35	2.09	26
		2604					(0.47)	(0.04)	(0.29)	(0.13)	(0.03)	(0.05)	(0.1)	(0.2)	(0.13)	(0.06)	(1.09)	
DHP-35	147	*2549*	4400	475	53984	a	73.85	0.31	14.43	2.04	0.09	0.46	2.35	4.38	1.99	0.13	1.58	15
		2609					(0.58)	(0.04)	(0.21)	(0.21)	(0.03)	(0.07)	(0.15)	(0.23)	(0.11)	(0.02)	(1.09)	
DHP-37	154	*2551*	4585	480	25859	a	71.09	0.45	14.99	2.52	0.09	0.74	2.93	4.29	2.75	0.20	1.93	9
		2610					(0.9)	(0.05)	(0.33)	(0.24)	(0.02)	(0.09)	(0.26)	(0.2)	(0.14)	(0.02)	(0.87)	
DHP-38	163	*2552*	4820	480	82158	a	76.85	0.25	12.77	1.58	0.07	0.38	2.37	3.90	1.68	0.20	1.49	24
		2605					(0.23)	(0.04)	(0.1)	(0.07)	(0.02)	(0.02)	(0.1)	(0.13)	(0.1)	(0.02)	(0.72)	
						b	77.54	0.23	12.78	1.52	0.07	0.32	2.09	3.65	1.67	0.19	3.04	10
							(0.07)	(0.04)	(0.09)	(0.05)	(0.02)	(0.03)	(0.06)	(0.11)	(0.08)	(0.02)	(1.64)	
DHP-39	165	*2893*	4875	480	85502	a	75.79	0.18	13.41	1.29	0.06	0.26	1.29	4.02	3.49	0.31	2.68	21
		2419					(0.53)	(0.06)	(0.27)	(0.12)	(0.03)	(0.04)	(0.13)	(0.19)	(0.15)	(0.05)	(1.6)	
DHP-40	172	*2572*	5060	475	4150	-	75.83	0.18	13.58	1.23	0.06	0.24	1.29	3.81	3.53	0.31	1.23	15
							(0.67)	(0.04)	(0.39)	(0.09)	(0.03)	(0.1)	(0.16)	(0.17)	(0.16)	(0.04)	(1.11)	
DHP-41	178	*2420*	5215	470	242	-	75.75	0.18	13.63	1.22	0.06	0.25	1.35	4.02	3.44	0.31	0.97	15
		2573					(0.23)	(0.03)	(0.21)	(0.1)	(0.02)	(0.05)	(0.08)	(0.12)	(0.12)	(0.04)	(0.9)	
DHP-42	186	*2574*	5425	465	948	-	75.21	0.19	13.85	1.31	0.05	0.26	1.42	4.04	3.34	0.33	2.08	14
							(0.57)	(0.06)	(0.4)	(0.15)	(0.02)	(0.06)	(0.19)	(0.18)	(0.16)	(0.04)	(0.89)	
DHP-43	190	*2421*	5530	460	874	a	75.92	0.19	13.47	1.24	0.06	0.25	1.25	3.83	3.60	0.33	1.48	30
		2575					(0.3)	(0.04)	(0.27)	(0.11)	(0.02)	(0.07)	(0.12)	(0.14)	(0.17)	(0.04)	(1.21)	

Table 3.2 (cont.): Average major element geochemical data for identifiable populations of analysed tephra samples (n > 10). (#) = standard deviation; FeOt = total iron oxide as FeO; H2Od = water by difference.

ID	Depth (ccd)	UA #	Modelled age (mean cal BP)	1SD	Shards/ $5cm^3$		SiO_2	TiO_2	Al_2O_3	FeO	MnO	MgO	CaO	Na_2O	K_2O	Cl	H_2O_d	*n*
DHP-44	194	*2576*	5635	450	13177	-	75.47	0.19	13.76	1.21	0.05	0.21	1.43	3.94	3.49	0.31	2.49	30
							(0.96)	(0.05)	(0.66)	(0.09)	(0.03)	(0.05)	(0.34)	(0.24)	(0.25)	(0.03)	(0.8)	
DHP-45	199	*2577*	5765	445	2627	a	75.61	0.19	13.53	1.25	0.05	0.25	1.26	4.00	3.54	0.33	2.63	11
							(0.52)	(0.03)	(0.23)	(0.14)	(0.02)	(0.07)	(0.14)	(0.2)	(0.12)	(0.03)	(1.33)	
						b	72.70	0.45	14.35	2.22	0.06	0.58	2.31	4.48	2.65	0.20	1.62	10
							(0.52)	(0.03)	(0.23)	(0.14)	(0.02)	(0.07)	(0.14)	(0.2)	(0.12)	(0.03)	(1.33)	
DHP-46	205	*2364, 2578*	5925	430	68559	-	75.78	0.18	13.50	1.22	0.06	0.24	1.32	4.04	3.47	0.30	1.95	56
		2762					(0.82)	(0.05)	(0.48)	(0.13)	(0.03)	(0.06)	(0.22)	(0.21)	(0.18)	(0.04)	(0.88)	
DHP-47	212	*2579*	6105	410	597	-	75.36	0.19	13.83	1.24	0.05	0.22	1.42	4.01	3.46	0.30	1.62	17
							(0.59)	(0.05)	(0.34)	(0.11)	(0.02)	(0.05)	(0.17)	(0.22)	(0.1)	(0.03)	(0.92)	
DHP-48	218	*2580*	6265	395	214	a	75.61	0.17	13.69	1.23	0.06	0.23	1.36	3.92	3.48	0.33	2.49	14
							(0.33)	(0.04)	(0.19)	(0.07)	(0.03)	(0.05)	(0.09)	(0.16)	(0.11)	(0.03)	(1.44)	
DHP-49	224	*2581*	6420	370	250	b	77.28	0.30	12.43	1.46	0.05	0.25	1.74	3.57	2.77	0.18	1.91	10
							(0.27)	(0.04)	(0.27)	(0.08)	(0.03)	(0.04)	(0.08)	(0.12)	(0.22)	(0.03)	(0.59)	
DHP-50	228	*2582*	6525	355	4058	a	64.93	0.89	15.48	5.63	0.15	1.94	4.88	4.24	1.72	0.17	1.98	11
							(1.17)	(0.04)	(0.4)	(0.36)	(0.03)	(0.23)	(0.4)	(0.13)	(0.16)	(0.02)	(0.85)	
						b	75.46	0.53	12.51	2.30	0.06	0.47	1.82	4.07	2.68	0.22	1.62	48
							(1.42)	(0.11)	(0.44)	(0.48)	(0.04)	(0.15)	(0.42)	(0.22)	(0.24)	(0.04)	(1.06)	
		2763				c	76.21	0.17	13.20	1.20	0.06	0.23	1.17	3.91	3.56	0.31	2.59	20
							(0.72)	(0.04)	(0.45)	(0.16)	(0.03)	(0.08)	(0.22)	(0.26)	(0.2)	(0.04)	(0.71)	
DHP-51	239	*2366*	6815	295	1834	a	65.60	1.11	15.47	5.25	0.17	1.40	3.69	4.68	2.59	0.15	1.90	39
		2583					(0.44)	(0.06)	(0.27)	(0.2)	(0.03)	(0.1)	(0.16)	(0.29)	(0.15)	(0.02)	(1.15)	
						b	75.37	0.40	12.67	1.87	0.06	0.30	1.40	3.64	3.99	0.43	1.76	10
							(1.23)	(0.07)	(0.58)	(0.21)	(0.03)	(0.11)	(0.33)	(0.26)	(0.14)	(0.06)	(0.97)	
DHP-52	246	*2584*	7000	245	566	-	75.30	0.17	13.93	1.21	0.06	0.24	1.46	3.89	3.51	0.29	1.98	10
							(0.42)	(0.04)	(0.35)	(0.07)	(0.03)	(0.04)	(0.17)	(0.06)	(0.16)	(0.03)	(0.79)	
DHP-53	266	*2585*	7490	125	1684	-	75.79	0.18	13.62	1.23	0.05	0.23	1.34	3.80	3.52	0.30	1.75	14
							(0.44)	(0.04)	(0.32)	(0.08)	(0.02)	(0.04)	(0.16)	(0.18)	(0.21)	(0.02)	(0.58)	
DHP-54	269	*2586*	7550	150	37936	a	73.04	0.50	14.17	2.20	0.07	0.59	2.28	4.22	2.74	0.21	2.50	16
		2764					(0.68)	(0.04)	(0.28)	(0.19)	(0.02)	(0.07)	(0.17)	(0.18)	(0.07)	(0.03)	(1.05)	
						b	77.43	0.20	13.09	1.22	0.09	0.29	2.07	3.85	1.63	0.15	2.39	16
							(0.22)	(0.04)	(0.13)	(0.08)	(0.03)	(0.06)	(0.1)	(0.15)	(0.08)	(0.02)	(0.69)	
DHP-56	288	*2879*	7935	240	12503	-	76.14	0.23	13.23	1.51	0.06	0.27	1.56	4.74	2.08	0.16	2.35	11
							(0.49)	(0.03)	(0.31)	(0.11)	(0.02)	(0.04)	(0.13)	(0.18)	(0.1)	(0.02)	(1.22)	

Table 3.2 (cont.): Average major element geochemical data for identifiable populations of analysed tephra samples (n > 10). (#) = standard deviation; FeOt = total iron oxide as FeO; H2Od = water by difference.

ID	Depth (ccd)	UA #	Modelled age (mean cal BP)	1SD	Shards/ 5cm^3		SiO_2	TiO_2	Al_2O_3	FeO	MnO	MgO	CaO	Na_2O	K_2O	Cl	H_2O_d	*n*
DHP-57	289	*2588*	7955	240	14083	a	76.90	0.23	13.18	1.46	0.06	0.22	1.53	4.14	2.19	0.16	2.08	28
							(0.46)	(0.03)	(0.28)	(0.08)	(0.03)	(0.03)	(0.12)	(0.19)	(0.08)	(0.03)	(0.84)	
						b	77.95	0.15	12.98	1.11	0.07	0.28	1.75	3.77	1.91	0.18	2.30	12
							(0.42)	(0.04)	(0.27)	(0.07)	(0.03)	(0.06)	(0.23)	(0.23)	(0.22)	(0.03)	(1.02)	
DHP-59	300	*2591*	8180	265	4541	-	76.16	0.18	13.49	1.24	0.05	0.23	1.26	3.90	3.46	0.30	1.42	11
							(0.53)	(0.05)	(0.44)	(0.07)	(0.01)	(0.04)	(0.17)	(0.26)	(0.2)	(0.03)	(1.66)	
DHP-61	320	*2592*	8585	270	679	-	75.90	0.18	13.51	1.27	0.06	0.24	1.26	3.75	3.62	0.31	2.11	11
							(0.36)	(0.05)	(0.2)	(0.07)	(0.02)	(0.03)	(0.11)	(0.15)	(0.14)	(0.04)	(1.4)	
DHP-62	335	*2368*	8890	250	125	a	67.70	0.78	15.26	4.94	0.14	0.93	3.33	5.00	2.04	0.15	1.49	19
		2593					(0.43)	(0.06)	(0.13)	(0.14)	(0.03)	(0.06)	(0.16)	(0.23)	(0.07)	(0.03)	(0.67)	
DHP-64	347	*2594*	9135	215	359	a	75.74	0.22	13.48	1.33	0.05	0.28	1.30	3.91	3.57	0.35	3.07	10
		2766					(0.41)	(0.07)	(0.21)	(0.1)	(0.03)	(0.04)	(0.15)	(0.14)	(0.18)	(0.03)	(1.84)	
DHP-67	177	*2883*	9560	110	71	-	72.84	0.48	13.54	3.82	0.15	0.58	2.89	4.58	0.95	0.18	2.52	12
							(0.22)	(0.03)	(0.08)	(0.25)	(0.02)	(0.07)	(0.1)	(0.24)	(0.07)	(0.02)	(0.7)	
DHP-71	213	*2599*	10420	90	87	-	69.11	0.57	15.47	4.09	0.18	0.56	2.21	5.07	2.58	0.20	2.32	25
							(0.35)	(0.05)	(0.27)	(0.12)	(0.03)	(0.05)	(0.1)	(0.22)	(0.1)	(0.02)	(1.36)	
DHP-74	232	*2600*	10485	50	537	-	67.85	1.21	14.24	4.86	0.08	1.35	3.53	3.88	2.94	0.06	3.10	11
							(0.4)	(0.06)	(0.09)	(0.16)	(0.04)	(0.1)	(0.12)	(0.24)	(0.09)	(0.01)	(0.56)	

Table 3.2 (cont.): Average major element geochemical data for identifiable populations of analysed tephra samples (n > 10). (#) = standard deviation; FeOt = total iron oxide as FeO; H2Od = water by difference.

3.3.2. Cryptotephra stratigraphy

The DHP174 tephrostratigraphy is split into five sections based on shard concentrations (highlighted in Figure 3.3): the early Holocene and peatland initiation (10,500-8000 cal yr BP), the early to mid-Holocene (8,000-5,000 cal yr BP), the mid- to late Holocene (split as 5,000-2,500 and 2,500-1,000 cal yr BP), and the period of reduced accumulation to the present day (<1,000 cal yr BP). Average geochemical data have been included in Table S3.2 for all identified glass populations, but for populations with low numbers of analyses it is not possible to tell if they represent detrital glass, multiple eruptions within a single sample, shards from nearby peaks, or if they reliably correlate with reference or published datasets. Therefore, only populations with >10 points are discussed in detail as these are most likely related to the glass concentration peak and represent the best-preserved records here (either due to their size, dominant wind direction, or proximity to the site) that may be found at other distal sites. Of the seventy-five tephra peaks analysed, these criteria are met for fifty-two samples representing sixty-four geochemical populations. Further, thirty-five of these sixty-four populations correlate with each other and will be discussed separately in section 3.2.5.

3.3.2.1. Early Holocene and peatland initiation (10,500-8000 cal yr BP)

The early Holocene has a relatively muted glass concentration signal, with only three eruptions of >500 shards/cm^3 before ~8,000 cal yr BP and the majority of peaks having fewer than 200 shards/5cm^3 (Figure 3.3). A total of fourteen samples were analysed from this period, seven of which meet the criteria for discussion here: two dacites (DHP-62a, -74), one rhyo-dacite (DHP-71), and four rhyolites (DHP-67 discussed here, DHP-59, -61, 64a discussed below in section 3.2.5). Major element geochemical data for these samples and relevant reference material are shown in Figure 3.5. It is unique to this period that four of the samples analysed near the base of the record (DHP-68, -69, -70 and -72) have geochemical data that are widely scattered and have no discernible populations.

Two dacitic samples are not correlated here to known eruptions. The oldest sample is DHP-74 with a modelled age of 10485±50 cal yr BP. The peak occurs at the first accumulation of peat at the site and is associated with a long tail of shards. DHP-62 occurs at 8890±250 cal yr BP and has a dominant dacitic population as well as two additional populations (one dacite, one rhyolite) with <10 points.

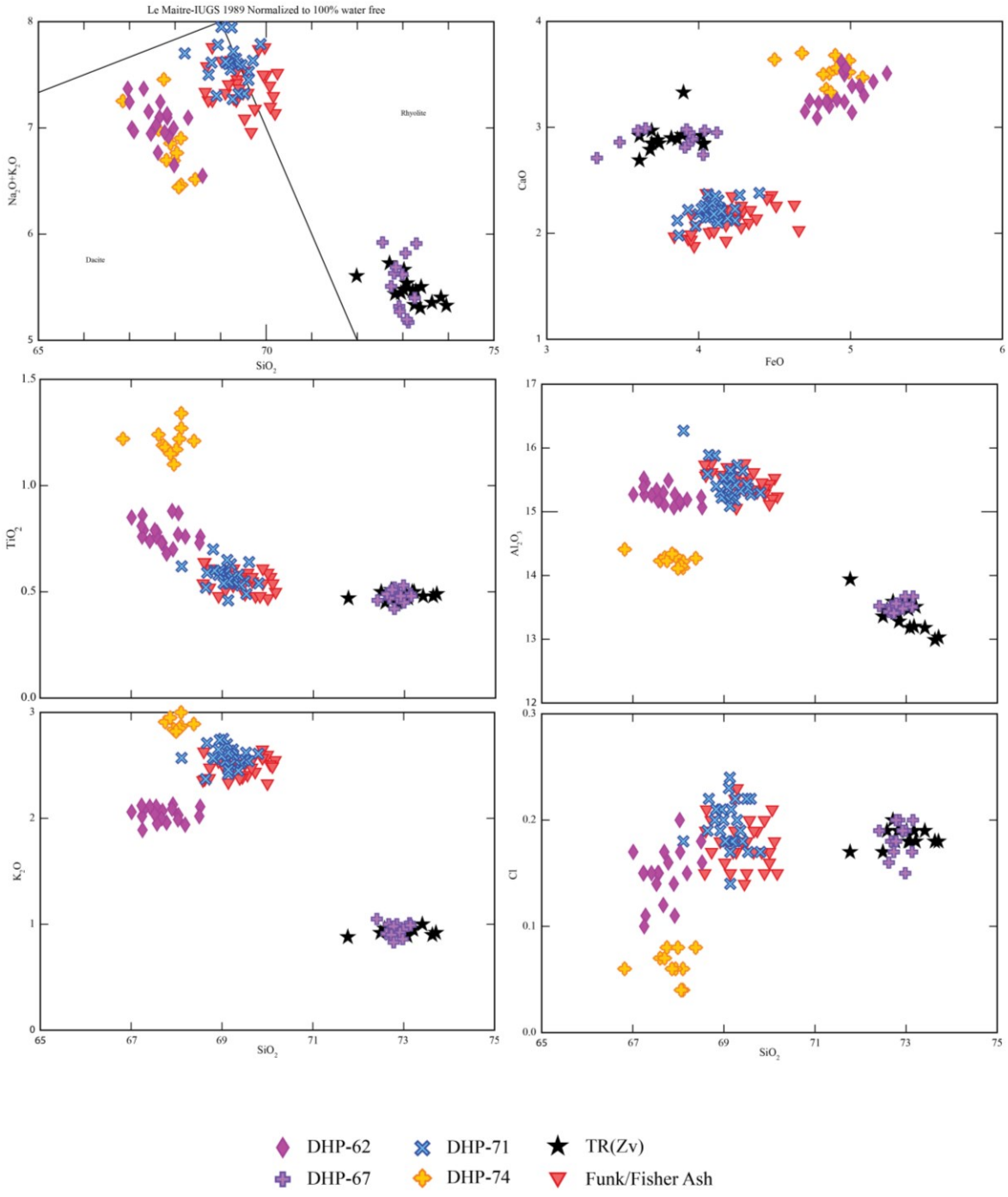

Figure 3.5 Major element glass geochemical plots for DHP174 tephra between 10,500-8000 cal yr BP. Published data for reference material from TR(Zv) (Derkachev et al., 2016) and data concurrently analysed for the Funk/Fisher Ash (Carson et al., 2002) are plotted for comparison.

DHP-71, a rhyo-dacite at 10420±90 cal yr BP, correlates with reference material for a sample from the caldera forming eruption of Fisher volcano, Unimak Island (Carson et al., 2002; Figure 2). Fisher caldera is one of the largest calderas in the Aleutain arc (Miller and Smith, 1977, 1987) and the associated multimodal Funk/Fisher tephra has bracketing ages of 9130±140 and 8425±350 ^{14}C years (Carson et al., 2002) resulting in a bracketing range of 9965-10485 cal yr BP for the eruption that overlaps with our age estimate.

The rhyolite DHP-67 is dated to 9560±110 cal yr BP and is correlated here to the TR(Zv) tephra from the caldera forming eruption of Zavaritsky volcano on Simushir Island, central Kurile Islands (Derkachev et al., 2016; Figure 2). It is noticeably different from the majority of the glass analyses presented here due to its low wt.% K_2O (0.95±0.07) and high wt.% FeO_t (3.82±0.25) This eruption has estimated ages of ~8.0 ka (Nakagawa et al., 2008) and ~8540±40 ^{14}C years (9500-9540 cal yr BP, Hasegawa et al., 2011); our age estimate agrees more closely with the latter. This is the farthest geographical correlation made in the DHP174 tephrostratigraphy as Zavaritsky volcano is ~4500 km from the site.

3.3.2.2. Early to mid-Holocene (8,000-5,000 cal yr BP)

Fifteen of the seventeen samples in the early to mid-Holocene meet the criteria for discussion here, representing twenty-one geochemical populations of >10 shards. Of these, one sample is predominantly dacitic (DHP-51) and one sample (DHP-50) has three populations, two of which (a, a rhyolite and b, a dacite) sit on trend together. The remaining eighteen populations are rhyolitic: ten have Mt. Churchill-like geochemistries (discussed below in section 3.2.5) and the remaining eight can be split using their relative wt.% K_2O: 1.5 to 2.3 (DHP-54b, -56a, -57-a,b), 2.5 to 3 (DHP-45b, -49, 54-a), and ~4 (DHP-51b). Major element geochemical data for these samples and relevant reference material are shown in Figure 3.6.

DHP-51 at 6815±295 cal yr BP has two unusual populations for the DHP174 record: DHP-51a has more analyses and is dacitic with some trachydactic points (65 to 66 wt.% SiO_2), DHP-51b is rhyolitic (74 to 77 wt.% SiO_2) and the only high-K calc-alkaline sample analysed. It has comparatively high wt.% K_2O and Cl, with lower Al_2O_3, MgO and CaO. Neither population is correlated here with a known source.

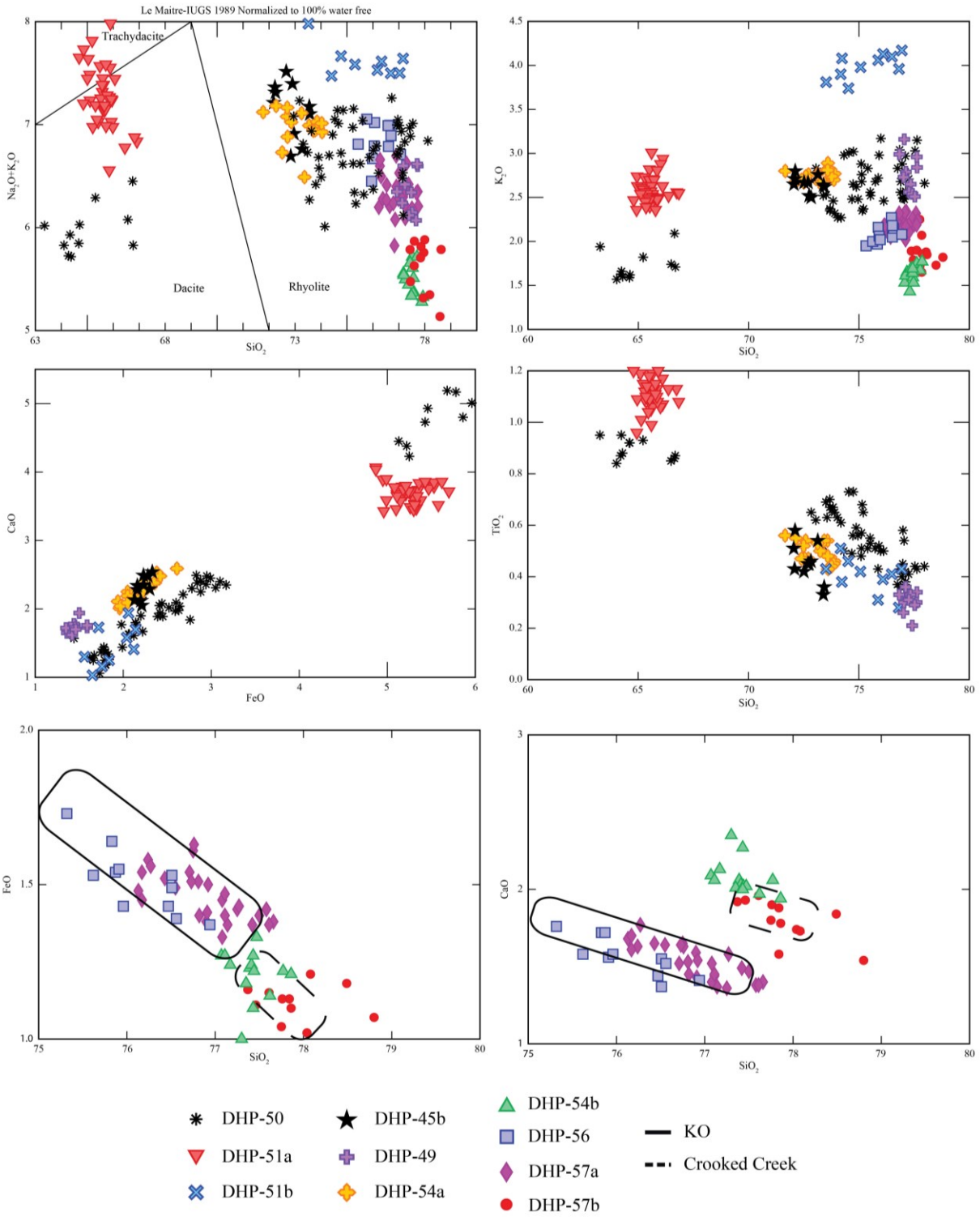

Figure 3.6 Major element glass geochemical plots for DHP174 tephra between 8,000-5,000 cal yr BP. Envelopes representing data for KO (Ponomareva, pers. comm.) and published data for Crooked Creek (Reger et al., 1995) are plotted for comparison.

DHP-50, dated to 6525±355 cal yr BP, has a dominant rhyolitic population (a, 74 to 77 wt.% SiO_2) with a smaller associated dacite (b, 64 to 66 wt.% SiO_2) and a further third population (c) which correlates with Mt. Churchill. DHP-50a and b plot well with analyses from Mulliken (2016) for the lower Oshetna tephra, which has a modelled age of 6640-6700 cal yr BP. It is unclear if the Oshetna tephra represents a single eruption, or multiple closely spaced eruptions from one or more sources given the heterogeneity of the samples analysed (Mulliken, 2016). DHP-50a and b appear similar to AT-3209 and AT-3196, however there is an offset to the overlap for wt.% CaO and K_2O, and the associated ages are at the limit of their associated errors.

3.3.2.2.1. Samples with 1.5 to 2.3 wt.% K_2O

Two of the largest concentrations of glass in this period are associated with four populations that have relatively low wt% K_2O: DHP-54b (7550±150 cal yr BP), DHP-56 (7935±240 cal yr BP) and DHP-57b (7955±240 cal yr BP).

All three populations are rhyolites with 75 to 78 wt.% SiO_2 but can be separated by comparing their FeO_t, CaO, and alkalis (Figure 3.6). One of these populations, DHP-56, plots well with reference material from the KO tephra – the largest Holocene eruption in Kamchatka associated with the Kuril-Lake Iliinsky caldera formation (Braitseva et al., 1997). The average age estimates for both DGP-56 is younger than the estimated age of KO - 7666±19 ^{14}C yr BP (Braitseva et al., 1997; ~8410-8455 cal yr BP) although it overlaps at the 2 sigma range.

The other two samples considered here have many elements that plot in a similar way to data reported for the Crooked Creek tephra in the eastern Cook Inlet area (Reger et al., 1995) – DHP-57b overlaps more thoroughly and is closest in age to the published estimate. This eruption is ^{14}C dated to ~8,500-9,500 cal yr BP and is therefore at least 500 years older than DHP-57b and ~1,000 years older than DHP-54b, but they may have the same eruptive source. Reger et al. (1995) suggested the Crooked Creek tephra may originate from Augustine but a proximal correlative is not known.

3.3.2.2.2. Samples with 2.5 to 3 wt.% K_2O

The remaining three samples in this period are rhyolites with mid-range wt.% K_2O values (Figure 3.6). DHP-49 has one dominant high wt.% SiO_2 (77 to 78) population with a modelled age of 6420±370 cal yr BP. This sample plots closely to reference material from the caldera

forming eruption of Kaguyak dated to 6650-7160 cal yr BP (Fierstein, 2007) although the wt.% CaO and alkalis are offset. Reported values for the Lower ash rib dated to 5660-6230 cal yr BP are described as similar to the Kaguyak co-ignembrite ash (Fierstein, 2007) but the full data are not available for comparison. While the age estimates of these samples match well a correlation with either the specific eruption or Kaguyak, as a source, require further analyses.

DHP-45b and -54a have relatively high wt.% FeO_t, TiO_2 and CaO with a dominant wt.% SiO_2 range of 72 to 74. These populations both correlate well for all elements analysed although the samples are stratigraphically separated by ~2 ka – DHP-45b dates to 5765±445 cal yr BP while DHP-54a occurs at 7550±150 cal yr BP. Published average data for one sample from Tephra 5 (Reger et al., 1995) and tephra J from Bear Lake (Riehle, 1985) match well with these samples (Figure 3.6). Given the location, grain size, and tephra thickness of tephra J, Riehle (1985) suggests Redoubt as a likely source, and Schiff et al. (2010, 2008) report activity at Redoubt for both of these time periods: three tephra layers in lake sediments that are 1 to 6 cm thick with maximum grain sizes of 1.5 to 7 mm between 5400±150 to 5680±110 cal yr BP, and two tephra layers that are 4 to 5 cm thick with maximum grain sizes of 4 to 14 mm at 7530±130 and 7560±130 cal yr BP. In the absence of reference data, this is not a confirmed correlation, however the timing and average published geochemistry are suggestive of a Redoubt source.

3.3.2.3. Mid to late Holocene

3.3.2.3.1. 5,000-2,500 cal yr BP

The mid to late Holocene has an increased number and frequency of large shard concentration peaks compared to the mid- and early-Holocene, particularly from 4,500 to 3,000 cal yr BP. A total of thirteen samples have populations with >10 points, all of which are rhyolitic, and only one (DHP-38) has more than one significant population analysed. Seven of the fourteen populations correlate to Mt. Churchill and are discussed below in section 3.2.5, the remaining seven are shown in Figure 3.7. Two of these are correlated here to known eruptions (DHP-31 and 34), two have suggested eruptive centres (DHP-38a, b) and the remaining three have unknown sources (DHP-37, 35 and 32).

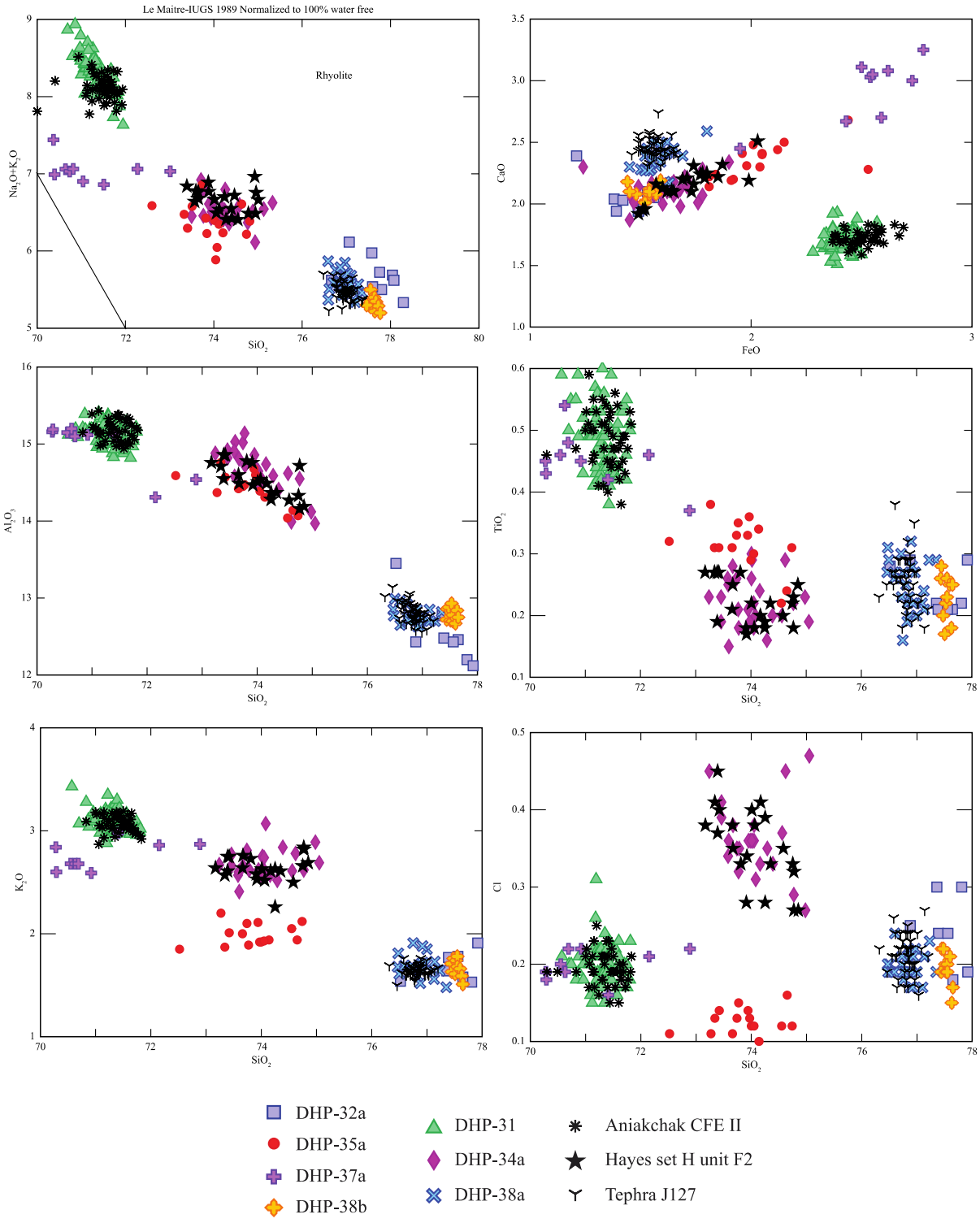

Figure 3.7 Major element glass geochemical plots for DHP174 tephra between 5,000-2,500 cal yr BP. Published data for reference material from Tephra J127 (Monteath et al., 2017) and data from concurrently analysed reference material of Aniakchak and Hayes set H unit F2 (Davies et al., 2016) are plotted for comparison.

DHP-38 is dated to 4820±480 and has two high wt.% SiO_2 rhyolite populations with low wt.% K_2O (1.6 to 1.8). The two populations are very similar geochemically and may be related, but there are subtle differences in their wt.% SiO_2, Al_2O_3 and MgO. This low wt.% K_2O range is not commonly reported for tephra sourced from Alaska and is related uniquely to Augustine and Kaguyak by Fierstein and Hildreth (2008) using whole rock analyses. One distal sample – tephra J127 from Jan Lake in eastern interior Alaska (Monteath et al., 2017) – matches DHP-38a geochemically (Figure 3.7) and has a modelled age of 4240-4820 cal yr BP which overlaps. More proximally, both DHP-38a and b also plot well with average data for Augustine produced from two sites on Augustine Island (Riehle et al., 1999; Figure 3.7), particularly sample C from site 49, and samples 33B and D from site 48. However, a correlation is not confirmed without point analyses for comparison, especially given the broad wt.% SiO_2 ranges of these samples (one s.d. of 0.75 to 3%).

Riehle et al. (1999) report mixed Augustine and Kayuyak like glass in two tephra deposits around this time although no associated glass analyses are published. Tephra F from Shuyak Island dates between 3360±25 and 3620±25 ^{14}C years, and Tephra D from Kamishak Creek, north of Kaguyak crater, dates between 3660±100 and 3850±100 ^{14}C years BP. These calibrate to age ranges of 3615-3910 and 3965-4280 cal yr BP, the latter estimate is ~ 700 years younger than DHP-38 but overlaps within error, while the former is ~1000 years younger. Hence, DHP-38a appears to correlate with tephra J127 (Monteath et al., 2017) and it is likely that both DHP-38a and -38b were sourced from Augustine or possibly Kaguyak, but they cannot be correlated to a known eruption with the current available data.

Both DHP-37a and DHP-35a are from unknown sources, and the samples contain three to four multiple populations suggesting either periods of increased activity or decreased peat accumulation. DHP-37a is a rhyolite with mid-range wt.% K_2O (2.6 to 2.9) with relatively high FeO_t, MgO and CaO. DHP-35 is also rhyolitic and has relatively low wt.% K_2O (1.9 to 2.1) and Cl (0.11-0.15). The modelled ages for DHP-37 (4585±480 cal yr BP) and DHP-35 (4400±475 cal yr BP) overlap within errors although they are separated by 7 cm of peat. DHP-34 has a modelled age of 4035±460 cal yr BP and correlates geochemically with the widespread Hayes set H unit F2 (Wallace et al., 2014; Figure 3.7). Hayes set H is a middle Holocene set of seven to eight tephra layers originally described by Riehle (1985) at a proximal locality known as site

23. Of these, tephra unit F2, as defined by Wallace et al. (2014) and correlated to the Jarvis Creek Ash (Begét et al., 1991) and unit G (Riehle, 1994), is the most widely reported and farthest travelled. This tephra is a key marker bed in Alaska and has a modelled age of 3910-4205 cal yr BP (Davies et al., 2016) which matches well with DHP-34. This peak is the largest of the time period, likely relating to the size of the eruption and Hayes volcano being located at the northern-most end of the Alaska arc, ~800 km from DHP174.

DHP-32 is another unknown rhyolite with a modelled age of 3695±435 cal yr BP. This high wt.% SiO_2 rhyolite has relative high CaO and low K_2O and is similar geochemically to DHP-38b although it has much lower wt.% Al_2O_3 (12.1 to 12.8). It may also correlate to Augustine but cannot be confirmed here.

DHP-31 has a modelled age of 3590±425 and correlates geochemically with the rhyolitic population of the widespread Aniakchak caldera-forming eruption (CFE) II (Figure 3.7). While Aniakchak has erupted frequently during the Holocene (Riehle et al., 1999; Neal et al., 2001; Bacon et al., 2014) the CFE II tephra is the most widely dispersed with distal visible deposits reported across western Alaska and cryptotephra deposits reported in central Alaska, the Chukchi Sea, Newfoundland and Greenland (Miller and Smith, 1987; Pearce et al., 2004; Denton and Pearce, 2008; Coulter et al., 2012; Pyne-O'Donnell et al., 2012; Monteath et al., 2017; Ponomareva et al., 2018). Using ^{14}C dates from multiple sites in Alaska, Aniakchak CFE II has a modelled age of 3290-3510 cal yr BP (Davies et al., 2016) that overlaps within error with the modelled age for DHP-31, but is younger than the associated Greenland ice core ages of either 3591±4 cal yr BP (GICC05, Vinther et al., 2006), or a corrected age of 3572±4 cal yr BP (Pearce et al., 2017) factoring a potential offset of -19±3 years between IntCal13 and GICC05 at 3600 cal yr BP (Muscheler et al., 2014; Adolphi and Muscheler, 2016). The modelled age for DHP-31 given here has too broad an error range to add weight to either estimate.

3.3.2.3.2. 2.5-1ka cal yr BP

This period has thirteen analysed tephra samples with seventeen identified populations of 10 shards or more. This is the key period of activity associated with Mt. Churchill – the main WRAn and WRAe eruptions are discussed here while the remaining ten populations that correlate are discussed in section 3.2.5 below. The five additional populations are measured from three samples (Figure 3.8) – one dacite (DHP-21a) and four rhyolites (DHP-7a, -8b, -21b, c).

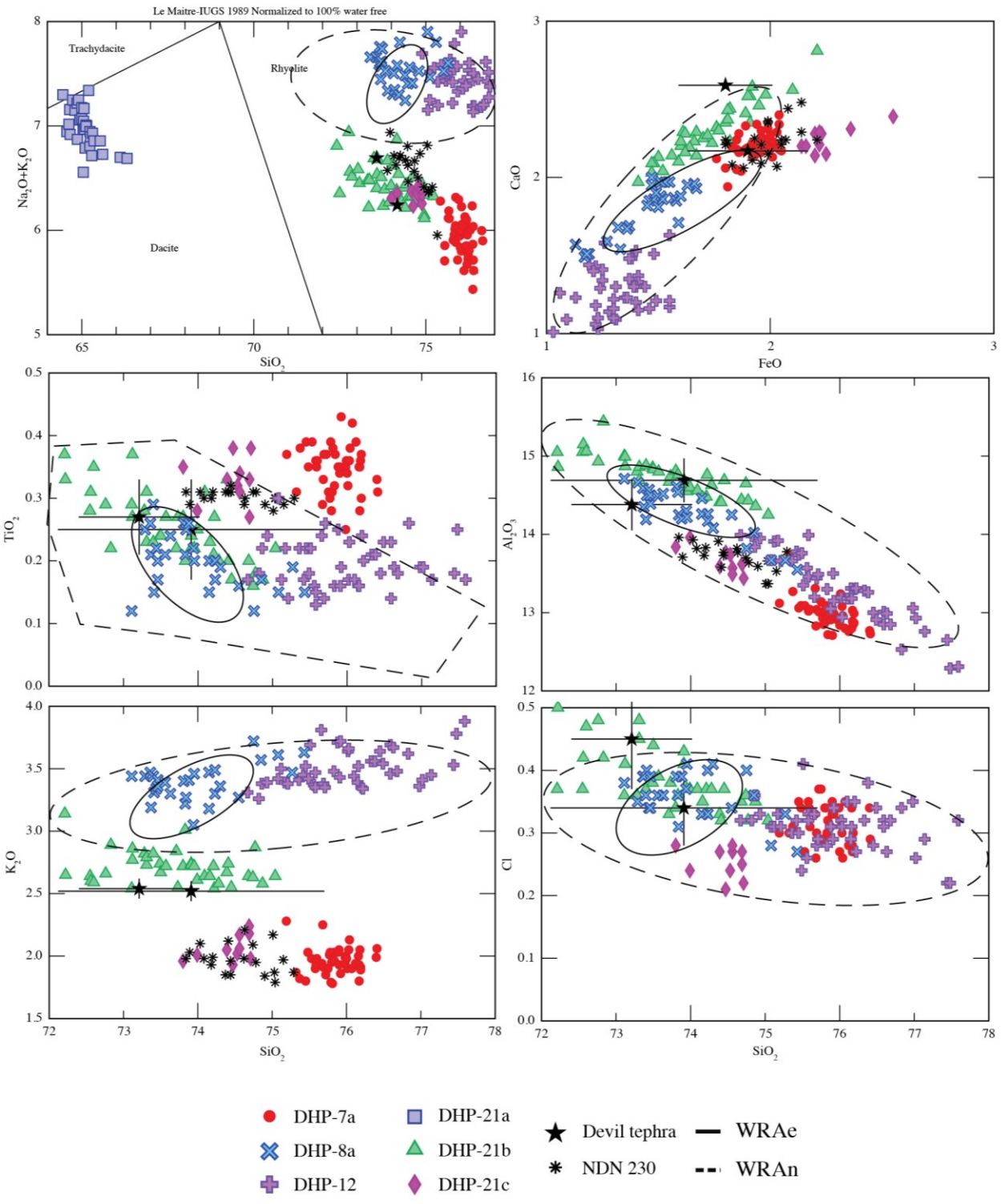

Figure 3.8 Major element glass geochemical plots for DHP174 tephra between 2,500-1,000 cal yr BP. Published data for the Devil tephra (Mulliken et al., 2015), NDN 230 (Pyne-O'Donnell et al., 2012), and areas representing data for the WRAe and WRAn (Preece et al., 2014) are plotted for comparison.

DHP-21 is the last sample analysed before a period of low glass deposition (<1,000 shards/5cm^{-3}) that lasts ~300 years, and has a modelled age of 2380±170 cal yr BP. It has three populations with >10 points – this may relate to the broad (4 cm wide) peak in glass concentration. DHP-21a is dacitic with wt.% SiO_2 ranging from 64.5 to 65.5 and is not correlated here to any known source or eruption.

DHP-21b has the largest number of analyses and relatively high wt.% Al_2O_3 (14.5 to 15.0) and Cl (0.3 to 0.4), and mid-range K_2O (2.55 to 2.85). It is geochemically similar to the Devil tephra (Figure 3.8) sourced from Hayes volcano, which has been traced across the middle Susitna valley, Alaska (Dilley, 1988; Dixon and Smith, 1990; Mulliken, 2016) and Hayes set H unit F2. However, its modelled age of 1725-1815 cal yr BP is ~600 years younger than DHP-21 and their ages do not overlap at the 2-sigma range. It is not correlated with the Devil tephra here but may be sourced from Hayes volcano given the geochemical similarities (e.g. relatively high wt.% Cl).

DHP-21c is also rhyolitic but has higher wt.% FeO_t (2.1 to 2.35) and relatively low K_2O (1.95 to 2.15). This population plots similarly to NDN 230 from Newfoundland (Pyne-O'Donnell et al., 2012) but is slightly offset as DHP-31c has higher wt.% FeO_t and lower MgO and Na_2O. The Ruppert tephra from the Brooks Range in Alaska (Monteath et al., 2017) with a modelled age of 2520-3230 cal yr BP is also geochemically similar, but also offset, as DHP-31c has lower wt.% Al_2O_3 and higher FeO_t. While a correlation was suggested with Augustine G (Pyne-O'Donnell et al., 2012), dated to 2000-2200 ^{14}C years BP (~1900 to 2300 cal yr BP, Waitt and Begét, 2009), the cryptotephra data do not directly correlate (e.g. Tappen et al., 2009; Figure 3.8).

The highest glass concentrations of the whole DHP174 record occur between 2,050 and 1,100 cal yr BP and have unique Mt. Churchill geochemistry's. The three largest peaks are DHP-16 (1890±190 cal yr BP), DHP-12 (1505±200 cal yr BP), and DHP-8a (1175±130 cal yr BP). DHP-8a has slightly different geochemical data than the other samples and is correlated to the WRAe, which has a modelled age of 1095-1170 cal yr BP (Davies et al., 2016) and a Greenland ice cire age of AD 853±1 (Toohey and Sigl, 2017) that agrees chronologically with DHP-8a. Geochemical data for DHP-16 and DHP-12 are both similar to WRAn (see section 3.2.5.2 below for details) and overlap with the associated modelled age of 1605-1805 cal yr BP (Davies et al., 2016). As DHP-12 has significantly higher glass concentrations (~2 millions shards/5cm^{-3}) this is interpreted as the main WRAn tephra.

DHP-8b and -7a have modelled ages of 1175±130 and 1095±85 cal yr BP, respectively. Both samples correlate well, and have relatively high wt.% SiO_2 (75.5 to 76.5) and low K_2O (1.8 to 2). These samples only occur in core DHP174-13 and are not found at all in DHP174-12. Both appear to correlate to Augustine, with two eruptions being recorded proximally at this time – tephra M at ~750 ^{14}C yr BP and tephra C at ~1,000-1,200 ^{14}C yr BP (Waitt and Begét, 2009). A correlation with Augustine C is more likely based on the chronology, although M cannot be ruled out as their geochemical data are reported as very similar (Waitt and Begét, 2009). As DHP-7a has a larger number of analyses and represents the main population of the sample it is suggested that DHP-8a may represent reworking of shards downwards in the profile as there are only 3 cm of peat between the two samples.

3.3.2.4. The last millennium and modern eruptions

Six samples were analysed from the past millennium, four of which are discussed here: DHP-2 and -4 in the 20th century and DHP-5 and -6 in a period with reduced accumulation from ~AD 900-1850. The shard concentrations range from ~4,000 to 36,000 shards/5cm^3 – this is lower than the average for peaks in the previous 2,000 years but similar to peak counts from 8,000 to 3,000 cal yr BP. Only DHP-4 has one single geochemical population present; DHP-2 and -5 have multiple populations with <10 points and DHP-6 has two dominant populations. Major element geochemical data for these samples and relevant reference material are shown in Figure 3.9.

DHP-6 has two main populations – a, an unknown dacite, and b, a rhyolite similar to Mount Churchill. The dacite DHP-6a does not match any previously published data for the age range (~AD 900-1850); it has 69 to 70 wt.% SiO_2 and an unusually broad spread in wt.% K_2O (2.8 to 3.8). DHP-5 has one main rhyolitic population, also similar to Mount Churchill; DHP-5 and -6b are discussed further in section 3.2.5 below.

Two of the four modern samples analysed can be correlated to known eruptions (Figure 3.9). DHP-4 is the oldest modern sample with the largest glass concentration in the recent record and has a single geochemical population that correlates with data for Novarupta-Katmai 1912 (Hildreth and Fierstein, 2000). To help constrain the ages for the modern period the date of this eruption was also included in the age model. DHP-2 has one main geochemical population, a rhyolite that correlates with reference material from Redoubt 1989-90 (Scott and McGimsey, 1994), which is supported by the age estimate of 1990±12.

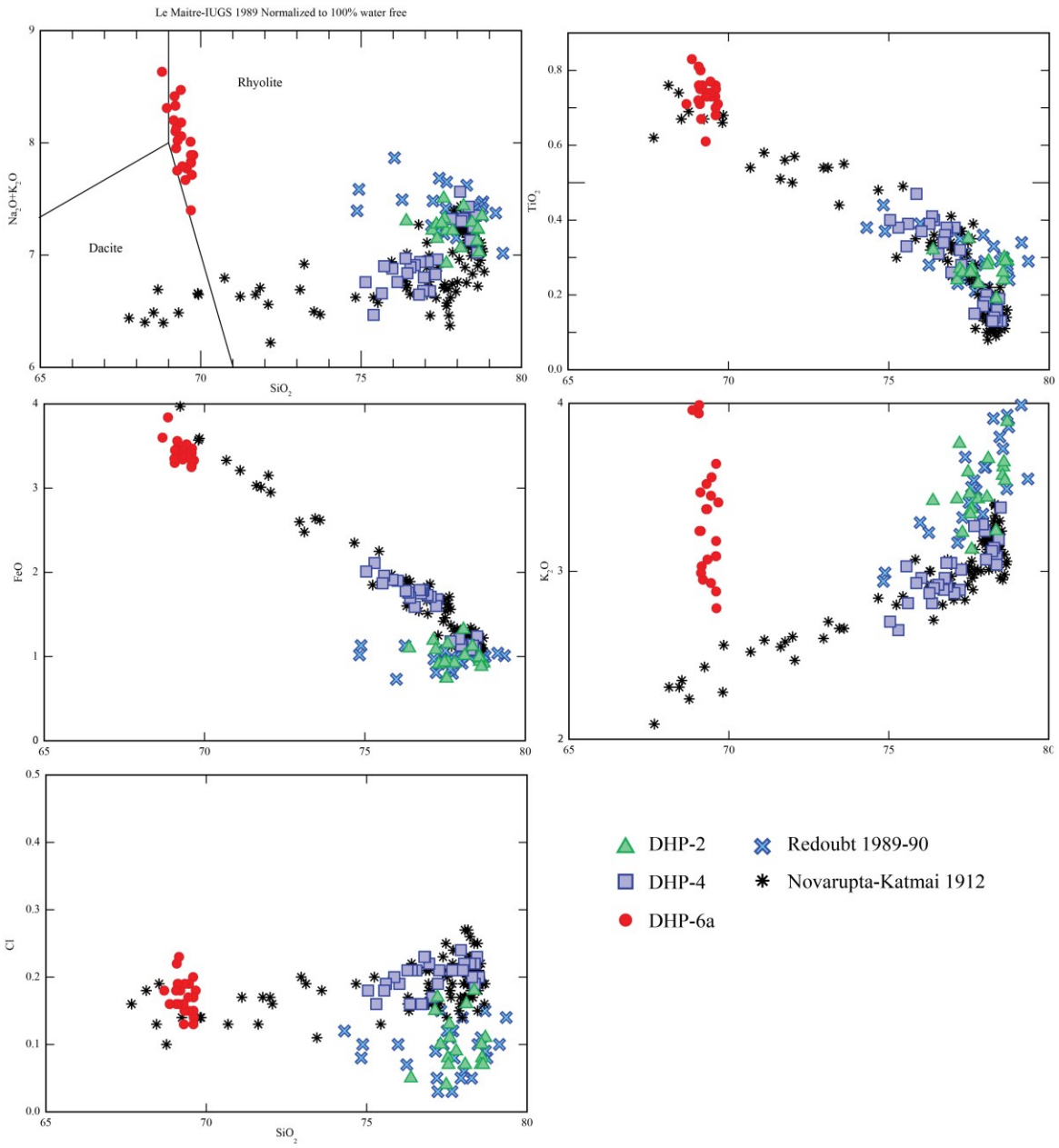

Figure 3.9 Major element glass geochemical plots for DHP174 tephra since 1,000 cal yr BP. Data from concurrently analysed reference material of Novarupta-Katmai 1912 and Redoubt 1989-90 (Davies et al., 2016) are plotted for comparison. It is not determined here if the vertical linear trend for wt.% K_2O of DHP-6a is related to the inclusion of small orthoclase crystals in the analyses as there is no similar effect seen in wt.% Al_2O_3 or FeO_t.

3.3.3. Mount Churchill

Data that are geochemically similar to Mt. Churchill are the most frequently occurring samples at DHP174, which is expected as Mt. Churchill is only ~450 km SW of DHP174 and is known to have been active during the Holocene. Previous reports of Mt. Churchill tephra include the widespread White River Ashes (WRA; Péwé, 1975) split in to the northern (~1700 cal yr BP) and eastern (~1135 cal yr BP) lobes; as well as a younger visible tephra at a proximal location (10cm above WRAe; Preece et al., 2014) and potentially both a younger and an older cryptotephra at a distal location in south-eastern Alaska (~300 cal yr BP and 6300 cal yr BP; Payne et al., 2008).

The record presented here, however, has far more frequent tephra preservation, with Mt. Churchill like glass occurring in thirty-five samples across the Holocene (Table 3.3; Figure 3.10). We do not suggest that these all represent primary airfall as the relative proximity to Mt. Churchill means it is more likely that glass will be reworked on the landscape given the higher concentrations of glass present. Also, although reworking within the sequence is limited to a few cm for most of the Holocene, the higher concentrations related to Mt. Churchill (e.g. ~2 million shards/5cm^3 associated with the WRAn) may facilitate more significant reworking and over-representation. Furthermore, the similarity in major and trace elements for glass from Mt Churchill does not allow easy separation of eruptions (Preece et al., 2014; Davies et al., 2016).

Despite these challenges, the presence of Mt. Churchill-like glass can still be used as indication of increased activity during the Holocene. The samples are categorised as five periods of activity where >10 analyses are present in a sample but may be a background signal: 8,200 to 9,200 cal yr BP, 4,900 to 7,500 cal yr BP, 2,500 to 3,400 cal yr BP, 1,100 to 2,000 cal yr BP, and <1,000 cal yr BP. These interludes are stratigraphically separated and contain intervening geochemically distinct tephra beds that lack Mt. Churchill analyses. Beyond this, specific definitions are made for ten ‘glass peaks’ where there is some limited confidence of a primary airfall event, and seven ‘eruptions’ with the highest level of confidence (see Figure 3.10, and Table 3.3 for the full list of sample details).

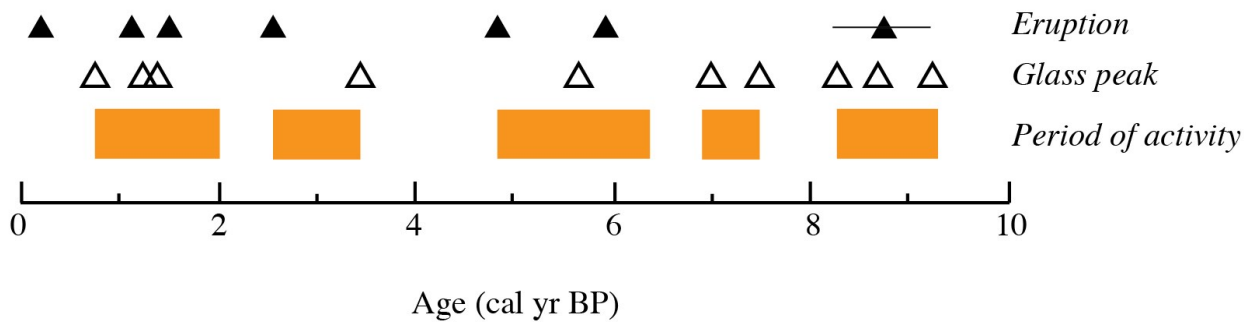

Figure 3.10: Holocene activity and major eruptions from Mt. Churchill interpreted from the DHP174 cryptotephra record. Glass peaks and eruptions refer to samples listed in Table 3.3. Periods of activity cover all samples with >10 glass analyses geochemically correlated to Mt. Churchill present.

a) Primary eruptions						
ID	**Depth (ccd)**	**Modelled age (mean cal BP)**	**1SD**	**Shards/5cm^3**	***n***	**Correlated eruption**
DHP-5	13	155	65	12038	21	**Lena?**
DHP-8	26	1175	130	248063	28	**WRAe**
DHP-12	38	1505	200	2149678	45	**WRAn**
DHP-22	76	2540	235	64266	47	--
DHP-39	165	4875	480	85502	21	--
DHP-46	205	5925	430	68559	56	--
b) Periods of activity (isochron/eruptions not identified)						
ID	**Depth (ccd)**	**Modelled age (mean cal BP)**	**1SD**	**Shards/5cm^3**	***n***	**Comments**
DHP-6	19	740	265	36421	22	Could be reworked post WRAe; similar geochem
DHP-9	30	1285	165	15392	21	In-between WRAe and WRAn (5 to 8 cm spacing) with smaller peaks in GC and similar geochem
DHP-11	35	1425	195	21209	19	
DHP-30	110	3430	410	11644	19	Small numbers of Mt. Churchill analyses in every sample from DHP-22 to -30 (over 35 cm; 100-10000 shards/5cm^{-3})
DHP-44	194	5635	450	13177	30	In-between two larger peaks of Mt. C glass with similar geochem; 10-30 cm between each
DHP-52	246	7000	245	566	10	Small peaks of glass but separated from other Mt. Churchill glass by 40 to 60 cm
DHP-53	266	7490	125	1684	14	
DHP-59	300	8180	265	4541	11	Likely first eruptive activity but also high risk for reworking and secondary deposition on peatland surface so primary airfall is not identified here
DHP-61	320	8585	270	679	11	
DHP-64	347	9135	215	359	10	

Table 3.3: Summary of records at DHP174 of individual eruptions and periods of activity of Mt. Churchill.

3.3.3.1. Chronostratigraphy of Mt. Churchill-like samples

Three samples in the DHP174 record represent the oldest occurrence of Mt. Churchill-like geochemistry and are also three of the four largest peaks in the early Holocene: DHP-59, -61, and -64. These correlate with proximal material (of a much younger age) from Mt. Churchill (Samples 11A and 16, Preece et al., 2014); a direct correlation to these samples is not proposed here given their ages, but Mt. Churchill is suggested as the likely source given the similarity.

The proximal samples are correlated to WRAn and have higher SiO_2 values (75 to 78%) than are typically found at other sites. These samples date to 9165±215 cal yr BP (DHP-64, ~359 shards/5cm^{-3}), 8585±270 cal yr BP (DHP-62, ~125 shards/5cm^{-3}), and 8180±265 cal yr BP (DHP-59, ~4541 shards/5cm^{-3}). Given the presence of samples lacking Churchill affinities between these peaks it is unlikely they represent reworking within the peat stratigraphy, but may represent re-deposition on the surface. DHP-64 in particular has 4 additional geochemical populations with <10 points, suggesting either a decrease in peat accumulation or increase in glass deposition (relating to increased volcanic activity or surficial reworking). These samples are interpreted as evidence for a period of early activity of Mt. Churchill, with at least one individual eruption.

After the initial appearance of Mt. Churchill like tephra in the Holocene, glass appears again in thirteen samples between 7,500 and 4,900 cal yr BP, after a period of ~700 years. At least two large primary eruptions are interpreted here. Eleven of these samples are unique populations, while two are multimodal with other geochemical populations present. DHP-53 and -52 are the oldest occurrences with modelled ages of 7490±125 and 7000±245 cal yr BP, respectively, and have relatively small peaks in glass concentration (500-1,700 shards/5cm^{-3}). As these are stratigraphically separated from the other tephra they are interpreted as a unique period of activity, but were likely small eruptive events.

DHP-46 (5925±430 cal yr BP) and DHP-39 (4875±480) are the largest peaks in shard concentration for the period (68,500 - 85,500 shards/5cm^3; Figure 3.3) and are interpreted here as primary airfall events. They are separated by 40 cm of peat accumulation (~1,100 years) and are hence unlikely to be reworked. DHP-46 is also the closest eruption chronologically to the cryptotephra MTR 146 reported at ~6300 cal yr BP in Payne et al. (2008) and overlaps within errors. DHP-44 (5635±450 cal yr BP) lies stratigraphically between these two samples. While it

has a relatively high glass concentration peak, it is significantly smaller than DHP-46 and -39 and is not geochemically distinct. Therefore, it may represent a separate eruption but is not interpreted as one with the data presented here. Additional samples from this interval with lower glass concentrations (200 to 4,000 shards/5cm^3) and/or multimodal geochemistries that are stratigraphically above and below these samples (DHP-40, -41, -42, -43, -45a, -47, -48, and -50c) are also not identified as clear separate primary airfall events.

Five samples have unique Mt. Churchill like geochemistry between 3,400 and 2,500 cal yr BP: DHP-22, -24, -25, -27, and -30. Of these, DHP-22 (2540±235 cal yr BP) has the highest glass concentrations (64,300 shards/5cm^{-3}; Figure 3.3) and is identified as primary airfall. DHP-30 (3430±410 cal yr BP) has relatively high glass concentrations (11,600 shards/5cm^{-3}) but is not clearly a distinct airfall event as it occurs at the start of a period where samples have relatively low numbers of Mt. Churchill like analyses (Table S2) and may represent reworking. The three samples in between are also not identified as primary airfall events here with the available data.

The three largest peaks between 1,900 and 1,100 cal yr BP (DHP-16, DHP-12 and DHP-8) have been discussed above in section 3.2.3.2. Given the abundance of glass present in DHP-12 it is not possible to determine whether any of the samples stratigraphically below (from DHP-13 to DHP-18) are primary airfall or glass reworked downwards, particularly as they are within the average maximum depth of active layer thaw for the site (>50 cm). DHP-9 and -11 have shard concentrations that are equivalent to less than 10% of the WRAe and WRAn deposits that they occur stratigraphically between (with ~3 cm of peat accumulation between each) and are geochemically similar to, respectively, so they cannot be confidently identified as unique airfall events. DHP-11, however, does have some unique geochemical characteristics (see section 3.2.5.2 below for details) that may add relate to either a separate eruption or a subunit of WRAn (Preece et al., 2014).

In the past 1000 years both DHP-5 and DHP-6b have Mt. Churchill like geochemical data and correlate well with each other (although DHP-5 has a wider SiO_2 range) but the 6 cm of peat accumulation between the two suggests they are separate eruptions. Modelled ages for DHP-5 and -6 are not likely reliable given the reduced accumulation between 12-20 ccd. The ^{14}C date at 14 ccd sits on a plateau in the ^{14}C calibration curve, resulting in modelled age estimates from AD

1675-1685, 1735-1780, and 1795-1810. DHP-5 directly overlies this and DHP-6 is located between this date and a lower ^{14}C date at 22 ccd which calibrates to AD 845±35.

3.3.3.2. Major element geochemical analyses of Mt. Churchill-like samples

The major element geochemical data of the Mt. Churchill like glass peaks and eruptions are consistent over the entire Holocene, with changes largely relating to the range of wt.% SiO_2 values. There are some subtle changes in FeO_t and MgO and CaO but these are often within the range of associated errors. Glass from Mt. Churchill is typically frothy and pumaceous and has numerous plagioclase microlites that can make analysing these samples, and obtaining high numbers of glass points without mineral inclusions, challenging. Figure 3.11 shows data for the samples discussed here plotted in brackets of their erupted time period with envelopes representing proximal data for WRAe and WRAn (Jensen et al., 2014; Preece et al., 2014). Solid symbols represent samples identified as primary airfall, while outlines are published data for WRAe and WRAn.

The oldest Mt. Churchill activity in the DHP174 record occurs between 9,200-8,200 cal yr BP (DHP-64, -61, and -59) and is geochemically similar to WRAn with wt.% SiO_2 ranges from 75 to 77, and some slight variance in the alkalis. DHP-53 and -52, starting the next period of activity at ~7,500-7,000 cal yr BP, have slightly lower wt.% SiO_2 ranges (from 74.5 to 76.5) and DHP-52 in particular sits between the data for WRAn and WRAe, with slightly lower wt.% FeO_t and MgO.

DHP-46 is the first high concentration peak interpreted as primary airfall and occurs ~1,100 years later at ~5,900 cal yr BP. Both DHP-46 and -44 also have the first evidence for wider wt.% SiO_2 ranges (74 to 78) that are similar to data for both WRAn and WRAe, and DHP-46 has a broader range of wt.% MgO and CaO. DHP-39 at ~4,900 cal yr BP has a slightly more constrained wt.% SiO_2 range from 75 to 77. DHP-30 at ~3,400 cal yr BP and DHP-22 at ~2,500 cal yr BP are both high concentration peaks and have more typical wt.% SiO_2 ranges of 75 to 77 that correlate well with data for WRAn although DHP-22 has a broader range of MgO.

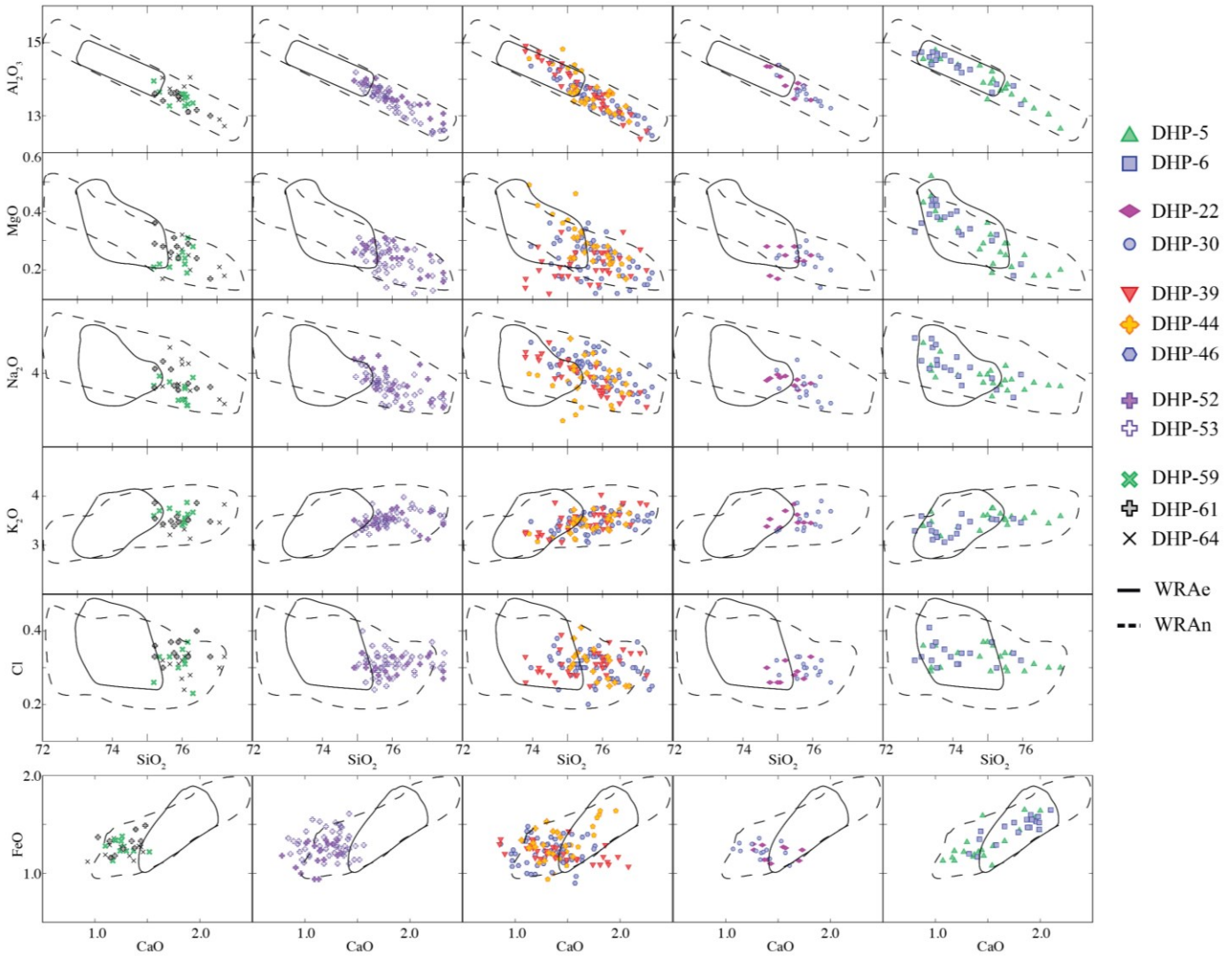

Figure 3.11 Major element glass geochemical plots for DHP174 tephra correlated to Mt. Churchill separated by age. a) <1000 cal yr BP; b) 2500-3500 cal yr BP; c) 4900-6000 cal yr BP; d) 7000-7500 cal yr BP; e) 8200-9200 cal yr BP. Envelopes representing published data for WRAn and WRAn (Preece et al., 2014) are plotted for comparison.

The tephra fall recorded by DHP-12 at 1505±200 cal yr BP is the largest glass concentration peak of the record and is correlated to the WRAn. The data have a wt.% SiO_2 range of 75 to 77 and match well both geochemically and chronologically. DHP-11 at 1425±195 cal yr BP postdates this peak by ~100 years and has a comparatively broad wt.% SiO_2 range of 72 to 76 with slightly lower wt.% FeO_t. DHP-9 at 1285±165 cal yr BP and DHP-8 at 1175±130 cal yr BP both have the lowest and most tightly constrained wt.% SiO_2 ranges of the data analysed here (73 to 74/75, respectively) and are correlated to the WRAe. It is not certain if DHP-9 represents a primary airfall event as the data for both samples match geochemically, have shard concentrations that are an order of magnitude different, and are only separated by 4 cm of peat.

Between ~AD 1900 and AD 1000, DHP-6b and -5 both have broader wt.% SiO_2 ranges of 72 to 77 and correlate well with published data for a visible tephra sample of WRA-Eb (Sample 12E) from Preece et al., 2014. Sample 12E was collected within 100 km of Mount Churchill's vent in western Yukon and was reported as having a likely genetic link to the magma source of the widespread WRAe tephra. The data are also similar to published values for the Lena tephra (Payne et al., 2008) and occur at a coincident time, but geochemically they differ slightly in wt.% FeO_t, CaO, MgO, and Na_2O so a correlation cannot be supported without further analysis.

3.4 Discussion

Abundant glass is recorded at DHP174 since peatland inception in the early Holocene. This is the first detailed contribution to a Holocene cryptotephra chronostratigraphy in northwestern North America, and demonstrates the potential for soligenic peatland archives in the zone of continuous permafrost. The key cryptotephra beds for future correlations and their identifying characteristics are outlined here before more general discussion of the DHP174 record as a stratigraphic archive of Holocene volcanic activity.

3.4.1. Key beds for a regional tephrostratigraphy

Within the DHP174 record there are a total of thirty-four identified cryptotephra that can contribute to a regional tephrostratigraphy. Their sample information and average major element glass geochemical data are summarised in Table 3.4. These key beds have a combination of features including significant glass concentrations, distinctive geochemical data, useful stratigraphic positions/timings, and potential correlation to other known records over a wide area.

ID	Depth (ccd)	Modelled age (mean cal BP)	1SD	Shards / 5cm^3		SiO_2	TiO_2	Al_2O_3	FeO	MnO	MgO	CaO	Na_2O	K_2O	Cl	H_2O_d	*n*	Correlated eruption	Suggested source/eruption
DHP-2	3	-40	12	8354	a	77.84	0.27	12.38	0.99	0.04	0.17	1.01	3.74	3.49	0.10	2.44	18	**Redoubt 1989-90**	Redoubt
		(1990)				0.65	0.04	0.39	0.15	0.03	0.09	0.22	0.19	0.19	0.04	0.56			
DHP-4	10	38	1	30084	-	77.01	0.29	12.57	1.56	0.05	0.24	1.15	3.97	3.00	0.20	3.31	28	**Novarupta -Katmai 1912**	Novarupta-Katmai
		(1912)				1.05	0.11	0.42	0.34	0.03	0.11	0.36	0.18	0.17	0.02	1.10			
DHP-5	13	155	65	12038	a	75.00	0.19	13.90	1.32	0.05	0.30	1.52	3.95	3.51	0.33	2.92	21	**(Lena?)**	Mt. Churchill
		(1795)				1.12	0.05	0.56	0.19	0.04	0.10	0.29	0.17	0.16	0.03	1.18			
DHP-6	19	735	280	36421	a	69.30	0.74	15.06	3.42	0.14	0.76	2.43	4.65	3.34	0.17	2.10	24	--	Unknown
						0.26	0.05	0.16	0.12	0.04	0.05	0.10	0.26	0.38	0.02	0.88			
DHP-7	23	1095	85	76117	a	75.86	0.35	12.99	1.94	0.06	0.41	2.20	3.96	1.96	0.31	2.11	42	--	Augustine C?
						0.28	0.04	0.19	0.07	0.03	0.03	0.09	0.16	0.11	0.03	1.19			
DHP-8	26	1180	135	248063	a	74.00	0.20	14.27	1.45	0.05	0.36	1.79	4.14	3.39	0.36	2.51	28	**WRAe**	Mt. Churchill
						0.64	0.04	0.31	0.16	0.03	0.06	0.17	0.12	0.15	0.04	1.06			
DHP-12	38	1510	215	~2,150, 000	-	76.00	0.20	13.30	1.32	0.05	0.24	1.24	3.88	3.50	0.31	2.27	45	**WRAn**	Mt. Churchill
						0.74	0.04	0.45	0.12	0.03	0.05	0.18	0.20	0.15	0.04	1.58			
DHP-21	70	2380	170	65993	a	65.03	1.10	16.13	5.08	0.17	1.47	3.93	4.92	2.06	0.12	1.03	33	--	Unknown
						(0.39)	(0.07)	(0.18)	(0.15)	(0.03)	(0.09)	(0.12)	(0.20)	(0.09)	(0.02)	(1.84)			
					b	73.69	0.25	14.74	1.73	0.08	0.50	2.29	3.72	2.71	0.38	3.21	38	--	Hayes?
						0.75	0.05	0.25	0.18	0.03	0.06	0.18	0.18	0.13	0.05	1.14			
					c	74.44	0.33	13.66	2.25	0.09	0.40	2.24	4.27	2.06	0.25	1.86	10	--	Unknown
						0.31	0.04	0.16	0.12	0.03	0.03	0.08	0.11	0.10	0.02	0.61			
DHP-22	76	2540	235	64266	a	75.98	0.19	13.38	1.30	0.05	0.23	1.23	3.81	3.53	0.31	1.53	47	--	Mt. Churchill
						0.67	0.05	0.43	0.13	0.02	0.05	0.19	0.17	0.17	0.03	1.09			
DHP-31	116	3590	425	69950	-	71.31	0.49	15.13	2.41	0.13	0.49	1.70	5.17	3.12	0.20	1.40	67	**Aniakchak CFE II**	Aniakchak
						0.27	0.05	0.14	0.05	0.03	0.03	0.08	0.19	0.16	0.03	1.12			
DHP-32	120	3695	435	10687	a	77.47	0.24	12.51	1.44	0.07	0.33	2.04	4.00	1.67	0.23	3.03	9	--	Unknown
						0.50	0.04	0.40	0.11	0.02	0.03	0.14	0.24	0.13	0.04	0.95			
DHP-34	133	4035	460	164555	a	74.03	0.22	14.64	1.62	0.08	0.48	2.12	3.85	2.67	0.35	2.09	26	**Hayes set H unit F2**	Hayes
						0.47	0.04	0.29	0.13	0.03	0.05	0.10	0.20	0.13	0.06	1.09			
DHP-35	147	4400	475	53984	a	73.85	0.31	14.43	2.04	0.09	0.46	2.35	4.38	1.99	0.13	1.58	15	--	Unknown
						0.58	0.04	0.21	0.21	0.03	0.07	0.15	0.23	0.11	0.02	1.09			
DHP-37	154	4585	480	25859	a	71.09	0.45	14.99	2.52	0.09	0.74	2.93	4.29	2.75	0.20	1.93	9	--	Unknown
						0.90	0.05	0.33	0.24	0.02	0.09	0.26	0.20	0.14	0.02	0.87			
DHP-38	163	4820	480	82158	a	76.85	0.25	12.77	1.58	0.07	0.38	2.37	3.90	1.68	0.20	1.49	24	**Tephra J127**	Augustine/ Kaguyak
						0.23	0.04	0.10	0.07	0.02	0.02	0.10	0.13	0.10	0.02	0.72			
					b	77.54	0.23	12.78	1.52	0.07	0.32	2.09	3.65	1.67	0.19	3.04	10	--	Augustine/ Kaguyak
						0.07	0.04	0.09	0.05	0.02	0.03	0.06	0.11	0.08	0.02	1.64			
DHP-39	165	4875	480	85502	a	75.79	0.18	13.41	1.29	0.06	0.26	1.29	4.02	3.49	0.31	2.68	21	--	Mt. Churchill
						0.53	0.06	0.27	0.12	0.03	0.04	0.13	0.19	0.15	0.05	1.60			

Table 3.4: Summary of the key tephra described within this study most useful for a regional tephrochronosratigraphy, listed in chronological order (oldest to youngest). Correlations to previously named tephra and volcanic sources are shown where relevant.

ID	Depth (ccd)	Modelled age (mean cal BP)	1SD	Shards / 5cm^3		SiO_2	TiO_2	Al_2O_3	FeO	MnO	MgO	CaO	Na_2O	K_2O	Cl	H_2O_d	*n*	Correlated eruption	Suggested source/eruption
DHP-45	199	5765	445	2627	b	72.70	0.45	14.35	2.22	0.06	0.58	2.31	4.48	2.65	0.20	1.62	10	--	Redoubt
						0.52	0.03	0.23	0.14	0.02	0.07	0.14	0.20	0.12	0.03	1.33			
DHP-46	205	5925	430	68559	-	75.78	0.18	13.50	1.22	0.06	0.24	1.32	4.04	3.47	0.30	1.95	56	--	Mt. Churchill
						0.82	0.05	0.48	0.13	0.03	0.06	0.22	0.21	0.18	0.04	0.88			
DHP-49	224	6420	370	250	b	77.28	0.30	12.43	1.46	0.05	0.25	1.74	3.57	2.77	0.18	1.91	10	--	Kaguyak?
						0.27	0.04	0.27	0.08	0.03	0.04	0.08	0.12	0.22	0.03	0.59			
DHP-50	228	6525	355	4058	a	64.93	0.89	15.48	5.63	0.15	1.94	4.88	4.24	1.72	0.17	1.98	11	--	Oshetna?
						1.17	0.04	0.40	0.36	0.03	0.23	0.40	0.13	0.16	0.02	0.85			
					b	75.46	0.53	12.51	2.30	0.06	0.47	1.82	4.07	2.68	0.22	1.62	48	--	Oshetna?
						1.42	0.11	0.44	0.48	0.04	0.15	0.42	0.22	0.24	0.04	1.06			
DHP-51	239	6815	295	1834	a	65.60	1.11	15.47	5.25	0.17	1.40	3.69	4.68	2.59	0.15	1.90	39	--	Unknown
						0.44	0.06	0.27	0.20	0.03	0.10	0.16	0.29	0.15	0.02	1.15			
					b	75.37	0.40	12.67	1.87	0.06	0.30	1.40	3.64	3.99	0.43	1.76	10	--	Unknown
						1.23	0.07	0.58	0.21	0.03	0.11	0.33	0.26	0.14	0.06	0.97			
DHP-54	269	7550	150	37936	a	73.04	0.50	14.17	2.20	0.07	0.59	2.28	4.22	2.74	0.21	2.50	16	--	Redoubt
						0.68	0.04	0.28	0.19	0.02	0.07	0.17	0.18	0.07	0.03	1.05			
					b	77.43	0.20	13.09	1.22	0.09	0.29	2.07	3.85	1.63	0.15	2.39	16	--	Augustine?
						0.22	0.04	0.13	0.08	0.03	0.06	0.10	0.15	0.08	0.02	0.69			
DHP-56	288	7935	240	12503	-	76.14	0.23	13.23	1.51	0.06	0.27	1.56	4.74	2.08	0.16	2.35	11	**KO**	Kuril-Lake Iliinsky, Kamchatka
						0.49	0.03	0.31	0.11	0.02	0.04	0.13	0.18	0.10	0.02	1.22			
DHP-57	289	7955	240	14083	a	76.90	0.23	13.18	1.46	0.06	0.22	1.53	4.14	2.19	0.16	2.08	28	KO	Kuril-Lake Iliinsky, Kamchatka
						0.46	0.03	0.28	0.08	0.03	0.03	0.12	0.19	0.08	0.03	0.84			
					b	77.95	0.15	12.98	1.11	0.07	0.28	1.75	3.77	1.91	0.18	2.30	12	--	Crooked creek
						0.42	0.04	0.27	0.07	0.03	0.06	0.23	0.23	0.22	0.03	1.02			Augustine?
DHP-62	335	8890	250	125	a	67.70	0.78	15.26	4.94	0.14	0.93	3.33	5.00	2.04	0.15	1.49	19	--	Unknown
						(0.43)	(0.06)	(0.13)	(0.14)	(0.03)	(0.06)	(0.16)	(0.23)	(0.07)	(0.03)	(0.67)			
DHP-67	177	9560	110	71	-	72.84	0.48	13.54	3.82	0.15	0.58	2.89	4.58	0.95	0.18	2.52	12	**TR(Zv)**	Zavaritsky. Kurile Islands
						(0.22)	(0.03)	(0.08)	(0.25)	(0.02)	(0.07)	(0.1)	(0.24)	(0.07)	(0.02)	(0.7)			
DHP-71	213	10420	90	87	-	69.11	0.57	15.47	4.09	0.18	0.56	2.21	5.07	2.58	0.20	2.32	25	**Funk/ Fisher**	Fisher
						(0.35)	(0.05)	(0.27)	(0.12)	(0.03)	(0.05)	(0.1)	(0.22)	(0.1)	(0.02)	(1.36)			
DHP-74	232	10485	50	537	-	67.85	1.21	14.24	4.86	0.08	1.35	3.53	3.88	2.94	0.06	3.10	11	--	Unknown
						(0.4)	(0.06)	(0.09)	(0.16)	(0.04)	(0.1)	(0.12)	(0.24)	(0.09)	(0.01)	(0.56)			

Table 3.4 (cont.): Summary of the key tephra described within this study most useful for a regional tephrochronosratigraphy, listed in chronological order (oldest to youngest). Correlations to previously named tephra and volcanic sources are shown where relevant.

3.4.1.1. Tephra with correlations with known eruptions

Eleven cryptotephra reported here can be correlated to known eruptions using major element EPMA data. These represent widespread, key marker beds on an international scale (Figure 3.12; a distribution for Tephra J127 is not shown as it only has confirmed reports at one site to date).

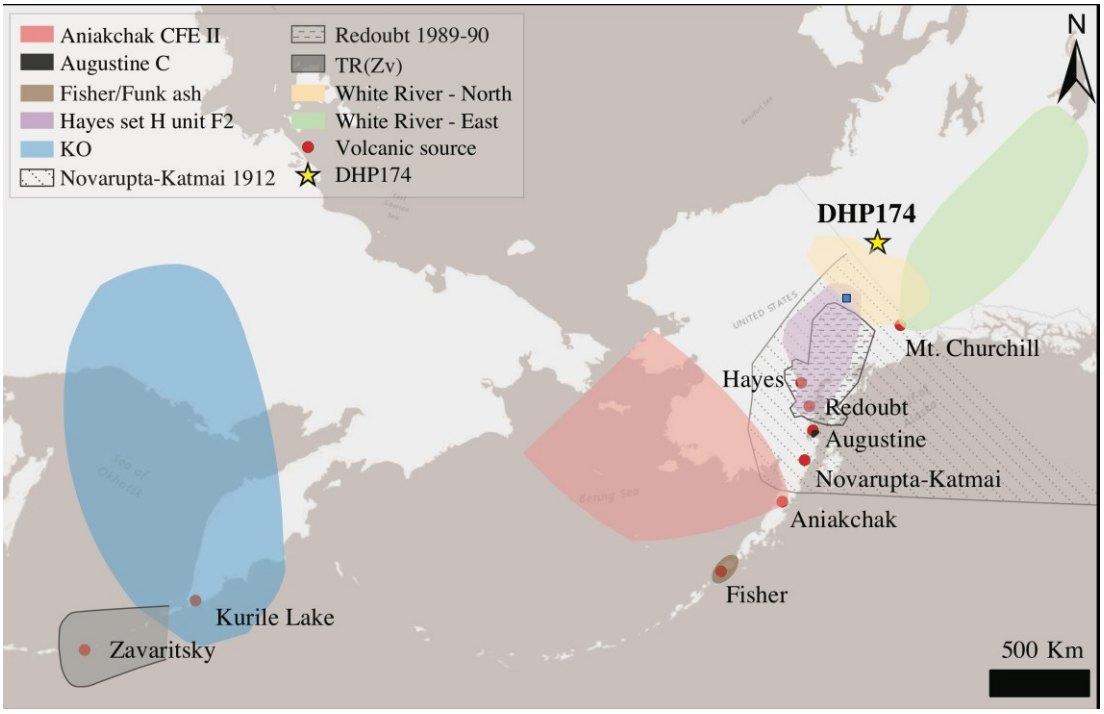

Figure 3.12: Map showing source volcanoes (circles) and the previous geographical distributions of known tephra correlated to samples at DHP174 (shown with a star symbol). Tephra J127 reported at Jan Lake is shown with a blue square (Monteath et al., 2017).Tephra distributions are based on published reports of visible tephra deposits and modern plume observations (Scott and McGimsey, 1994; Carson et al., 2002; Hildreth and Fierstein, 2012; Davies et al., 2016; Derkachev et al., 2016; Ponomareva et al., 2017a). Aniakchak CFE II has been found beyond the area shown as a cryptotephra in multiple locations across Alaska and beyond (e.g. Dunning, 2011; Lakeman et al., 2008; Payne and Blackford, 2008; Pearce et al., 2017; Zdanowicz et al., 2014).

In the early Holocene, the Funk/Fisher ash (DHP-71, 10420±90 cal yr BP), TR(Zv) tephra (DHP-67, 9560±110 cal yr BP) and KO tephra (DHP-56, 7955±240) are the furthest travelled glass recorded in the DHP174 record. These all have relatively small glass concentration signals that are part of double- or triple-peaks but their major element geochemistries are easily differentiated – Funk/Fisher ash is dacitic with low wt.% TiO_2 and relatively high Na_2O; TR(Zv)

and KO both have relatively higher wt.% FeO_t and lower K_2O than glass from Alaska or the Aleutians (Figures 4 and 5).

After this there is a period with very little glass correlating to known eruptions until DHP-38a at 4820±480 cal yr BP. This tephra has not been reported proximally but correlates well with the visible Tephra J127 in Jan Lake (Monteath et al., 2017). It has a high glass concentration signal at DHP174 (with the sample containing two geochemical populations) and is geochemically distinct due to its low wt.% K_2O, relatively low Al_2O_3, and higher CaO (Figure 6).

Two of the most widely and frequently reported Holocene distal tephra in Alaska (Figure 3.12) occur within 500 years of each other: Hayes set H unit F2 (DHP-34a, 4035±460 cal yr BP) and Aniakchak CFE II (3590±425 cal yr BP). These represent major contributions to a tephrostratigraphy as they can be used to link many sites and records together. Both tephra have some of the highest (non-Mt. Churchill) glass concentrations recorded at DHP174 and can be easily identified by correlation with their well characterised reference samples.

The WRAs are both identified at DHP174 and have very high to extremely high glass concentrations (WRAn - DHP-12, 1505±200 cal yr BP; WRAe – DHP-8a, 1175±130 cal yr BP). These tephra are widespread visibly in the Yukon Territory and western Canada, and the WRAe particularly has been found visibily into the Northwest Territories (Robinson, 2001; Patterson et al., 2017) and as a cryptotephra in eastern Canada (Pyne-O'Donnell et al., 2012), USA (Mackay et al., 2016), Greenland and Europe (Jensen et al., 2014). Their geochemical data plot closely, given they are from the same source, but differences in their range of wt.% SiO2 can be used to distinguish them as well as their estimated ages (Figure 10).

Shortly after the WRAe, DHP-7a has a modelled age of 1095±85 cal yr BP and is correlated with Augustine C. This tephra is recorded in proximal records around Augustine volcano (e.g. Waitt and Begét, 2009) but has not been reported distally. It has a relatively high glass concentration peak, although this may also be attributed to a secondary population of glass correlated with Mt. Churchill. Its major element geochemistry is distinctive due to its high wt.% SiO_2, FeO_t, and Cl, and low K_2O (Figure 7).

Two eruptions are identified in the modern period: Novarupta-Katmai 1912 (DHP-4), the largest 20^{th} century eruption in Alaska, and Redoubt 1989-90 (DHP-2a). Both of these tephra are found

across southern and central Alaska, and observations of their plumes and trajectories suggested ash would likely travel over Yukon Territory (Davies et al., 2016). Both eruptions have similar major element geochemical data, but can be differentiated most clearly from each other using the range of wt.% SiO_2 analysed (which can be much higher for Novarupta-Katmai 1912) and their wt.% FeO_t, K_2O and Cl (Figure 8).

3.4.1.2. Tephra with suggested correlations to known sources

Eleven of the key cryptotephra reported here have suggested correlations to a specific volcanic source: four to Mt. Churchill, four to Augustine and/or Kaguyak, two to Redoubt, and one to Hayes.

Mt. Churchill has previously published evidence for two and perhaps three Holocene eruptions (Payne et al., 2008; Preece et al., 2014) that are both younger and older than the WRAn and WRAe. Here we suggest there may be at least four additional eruptions that vary in size and plume trajectory. Modelled ages for eruptions preceding the WRAn are: 5925±430, 4875±480 and 2540±235 cal yr BP. One eruption post-dates the WRAe, but due to a period of reduced peat accumulation it's modelled age (155±65 cal yr BP) may not be precise. This sample may correlate with previously published tephra that are reported as 10cm above WRAe (Preece et al., 2014) and Lena tephra at 285-310 cal yr BP (Payne et al., 2008) but this cannot be confirmed given the uncertain chronological data at DHP174 and geochemical offsets from the published data.

While Augustine has a well-defined proximal stratigraphy for the last 2,500 years, it is believed to have been relatively inactive in the early Holocene (Waitt and Begét, 2009) although there are several distal tephra which are reported as potential correlatives (e.g. Reger et al., 1995; Riehle et al., 1999). DHP-57b (7955±240 cal yr BP) and DHP-54a (7550±150 cal yr BP) plot closely to average EPMA major element geochemical data published for Crooked Creek tephra (Reger et al., 1995), which is suggested to have originated from Augustine. DHP-49 (6420±370 cal yr BP) and DHP-38 (4820±480 cal yr BP) have relatively low wt.% K2O which is distinctive for Alaska and Aleutian tephra and is tentatively linked to either Augustine or Kaguyak (Fierstein and Hildreth, 2008).

Redoubt has few proximal records of activity during the Holocene that would likely have produced large volumes of ash, but nearby lake records suggest that there may have been several periods producing visible tephra that are suggested to originate from Redoubt given their location and grain size data (Riehle, 1985; Schiff et al., 2008, 2010). DHP-54b (7550±150 cal yr BP) and DHP-45b (5765±445 cal yr BP) have similar major element geochemical data to published averages for material from Redoubt (rhyolites with relatively high wt.% FeO_t, CaO, and mid-range K_2O) and occur at the same time as visible tephra deposits in lake records close to Redoubt volcano (Riehle, 1985; Schiff et al., 2008, 2010).

DHP-21 (2380±170 cal yr BP) has multiple geochemical populations, but the dominant rhyolite (DHP-21b) is similar to the Devil tephra and unit F2 of set H, both sourced from Hayes volcano (Wallace et al., 2014; Mulliken, 2016). This tephra has mid-range wt.% K_2O and relatively high Cl (Figure 7) but is significantly older (~600 years) than the Devil tephra and therefore occurs between known eruptions from Hayes volcano.

3.4.1.3. Unknown tephra

There are twelve remaining cryptotephra described here for which there are no obvious correlations with either a known eruption or volcanic source. As some of these tephra occur in periods with few/no identified distal tephra correlations, and often have distinct major element geochemical data, they are important additions to the well-known key beds and sources discussed. Three of these samples are dacites, four are rhyolites, and two have bimodal populations (dacitic and rhyolitic) and may represent either one eruption with a broad geochemical range or two concurrent eruptions.

Two of the dacites are recorded in the early Holocene at 10485±50 cal yr BP (DHP-74) and 8890±250 cal yr BP (DHP-62a), while the other (DHP-6a) is recorded in the period of reduced peat accumulation in the last 1ka and has an imprecise modelled age of 740±265 cal yr BP. The rhyolites all occur in the late Holocene: two samples precede Hayes set H unit F2 (DHP-37a, 4585±480 cal yr BP; DHP-35a, 4400±475 cal yr BP), one lies between Hayes F2 and Aniakchak CFE II (DHP-32a, 3695±435 cal yr BP), and one is a sub-population present in the same sample as a likely Hayes correlative tephra (DHP-21c, 2380±170). DHP-37a has distinctive major

element geochemical data with relatively high wt.% Al_2O_3, FeO_t, and MgO, and a SiO_2 range of 70 to 72.

The remaining three rhyolites all have low wt.% K_2O but a correlation is not clear as there are no reported of activity or distal deposits for either Augustine or Kaguyak at this time and no other similarities for the major element geochemical data. DHP-35a has relatively low wt.% K_2O (1.9 to 2.1) but higher Al_2O_3 and FeO_t and lower Cl than is typical from Augustine or Kaguyak. DHP-32a has a high constrained range of wt.% SiO_2 (77 to 78) with relatively low Al_2O_3, and low K_2O (1.5 to 1.8). DHP-21c has constrained mid-range wt.% SiO_2 (74 to 75) with relatively low wt.% K_2O (1.95 to 2.15). This sample has a similar timing and geochemistry to multiple other reported cryptotephra with suggested correlations to Augustine (e.g. Monteath et al., 2017; Pyne-O'Donnell et al., 2012), however these all have slight offsets in their geochemical analyses which persist even when analysed concurrently.

The split dacite/rhyolite samples occur 300 years apart in the mid-Holocene: DHP-51 has a modelled age of 6815±295 cal yr BP while DHP-50 is slightly younger at 6525±355 cal yr BP. Populations of DHP-50 and -51 both have wt.% SiO2 ranges between 64 to 66 and 74 to 77 but they do not correlate as their major element geochemical signatures are different. These samples both occur at a similar time to the reported Oshetna tephra which has multiple reported geochemical populations (Child et al., 2013; Mulliken, 2016) and may be related to the eruption(s) contributing to those, or additional concurrent ash transport.

3.4.2. Issues of preservation and identification

Glass from numerous volcanic sources is recorded at DHP174, but there are frequent overlaps in eruptions, with multiple geochemical populations identified within a single glass concentration peak or sample. Even with 1 cm resolution analyses it is not possible to discern if all the populations analysed in a single sample relate to the depth of the analysed peak (representing 20 to 25 years for most of the Holocene record). The proportional number of analyses that a population has may relate to differences in eruption size, distance from source, and differential processes during transportation and deposition. An alternative interpretation could be that populations with smaller number of analyses have their primary airfall in the few cm above or below the peak and the analyses are shards from the 'tail' of their distribution. Increased resolution of analyses could help with this problem, but at the scale of the record here would

require significantly more time and analyses and would likely not yield sufficiently improved results. Instead, for this meso-distal location, it is recommended to use clear peaks with dominant numbers of glass analyses for correlations as they are likely the most reliable.

While a background signal of glass is present, the majority of the record has identifiable peaks above this level and the geochemical data, where unique, show little evidence of reworking of more than a few cm (as is typical for ombrotrophic peatland records – e.g. Payne and Gehrels, 2010). Exceptions to this are found at the base of the record where there are several samples with mixed or scattered geochemical data that implies reworking either within the peat sequence or re-deposition on the surface. As the onset of peatland initiation occurred at the very beginning of the Holocene there would have likely been reduced surface vegetation and more potential for wind erosion and detrital glass deposition, however this trend is not consistent over time as some tephra at that time have clear peaks with single geochemical populations. One further complication for the stratigraphic preservation relates to glass from Mt. Churchill – as it lies much closer geographically to DHP174 (~ 450 km) than most of the sources in Alaska and the Aleutians (ranging from ~ 800 km to Hayes volcano to 4500 km for Zavaritsky volcano) and has known plume trajectories in this direction (e.g. WRAn) the associated concentrations of glass measured here are often very high. If Mt. Churchill samples are not stratigraphically separated or have distinct tephra from other sources in between it is not possible to tell from EPMA data alone if they represent unique eruptions/primary airfall or reworking on the landscape or within the active layer of the peat sequence (typically up to 30 cm deep during summer from modern measurements). This is particularly problematic in the 20 cm of peat below the depth of the peak correlated to the WRAn.

From observations of historical volcanic activity, it is not surprising that we see a complex record over the Holocene. Historically there are multiple large explosive eruptions happening on an annual basis (Alaska Volcano Observatory, 2017) that can erupt for a period of days to months. Additional complications affecting the transport and deposition of ash from these eruptions include changing wind direction and broad scale atmospheric circulation (e.g. changes in the Arctic Oscillation or Pacific Decadal Oscillation). DHP-21 represents one particular example of a complex peak – three geochemical populations are identified: one dacite of unknown origin, and two rhyolites with suggested correlations to Hayes and Augustine

volcanoes. Both of these volcanoes have detailed proximal stratigraphy's but there are with no records of activity from either source at this time (~2400 cal yr BP).

Not all of the observed modern eruptions from Alaska that may be expected in the Yukon Territory are recorded at DHP174 - Crater Peak 1992, for example, has plume trajectories that suggest ash deposition in the Yukon Territory, but it is not recorded here. One possibility is that glass from smaller eruptions or those less represented at DHP174 may be lost in the background signal or overwhelmed by larger eruptions. For example, while 1 cm at DHP174 represents ~10 years for the past century, glass from Novarupta-Katmai 1912 may obscure two to four decades of eruptions with only minimal reworking. Several modern eruptions are from sources that are >1000 km from DHP174, and there are also no published glass reference major element data for eruptions from some of the closest sources (e.g. Trident, Iliamna, Veniaminof), which may therefore be present in small amounts, but unidentified.

For Holocene eruptions histories, the record described here provides a new location for cryptotephra twenty-two eruptions, eighteen of which have not been previously reported outside of Alaska or this far from their source areas (including Kamchatka and the Kurile Islands). This demonstrates significant complementary research on the geographical distribution, major element geochemistry and chronology of these tephra. For tephra linked to source volcanoes, including Mt. Churchill, Augustine, Kaguyak and Redoubt, this record also adds support to previously reported samples from single locations or research areas and may imply increased Holocene activity beyond their currently defined eruption histories. Without a closer comparison to single point major element geochemical data and reference samples, however, this cannot be confirmed. The twelve unknown tephra reported here are also of interest, particularly the dacitic samples - there are seven dacitic populations present at DHP174, several with large glass concentrations and only one of which has a known correlative here. While dacitic tephra have been found proximally, and as distal visible layers in older time periods (e.g. Preece et al., 2011) they represent a field of Holocene cryptotephra which is currently not well established.

Many of the cryptotephra found at DHP174 are from large caldera-forming eruptions, including Novarupta-Katmai, Aniakchak, Kuril-Lake Iliinsky, Zavaritsky, and Fisher. There are many reported caldera-formations from proximal studies that are not reported here, including Black Peak, Okmok, Veniaminof, Akutan, and Makushin (Miller and Smith, 1987). This lack of

recognition may also relate to a lack of published major element glass geochemical data for proximal/reference samples. Additionally, the furthest travelled cryptotephra in the record, sourced from the mid-Aleutian arc to the Kurile Islands, occur in the early Holocene but large eruptions from these areas are not recorded in the mid to late Holocene. This could be an issue of small glass concentrations being overwhelmed by glass from sources that are geographically closer but could also be explained by changing atmospheric circulation in the region. The order of magnitude shift in shard concentrations that occurs in the mid Holocene, for example, can most easily be explained by changes in atmospheric circulation, an increase in the frequency or explosivity of volcanic eruptions upwind, or significant change in peat accumulation rate.

A final consideration regarding the contribution of data from the DHP174 record to a regional tephrostratigraphy is the modelled ages of eruptions. Cryptotephra have significant potential as chronostratigraphic tools in northern records if they are well defined isochrons that can be incorporated where other methods are unsuitable. While nine of the cryptotephra reported at DHP174 that correlate with key Holocene tephra overlap within errors with previous age estimates (Redoubt 1989-90, Augustine C, WRAe, WRAn, Aniakchak CFE II, Hayes set H unit F2, Tephra J127, TR(Zv), and Funk/Fisher ash), one eruption has an age estimate that is younger (KO) than previously published. The modelled ages of these tephra overlap at the two-sigma error range, but this represents up to 500 years offset in the average ages.

3.5 Conclusions

The DHP174 cryptotephra record represents a significant advance for palaeo-records and a template in northwestern North America. There are few full Holocene records from northwestern Canada, but the combination of an ice-free area in the Yukon and early peatland initiation has resulted here in near continuous Holocene accumulation. This also is the first published use of cores from a soligenic peatland in the zone of continuous permafrost and they are shown to be an effective trap and archive of airfall material. There is little to no evidence that either colluvial processes or cryoturbation have affected peat accumulation and the cryptotephra record.

The datasets included here are a major contribution to a regional tephrostratigraphy in northwestern North America. The identification and description of thirty-four key cryptotephra for distal correlations is an important resource for chronostratigraphic correlations and doubles the number of tephra previously identified in the area. This is also the first report of tephra from

the Kurile Islands and Kamchatka in western Canada and significantly extends the known frequency and/or geographical distributions of tephra from Fisher, Augustine, Redoubt, Hayes and Mt. Churchill.

Of the thirty-four key cryptotephra identified here, six are widely reported (Hayes set H unit F2, Aniakchak CFE II, WRAn, WRAe, Novarupta-Katmai 1912, Redoubt 1989-90), three are previously reported at sites in Alaska (Funk/Fisher ash, Tephra J127, Augustine C), and two are ultra-distal (TR(Zv), KO). Seven cryptotephra have suggested correlations to Augustine, Kaguyak, Redoubt, and Hayes, and at least four additional Holocene eruptions from Mt. Churchill are proposed. Twelve cryptotephra, including six dacites, have unknown correlated eruptions or volcanic sources but are well characterised for comparison with data in future research.

By complementing and adding to the existing proximal and ultra-distal records produced on either coast of northern North America, these data demonstrate the volume and value of cryptotephra preserved across the continent and beyond. They have particular implications for our understanding of eruptive frequencies, volcanic hazards, and mechanisms of transportation (including air circulation) throughout the Holocene. While these data are not without their challenges, including the high-frequency of eruptions, their overlapping occurrence in time, and similarities in major element glass geochemistry, they provide a wealth of opportunities for further research and moving beyond descriptions to direct applications.

3.6 References

Abbott, P.M., Davies, S.M., 2012. Volcanism and the Greenland ice-cores: The tephra record. Earth-Science Rev. 115, 173–191. https://doi.org/10.1016/j.earscirev.2012.09.001

Adolphi, F., Muscheler, R., 2016. Synchronizing the Greenland ice core and radiocarbon timescales over the Holocene-Bayesian wiggle-matching of cosmogenic radionuclide records. Clim. Past 12, 15–30. https://doi.org/10.5194/cp-12-15-2016

Alaska Volcano Observatory, n.d. Alaska Volcano Observatory Online Library [WWW Document]. URL www.avo.alaska.edu/downloads/. (accessed 6.30.17).

Bacon, C.R., Neal, C.A., Miller, T.P., McGimsey, R.G., Nye, C.J., 2014. Postglacial eruptive history, geochemistry, and recent seismicity of Aniakchak volcano, Alaska Peninsula, U.S. Geological Survey Professional Paper.

Begét, J.E., Reger, R.D., Pinney, D., Gillispie, T., Campbell, K., 1991. Correlation of the Holocene Jarvis Creek, Tangle Lakes, Cantwell, and Hayes Tephras in South-Central and Central Alaska. Quat. Res. 35, 174–189. https://doi.org/10.1016/0033-5894(91)90065-D

Blockley, S.P.E., Pyne-O'Donnell, S.D.F., Lowe, J.J., Matthews, I.P., Stone, A., Pollard, A.M., Turney, C.S.M., Molyneux, E.G., 2005. A new and less destructive laboratory procedure for the physical separation of distal glass tephra shards from sediments. Quat. Sci. Rev. 24, 1952–1960. https://doi.org/10.1016/j.quascirev.2004.12.008

Braitseva, O. a., Ponomareva, V. V., Sulerzhitsky, L.D., Melekestsev, I. V., Bailey, J., 1997. Holocene Key-Marker Tephra Layers in Kamchatka, Russia. Quat. Res. 47, 125–139. https://doi.org/10.1006/qres.1996.1876

Bronk Ramsey, C., 2009. Bayesian Analysis of Radiocarbon Dates. Radiocarbon 51, 337–360. https://doi.org/10.1017/S0033822200033865

Bronk Ramsey, C., 2008. Deposition models for chronological records. Quat. Sci. Rev. 27, 42–60. https://doi.org/10.1016/j.quascirev.2007.01.019

Bronk Ramsey, C., Albert, P.G., Blockley, S.P.E., Hardiman, M., Housley, R.A., Lane, C.S., Lee, S., Matthews, I.P., Smith, V.C., Lowe, J.J., 2015. Improved age estimates for key Late Quaternary European tephra horizons in the RESET lattice. Quat. Sci. Rev. 118, 18–32. https://doi.org/10.1016/j.quascirev.2014.11.007

Calmels, F., Gagnon, O., Allard, M., 2005. A portable earth-drill system for permafrost studies. Permafr. Periglac. Process. 16, 311–315. https://doi.org/10.1002/ppp.529

Carson, E.C., Fournelle, J.H., Miller, T.P., Mickelson, D.M., 2002. Holocene tephrochronology of the Cold Bay area, southwest Alaska Peninsula. Quat. Sci. Rev. 21, 2213–2228. https://doi.org/10.1016/S0277-3791(02)00023-9

Child, J.K., Begét, J.E., Werner, A., 2013. Three Holocene Tephras Identified in Lacustrine Sediment Cores from the Wonder Lake Area , Identified in Lacustrine Sediment from Holocene the Three Cores Tephras Denali National Park Lake Preserve , Alaska , Area ,.

Clague, J.J., Evans, S.G., Rampton, V.N., Woodsworth, G.J., 1995. Improved age estimates for the White River and Bridge River tephras, western Canada. Can. J. Earth Sci. 32, 1172–1179. https://doi.org/10.1139/e95-096

Coulter, S.E., Pilcher, J.R., Plunkett, G., Baillie, M., Hall, V.A., Steffensen, J.P., Vinther, B.M., Clausen, H.B., Johnsen, S.J., 2012. Holocene tephras highlight complexity of volcanic signals in Greenland ice cores. J. Geophys. Res. Atmos. 117, 1–11. https://doi.org/10.1029/2012JD017698

Davies, L.J., Jensen, B.J.L., Froese, D.G., Wallace, K.L., 2016. Late Pleistocene and Holocene tephrostratigraphy of interior Alaska and Yukon: Key beds and chronologies over the past 30,000 years. Quat. Sci. Rev. 146, 28–53. https://doi.org/10.1016/j.quascirev.2016.05.026

Davies, S.M., 2015. Cryptotephras: The revolution in correlation and precision dating. J. Quat. Sci. 30, 114–130. https://doi.org/10.1002/jqs.2766

Denton, J.S., Pearce, N.J.G., 2008. Comment on "A synchronized dating of three Greenland ice cores throughout the Holocene" by B. M. Vinther et al.: No Minoan tephra in the 1642 B.C. layer of the GRIP ice core. J. Geophys. Res. Atmos. 113, 1–7. https://doi.org/10.1029/2007JD008970

Derkachev, A.N., Nikolaeva, N.A., Gorbarenko, S.A., Portnyagin, M. V., Ponomareva, V. V., Nürnberg, D., Sakamoto, T., Iijima, K., Liu, Y., Shi, X., Lv, H., Wang, K., 2016. Tephra layers of in the quaternary deposits of the Sea of Okhotsk: Distribution, composition, age and volcanic sources. Quat. Int. 425, 248–272. https://doi.org/10.1016/j.quaint.2016.07.004

Dilley, T.E., 1988. Holocene tephra stratigraphy and pedogenesis in the Middle Susitna River Valley, Alaska. University of Alaska, Fairbanks.

Dixon, E.J., Smith, G.S., 1990. A regional application of tephrochronology in Alaska, in: Lasca, M.P., Donahue, J. (Eds.), Archaeological Geology of North America, Centennial Special Volume 4. Geological Society of America, Boulder, Colorado, pp. 383–398.

Donovan, J., Kremser, D., Fournelle, J.H., Goemann, K., 2015. Probe for EPMA: Acquisition, automation and analysis.

Dugmore, A.J., Larsen, G., Newton, A.J., 1995. Seven tephra isochrones in Scotland. The Holocene 5, 257–266. https://doi.org/10.1177/095968369500500301

Duk-Rodkin, A., 1999. Glacial limits map of Yukon Territory; Geological Survey of Canada, Open File 3694, Indian and Northern Affairs Canada Geoscience Map 1999-2, scale 1:1 000 000. https://doi.org/10.4095/210739

Dunning, H.A., 2011. Extending the applications of tephrochronology in Northwestern North America. University of Alberta.

Environment and Climate Change Canada, n.d. Canadian Climate Normals. [WWW Document]. URL http://climate.weather.gc.ca/climate_normals/index_e.html (accessed 6.30.17).

Fierstein, J., 2007. Explosive eruptive record in the Katmai region, Alaska Peninsula: An overview. Bull. Volcanol. 69, 469–509. https://doi.org/10.1007/s00445-006-0097-y

Fierstein, J., Hildreth, W., 2008. Kaguyak dome field and its Holocene caldera, Alaska Peninsula. J. Volcanol. Geotherm. Res. 177, 340–366. https://doi.org/10.1016/j.jvolgeores.2008.05.016

Hasegawa, T., Nakagawa, M., Yoshimoto, M., Ishizuka, Y., Hirose, W., Seki, S., Ponomareva, V., Alexander, R., 2011. Tephrostratigraphy and petrological study of Chikurachki and Fuss volcanoes, western Paramushir Island, northern Kurile Islands: Evaluation of Holocene eruptive activity and temporal change of magma system. Quat. Int. 246, 278–297. https://doi.org/10.1016/j.quaint.2011.06.047

Hildreth, W., Fierstein, J., 2012. The Novarupta-Katmai Eruption of 1912 — Largest Eruption of the Twentieth Century: Centennial Perspectives. US Geol. Surv. Prof. Pap. 259.

Hildreth, W., Fierstein, J., 2000. Katmai volcanic cluster and the great eruption of 1912. Bull. Geol. Soc. Am. 112, 1594–1620. https://doi.org/10.1130/0016-7606(2000)112<1594:KVCATG>2.0.CO;2

Hua, Q., Barbetti, M., Rakowski, A.Z., 2013. Atmospheric radiocarbon for the period 1950-2010. Radiocarbon 55, 2059–2072. https://doi.org/10.2458/azu_js_rc.v55i2.16177

Jensen, B.J.L., Froese, D.G., Preece, S.J., Westgate, J.A., Stachel, T., 2008. An extensive middle to late Pleistocene tephrochronologic record from east-central Alaska. Quat. Sci. Rev. 27, 411–427. https://doi.org/10.1016/j.quascirev.2007.10.010

Jensen, B.J.L., Pyne-O'Donnell, S., Plunkett, G., Froese, D.G., Hughes, P.D.M., Sigl, M., McConnell, J.R., Amesbury, M.J., Blackwell, P.G., van den Bogaard, C., Buck, C.E., Charman, D.J., Clague, J.J., Hall, V.A., Koch, J., Mackay, H., Mallon, G., McColl, L., Pilcher, J.R., 2014. Transatlantic distribution of the Alaskan White River Ash. Geology 42, 875–878. https://doi.org/10.1130/G35945.1

Jensen, B.J.L., Reyes, A. V., Froese, D.G., 2013. Marine tephrostratigraphy in the Gulf of Alaska and comparison to terrestrial records from eastern Beringia, in: Program and Abstracts, CANQUA-CGRG Biannual Meeting. University of Alberta, Edmonton, Alberta.

Kuehn, S.C., Froese, D.G., Carrara, P.E., Foit, F.F., Pearce, N.J.G., Rotheisler, P., 2009. Major- and trace-element characterization, expanded distribution, and a new chronology for the latest Pleistocene Glacier Peak tephras in western North America. Quat. Res. 71, 201–216. https://doi.org/10.1016/j.yqres.2008.11.003

Kuehn, S.C., Froese, D.G., Shane, P.A.R., 2011. The INTAV intercomparison of electron-beam microanalysis of glass by tephrochronology laboratories: Results and recommendations. Quat. Int. 246, 19–47. https://doi.org/10.1016/j.quaint.2011.08.022

Lakeman, T.R., Clague, J.J., Menounos, B., Osborn, G.D., Jensen, B.J.L., Froese, D.G., 2008. Holocene tephras in lake cores from northern British Columbia, Canada. Can. J. Earth Sci. 45, 935–947. https://doi.org/10.1139/E08-035

Lane, C.S., Lowe, D.J., Blockley, S.P.E., Suzuki, T., Smith, V.C., 2017. Advancing tephrochronology as a global dating tool: Applications in volcanology, archaeology, and palaeoclimatic research. Quat. Geochronol. 40, 1–7. https://doi.org/10.1016/j.quageo.2017.04.003

Lowe, D.J., 2011. Tephrochronology and its application: A review. Quat. Geochronol. 6, 107–153. https://doi.org/10.1016/j.quageo.2010.08.003

Lowe, D.J., Blaauw, M., Hogg, A.G., Newnham, R.M., 2013. Ages of 24 widespread tephras erupted since 30,000 years ago in New Zealand, with re-evaluation of the timing and

palaeoclimatic implications of the Lateglacial cool episode recorded at Kaipo bog. Quat. Sci. Rev. 74, 170–194. https://doi.org/10.1016/j.quascirev.2012.11.022

Mackay, H., Hughes, P.D.M., Jensen, B.J.L., Langdon, P.G., Pyne-O'Donnell, S.D.F., Plunkett, G., Froese, D.G., Coulter, S.E., Gardner, J.E., 2016. A mid to late Holocene cryptotephra framework from eastern North America. Quat. Sci. Rev. 132, 101–113. https://doi.org/10.1016/j.quascirev.2015.11.011

Miller, T.P., Smith, R.L., 1987. Late Quaternary caldera-forming eruptions in the eastern Aleutian arc, Alaska. Geology 15, 434–438. https://doi.org/10.1130/0091-7613(1987)15<434:LQCEIT>2.0.CO;2

Miller, T.P., Smith, R.L., 1977. Spectacular mobility of ash flows around Aniakchak and Fisher calderas, Alaska. Geology 5, 173. https://doi.org/10.1130/0091-7613(1977)5<173:SMOAFA>2.0.CO;2

Monteath, A.J., van Hardenbroek, M., Davies, L.J., Froese, D.G., Langdon, P.G., Xu, X., Edwards, M.E., 2017. Chronology and glass chemistry of tephra and cryptotephra horizons from lake sediments in northern Alaska, USA. Quat. Res. 88, 169–178. https://doi.org/10.1017/qua.2017.38

Morgan, G.B., London, D., 2005. Effect of current density on the electron microprobe analysis of alkali aluminosilicate glasses. Am. Mineral. 90, 1131–1138. https://doi.org/10.2138/am.2005.1769

Mulliken, K., 2016. Holocene Volcanism and Human Occupation in the Middle Susitna River Valley, Alaska. University of Alaska, Fairbanks.

Muscheler, R., Adolphi, F., Knudsen, M.F., 2014. Assessing the differences between the IntCal and Greenland ice-core time scales for the last 14,000 years via the common cosmogenic radionuclide variations. Quat. Sci. Rev. 106, 81–87. https://doi.org/10.1016/j.quascirev.2014.08.017

Nakagawa, M., Ishizuka, Y., Hasegawa, T., Baba, A., Kosugi, A., 2008. Preliminary Report on Volcanological Research of KBP 2007-08 Cruise by Japanese Volcanology group. Sapporo. https://doi.org/10.6067/XCV8668F2H

Neal, C. a., McGimsey, R.G., Miller, T.P., Riehle, J.R., Waythomas, C.F., 2001. Preliminary Volcano-Hazard Assessment for Aniakchak Volcano , Alaska. USGS Open-File Rep. 00–519, 1–35.

Nielsen, C.H., Sigurdsson, H., 1981. Quantitative methods for electron microprobe analysis of sodium in natural and synthetic glasses. Am. Mineral. 66, 547–552.

Nilsson, M., Klarqvist, M., Possnert, G., 2001. Variation in 14C age of macrofossils and different fractions of minute peat samples dated by AMS. The Holocene 11, 579–586. https://doi.org/10.1191/095968301680223521

Patterson, R.T., Crann, C.A., Cutts, J.A., Courtney Mustaphi, C.J., Nasser, N.A., Macumber, A.L., Galloway, J.M., Swindles, G.T., Falck, H., 2017. New occurrences of the White River Ash (east lobe) in Subarctic Canada and utility for estimating freshwater reservoir effect in lake sediment archives. Palaeogeogr. Palaeoclimatol. Palaeoecol. 477, 1–9. https://doi.org/10.1016/j.palaeo.2017.03.031

Payne, R., Blackford, J., van der Plicht, J., 2008. Using cryptotephras to extend regional tephrochronologies: An example from southeast Alaska and implications for hazard assessment. Quat. Res. 69, 42–55. https://doi.org/10.1016/j.yqres.2007.10.007

Payne, R.J., Blackford, J.J., 2008. Extending the late holocene tephrochronology of the central Kenai Peninsula, Alaska. Arctic 61, 243–254.

Payne, R.J., Gehrels, M., 2010. The formation of tephra layers in peatlands: An experimental approach. Catena 81, 12–23. https://doi.org/10.1016/j.catena.2009.12.001

Pearce, C., Varhelyi, A., Wastegärd, S., Muschitiello, F., Barrientos, N., O'Regan, M., Cronin, T.M., Gemery, L., Semiletov, I., Backman, J., Jakobsson, M., 2017. The 3.6ka Aniakchak tephra in the Arctic Ocean: A constraint on the Holocene radiocarbon reservoir age in the Chukchi Sea. Clim. Past 13, 303–316. https://doi.org/10.5194/cp-13-303-2017

Pearce, N.J.G., Westgate, J.A., Preece, S.J., Eastwood, W.J., Perkins, W.T., 2004. Identification of Aniakchak (Alaska) tephra in Greenland ice core challenges the 1645 BC date for Minoan eruption of Santorini. Geochemistry, Geophys. Geosystems 5. https://doi.org/10.1029/2003GC000672

Péwé, T.L., 1975a. Quaternary stratigraphic nomenclature in unglaciated Central Alaska. U.S. Geol. Surv. Prof. Pap. 862, 1.

Péwé, T.L., 1975b. Quaternary Geology of Alaska. U.S. Geol. Surv. Prof. Pap., Geological Survery Professional Paper 835.

Péwé, T.L., Westgate, J.A., Preece, S.J., Brown, P.M., Leavitt, S.W., 2009. Late pliocene dawson cut forest bed and new tephrochronological findings in the Gold Hill Loess, east-central Alaska. Bull. Geol. Soc. Am. 121, 294–320. https://doi.org/10.1130/B26323.1

Ponomareva, V., Polyak, L., Portnyagin, M., Abbott, P.M., Zelenin, E., Vakhrameeva, P., Garbe-Schönberg, D., 2018. Holocene tephra from the Chukchi-Alaskan margin, Arctic Ocean: Implications for sediment chronostratigraphy and volcanic history. Quat. Geochronol. 45, 85–97. https://doi.org/10.1016/j.quageo.2017.11.001

Ponomareva, V., Polyak, L., Portnyagin, M., Abbott, P.M., Zelenin, E., Vakhrameeva, P., Garbe-Schönberg, D., 2017. Holocene tephra from the Chukchi-Alaskan margin, Arctic Ocean: Implications for sediment chronostratigraphy and volcanic history. Quat. Geochronol. https://doi.org/10.1016/j.quageo.2017.11.001

Preece, S.J., McGimsey, R.G., Westgate, J.A., Pearce, N.J.G., Hart, W.K., Perkins, W.T., 2014. Chemical complexity and source of the White River Ash, Alaska and Yukon. Geosphere 10, 1020–1042. https://doi.org/10.1130/GES00953.1

Preece, S.J., Pearce, N.J.G., Westgate, J.A., Froese, D.G., Jensen, B.J.L., Perkins, W.T., 2011a. Old Crow tephra across eastern Beringia: A single cataclysmic eruption at the close of Marine Isotope Stage 6. Quat. Sci. Rev. 30, 2069–2090. https://doi.org/10.1016/j.quascirev.2010.04.020

Preece, S.J., Westgate, J.A., Froese, D.G., Pearce, N.J.G., Perkins, W.T., Fisher, T., 2011b. A catalogue of late Cenozoic tephra beds in the Klondike goldfields and adjacent areas, Yukon Territory 1 1 Yukon Geological Survey Contribution 010. Can. J. Earth Sci. 48, 1386–1418. https://doi.org/10.1139/e10-110

Preece, S.J., Westgate, J.A., Stemper, B.A., Péwé, T.L., 1999. Tephrochronology of late Cenozoic loess at Fairbanks, central Alaska. Bull. Geol. Soc. Am. 111, 71–90. https://doi.org/10.1130/0016-7606(1999)111<0071:TOLCLA>2.3.CO;2

Pyne-O'Donnell, S.D.F., Cwynar, L.C., Jensen, B.J.L., Vincent, J.H., Kuehn, S.C., Spear, R., Froese, D.G., 2016. West Coast volcanic ashes provide a new continental-scale Lateglacial isochron. Quat. Sci. Rev. 142, 16–25. https://doi.org/10.1016/j.quascirev.2016.04.014

Pyne-O'Donnell, S.D.F., Hughes, P.D.M., Froese, D.G., Jensen, B.J.L., Kuehn, S.C., Mallon, G., Amesbury, M.J., Charman, D.J., Daley, T.J., Loader, N.J., Mauquoy, D., Street-Perrott, F.A., Woodman-Ralph, J., 2012. High-precision ultra-distal Holocene tephrochronology in North America. Quat. Sci. Rev. 52, 6–11. https://doi.org/10.1016/j.quascirev.2012.07.024

Reger, R.D., Pinney, D.S., Burke, R.M., Wiltse, M.A., 1995. Catalog and initial analyses of geologic data related to middle to late Quaternary deposits, Cook Inlet region, Alaska. Report of Investigations 95-6.

Reimer, P.J., Bard, E., Bayliss, A., Beck, J.W., Blackwell, P.G., Bronk Ramsey, C., Buck, C.E., Cheng, H., Edwards, R.L., Friedrich, M., Grootes, P.M., Guilderson, T.P., Haflidason, H., Hajdas, I., Hatté, C., Heaton, T.J., Hoffmann, D.L., Hogg, A.G., Hughen, K.A., Kaiser, K.F., Kromer, B., Manning, S.W., Niu, M., Reimer, R.W., Richards, D.A., Scott, E.M., Southon, J.R., Staff, R.A., Turney, C.S.M., van der Plicht, J., 2013. IntCal13 and Marine13 Radiocarbon Age Calibration Curves 0–50,000 Years cal BP. Radiocarbon 55, 1869–1887. https://doi.org/10.2458/azu_js_rc.55.16947

Reyes, A. V., Jensen, B.J.L., Zazula, G.D., Ager, T.A., Kuzmina, S., La Farge, C., Froese, D.G., 2010. A late-Middle Pleistocene (Marine Isotope Stage 6) vegetated surface buried by Old Crow tephra at the Palisades, interior Alaska. Quat. Sci. Rev. 29, 801–811. https://doi.org/10.1016/j.quascirev.2009.12.003

Riehle, J.R., 1994. Heterogeneity, Correlatives, and Proposed Stratigraphic Nomenclature of Hayes Tephra Set H, Alaska. Quat. Res. 41, 285–288. https://doi.org/10.1006/qres.1994.1032

Riehle, J.R., 1985. A reconnaissance of the major Holocene tephra deposits in the upper Cook Inlet region, Alaska. J. Volcanol. Geotherm. Res. 26, 37–74. https://doi.org/10.1016/0377-0273(85)90046-0

Riehle, J.R., Meyer, C.E., Miyaoka, R.T., 1999. Data on Holocene tephra (volcanic ash) deposits in the Alaska Peninsula and lower Cook Inlet region of the Aleutian volcanic arc, Alaska. U.S. Geological Survey Open-File Report 99-0135.

Robinson, S.D., 2001. Extending the late Holocene White River ash distribution, northwestern Canada. Arctic 54, 157–161.

Roland, T.P., Mackay, H., Hughes, P.D.M., 2015. Tephra analysis in ombrotrophic peatlands: A geochemical comparison of acid digestion and density separation techniques. J. Quat. Sci. 30, 3–8. https://doi.org/10.1002/jqs.2754

Schiff, C.J., Kaufman, D.S., Wallace, K.L., Ketterer, M.E., 2010. An improved proximal tephrochronology for Redoubt Volcano, Alaska. J. Volcanol. Geotherm. Res. 193, 203–214. https://doi.org/10.1016/j.jvolgeores.2010.03.015

Schiff, C.J., Kaufman, D.S., Wallace, K.L., Werner, A., Ku, T.L., Brown, T.A., 2008. Modeled tephra ages from lake sediments, base of Redoubt Volcano, Alaska. Quat. Geochronol. 3, 56–67. https://doi.org/10.1016/j.quageo.2007.05.001

Scott, W.E., McGimsey, R.G., 1994. Character, mass, distribution, and origin of tephra-fall deposits of the 1989-1990 eruption of redoubt volcano, south-central Alaska. J. Volcanol. Geotherm. Res. 62, 251–272. https://doi.org/10.1016/0377-0273(94)90036-1

Spray, J.G., Rae, D.A., 1995. Quantitative electron-microprobe analysis of alkali silicate glasses: a review and user guide. Can. Mineral. 33, 323–332.

Tappen, C.M., Webster, J.D., Mandeville, C.W., Roderick, D., 2009. Petrology and geochemistry of ca. 2100-1000 a.B.P. magmas of Augustine volcano, Alaska, based on analysis of prehistoric pumiceous tephra. J. Volcanol. Geotherm. Res. 183, 42–62. https://doi.org/10.1016/j.jvolgeores.2009.03.007

Toohey, M., Sigl, M., 2017. Volcanic stratospheric sulfur injections and aerosol optical depth from 500 BCE to 1900 CE. Earth Syst. Sci. Data 9, 809–831. https://doi.org/10.5194/essd-9-809-2017

Vinther, B.M., Clausen, H.B., Johnsen, S.J., Rasmussen, S.O., Andersen, K.K., Buchardt, S.L., Dahl-Jensen, D., Seierstad, I.K., Siggaard-Andersen, M.L., Steffensen, J.P., Svensson, A., Olsen, J., Heinemeier, J., 2006. A synchronized dating of three Greenland ice cores

throughout the Holocene. J. Geophys. Res. Atmos. 111. https://doi.org/10.1029/2005JD006921

Waitt, R.B., Begét, J.E., 2009. Volcanic processes and geology of augustine volcano, Alaska. US Geol. Surv. Prof. Pap. 1–78.

Wallace, K.L., Coombs, M.L., Hayden, L.A., Waythomas, C.F., 2014. Significance of a near-source tephra-stratigraphic sequence to the eruptive history of Hayes Volcano, south-central Alaska. U.S. Geological Survey Scientific Investigations Report 2014-5133.

Westgate, J.A., Smith, D., Tomlinson, M., 1970. Late Quaternary tephra layers in southwestern Canada, in: Smith, R.A., Smith, J.W. (Eds.), Early Man and Environments in Northwest North America. Calgary, Alberta, pp. 13–34.

Zdanowicz, C., Fisher, D., Bourgeois, J., Demuth, M., Zheng, J., Mayewski, P., Kreutz, K., Osterberg, E., Yalcin, K., Wake, C., Steig, E.J., Froese, D., Goto-Azuma, K., 2014. Ice Cores from the St. Elias Mountains, Yukon, Canada: Their Significance for Climate, Atmospheric Composition and Volcanism in the North Pacific Region. Arctic 67, 35. https://doi.org/10.14430/arctic4352

CHAPTER 4: HIGH-RESOLUTION AGE MODELLING OF PEAT BOGS FROM NORTHERN ALBERTA, CANADA, USING PRE- AND POST-BOMB ^{14}C, ^{210}PB AND HISTORICAL CRYPTOTEPHRA

4.1 Introduction

Holocene peat records preserve abundant organic material and small amounts of other constituents that can record both natural and anthropogenic disturbances over time (e.g. Barber, 1993; Blackford, 2000; Charman et al., 2001; Swindles et al., 2012; Zhao et al., 2007). Ombrotrophic bogs – peatlands that receive water and nutrients almost exclusively from precipitation - are commonly studied as they predominantly receive inputs by atmospheric deposition and can be exceptional archives of past environmental change (Charman et al., 2009; Booth et al., 2010). These archives retain atmospheric inputs, such as particulate matter, and preserve a chronological record of their deposition. Records of particular interest include pollutants (e.g. PCBs and PAHs - Bracewell et al., 1993; Berset et al., 2001; Dreyer et al., 2005; Zaccone et al., 2009; Bao et al., 2014; major and trace metals – Shotyk et al., 1992, 1996; Zaccone et al., 2008; de Vleeschouwer et al., 2009; Martínez and McBride, 1999; Roos-Barraclough et al., 2002; proxies for fossil fuel combustion - Oldfield et al., 1981) and atmospheric dusts (e.g. Fiałkiewicz-Kozieł et al., 2016; Le Roux et al., 2012; Sapkota et al., 2007). To interpret palaeoenvironmental records from peatlands, however, an understanding of both the external forcing and internal processes is required (Barber and Charman, 2014).

Due to variable rates of peat accumulation and decomposition, the interpretation of age-depth relationships in these archives can be complex and subject to uncertainty (e.g. Belyea and Warner, 1994); at the same time, without reliable chronological control, the records they preserve are of limited use. Several chronological approaches are commonly applied to dating peat sequences (see Turetsky et al. (2004) for a full review) including radiocarbon (^{14}C; e.g. Piotrowska et al., 2011) or lead dating (^{210}Pb; e.g. Appleby et al., 1988; Le Roux and Marshall, 2011) and chronostratigraphic markers such as fallout isotopes, pollen markers, spheroidal carbonaceous particles (SCPs), and cryptotephra can provide additional information (e.g. Barber et al., 1998; Swindles et al., 2010; Van der Plicht et al., 2013; Yang et al., 2001). There has been little consensus in the literature on

which approach is best. This relates in part to the variable nature of peatlands – small-scale features such as hummocks, hollows, pools, and lawns typically vary in length (Baird et al., 2009) and can have different plant communities, biogeochemical behaviour, and water table characteristics (Belyea and Clymo, 2001). Relatively short-term disturbances such as fires and surface peat burning, permafrost development and degradation, or the preservation of relict features, do not necessarily have uniform effects on a peatland or reflect systems in equilibrium (e.g. Halsey et al., 1995). The combination of these factors causes inherent variability in peat profiles.

Peat is composed primarily of organic matter and is therefore well suited for ^{14}C dating. High-resolution age models have been produced from studies using both pre- and post-bomb ^{14}C dates or wiggle-matching techniques (van Geel and Mook, 1989; Blaauw et al., 2004; Goslar et al., 2005; van der Linden et al., 2008). As different chemical and particulate fractions may produce different ages, however, the material dated must be considered and bulk dates may differ from individually picked plant macrofossils (e.g. Blaauw et al., 2003; Brock et al., 2011; Chambers et al., 1979; Charman and Garnett, 2005; Holmquist et al., 2016; Kilian et al., 1995; Nilsson et al., 2001; Shore et al., 1995). The type of material available may also change through a sequence due to shifts in the plant communities present or the degree of decomposition.

^{210}Pb dating is commonly applied to modern records (e.g. Appleby et al., 1997; Clymo et al., 1990; Le Roux and Marshall, 2011; MacKenzie et al., 1997; Sanchez-Cabeza and Ruiz-Fernández, 2012), and requires corroboration from independent chronostratigraphic markers (Oldfield et al., 1995). A common criticism of ^{210}Pb dating is the potential for mobilisation of ^{210}Pb and other associated chronological markers (e.g. ^{137}Cs) within peat sequences (e.g. Ali et al., 2008; Parry et al., 2013; Sanders et al., 1995; Urban et al., 1990). This has been disputed experimentally (e.g. Vile et al., 1999) and studies have shown good agreement between ^{210}Pb ages and other chronometers (e.g. El-Daoushy et al., 1982; MacKenzie et al., 1997; Shotyk et al., 1997; Wieder et al., 1994). Attempts to combine overlapping ^{14}C and ^{210}Pb dates have had mixed success – in some instances bomb-peak ^{14}C dates match ^{210}Pb dates well (e.g. Le Roux et al., 2005; Rausch et al., 2005; Roos-Barraclough and Shotyk, 2003), while in others significant offsets are present between the two methods, particularly further back in time (e.g. Bauer et al., 2009;

Fiałkiewicz-Kozieł et al., 2015; Goodsite et al., 2001; Piotrowska et al., 2010; van der Plicht et al., 2013).

Records of cryptotephra - non-visible horizons of volcanic ash from distal sources- are well established in peatlands globally (e.g. Dugmore et al., 1996; Lowe et al., 2013; Mackay et al., 2016; Payne et al., 2008; Pyne-O'Donnell et al., 2012; Zaretskaia et al., 2001) and are a useful chronostratigraphic tool (Pilcher et al., 1995; Plunkett, 2006; Swindles et al., 2010). If correlations can be made with well-dated tephra (e.g. historical eruptions, or tephra preserved within annually resolved records) then these tightly constrained ages can be included in age-depth models (e.g. Schoning et al., 2005) and used as an independent test of other chronological methods applied to the same material (e.g. Oldfield et al., 1997). Ombrotrophic peatlands downwind of active volcanic sources are ideal traps for cryptotephra as they can preserve more cryptotephra layers than nearby lakes (Watson et al., 2016) and are thought to be subject to less reworking within a stratigraphic sequence than lacustrine or marine records (Beierle and Bond, 2002; Clymo and Mackay, 1987; Griggs et al., 2015; Payne et al., 2005; Pyne-O'Donnell, 2011). However, the potential close history between peatlands and human activity (e.g. human and animal traffic, peat removal for fuel) means anthropogenic effects must be considered (Swindles et al., 2013). There is also no guarantee that ash from a given eruption will be preserved in identifiable concentrations, and where it is preserved, layers may be discontinuous (e.g. Bergman et al., 2004; Payne and Gehrels, 2010; Zoltai, 1989) or re-deposited after the initial eruption (Davies et al., 2007). Variation is common between records preserved within a local area or a given peatland due to the interaction of regional and local factors affecting deposition and preservation (Watson et al., 2015).

When considering the modern period, dating peat can be difficult due to the signals being studied occurring within the acrotelm – the living section of a peat bog with relatively loose material, large pore spaces, and periodic saturation by water. The acrotelm has high permeability and rates of decomposition compared to the catotelm, which is permanently saturated, commonly dense, compressed peat with low permeability. This simple two-dimensional model has been widely used to understand peat hydrology and ecology, modelling and budgeting since the 1970s (e.g. Ingram, 1978), and the boundary between the two 'layers' in a peatland varies over time based on the water table depth. While the

depth of this boundary is also different between, and potentially within, peatlands, anthropogenic influences will certainly be preserved within it, and recent climatic anomalies such as the Little Ice Age will be affected by changes in signal preservation and taphonomic processes (e.g. transportation, burial, and decomposition) across the boundary. While high peat accumulation rates and increased precision of analytical techniques may imply certain resolutions are obtainable (e.g. annual, seasonal), such variable taphonomic influences and subsequent preservation of the different proxies within the peat sequence will likely increase the observed signal noise and place a limit on interpretation.

Here, we compare three different techniques commonly applied to dating peat sequences (accelerator mass spectrometry - ^{14}C; gamma spectrometry - ^{210}Pb, ^{137}Cs and ^{241}Am; and cryptotephra) and combine and model the results using Bayesian statistics to produce more accurate and precise age-depth models. Bayesian statistical techniques have been utilised in a wide range of fields to produce detailed age-depth models based on a relatively small number of dates (e.g. Christen et al., 1995; Litton and Buck, 1995). Bayesian models, through their inclusion of additional (prior) information, provide more precise interpolations than using raw dates alone (e.g. Blaauw and Christen, 2005; Bronk Ramsey, 2008) and provide additional benefits for identifying outliers or anomalous circumstances in the archived sequences (e.g. hiatuses, reversals).

The combination of multiple chronometers and sediment accumulation rates has been used to highlight differences between chronological methods and produce a more accurate final age-model in lacustrine sediments (Tylmann et al., 2016). Additional supporting data preserved within peat cores can also be used to constrain and model peat accumulation. Changes in plant macrofossil composition can affect peat accumulation rates (e.g. Yeloff et al., 2006), and stratigraphic units relating to records of local fires, permafrost development, shifts in the dominant plant species present, peat humification, etc, can therefore be defined and linked to abrupt changes in peat archives.

The peatlands of western interior Canada have been extensively studied over both modern and Holocene timescales (e.g. Beilman et al., 2001; Campbell et al., 2000; Turetsky et al., 2007; Vitt et al., 1994; Yu et al., 2003; Zoltai and Vitt, 1990). We focus

on the Fort McMurray region here as the study of local and regional atmospheric trace elements and organic compounds (e.g. Shotyk et al., 2017, 2016; Zhang et al., 2016) require chronological accuracy and precision on a sub-centennial, and ideally sub-decadal timescale.

Alberta is also downwind of many active volcanoes (Alaska Volcano Observatory; Miller et al., 1998) and has well-established records of visible tephra (e.g. Clague et al., 1995; Jensen and Beaudoin, 2016; Kuehn et al., 2009; Osborn, 1985; Westgate et al., 1970, 1969; Zoltai, 1989). It is likely that tephra can be used to constrain the age models (as their associated errors are smaller than those produced with other methods, e.g. ^{14}C) and to highlight and help to interpret any potential differences in the other chronometers. Key potential tephra here are modern eruptions from sources in Alaska (Davies et al., 2016) or the regionally widespread eastern lobe of the White River Ash (WRAe; Péwé, 1975) that has precise associated ages from wiggle matching of buried tree stumps and Greenland ice core chronologies (Coulter et al., 2012; Jensen et al., 2014; Toohey and Sigl, 2017).

Here we report data from six ombrotrophic peatlands in Alberta, Canada. Multiple peat sequences allow us to assess regional variation by determining how well the chronometers are represented at each site, if there are observable patterns when comparing methods and if our approach for combining and modelling the chronometers using Bayesian statistics is successful across a variety of cores and locations.

4.1.1. Regional setting

Cores were collected from six peatlands within the boreal plains of northern Alberta in the summers of 2013 and 2014: five from the Fort McMurray area (Anzac, ANZ; McKay, McK; McMurray, McM; Mildred, MIL; and Jack Pine Hills, JPH-4) and one from a bog located north of Utikuma Lake (UTK) (Figure 4.1). Both areas have an estimated 10-30% peatland surface cover with typical depths of 2.5-4.0 m (Vitt et al., 2000).

Fort McMurray is located in north-eastern Alberta and has a dry boreal climate with average daily temperatures ranging from -17°C in January to +17°C in July (1981-2010 data; Environment and Climate Change Canada, 2017). It lies within the zone of sporadic permafrost (Zoltai, 1995; Beilman et al., 2001) and receives ~420 mm average annual

precipitation, mainly falling in the summer months (1981-2010 data; Environment and Climate Change Canada, 2017).

UTK is located in north-central Alberta, ~260 km southwest of the Fort McMurray sites. This is within the Utikuma Region Study Area (URSA) that has been a focus of long-term studies of peatland hydrology and biogeochemistry in Alberta (Devito et al., 2012, 2016; Petrone et al., 2016). It has a boreal climate with average daily temperatures ranging from -14°C in January to +15°C in July (1971-2000 data for Slave Lake; Environment and Climate Change Canada, 2017). The region is located outside the present-day southern limit of permafrost distribution and has relatively higher average annual precipitation (~500 mm) than the Fort McMurray area, which is also focused in the summer months.

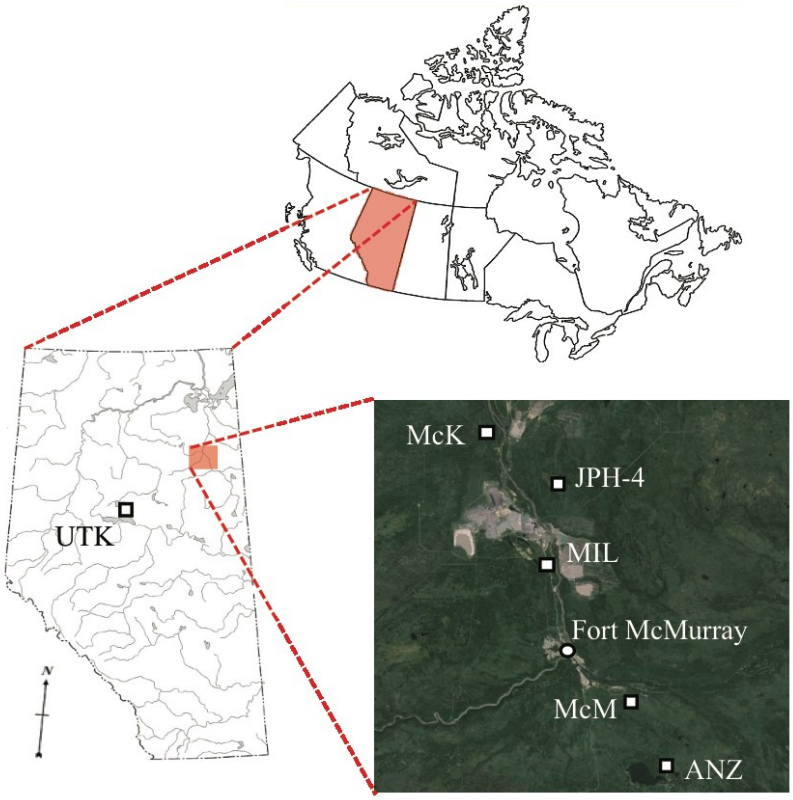

Figure 4.1 Map showing peatland coring locations discussed in the text. Inset shows detailed locations in the Fort McMurray area. Reproduced from van Bellen et al. (in press).

4.2 Material and Methods

The cores used within this study have been previously discussed by other collaborative investigations (e.g. Shotyk et al., 2016a, 2017; Zhang et al., 2016; Mullan-Boudreau et al., 2017; Magnan et al., 2018; van Bellen et al., in press). The subsampling protocol for the peat samples is detailed in Appendix A. Information regarding the environmental histories, three independent chronometers, and resulting Bayesian models is outlined in the subsections below.

4.2.1. Environmental histories

Supporting data produced from the cores were used to identify potential significant changes in peat accumulation or preservation. Proxies used include plant macrofossils including macroscopic charcoal and charred plant remains (Magnan et al., 2018), testate amoeba assemblages (van Bellen et al., in press), measurements of dry density, pH, ash content (Mullan-Boudreau et al., 2017), and the degree of peat humification, evaluated using the main atomic ratios (C:N, H:C, O:C) in conjunction with stable isotope analyses ($\delta^{13}C$ and $\delta^{15}N$). When considered together, these data highlight periods of environmental importance such as permafrost development and/or degradation (i.e. drier bog surface and the establishment of xerophilous vegetation); local fires from peaks of macroscopic charcoal >1 mm and charred plant macrofossils; changes in surface wetness from testate amoeba assemblages, moss species, and increased presence of *Picea* needles; and peatland succession (e.g. fen-bog transitions shown with changes in dominant bryophytes, decreasing ash content and pH). At the depths of these changes additional information can be used as input for the age-depth models to more accurately represent the preserved records (see *Section 3.4* for details).

Five of these sites have been ombrotrophic for the entire period covered by the cores collected; MIL has a shallow ombrotrophic zone near the surface and was minerotrophic preceding this (Mullan-Boudreau et al., 2017).

4.2.2. Cryptotephra analysis

No visible tephra were identified in any of the peat cores. Targeted cryptotephra analyses were undertaken using contiguous 1 cm subsamples from the uppermost sections of the

cores (to identify modern ash-fall events) and at a 2 cm resolution for a targeted 20 cm period near the base of the cores (to identify WRAe). The depths to be analysed were determined using ^{14}C dates from the modern day back to ~AD 1850 and for up to 800 years surrounding the AD 853 eruption of WRAe.

Standard methods were used to produce glass shard concentration profiles (Blockley et al., 2005) and the heavy liquid Lithium Heteropolytungstate (LST) was used for density separations. Glass shards for geochemical analysis were re-extracted from peaks in shard concentration using acid digestion (Dugmore et al., 1995), which has been shown to efficiently remove peat fibres without chemically altering or degrading the glass shards (Roland et al., 2015). Samples were mounted in an epoxy puck and polished to expose glass surfaces before being carbon coated prior to electron probe microanalysis (EPMA). New data are reported here from glass shards analysed on a JEOL 8900 Superprobe and Cameca SX100 at the University of Alberta by wavelength dispersive X-ray spectroscopy (WDS) following established protocols (e.g. Jensen et al., 2008).

A standard suite of ten elements (Si, Ti, Al, Fe, Mn, Mg, Ca, Na, K, Cl) were measured using a 5 μm beam with 15 keV accelerating voltage and 6 nA beam current to minimise alkali migration during analyses (Spray and Rae, 1995; Morgan and London, 2005). Where intensity data loss does occur, it has been shown that empirical corrections can be applied if the data demonstrate linear variance over time (Nielsen and Sigurdsson, 1981). Here both Si and Na were corrected for Time Dependent Intensity (TDI) loss (or gain) using a self-calibrated correction with Probe for EPMA software (Donovan et al., 2015).

Two secondary standards of known composition were run concurrently with all tephra samples: ID 3506, a Lipari rhyolite obsidian, and a reference sample of Old Crow tephra, a well-characterized, secondarily hydrated tephra bed (e.g. Kuehn et al., 2011). All results were normalized to 100% and presented as weight percent (wt%) oxides. New major-element geochemical data and associated standard measurements, as well as data points for relevant reference material, are reported in the Supplementary Information (Table S1).

4.2.3. Radiometric dating

4.2.3.1. ^{14}C dating

A total of 63 pre- and post-bomb ^{14}C dates were produced for the six cores (representing nine to eleven dates per core) from identified plant macrofossils. *Sphagnum* remains were preferred where possible as they yield the most reliable ^{14}C dates (Nilsson et al., 2001), however other terrestrial plant macrofossils (e.g. twigs, needles, leaves, seeds) were used in some samples to provide sufficient mass for analysis.

All ^{14}C samples were pre-treated at the University of Alberta following standard procedures (e.g. Reyes et al., 2010) and analysed at the Keck-Carbon Cycle AMS facility (University of California, Irvine). Two secondary standards were also pre-treated concurrently (a last interglacial non-finite-age wood, AVR-PAL-07; middle Holocene wood, FIRI-F standard) and the resulting ^{14}C values were within expected ranges (Table S2). The unknown ^{14}C ages were calibrated using Bomb13NH1 (Hua et al., 2013) and IntCal13 (Reimer et al., 2013) calibration curves as appropriate with Oxcal v4.2 (Bronk Ramsey, 2009a).

4.2.3.2. ^{210}Pb, ^{137}Cs and ^{241}Am dating

The uppermost sections of the six peat cores were analysed by gamma spectrometry for the natural fallout radionuclide ^{210}Pb and artificial fallout radionuclides ^{137}Cs and ^{241}Am. The measurements were carried out using ultralow background gamma spectrometers (ORTEC, Oak Ridge, TN, USA) at the University of Alberta equipped with ORTEC GWL-250-15 HPGe well detectors (with OFHC Cu endcap and high purity Al well tube) in an ultralow background J-type cryostat surrounded by a virgin lead shield (15 cm thick) with nitrogen purge port. Full details are reported in Appendix B.

Unsupported ^{210}Pb activity was calculated by subtracting supported ^{210}Pb (assumed to be in equilibrium with ^{226}Ra activity) from the measured total ^{210}Pb activity. Since individual ^{226}Ra measurements at some sites (ANZ, UTK, McM) had very large relative uncertainties (70% on average), supported ^{210}Pb activity was in practice calculated as the running average of the nearest three ^{226}Ra values. A similar smoothing process was applied to the raw ^{241}Am data.

Raw ^{210}Pb dates were calculated using Constant Rate of Supply Model (Appleby and Oldfield, 1978). This assumes a constant rate of supply of unsupported ^{210}Pb to the peat surface despite variable sedimentation rates - an appropriate assumption for ombrotrophic peatlands where mass specific concentrations can change through time as the result of organic decay. Peaks in the ^{137}Cs and ^{241}Am records were used to identify, where possible, the 1963 depth, which relates to the maximum fallout values of these radionuclides from the atmospheric testing of nuclear weapons.

4.2.4. Bayesian age modelling

Age-depth models were constructed using OxCal's Poisson process model (P_Sequence, Bronk Ramsey, 2008). Two steps were followed for each site: first, independent models for each chronometer were visually compared for the initial detection of outliers and/or offsets between the dating methods. This is more effective as a first approach than using statistical techniques that can be biased by, for example, the high number and tight distribution of ^{210}Pb dates presented here. Cryptotephra isochrons were used as independent checks for both radiometric methods and the data were corrected where necessary. The resulting radiometric data for each site were then combined in one P_Sequence model and outliers were judged statistically using OxCal's agreement indices (AI), showing the extent to which the modelled posterior distributions overlap with the original distributions, and a student t-distribution outlier model (Bronk Ramsey, 2009b).

The P_Sequence model in OxCal v4.2 is the most appropriate for modelling peat ages as it allows variable accumulation rates. Here the k parameter - deposition events defined as increments per unit length, controlling model rigidity and resolution - was set as variable rather than fixed to increase flexibility of the model (Bronk Ramsey, 2013). Furthermore, OxCal's boundary function can constrain the models using identified changes from supporting data (detailed in *Section 3.1*). This function does not force a change or require a hiatus to occur, but instead allows a break point in accumulation rates if the dates are best modelled that way.

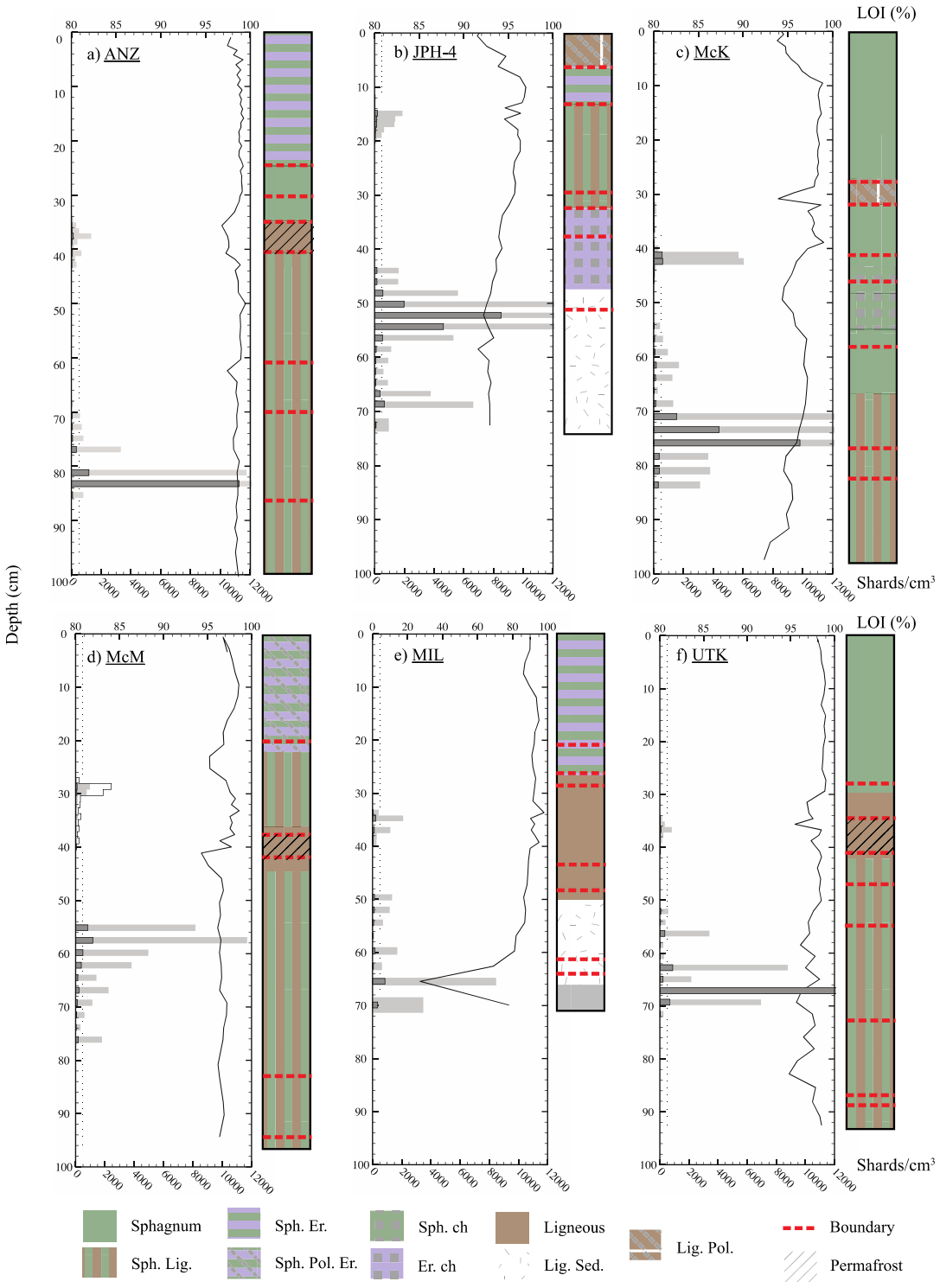

Figure 4.2 Stratigraphic details of six peat cores, including sedimentology, glass shard concentration profiles, boundaries, ^{14}C sample depths and LOI data. Dark grey bars for shard concentrations are raw data (shards/cm^3), light grey bars are 10x magnification. Black outline for McM shows 25x magnification for further clarification.

4.3 Results

Summaries of core data produced from all six sites are plotted in Figure 4.2, including stratigraphic units, event boundaries, cryptotephra shard concentration profiles, and loss on ignition percentages (LOI). The individual model components (age data and event boundaries) are discussed in detail before the full models are assessed. We focus on the post-industrial period (post AD 1850) as all three methods have data available and a more thorough comparison is therefore possible. This period also relates to peat depths that will contain the acrotelm/catotelm boundary. Multiple model iterations were developed for each site as new data (ages and event histories) were produced– these are fully documented in Figure S4.1, and only the final versions are presented here.

4.3.1. Event histories

Proxy data used to define events in the core histories that are included as boundaries in our models are shown in Table 4.1, and the event depths are presented as red dashed lines in Figure 4.2 and Figures 4.5-4.7.

Recorded events at these peatlands are predominantly local fires interpreted using abundances of charcoal >1 mm and charred macrofossil remains (e.g. *Picea* needles, *Sphagnum*, Ericaceae leaves; (Magnan et al., 2018). These fires may have burned some of the upper peat layers and created a hiatus in the peat sequence. After a fire, some studies have shown that mechanisms of interception and retention may change - as organic matter becomes more hydrophobic re-wetting is reduced and runoff increases (e.g. Certini, 2005, and references therein). Shifts towards drier surface conditions, as interpreted from changes in moss assemblages and the increased presence of conifers, could have changed rates of peat accumulation or decomposition. Three sites (ANZ, McM and UTK) have evidence for permafrost aggradation interpreted from drying of the bog surface (reconstructed using testate amoebae; van Bellen et al., in press), increased degree of peat humification, changes in plant communities, and stable isotope signature (Magnan et al., 2018). The permafrost at these sites most likely formed as ice lenses that would have caused an upheaval and drying of the peat surface, a major slowdown in peat accumulation, and the development of internal lawn after thaw (Zoltai and Tarnocai, 1975; Vitt et al., 1994).

Site	Boundary depth	Proxy information	Event	In model?
ANZ	24.67	S. Fuscum established		Y
	30.28	WTD, H/C	Permafrost thaw	Y
	36.59-40.75	WTD, H/C, charcoal >1mm, charred needles	Permafrost aggradation and fire	Y/Y
	61.36	Charcoal >1mm, charred needles	Local fire	Y
	69.62	Charred needles, some charcoal >1mm	Local fire	N
	86.36	Charcoal >1mm	Possible fire	N
JPH	0-5.24	WTD, Picea needles	Dry conditions, Picea trees	Y
	12.89	S. Acutfolia established		Y
	28.65-32.75	Charcoal >1mm, charred macros, WTD	Dry phase, local fires	N/N
	36.77	Charcoal >1mm, charred macros	Local fire	Y
	51.22	Cyperaceae, C/N	Wet to dry transition	Y
McK	27.46-31.96	Polytrichum	Drying	Y/Y
	41.18	WTD, Polytrichum	Wet to dry shift	Y
	45.92-57.9	Charcoal >1mm, charred needles	Multiple local fires	N/Y
	77.08-82.29	Charcoal >1mm, charred needles	Local fires	N/N
McM	19.61	S. Acutfolia established		Y
	37.68	Abundant charcoal >1mm	Local fire, dry to wet shift	Y
	42.29	Abundant charcoal >1mm	Local fire	Y
	84.3-94.32	Abundant Picea needles	Dry period?	N/N
MIL	20.67	Large decrease in pH		Y
	26.09	S. Acutfolia established		Y
	28.25	Charred Sphagnum	Possible fire	Y
	43.77	Charcoal >1mm, charred macros	Local fire	Y
	48.44	Charcoal >1mm, charred macros	Local fire	N
	61.12-64.08	Charcoal >1mm, charred macros	One/multiple local fires	Y/N
UTK	28.32	Shift to S. Acutfolia; C/N increase		Y
	34.59-42.84		Permafrost possible	Y/Y
	47.01	Charcoal >1mm, charred needles	Local fire	Y
	55.22	Charcoal >1mm, charred needles	Local fire	Y
	72.58	Shift to S. Acutfolia, charcoal >1mm, charred needles	Local fire	N
	86.75-89.53	Charcoal >1mm, charred needles	One/multiple local fires	N/N

Table 4.1: Event histories for the cores analysed from each site, including the depth of the inferred changes and the proxy data used to support this. Events included in the final age models as boudnaries are shown with a Y; those not included are shown with an N. WTD = water table depth; C/N and H/C refer to measurements of isotopic ratios.

Not all events are included in the models – particularly further back in time where multiple boundaries may occur between measured dates and including both boundaries would cause a break in the model. However, peat accumulation rates in these periods are an order of magnitude lower relative to the modern period (0.01-0.05 cm/year vs 0.25-1.55 cm/year) as the peat has been compressed and has been subjected to a longer period of decay before burial in the catotelm, and it is unlikely that boundaries relating to short-term events (e.g. fires in one season/year) would significantly impact accumulation rates.

4.3.2. Cryptotephra results

Glass shards are present at all sites in both intervals sampled (<~200 yr BP, and surrounding AD 853), although the shard concentration profiles vary between sites. Figure 2 shows the profiles for both intervals, with light grey bars showing 10x values as the shard counts in the two periods differ by an order of magnitude. The sites preserve different numbers of peaks within the studied intervals and have different physical taphonomic processes affecting shard preservation (e.g. maximum peak concentrations, shard dispersion below the identified peak).

Sixteen potential airfall peaks were identified for geochemical analysis. Table 4.2 and Figures 4.3 and 4.4 show the samples analysed, the average major element data EPMA for identified geochemical populations, and any possible geochemical correlations to known eruptions with associated chronological data that can be included in our age models. Full normalised single point major element EPMA datasets are provided in Table S4.1.

Nine samples can be used as isochrons as they are identified as primary airfall events (where one dominant geochemical population is present) and correlate with reference material for known eruptions (Novarupta-Katmai 1912, UA 1364, and the eastern lobe of the White River Ash, WRAe, UA 1119; UA reference collection samples, details provided in Table 2). Six of the remaining samples (McK 36, ANZ 40-44, MIL 57) have mixed geochemical data likely resulting from disrupted peat accumulation and/or preservation (e.g. removal of organic material by fire) and one sample (UTK 36) has insufficient data for comparison.

a) Samples used as isochrons

Site	Depth (cm)	Sample #	UA #	SiO_2	TiO_2	Al_2O_3	FeO_t	MnO	MgO	CaO	Na_2O	K_2O	Cl	Total	$H2O_d$	n	Correlation
ANZ	37.60	39	2969	77.98	0.15	12.27	1.13	0.05	0.10	0.72	4.15	3.26	0.24	100	1.48	31	Novarupta-Katmai 1912
				(0.23)	(0.04)	(0.13)	(0.04)	(0.03)	(0.01)	(0.03)	(0.23)	(0.08)	(0.09)		(1.38)		
	83.22	83	2919	74.42	0.19	14.15	1.35	0.04	0.32	1.72	3.99	3.46	0.35	100	0.86	19	Mt. Churchill - WRAe
				(0.99)	(0.05)	(0.52)	(0.24)	(0.02)	(0.08)	(0.25)	(0.15)	(0.23)	(0.03)		(1.17)		
JPH	14.86	16	2913	77.71	0.16	12.31	1.17	0.05	0.13	0.81	4.19	3.25	0.23	100	2.55	15	Novarupta-Katmai 1912
				(1.39)	(0.07)	(0.67)	(0.17)	(0.02)	(0.09)	(0.3)	(0.32)	(0.11)	(0.04)		(1.4)		
	53.22	54	2873	74.00	0.20	14.30	1.40	0.05	0.34	1.81	4.07	3.56	0.36	100	1.34	34	Mt. Churchill - WRAe
				(0.87)	(0.05)	(0.47)	(0.18)	(0.02)	(0.09)	(0.19)	(0.24)	(0.19)	(0.03)		(1.51)		
McK	75.83	65	2877	73.88	0.20	14.29	1.46	0.05	0.35	1.71	4.24	3.54	0.35	100	1.21	33	Mt. Churchill - WRAe
				(0.83)	(0.05)	(0.35)	(0.19)	(0.02)	(0.08)	(0.25)	(0.38)	(0.29)	(0.04)		(1.42)		
McM	28.66	26	2968	77.88	0.17	12.33	1.17	0.05	0.11	0.76	4.10	3.27	0.22	100	1.37	30	Novarupta-Katmai 1912
				(0.38)	(0.05)	(0.17)	(0.1)	(0.03)	(0.04)	(0.12)	(0.22)	(0.1)	(0.04)		(1.56)		
	57.49	51	2920	73.76	0.20	14.28	1.44	0.06	0.35	1.53	4.24	3.78	0.36	100	1.16	15	Mt. Churchill - WRAe
				(0.96)	(0.05)	(0.32)	(0.21)	(0.03)	(0.08)	(0.37)	(0.43)	(0.57)	(0.04)		(2.4)		
MIL	34.72	32	2914	78.17	0.15	12.07	1.11	0.04	0.11	0.73	4.17	3.22	0.23	100	0.75	16	Novarupta-Katmai 1912
				(0.25)	(0.03)	(0.16)	(0.04)	(0.02)	(0.01)	(0.02)	(0.24)	(0.12)	(0.03)		(2.46)		
UTK	67.11	65	2924	74.05	0.18	14.25	1.41	0.05	0.34	1.73	4.02	3.63	0.36	100	1.71	18	Mt. Churchill - WRAe
				(1.04)	(0.05)	(0.52)	(0.23)	(0.03)	(0.11)	(0.25)	(0.31)	(0.37)	(0.05)		(1.69)		

b) Other samples analysed

Site	Depth (cm)	Sample #	UA #	SiO_2	TiO_2	Al_2O_3	FeO_t	MnO	MgO	CaO	Na_2O	K_2O	Cl	Total	$H2O_d$	n	Correlation
ANZ	38.62	40	2907	73.80	0.21	14.35	1.49	0.04	0.39	1.81	4.13	3.40	0.37	100	2.21	6	Mt. Churchill
				(0.24)	(0.02)	(0.15)	(0.12)	(0.02)	(0.07)	(0.12)	(0.25)	(0.2)	(0.03)		(1.51)		
				78.05	0.15	12.10	1.13	0.05	0.13	0.72	4.24	3.22	0.21	100	1.58	4	Novarupta-Katmai 1912
				(0.3)	(0.02)	(0.02)	(0.03)	(0.03)	(0.02)	(0.03)	(0.21)	(0.13)	(0.01)		(0.2)		
	40.75	42	2971	76.05	0.38	12.82	2.11	0.05	0.41	2.19	3.58	2.27	0.17	100	1.24	5	Unknown
				(0.92)	(0.05)	(0.27)	(0.26)	(0.01)	(0.08)	(0.26)	(0.25)	(0.14)	(0.03)		(0.55)		
			2908, 2971	74.89	0.18	14.34	1.54	0.05	0.31	1.67	4.54	2.39	0.11	100	1.70	10	Mt. St. Helens ash bed Z
				(0.7)	(0.04)	(0.3)	(0.21)	(0.02)	(0.03)	(0.18)	(0.4)	(0.12)	(0.02)		(0.89)		
				(0.38)	(0.08)	(0.36)	(0.08)	(0.02)	(0.03)	(0.1)	(0.32)	(0.02)	(0.02)		(0.63)		
				72.81	0.42	14.59	1.86	0.04	0.46	1.61	5.14	2.90	0.20	100	1.42	5	Unknown
				(0.88)	(0.05)	(0.16)	(0.3)	(0.03)	(0.08)	(0.18)	(0.42)	(0.3)	(0.03)		(0.85)		
	41.82	43	2967	74.20	0.19	14.14	1.63	0.01	0.31	1.44	3.70	4.25	0.17	100	4.05	3	Unknown
				(0.39)	(0.02)	(0.28)	(0.02)	(0.01)	(0.03)	(0.15)	(0.34)	(0.21)	(0.05)		(0.89)		

Table 4.2: Average major element geochemical data for identifiable populations of analysed tephra samples and suggested correlations. (#) = standard deviation; FeO_t = total iron oxide as FeO; $H2O_d$ = water by difference.

b cont.) Other samples analysed

Site	Depth (cm)	Sample #	UA #	SiO_2	TiO_2	Al_2O_3	FeO_t	MnO	MgO	CaO	Na_2O	K_2O	Cl	Total	$H2O_d$	n	Correlation
				76.95	0.04	12.98	0.80	0.10	0.04	0.56	3.73	4.73	0.08	100	5.55	3	Unknown
				(0.53)	(0.02)	(0.27)	(0.29)	(0.08)	(0.03)	(0.02)	(0.15)	(0.3)	(0.01)		(0.2)		
	42.89	44	2909	74.63	0.22	14.18	1.67	0.04	0.33	1.66	4.76	2.40	0.11	100	2.32	5	Mt. St. Helens ash bed Z
				(0.09)	(0.04)	(0.05)	(0.05)	(0)	(0.03)	(0.03)	(0.22)	(0.08)	(0.03)		(1.11)		
McK	41.18	36	2966	73.94	0.28	14.05	1.71	0.03	0.28	1.22	4.03	4.39	0.10	100	1.91	9	Unknown
				(0.28)	(0.06)	(0.13)	(0.06)	(0.03)	(0.01)	(0.04)	(0.29)	(0.09)	(0.01)		(0.72)		
				75.22	0.36	13.65	1.31	0.03	0.31	1.22	4.37	3.41	0.14	100	2.45	5	Unknown
				(0.35)	(0.03)	(0.26)	(0.06)	(0.01)	(0.04)	(0.08)	(0.12)	(0.17)	(0.03)		(1.4)		
				74.10	0.21	14.31	1.44	0.07	0.36	1.67	3.84	3.71	0.37	100	2.48	3	Unknown
				(0.96)	(0.09)	(0.5)	(0.28)	(0.02)	(0.14)	(0.26)	(0.19)	(0.4)	(0.04)		(0.88)		
				75.65	0.07	13.24	1.17	0.04	0.03	0.57	4.25	4.90	0.10	100	3.26	5	Unknown
				(1.2)	(0.02)	(0.54)	(0.16)	(0.03)	(0.02)	(0.09)	(0.18)	(0.3)	(0.02)		(0.99)		
MIL	65.45	57	2922	73.86	0.19	14.20	1.33	0.05	0.33	1.72	3.52	4.43	0.36	100	2.57	8	Mt. Churchill - WRAe
				(0.78)	(0.04)	(0.36)	(0.19)	(0.02)	(0.08)	(0.24)	(0.59)	(1.03)	(0.03)		(1.94)		
				64.60	0.96	15.84	5.54	0.18	1.80	4.30	4.11	2.53	0.15	100	1.28	7	Low SiO2 mix
				(3.84)	(0.22)	(0.32)	(2.14)	(0.03)	(0.91)	(1.63)	(0.9)	(0.53)	(0.04)		(1.19)		
UTK	36.69	36	2970	78.07	0.14	12.29	1.17	0.03	0.10	0.73	3.95	3.32	0.25	100	2.03	3	Novarupta-Katmai 1912
				(0.21)	(0.05)	(0.02)	(0.03)	(0.02)	(0.01)	(0.02)	(0.24)	(0.11)	(0.02)		(0.4)		

c) Reference material analysed concurrently

Site	UA #	SiO_2	TiO_2	Al_2O_3	FeO_t	MnO	MgO	CaO	Na_2O	K_2O	Cl	Total	$H2O_d$	n	Correlation
Carmacks, Yukon Territory	1119	73.55	0.23	14.58	1.50	0.05	0.37	1.80	4.28	3.35	0.34	100	2.68	28	Mt. Churchill - WRAe
		(0.5)	(0.05)	(0.28)	(0.15)	(0.03)	(0.06)	(0.15)	(0.21)		(0.02)		(0.89)		
Kodiak Island, Alaska	1364	74.93	0.37	13.15	2.06	0.06	0.42	1.69	4.23	2.91	0.19	100	1.14	42	Novarupta-Katmai 1912
		(3.41)	(0.21)	(1.13)	(0.96)	(0.03)	(0.36)	(0.99)	(0.25)	(0.31)	(0.03)		(1.3)		(all data)
		78.03	0.15	12.16	1.19	0.05	0.11	0.79	4.15	3.19	0.22	100	1.03	16	Novarupta-Katmai 1912
		(0.26)	(0.04)	(0.18)	(0.06)	(0.02)	(0.03)	(0.09)	(0.23)	(0.1)	(0.02)		(0.85)		(high SiO2 popn only; >77%)
Washington	2310	75.24	0.23	13.90	1.54	0.04	0.27	1.52	4.72	2.46	0.10	100	2.20	21	Mt. St. Helens ash bed Z
		(0.68)	(0.03)	(0.39)	(0.13)	(0.02)	(0.05)	(0.18)	(0.23)	(0.13)	(0.02)		(1.63)		

Table 2 (cont.): Average major element geochemical data for identifiable populations of analysed tephra samples and suggested correlations. (#) = standard deviation; FeO_t = total iron oxide as FeO; $H2O_d$ = water by difference.

In the late Holocene interval analysed here (up to 800 years surrounding AD 853), four of the sites preserve a clear peak in glass concentration of thousands of shards/cm^3 (ANZ, UA 2919; JPH, UA 2873; McK, UA 2877; and UTK, UA 2924). A smaller peak (~1500 shards/cm^3) is present in McM (UA 2920) and MIL has background level counts. There are additional geochemically distinct secondary peaks present stratigraphically below the primary peak at JPH and above the primary peak at McK and UTK (Figure 2). These are not discussed further here as they have not been correlated between the cores and do not have associated chronological information.

The primary peaks identified at five sites correlate geochemically with the WRAe tephra (Figure 4.3). Glass from MIL is mixed – geochemically some shards correlate with WRAe, as well as other more mafic populations. An isochron is not defined here as the shard concentration profile is likely reworked given the relatively low shard counts with mixed geochemistry and the increased presence of silts (20-70% mineral content) in this minerotrophic section of the core.

Shard concentrations for the surface peat records are shown in more detail in Figure 4.5 alongside summarised age modelling data (see *Section 4.3* for details). Both ANZ and McK were analysed from the surface back to ~AD 1800 and significant concentrations of glass were absent for most of the 20th century. A primary peak of ~80-210 shards/cm^3 is seen at all sites, with samples at McK having higher concentrations of up to ~600 shards/cm^3. The shard profiles are highly variable between sites with some features only present at selected sites e.g. an older secondary peak at ANZ; significant tails of shards at JPH and McM (Figure 4.2).

Glass correlating to the Alaska eruption of Novarupta-Katmai in 1912 is present at four sites (ANZ, UA 2969; JPH, UA 2913; McM, UA 2920; and MIL, UA 2914; Figure 4.3). This is the southern-most occurrence of Novarupta-Katmai 1912 to date, and the second reported identification in North America outside of Alaska. The only previous distal correlation of Novarupta-Katmai 1912 is with glass in Greenland's North Grip ice core (Coulter et al., 2012).

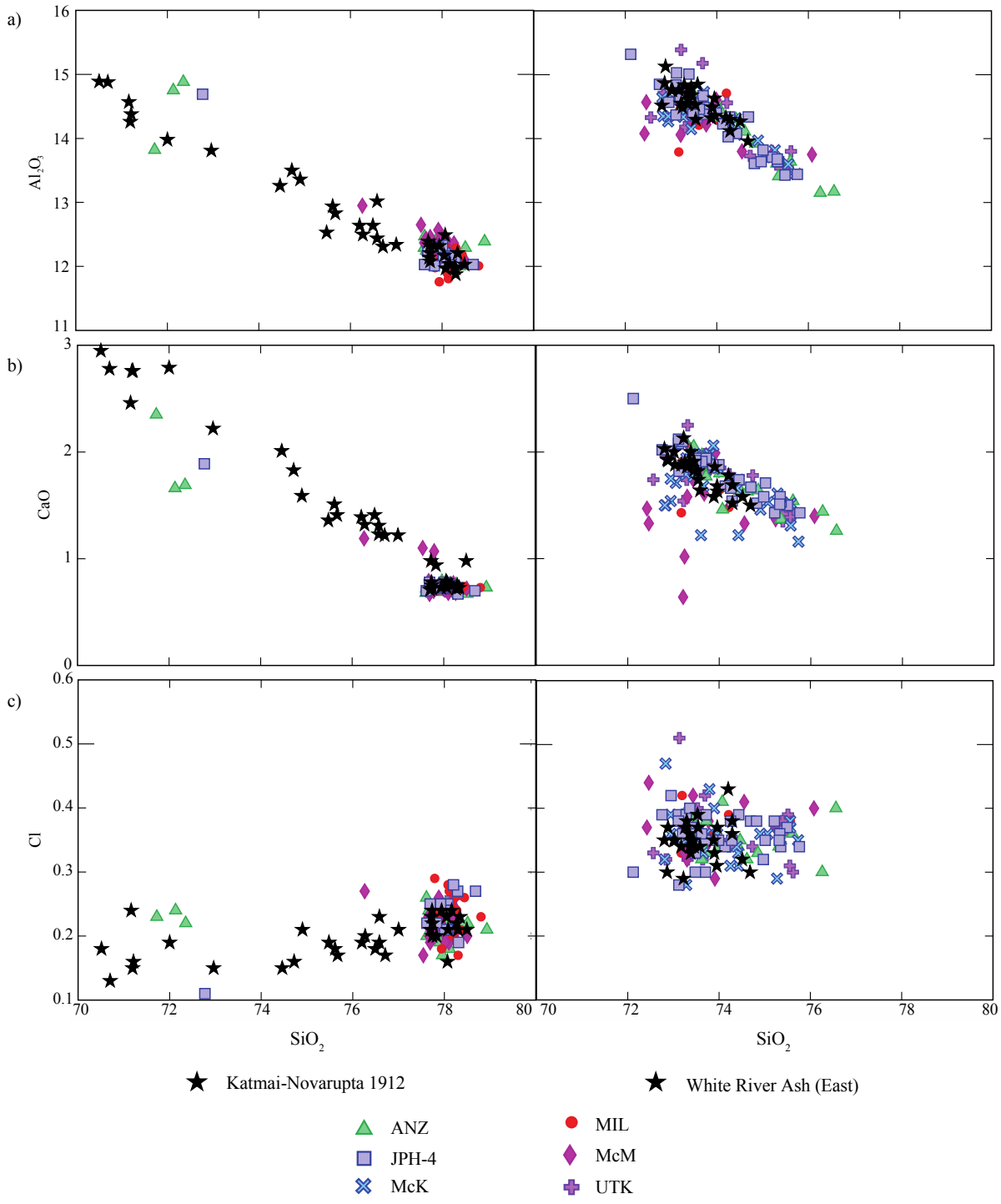

Figure 4.3 Major-element glass geochemical plots showing the correlation between material from the northern Alberta peat cores and proximal reference material from Novarupta-Katmai 1912 and WRAe. Full details of the proximal reference material are provided in Table 4.2.

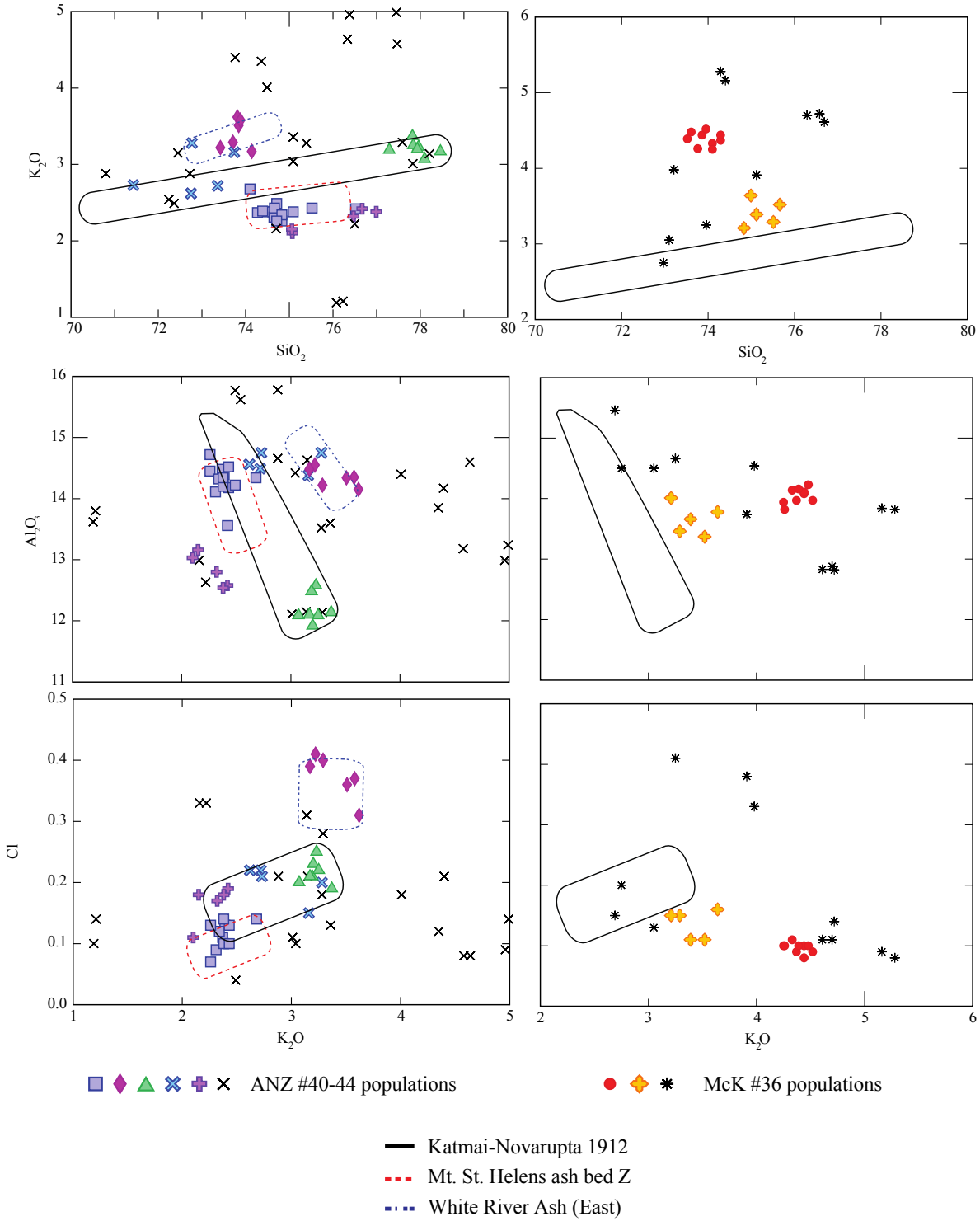

Figure 4.4 Major element glass geochemical plots showing the multiple populations present in samples from ANZ and McK, compared with outlines representing analyses of reference material from Novarupta-Katmai 1912 (solid black), Mt. Churchill (WRAe; dashed blue), and Mt. St. Helens ash bed Z (dashed red). Full details of the proximal reference material are provided in Table 4.2.

The primary peak in McK (UA 2966) has at least three distinct geochemical populations that appear Aleutian in origin (although their alkali totals are relatively high) but have no identified correlations (Figure 4.4). As the peak shard counts are significantly higher than recorded at other sites this is interpreted as an over-concentration of glass, most likely caused by a period of reduced peat accumulation or the removal of organic material. Supporting proxy data show a shift at this depth from wet to dry conditions but no evidence of fire.

The broad peak of shards at ANZ from 38.62-42.89 cm (UA 2907, 2908, 2909, 2967, 2971) contains multiple geochemical populations - two can be correlated to Novarupta-Katmai 1912 and Mt. Churchill, and one appears correlate to ash bed Z, a mid-1600s eruption of Mt. St. Helens (Figure 4.4). Ash bed Z is recorded proximally in Washington as a thin deposit of fine ash with a NE trajectory, maximum thickness of 15cm, and a similar geochemical composition to the pre-1980 summit dome (Mullineaux, 1996). Stratigraphically, it occurs between set X (~AD 1500s) and set T (~AD 1800s) and is estimated to have erupted in the mid-1600s (Yamaguchi and Hoblitt, 1995). Ash bed Z is interpreted as a co-ignimbrite ash that would be unlikely to travel as far north but there are no other known Mt. St. Helens eruptions that have the same high wt.% SiO_2 content. The most recent eruptive activity from Mount Churchill is reported at ~AD 1640-1665 (Payne et al., 2008).

4.3.3. Radiometric data

4.3.3.1. ^{14}C dates

All ^{14}C dates reported here followed their observed stratigraphic order and no age-reversals were present (Table 4.3). Several dates were bimodal when calibrated, or located on radiocarbon plateaus – especially around the 19th century. At McM (#38 – 42.49 cm, #42 – 47.02 cm) and McK (#40 – 45.92 cm, #50 – 57.90 cm) large apparent jumps between dated samples occurred, indicating the presence of either hiatuses or significant changes in accumulation rate. At the three of the four sites (excluding MIL) where Novarupta-Katmai 1912 is present the cryptotephra peak agrees with the ^{14}C one sigma error range.

Sample ID	UCIAMS #	Depth (cm)	Description	F ^{14}C	±	^{14}C age (BP)	±	Calibrated age (cal BC/AD)			
								68.2% range		95.4% range	
ANZ-W3 #05	170621	5.99	*Sphagnum* stems	1.0634	0.0017	---	---	2005-2006	---	2005-2008	1956-1957
ANZ-W3 #10	170623	10.62	*Sphagnum* stems	1.0675	0.0019	---	---	2004-2006	---	2003-2007	1956-1957
ANZ-W3 #15	154027	14.98	*Sphagnum* stems	1.1521	0.0023	---	---	1990-1991	---	1957-1958	1989-1991
ANZ-W3 #20	154026	19.20	*Sphagnum* stems	1.2131	0.0022	---	---	1960-1961	1984-1985	1959-1961	1983-1985
ANZ-W3 #25	154025	23.75	*Sphagnum* stems	1.3133	0.0025	---	---	1978-1979	---	1962	1977-1979
ANZ-W3 #30	154024	28.45	*Sphagnum, Ericaceae* leaves	1.4155	0.0025	---	---	1962	1974	1962-1963	1973-1974
ANZ-W3 #40	142039	38.62	Twig material	---	---	170	20	1669-1682; 1736-1780; 1799-1805	1935-1944	1665-1693; 1727-1785; 1793-1813	1919-
ANZ-W3 #50	152367	49.01	*Sphagnum* stems, *Picea* needles	---	---	330	15	1514-1528	1553-1599; 1617-1633	1490-1603	1613-1637
ANZ-W3 #60	142038	59.31	*Sphagnum* stems	---	---	325	20	1516-1530; 1539-1596	1618-1635	1490-1603	1612-1642
ANZ-W3 #70	152362	69.62	*Sphagnum* stems and branches, *Picea* needles, *Chamaedaphne calyculata* seed	---	---	910	15	1049-1085	1124-1137; 1150-1160	1041-1108	1116-1165
ANZ-W3 #80	142043	80.15	*Sphagnum* stems and leaves	---	---	1245	25	689-751	760-775	682-779	790-869
JPH4-W1 #5	154012	4.31	*Sphagnum, Picea* needles	1.2789	0.0023	---	---	1979-1980	---	1959; 1961-1962	1979-1980; 1981
JPH4-W1 #10	154011	9.08	*Sphagnum* stems	1.7993	0.0033	---	---	1965	---	1963-1965	---
JPH4-W1 #14	154009	12.89	*Sphagnum* stems	1.2479	0.0023	---	---	1981-1982	---	1959; 1961-1962	1980-1982
JPH4-W1 #20	154008	18.93	*Sphagnum* stems, *V. oxycoccos* charred leaves, *Picea* charred needles	---	---	95	15	1698-1724	1815-1835; 1878-1395; 1903-1917	1694-1728	1812-1919
JPH4-W1 #30	142066	28.65	*Sphagnum* stems	---	---	490	40	1411-1445	---	1324-1346	1393-1464
JPH4-W1 #39-40	152359	38.30	*Sphagnum* stems, *Conifer/Ericaceae* bark, *Carex* seeds, *Picea* charred needles	---	---	605	20	1306-1329; 1341-1363	1385-1396	1299-1370	1380-1404
JPH4-W1 #50	142037	49.13	Bark	---	---	955	20	1029-1047	1091-1121; 1140-1148	1022-1059	1069-1155
JPH4-W1 #59	152360	58.47	*Carex* seeds, Conifer bark, *Ericaceae* stems	---	---	1290	15	678-710	746-764	670-723	740-768
JPH4-W1 #70	142045	70.07	Stem and fragments (ligneous)	---	---	2405	20	*448-409*	---	*703-696*	*541-402*
McK-W2 #10	154007	11.76	*Sphagnum* stems	1.1453	0.0025	---	---	1990-1992	---	1957-1958	1990-1992
McK-W2 #15	154006	17.39	*Sphagnum* stems	1.2336	0.0022	---	---	1960	1982-1983	1959-1960; 1961-1962	1982-1983
McK-W2 #20	154005	22.96	*Sphagnum* stems	1.5258	0.0033	---	---	1970	1971	1969-1971	---
McK-W2 #25	154004	28.58	*Sphagnum*, Rhododendron leaves	1.7272	0.0031	---	---	1966	---	1965-1966	---
McK-W2 #40	142064	45.92	*Sphagnum* stems and leaves	---	---	280	20	1528-1551	1634-1651	1521-1576; 1584-1591	1626-1662

Table 4.3: Summary of ^{14}C dates produced from the six peat cores. BC dates are shown in blue italics; starred (*) dates are interpreted as anomolous. ^{14}C dates were calibrated using Bomb13NH1 (Hua et al., 2013) and IntCal13 (Reimer et al., 2013) calibration curves as appropriate in Oxcal v4.2 (Bronk Ramsey, 2009a).

Sample ID	UCIAMS #	Depth (cm)	Description	F ^{14}C	±	^{14}C age (BP)	±	Calibrated age (cal BC/AD)			
								68.2% range		95.4% range	
McK-W2 #50	152365	57.90	*Picea* charred needles, *Sphagnum* stems	---	---	1135	15	889-901	921-953	882-972	---
McK-W2 #60	142065	69.77	*Sphagnum* stems and leaves	---	---	1220	20	728-737; 768-779	790-829; 838-865	713-744	765-885
McK-W2 #70	152366	82.29	*Picea* charred needles, Ericaceae charred leaves, *Sphagnum* stems	---	---	1575	15	429-436; 446-472	487-498; 505-535	426-538	---
McK-W2 #77	142068	91.60	*Sphagnum* stems and leaves	---	---	1920	45	25-130	---	*21-11*	*2*-216
MCM W3 #05	170644	5.02	*Sphagnum* stems	1.0901	0.0017	---	---	2000-2001	---	1999-2002	1957
McM-W3 #11	170627	11.74	*Sphagnum* stems	1.1318	0.0017	---	---	1993	---	1992-1994	1957-1958
McM-W3 #17	170634	18.48	*Sphagnum* stems	1.1621	0.0017	---	---	1989-1990	---	1988-1990	1957-1958
McM-W3 #23	170629	25.27	*Sphagnum* stems	1.0004	0.0015	0	15	1954-1955	---	1954-1955	1956-1957
MCM W3 #29	170639	32.06	*Sphagnum* stems	0.9881	0.0017	95	15	1698-1724; 1815-1835	1878-1895; 1903-1917	1812-1919	1694-1728
McM-W3 #35	170626	38.83	*Sphagnum* stems	0.9854	0.0015	120	15	1833-1880; 1915-1926	1688-1706; 1720-1730; 1809-1819	1806-1893	1683-1735; 1907-1930
McM-W3 #38	154002	42.29	Charred *Picea* and *Larix* leaves	---	---	210	20	1655-1670; 1779-1799	1943-	1648-1682; 1739-1744; 1752-1803	1937-
McM-W3 #42	163396	47.02	*Sphagnum* stems and charred *Larix* leaves	---	---	985	15	1018-1039	---	1016-1047	1092-1122;1140-1148
McM-W3 #52	163398	53.96	*Sphagnum* stems	---	---	950	20	1030-1049	1085-1124; 1137-1150	1025-1059	1065-1155
McM-W3 #60	154001	68.03	*Sphagnum stems*	---	---	1220	20	728-737	768-779; 790-829; 838-865	713-744	765-885
McM-W3 #80	154000	91.50	*Larix leaves, Picea leaves*	---	---	1905	15	76-91	99-124	65-130	---
MIL-W1 #10	154023	10.82	*Sphagnum* stems	1.1235	0.0020	---	---	1993-1995	---	1957-1958	1993-1995
MIL-W1 #15	154022	16.24	Sphagnum, Ericaceae leaves	1.1843	0.0021	---	---	1958-1959	1986-1988	1958-1959	1986-1988
MIL-W1 #20	154021	21.78	*Sphagnum* stems	1.3382	0.0024	---	---	1977	---	1976-1977	1978
MIL-W1 #25	154018	27.17	*Sphagnum* stems	1.2256	0.0022	---	---	1959-1960; 1961	1983-1984	1959-1962	1982-1985
MIL-W1 #30	154017	32.56	*Sphagnum* stems	1.0587	0.0021	---	---	2006-2008	2009-2014	1956	2005-2014
MIL-W1 #35	154016	38.10	*Sphagnum* stems	---	---	25	15	1896-1904	---	1891-1907	---
MIL-W1 #40	142040	43.77	Bark of twigs, twig, woody fragments, seeds	---	---	110	20	1694-1710; 1718-1727	1813-1890; 1910-1917	1685-1733	1807-1896; 1903-1928
MIL-W1 #44	152363	48.44	Charred *Picea*, *Larix* needles and Ericaceae leaves	---	---	675	15	1282-1299	1372-1378	1278-1305	1365-1385

Table 4.3 (cont.): Summary of ^{14}C dates produced from the six peat cores. BC dates are shown in blue italics; starred (*) dates are interpreted as anomolous. ^{14}C dates were calibrated using Bomb13NH1 (Hua et al., 2013) and IntCal13 (Reimer et al., 2013) calibration curves as appropriate in Oxcal v4.2 (Bronk Ramsey, 2009a).

Sample ID	UCIAMS #	Depth (cm)	Description	F ^{14}C	±	^{14}C age (BP)	±	Calibrated age (cal BC/AD)			
								68.2% range		95.4% range	
*MIL-W1 #50	142041	55.56	Stems	1.3667	0.0029	---	---	1975-1976	---	1974-1976	---
MIL-W1 #50-51	152364	55.56	Coniferous bark (peridermis)	---	---	990	15	1018-1035	---	1012-1045	1095-1121
MIL-W1 #55	152361	62.60	Charred *Picea* needles	---	---	1135	15	889-901	921-953	882-972	---
MIL-W1 #58	142042	66.98	Charcoal particles	---	---	1500	20	551-593	---	478-482	536-620
UTK W2 #05	170646	4.87	*Sphagnum stems*	1.0489	0.0017	---	---	2007-2009	---	2007-2009	1956-1957
UTK W2 #11	170641	11.06	*Sphagnum stems*	1.0846	0.0018	---	---	2001-2002	---	2000-2003	1957
UTK-W2 #17	170630	17.10	*Sphagnum stems*	1.1349	0.0018	---	---	1992-1993	---	1991-1994	1957-1958
UTK W2 #23	170642	23.18	*Sphagnum stems*	1.2225	0.0021	---	---	1983-1984	1959-1960	1983-1985	1959-1962
UTK-W2 #29	170624	29.36	*Sphagnum stems*	1.3755	0.0023	---	---	1974-1976	---	1974-1976	1962
UTK-W2 #32	163401	32.50	*Sphagnum stems*	1.5449	0.0025	---	---	1969-1970	---	1968-1970	1971
UTK-W2 #42	154015	42.85	*Sphagnum stems*	---	---	55	20	1710-1718	1828-1832; 1890-1910	1697-1725	1814-1835; 1877-1918
UTK-W2 #48	163397	49.07	*Sphagnum stems*	---	---	220	15	1660-1666	1784-1796	1648-1670; 1780-1800	1943-
UTK-W2 #54	163402	55.22	*Sphagnum stems*	---	---	320	15	1522-1530; 1539-1591	1620-1635	1497-1506; 1512-1601	1616-1643
UTK-W2 #62	154014	63.83	*Sphagnum*	---	---	1100	15	901-921	950-980	895-929	939-988
UTK-W2 #84	154013	89.53	*Sphagnum stems*	---	---	2485	15	*594-546*	*648-610; 670-663; 689-681; 754-735*	*696-540*	*721-702; 766-727*

Table 4.3 (cont.): Summary of ^{14}C dates produced from the six peat cores. BC dates are shown in blue italics; starred (*) dates are interpreted as anomolous. ^{14}C dates were calibrated using Bomb13NH1 (Hua et al., 2013) and IntCal13 (Reimer et al., 2013) calibration curves as appropriate in Oxcal v4.2 (Bronk Ramsey, 2009a).

4.3.3.2. ^{210}Pb, ^{137}Cs and ^{241}Am dates

Key parameters associated with each core, including the maximum ^{210}Pb activity, the ^{210}Pb and ^{137}Cs inventories, and the mean ^{210}Pb flux, are summarised in Table 4, and full details of the radiometric data determined for each core are shown in Table S3a. Measured ^{226}Ra concentrations were an order of magnitude lower than those typical of mineral soils with mean values of around 5 Bq kg^{-1} - this is assumed to reflect the high organic matter content of the bogs. The ^{210}Pb radiometric inventories are broadly similar and correspond to mean ^{210}Pb supply rates of between 73-119 Bq m^{-2} y^{-1}, with a mean value of 97 Bq m^{-2} y^{-1}. Although there is very little data on ^{210}Pb fallout in this region, these are comparable to published values for atmospheric flux (e.g. Appleby and Oldfield, 1983; Bauer et al., 2009; Turetsky et al., 2007; Wieder et al., 2016).

Records of ^{137}Cs activity versus depth and initial ^{210}Pb dates calculated using the CRS model for all sites are shown in Figure 5. Many of the cores show evidence of significant modification of the ^{137}Cs fallout record that is expected to reflect fallout from the atmospheric testing of nuclear weapons beginning in the mid-1950s and reaching a peak in 1963. Implementation of the atmospheric test ban treaty in 1963 resulted in a rapid decline in fallout to very low levels by the mid-1980s, and fallout from the 1986 Chernobyl accident in this region was negligible. Post-depositional transport processes have resulted in significant discrepancies between the bog records and the fallout record (Figure 5), making identification of the 1963 depth problematic. Unusual features include multiple peaks and increasing concentrations towards the top of the core. Regarding the surficial peaks, the enrichment of alkali metals at the surface of bogs is known to be related to biological uptake by plants (Damman, 1978) rather than a reflection of direct atmospheric inputs. Cs-137 is recorded elsewhere as being mobile in acidic peat bog profiles (e.g. Appleby et al., 1997; MacKenzie et al., 1997; Schleich et al., 2000; Zaccone et al., 2007).

While the 1963 dates for these cores are lacking in precision, they are in reasonable agreement with the ^{210}Pb dates (Table 5) but only three cores (ANZ, McK, UTK) had ^{137}Cs records that could be used to establish the 1963 depth with some confidence.

Site	Unsupported ^{210}Pb								^{137}Cs			^{241}Am peak depth (cm)	Comments
	Maximum activity		Inventory		Flux		Equilibrium depth (cm)	Unsupported ^{210}Pb activity	Inventory		Peak depth (cm)		
	Bq kg^{-1}	±	Bq m^{-2}	±	Bq m^{-2}y^{-1}	±			Bq m^{-2}	±			
ANZ	167	40	3820	73	119	3	40-50	Relatively uniform <20 cm; below this decline is more or less exponential with depth	766	10	1, 18-21, 31.5	35	
JPH	323	21	2340	55	73	2	25	Varied non-monotonically with depth 0-6 cm Decline more regular in deeper layers; small non-monotonic feature at 18 cm ^{210}Pb concentrations in dense layers >20 cm close to/below the minimum level of detection	1164	17	*1.5*, *6*, 13	11-13	High values of ^{137}Cs activity in the uppermost layers is unlikely to be a record of atmospheric fallout
McK	361	29	3639	84	113	3	40	Varied non-monotonically with depth 0-30 cm	1428	18	*1, 7*, 30	*21*, 29, *36*	High values of ^{137}Cs activity in the uppermost layers is unlikely to be a record of atmospheric fallout
McM	286	27	3307	80	103	3	40	Decline irregular with depth, but no major non-monotonic features Gradient of the decline is significantly steeper >24 cm; lower net peat accumulation rates in the deeper layers Abrupt termination >42 cm may relate to the abrupt change in the nature of the peat at 38 cm	1565	22	17-19, 23	20-27	Small, diffuse peak in ^{241}Am concentrations 20-27 cm implies the secondary ^{137}Cs peak at 23 cm may be a better indicator of the 1963 depth
MIL	233	26	2988	55	93	2	43	Decline more regular Several non-monotonic features that may record brief changes in net peat accumulation	1014	14	24, 31-34	28-34	Two ^{137}Cs peaks are separated by a non-monotonic feature - both features may date from the early 1960s
UTK	285	16	2556	37	80	3	46	0-18 cm: concentrations decline exponentially with depth 21-33 cm: concentrations constant; separated from the uppermost zone by a small non-monotonic feature >33 cm: concentrations decline steeply with depth, may be related > peat density here	820	11	30-34		

4.4 Key radiometric parameters associated with each core including the maximum ^{210}Pb concentration, the ^{210}Pb and ^{137}Cs inventories, and the mean ^{210}Pb flux.

Although the ^{137}Cs record in ANZ has two distinct peaks, at 18-21 cm and 32-37 cm, evidence that the deeper peak records 1963 is provided by its location below the 28.45 cm sample dated by ^{14}C to 1974, and the presence at around the same depth (34-37 cm) of a small but significant ^{241}Am peak. McK and UTK both have single prominent well-defined ^{137}Cs peaks, at 30 cm (McK) and 30-34 cm (UTK). 1963 dates for these features are supported by the fact that both lie just below samples dated by ^{14}C to the mid to late 1960s: the 28.58 cm in McK is dated 1965-6, and the 32.5 cm in UTK sample is dated 1969-70. In UTK there is also a small but significant ^{241}Am peak at the same depth as the ^{137}Cs peak. The raw ^{210}Pb dates for these cores are also in general agreement with the ^{137}Cs dates - at the McK core they place 1963 at a depth of 30 cm, very close to the ^{137}Cs peak. However, there is a small discrepancy for UTK as the raw ^{210}Pb calculations place 1963 at 34.75 cm, and a slightly larger discrepancy for ANZ where 1963 is placed at a depth of 31.2 cm.

In the other three cores it was only possible to give some general indication as to the 1963 depth. In JPH the ^{137}Cs record has two prominent peaks, at 1.5 cm and 6 cm, neither of which are likely to record the 1963 fallout maximum. It may however be recorded by a small but diffuse ^{241}Am peak at 11-14 cm. In McM there is a broad ^{137}Cs feature that includes two distinct peaks, at 17-19 cm and 23 cm. Small concentrations of ^{241}Am between 20-27 cm suggest that the deeper though smaller ^{137}Cs peak dates from the early 1960s. In MIL there are again two well-resolved peaks, the larger at 24 cm and the smaller at 31-34 cm. Traces of ^{241}Am were recorded between 28 and 34 cm.

For comparisons with the cryptotephra data, the raw CRS model dates for ANZ place 1912 at a depth of 37.8 cm, in good agreement with the Novarupta-Katmai tephra date for this core (1912=37.6 cm). At the other four sites with this marker, however, there are significant discrepancies between the tephra and ^{210}Pb dates (Table 4.5). Causes of these discrepancies, and those between ^{210}Pb and ^{137}Cs dates, include variations in the rate of supply of ^{210}Pb due to localised changes at the surface of the bog, post-depositional downwards migration of ^{210}Pb, and hiatuses in the core record. These can all result in failure of the ^{210}Pb record to fully meet the assumptions of the CRS model. Corrected ^{210}Pb dates can be obtained by instead applying the CRS model in a piecewise way using those clearly identifiable chronostratigraphic dates as reference points (Appleby 2001).

Pb-210 dates determined by this method are given in Table S4.3b. ^{137}Cs and tephra dates used as reference points in the calculations are shown in bold.

	1963 depth (cm)		1912 depth (cm)		Reference points used for final age models*
	^{137}Cs/^{241}Am	^{210}Pb	Tephra	^{210}Pb	
ANZ	32-37	31.2	37.6	37.8	1963 & 1912
JPH	11-14?	12.5	14.86	19	1912
McK	30	30	None	35.9	None
McM	20-27?	26.3	18.66	37.75	1912
MIL	28-34?	30.15	34.72	40.2	1912
UTK	30-34	34.75	N/A†	40.85	1912

Table 4.5: Comparison of reference dates for AD 1963 (137Cs) and 1912 (cryptotephra) in each core with 210Pb CRS model data. *see also: Table S3b. † No isochron defined.

4.3.4. Age-depth modelling and comparison of chronometers

As a manual first pass to compare the radiometric methods, dates produced from ^{14}C and ^{210}Pb were modelled in separate P_Sequence models and compared with each other and the independent chronostratigraphic markers (^{137}Cs, ^{241}Am, and cryptotephra). Figure 4.5 shows the mean modelled ^{14}C and ^{210}Pb values for each sample plotted with 1 sigma error ranges. At UTK the initial ^{210}Pb, ^{14}C, and ^{137}Cs data agree well - most offsets are less than 5 years. The upper section of MIL is similarly agreeable. At the remaining four sites, ^{210}Pb dates are commonly offset from ^{14}C dates by ~10 years back until 1960, and consistently underestimate the modelled ^{14}C ages by 20 to more than 100 years from 1960-1850.

Figure 4.6 shows that the recalculated CRS ages (^{210}Pb corrected, where possible, using cryptotephra and ^{137}Cs) for MIL and McM are in better agreement with the ^{14}C ages, while JPH has agreement between the ^{210}Pb dates, ^{137}Cs, and tephra record but the ^{14}C dates are offset. ^{210}Pb data from ANZ were not corrected as the offset in the lowest three dates from 36-40 cm appears to be directly related to the presence of permafrost. Instead, a calendar date for the 1912 eruption was included in the model.

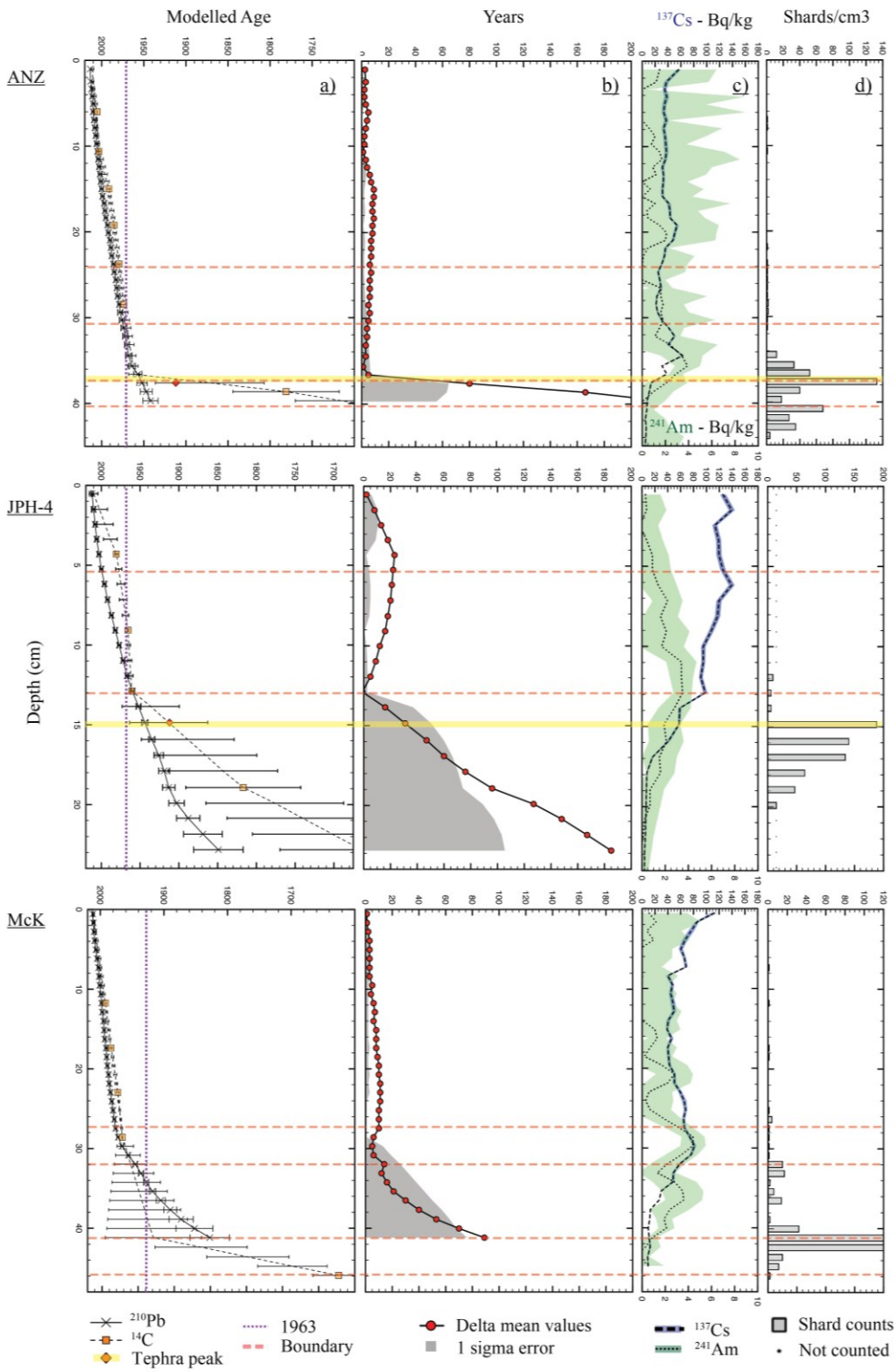

Figure 4.5: Individual core age models for the modern period, showing a) ^{14}C, ^{210}Pb and cryptotephra dates; b) delta values between the median chronometer values at each depth and the associated error; c) ^{137}Cs and ^{241}Am profiles; d) tephra shard concentration profiles.

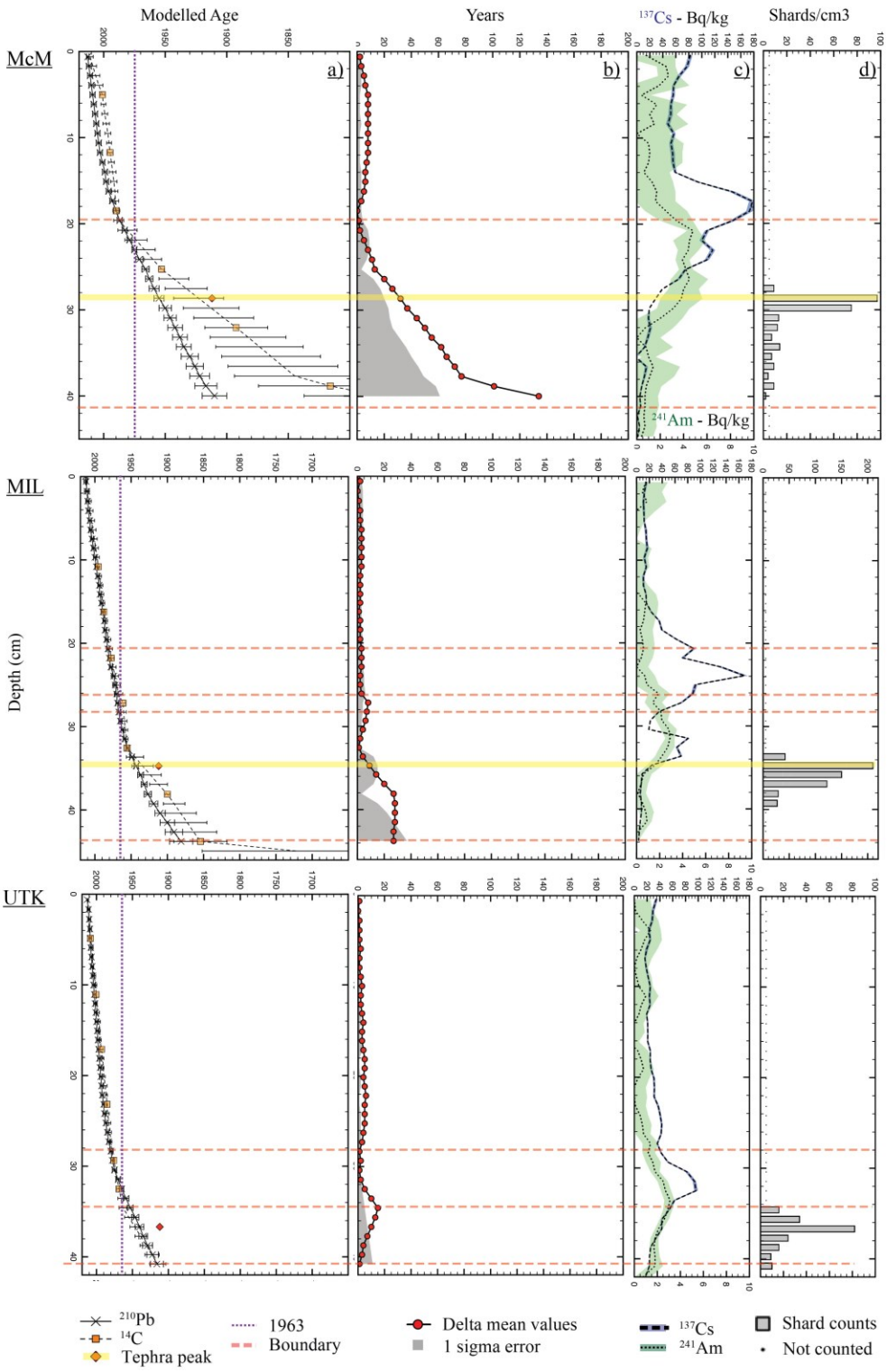

Figure 4.5 (cont.): Individual core age models for the modern period, showing a) ^{14}C, ^{210}Pb and cryptotephra dates; b) delta values between the median chronometer values at each depth and the associated error; c) ^{137}Cs and ^{241}Am profiles; d) tephra shard concentration profiles.

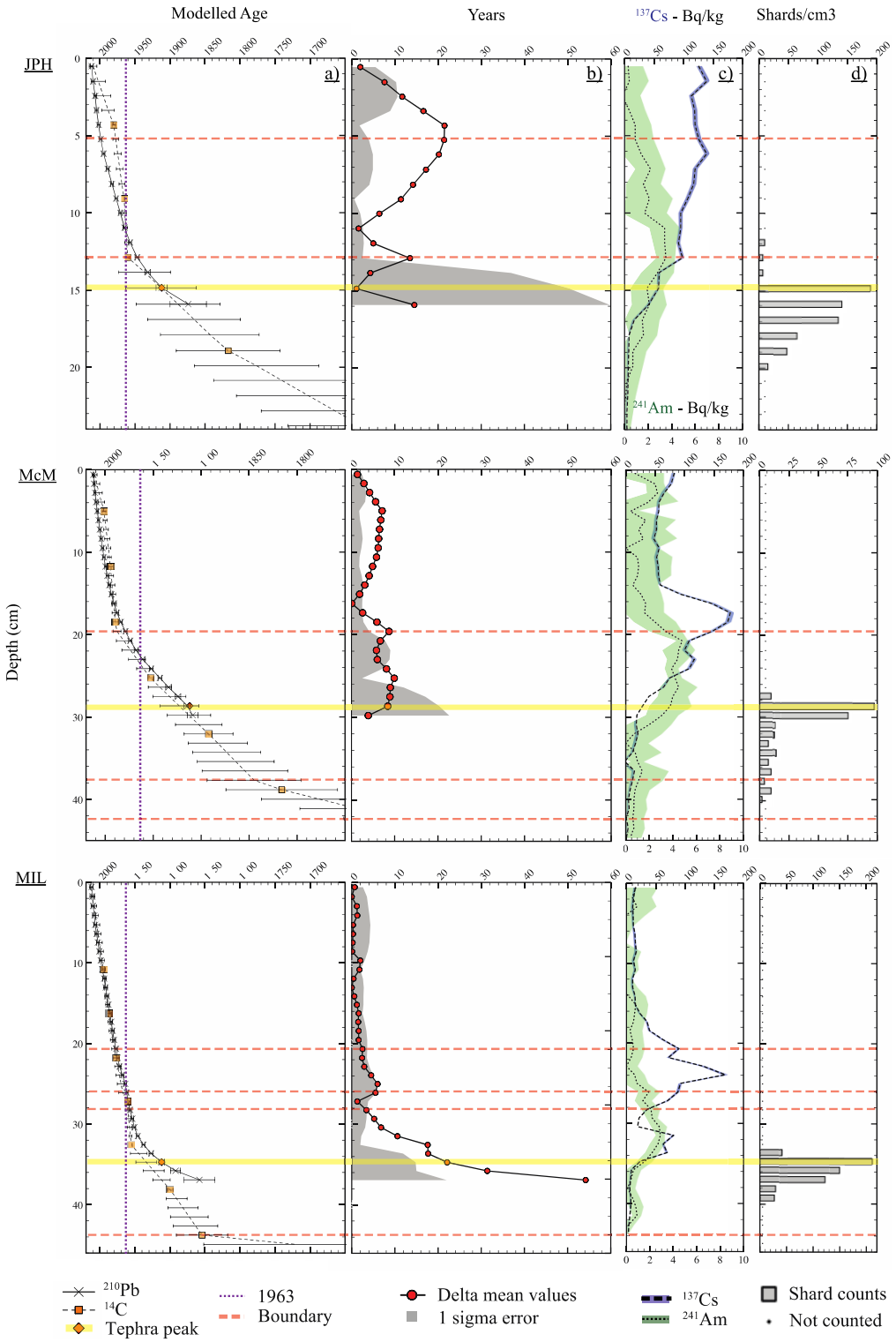

Figure 4.6 Individual core age models with tephra-corrected ^{210}Pb data for AD 1650-2015 at JPH, MIL, and McM. a) ^{14}C, ^{210}Pb and cryptotephra dates; b) delta values between the median chronometer values at each depth and the associated error; c) ^{137}Cs and ^{241}Am profiles; d) tephra shard concentration profiles.

The resulting P_Sequence models for five of the six sites (Figure 4.7) have improved agreement indices (AI), more realistic accumulation rates, and improved precision when compared with any one chronometer alone. For the 20th century, the combined models for four sites (ANZ, JPH, McK, McM) have standard deviations of less than 5 years for all samples. MIL and UTK have one and five samples respectively that have standard deviations of up to 7 years. UTK has a number of increased errors at the start of 20th century due to the presence of permafrost directly above two radiocarbon-plateau dates which cannot be more tightly constrained with the current prior dataset.

The models are classified here as simple (MIL, UTK), advanced (McM, ANZ), and complex (JPH, McK). Simple models are well constrained and have good agreement between the chronometers with little to no additional work needed. Advanced models have some complications, e.g. prolonged disruptions to accumulation by the presence of permafrost or local surface peat combustion, but the corrected data agree well when this additional information is included in the model. Complex models have disagreements between chronometers which cannot be fully resolved with the current data sets or cannot be fully explained.

Using outlier analysis, 1-3 dates from the period back to ~AD 1850 are rejected at each site (excluding UTK which includes all dates), as well as one date from the older section at McM and MIL. At MIL three dates from 32-36 cm are identified as outliers (one ^{14}C, two ^{210}Pb; Figure 5); this period is also associated with changes in dry density, C/N and ligneous roots. For JPH a successful model only includes the tephra-corrected ^{210}Pb data and excludes all three modern ^{14}C dates.

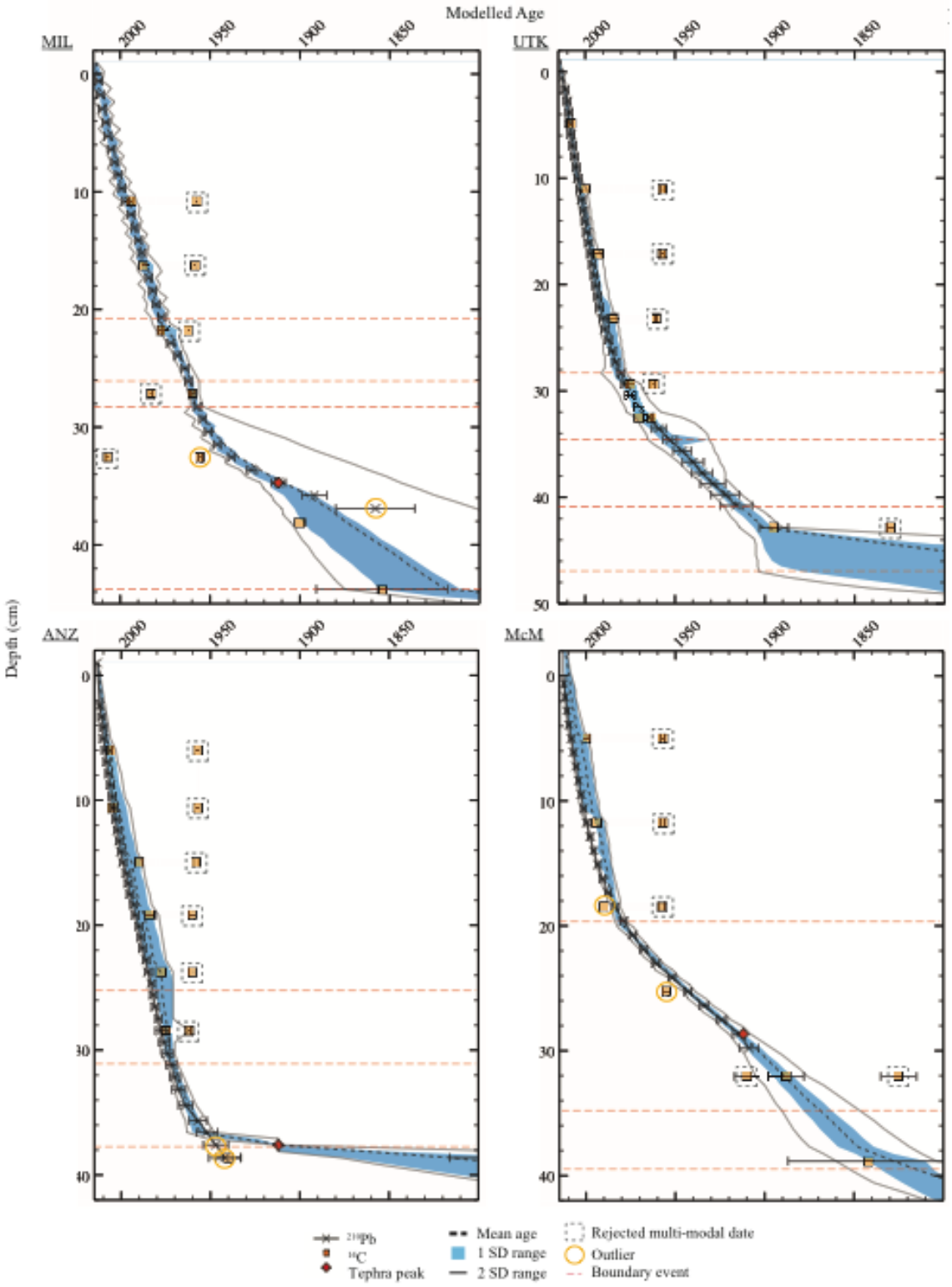

Figure 4.7: Final Bayesian P_Sequence core age models. Blue areas show 1 sigma error ranges; grey lines bound 2 sigma error ranges. Median values are shown with the dashed line.

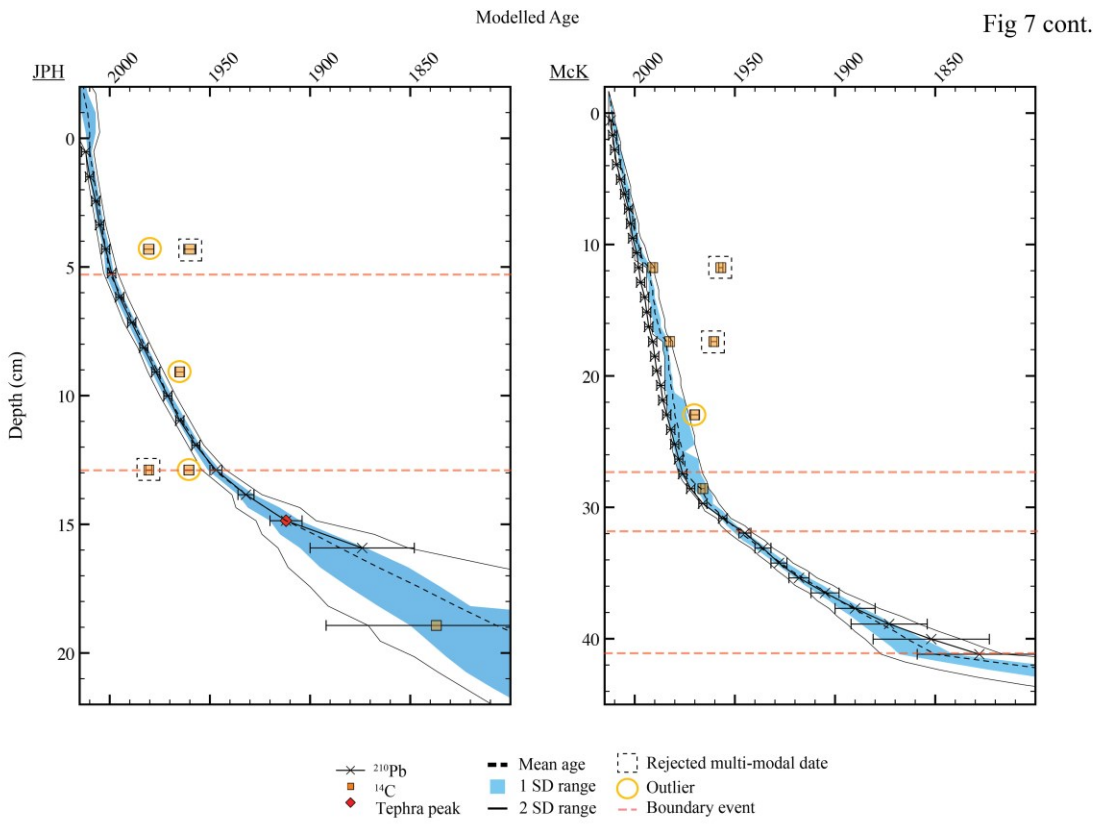

Figure 4.7 (cont.): Final Bayesian P_Sequence core age models. Blue areas show 1 sigma error ranges; grey lines bound 2 sigma error ranges. Median values are shown with the dashed line.

4.4 Discussion

The data shown here demonstrate the range of variability that can occur when constructing age-depth models for peatland records, even within one region. None of the chronological methods are intrinsically problematic, but they rely on assumptions of relatively uniform peat accumulation and signal preservation that may be invalid for parts of records or changes over time. While some sites can be modelled simply, at most sites a more detailed comparison using multiple chronometers and environmental proxies that affect peat accumulation and preservation is useful to assess accuracy. Dating modern peat cores with a single chronometer can mask this complexity, particularly in peatlands affected by strong environmental changes (e.g. permafrost formation or surface drying that may affect accumulation rates) with the caveat that inaccuracies in age models can lead to incorrect interpretations of associated proxy data.

4.4.1. Environmental histories

Environmental histories record events which may have impacted the peatland archives, but here they have not all noticeably affected the peat surface and resulting modelled accumulation rates. For example, possible fires recorded at MIL and UTK do not appear to have combusted peat surface material at the coring locations, although an older local fire at MIL at 44 cm coincides with a sharp change in accumulation rate. At five sites, there is an ecological shift towards a dominance of *Sphagnum* section *Acutifolia* during the 20th century. These changes are not coincident, with JPH starting in ~1956, MIL in ~1965, and ANZ, McM and UTK, all in 1980-1985, but this change only appears to affect accumulation rates at two of the preserved records (McM and UTK).

Three sites have apparent hiatuses through either loss of organic material or significant reductions in accumulation. At ANZ, ~200 years of peat is missing from ca. AD 1700-1900 during a period of permafrost and local fires as shown by the bracketing ^{14}C and tephra data. Bracketing ^{14}C dates at McM show an apparent hiatus during the period of permafrost and local fires which coincides with the Little Ice Age (47.02 cm = ~AD 1100, 42.29 cm = ~AD 1700). At McK, a level corresponding to a wet to dry shift in the late 19th century (42 cm) has a concentration of glass from at least three different eruptions, interpreted here as evidence for a near stationary peatland surface that accumulated multiple tephra falls. These 'hiatuses' occur over discrete depths of the peat records, and can only be properly accounted for when recognised using multiple techniques.

Permafrost, surface drying, local fires, and ligneous roots are the features most commonly associated with complications in the resulting age-depth models. Possible permafrost development was identified at three sites, although the timing is not fully coincident. Both McM and ANZ record an early onset (AD 1300 & 1600) while UTK has 20th century onset (~AD 1900). McM shows the earliest disappearance at ~AD 1850, while at ANZ and UTK permafrost has persisted until 1960-1970.

The inclusion of environmental histories that may have affected peat accumulation rates as boundaries in OxCal P_Sequence models is appropriate to judge the relative importance of events identified from proxy data as the dates can confirm if events had

coincident changes in peat accumulation rates. The models produced here show that this information is important for obtaining an accurate representation of peat accumulation, particularly where hiatuses and significant peat accumulation changes have occurred. Using environmental information to produce a Bayesian model of ^{210}Pb data calculated using the CRS model also combines the two methods in a way that provides better agreement with other complimentary data and results in dates based on physical principles.

The precise age of these boundaries must be considered cautiously, however –if intervals do not have *a priori* constraining dates close to the depths of the boundary change they will have relatively broad associated errors and ranges of possible accumulation rates above and below. Several dates here were sampled at the exact depth of the boundary and it is not necessarily clear if they represent maximum or minimum constraints e.g. for local fires the material may be the subsequent new peat growth or the lowest depth burned down to. This can be addressed by dating directly below the event/boundary to obtain a maximum age if the event is of particular interest.

4.4.2. Cryptotephra data

Tephra data from these sites extend the known geographical limits for deposition of Novarupta-Katmai 1912 and the regionally widespread WRAe. While our tephra profiles are not fully comprehensive late Holocene records for the area, they demonstrate the preservation of tephra that are both locally important and widespread, and hence the possibilities for correlation with other regional to hemispheric records.

The identification of 17th century tephra including a Mt. Churchill correlative and the MSH ash bed Z shows the potential for other cryptotephra horizons in the region. Both tephra were erupted within the bracketing ^{14}C dates at ANZ (Table 3). Only 2 cm of peat is present between tephra peaks from 1912 and the mid 17th century beds and this is coincident with the presence of increased charcoal and charred macrofossils. We interpret this as burning of surface peat at ANZ before AD 1900 that removed peat accumulated since ~AD 1700 and concentrated glass preserved from this period.

The shard profiles reported here support previous work reporting spatial variability of the number of tephra and shard concentrations preserved regionally (e.g. Watson et al., 2015;

Zoltai, 1989): Novarupta-Katmai 1912 was seemingly absent from McK; WRAe was not identified at MIL, though this is not surprising given that the peatland was a fen at the time and not ombrotrophic.

4.4.3. Age-depth models

Age-depth models incorporate information from multiple analyses and additional supporting methodologies, and can highlight periods of disagreement between dating methods that have their own inherent strengths and weaknesses. It is not implied here that a given method is inherently better than any other — a positive outcome from this study is that using a range of independent techniques allows the slight biases that exist within a method to be interrogated and considered within the light of the total chronological information available, ultimately providing more robust chronologies.

C-14 dates are commonly used for peatland age models, but often only pre-bomb dates will be connected to the bottom of a ^{210}Pb record. Three sites here show good agreement between post-bomb ^{14}C dates and ^{210}Pb, with both methods producing well-constrained age models back through the 1960s. However, at JPH three post-bomb dates were shown to be outliers and statistically rejected from the Bayesian models. As macrofossils were carefully picked and identified it is unlikely that these outliers were the result of, for example, root contamination. Instead, very low rates of peat accumulation for the upper layers likely means each dated sample is comprised of material from multiple years of accumulation (Garnett and Stevenson, 2004) and the resolution of ^{14}C analysis is not comparable to the ^{210}Pb dates.

It is generally accepted that ^{210}Pb dating in peatlands needs independent corroboration (Oldfield et al., 1995) and there was reasonable agreement between the raw CRS model ^{210}Pb dates and the ^{137}Cs dates where they could be discerned. In this study, we analysed cores primarily for the reconstruction of atmospheric deposition of contaminants in the Athabasca Bituminous Sands region since commercial development in AD 1967. The time frame of importance for these studies, focused on the post-bomb interval, is well constrained within these cores and the age differences between the methods are relatively small.

Offsets between ^{14}C and ^{210}Pb are more common for the pre-bomb interval through the 20th century where both methods have increased uncertainties, but ^{14}C dates helped highlight large hiatuses from reduced peat accumulation or lost organic material that were not clearly shown in the ^{210}Pb profiles. Discrepancies between the raw ^{210}Pb dates and the chronostratigraphic dates were largely resolved by applying the CRS model in a piecewise way using the methods outlined in Appleby (2001).

Pre-bomb ^{210}Pb dates are consistently younger than ^{14}C dates from the same levels. This is unlike some previously reported discrepancies between ^{210}Pb and ^{14}C dates from European peats (e.g. Fiałkiewicz-Kozieł et al., 2015; Goodsite et al., 2001; Van der Plicht et al., 2013), and instead the trend is similar to that reported from Sweden (Oldfield et al., 1997), Poland (Piotrowska et al., 2010), and Saskatchewan (Bauer et al., 2009). Uncertainty in raw ^{210}Pb dates calculated using either of the standard simple models are less securely known as the records extend beyond the ^{137}Cs peak to ~100 years. By the early 20th century ^{210}Pb concentrations have decayed to just 4% of their original value. Discrepancies in the older parts of the records here where there is recorded ^{210}Pb activity below its excepted depth of equilibrium are most probably due to some downwards migration of ^{210}Pb within the sequence. Possible causes include chemical and physical diffusion, and may relate to the development of permafrost and movement of water within the peatland (see *section 5.4* for full discussion).

Cryptotephra primary air-fall peaks and overlapping ^{14}C dates provide additional data for the age models by highlighting periods of complexity (e.g. permafrost, hiatuses). This represents a novel use of historic cryptotephra — i.e. having a reliable early 20th century chronostratigraphic date to identify and correct errors in the ^{210}Pb dates for that part of the record. This tephra is particularly well timed for such a comparison as it occurs just after the plateau in the radiocarbon calibration curve that causes increased errors in ^{14}C dates from ~AD 1700-1900 and over just 4 half-lives of ^{210}Pb before the present day, when the signal uncertainty is increased. Furthermore, interruptions to peat accumulation are reported here at several sites in Alberta at this time; these events can be constrained more thoroughly when associated with tephra air-fall peaks.

4.4.4. Chronological signal preservation and limits to age-depth model resolution

The measured signal for each chronological technique has different physical properties and therefore differing potential for offset from the true age of the record. For example, our results show that post-depositional migration had a much greater impact on the ^{137}Cs records than ^{210}Pb or cryptotephra shards. While this is expected given previous studies on the mobility of ^{137}Cs within ombrotrophic bogs (e.g. Appleby et al., 1997; Schell et al., 1989; Schleich et al., 2000; Zaccone et al., 2007) variation in chronological signal stability and preservation for the methods used (^{14}C, ^{210}Pb, ^{137}Cs, ^{241}Am, cryptotephra) is discussed here. A variety of processes affecting signal variation and the physical characteristics of the peat substrate must be considered as well as the chronological signal. Together, these factors relate directly to the realistic limit of the accuracy of age-depth models and the temporal resolution of proxy records from peat archives. This is assessed here using four key questions – What is the measured signal? How is this signal fixed in peat deposits? How can this signal change or be mobilised? And what external characteristics are important for accurate signal preservation?

There is a large body of literature addressing each aspect considered here and this is not an exhaustive review — we summarise central themes and focus on the most relevant points for the data presented here. Analytical uncertainty associated with the processing and measurement of sample signals are not discussed here as they are assumed to have been accounted for in the error propagation for individual dates, the initial evaluation and inter-comparison of the datasets, and the statistical age-depth modelling process. We also do not directly address whether there is an offset between the age-depth relationship for the peat and the age-depth relationship for the associated environmental proxies. Given the observable differences in factors affecting preservation this may occur, although to what degree needs further investigation.

For signal source, ^{14}C values result from the fixing of atmospheric CO_2 during photosynthesis while the other methods rely on atmospheric fallout and retention of inorganic particles. C-14 signals are set when the living material dies as the organism is no longer in equilibrium with the atmosphere. Anomalous results can result from the sample having a misleading signal due to uptake of old or modern carbon sources - ^{14}C

values can be dampened by uptake of old-carbon from older plant material within the sequence (e.g. Goslar et al., 2005; Kilian et al., 1995) or industrial pollution (e.g. Chambers et al., 1979; Charman and Garnett, 2005). While mosses do not have roots, and absorb water and nutrients mainly through their leaves instead of the substrate, it is possible for material from other plants and organisms in the peatland to be affected by these issues. Mosses are most likely affected by material being preserved at a different stratigraphic position from the contemporary surface due to mechanical processes (e.g. reburial or re-deposition of organic material, penetration of living rootlets in to older layers), or the assimilation of material from multiple years in one analysed sample (Garnett and Stevenson, 2004; Piotrowska et al., 2010). As ^{14}C dates are independent of each other, it is possible that changes in peat accumulation may not be fully constrained by the number of dates produced if they occurred between dated intervals, or within only a few cm of accumulation.

For the inorganic particles, a stratigraphic signal is preserved by the chemical or physical retention of the particles by the peat matrix after direct air-fall on to the bog surface. Variations in the relative concentration of the signal imply changes in the surface retention over time, assumed to relate to changing atmospheric concentrations and peat accumulation rates. However, there can be variations in the initial infiltration depth of the particles at the surface (e.g. Dörr, 1995; Olid et al., 2016), the effective preservation rate of the atmospheric signal (e.g. particle interception, the physical entrapment of particles by the peat matrix, location specific factors), and surficial reworking before the signal is fixed (e.g. microtopography, snow cover). Once associated with the peat surface, signal retention can be linked broadly to chemical (e.g. adsorption and complexation of particles and ions to peat surfaces, affected by redox potential, pH and organic acids in pore waters), biological (e.g. root uptake, plant growth), and hydrological controls (e.g. infiltration with precipitation, water table change, permafrost, downwashing, evapotranspiration).

The majority of cryptotephra shards have been shown to remain at the surface where they were deposited. There is evidence for some migration laterally within a peatland, and vertically in a peat sequence, but this does not tend to obscure the primary depositional horizon (Payne et al., 2005; Payne and Gehrels, 2010; Watson et al., 2015). Vertical

displacement is most likely to occur soon after deposition unless it is caused by external disturbances (e.g. fires; Payne and Gehrels, 2010). While there is no discussion of the mechanism by which shards are fixed to peat deposits in the literature, it is assumed this is a physical rather than chemical process. Movement within the peat stratigraphy can be observed as tails above or below a primary shard concentration peak or mixed geochemical signals where different populations are combined, while lateral movement results in variable peak concentrations between cores. These effects, however, can both also be caused by secondary deposition if tephra shards are reworked on the landscape. This is unlikely to be significant within an ombrotrophic peatland, although deforestation and increased wind erosion in the surrounding area could be a significant external influence.

In mineral soils, the relative mobility of a metal ion is a function of both the physical and chemical characteristics of the metals themselves (mainly ionic radius and electrical charge), as well as soil features, including pH and redox potential, and abundance of clay minerals, oxyhydroxides, and organic matter content (Degryse et al., 2009). Lead ions, for example, form stable complexes with organic matter, oxyhydroxides, and clay minerals which act in concert to reduce the mobility of Pb^{2+} (Ferraz and Lourençlo, 2000; Strawn and Sparks, 2000; Trivedi et al., 2003; Syrovetnik et al., 2007). However, while free ions in solution are typically the most reactive species, ^{210}Pb and other forms of atmospheric Pb are not predominantly in ionic form and other mechanisms are required to understand metal retention at the air-bog interface, starting with mosses (Shotyk et al., 2015). Variations in pH can profoundly affect Pb adsorption (Grybos et al., 2007) and it has been suggested that ^{210}Pb may undergo some detachment from its host aerosol in response to the low pH of bog surface water (approximately pH 4) or acidic rainwater (Shotyk et al., 2015).

Several studies have examined the potential mobility of stable and radioactive Pb isotopes in peat sequences in recent decades after reported findings of profiles or flux values that do not correlate with independent markers, or differences between features such as hummocks and hollows within one peatland (Damman, 1978; Oldfield et al., 1979; Urban et al., 1990; Lamborg et al., 2002; Hansson et al., 2014). For some peat profiles in Alberta it has been reported that ^{210}Pb concentrations did not decrease

exponentially with depth or approach a low constant value (Turetsky et al., 2000; Wieder et al., 2016) and ^{210}Pb dating is therefore not possible due to insufficient signal preservation. Multiple studies internationally, however, have produced measured profiles and comparisons with established pollen-stratigraphies, pollutant histories, independent chronological techniques, herbarium samples and records from other sites, leading to the conclusion that there was no measurable post-depositional migration (Jones and Hao, 1993; Shotyk, 1996; Appleby et al., 1997; Vile et al., 1999; Weiss et al., 1999; de Vleeschouwer et al., 2009; Novák et al., 2011; Pratte et al., 2013; Shotyk et al., 2016b).

For the other radioisotopes analysed here ^{241}Am is considered to be relatively stable and in good agreement with other chronometers (Oldfield et al., 1995; Smith et al., 1997; Testa et al., 1999; Schleich et al., 2000; Gallagher et al., 2001; Łokas et al., 2013). Cs-137 records are more variable. Some studies show expected peaks and good agreement with established chronometers, but the isotope can be highly mobile in acidic bog-water or decomposing organic material, although a small percentage of mineral matter may improve its retention (Schell et al., 1989; MacKenzie et al., 1997; Sokolik et al., 2002; Zaccone et al., 2007; Lusa et al., 2015). Even with some degree of post-depositional migration, these fallout radionuclides can still be used to evaluate other chronometers if there is a peak in the profile corresponding to the zenith of atmospheric fallout. Multiple peaks or a blurred signal, however, are not easy to utilise.

The inorganic particles used here differ in size by orders of magnitude (Figure 8a) – ^{210}Pb, ^{137}Cs, and ^{241}Am are attached to sub-micron aerosols (~0.5 μm in diameter) while cryptotephra shards are typically 10-100 μm. These differences will affect particle interception by the bog surface (differential deposition) as well as the retention of these two types of particles (diagenetic modification). Locally important processes of redistribution for any particles within a peatland include (Figure 8b): i) variable microtopography allowing particles to be blown or washed from exposed areas to hollows ; ii) direct airfall on to snow, with redistribution by surface winds, and secondary deposition from the temporary surface position after melt (e.g. Bergman et al., 2004); iii) disturbance events (e.g. fires, human impacts) mobilising or removing particles; iv) vegetation interception, roots facilitating downward migration, or plant growth causing

upwards or lateral migration of attached particles; and v) changes in the water table and percolation/downwash causing vertical movement, including complications from vi) permafrost formation or vii) permafrost thaw.

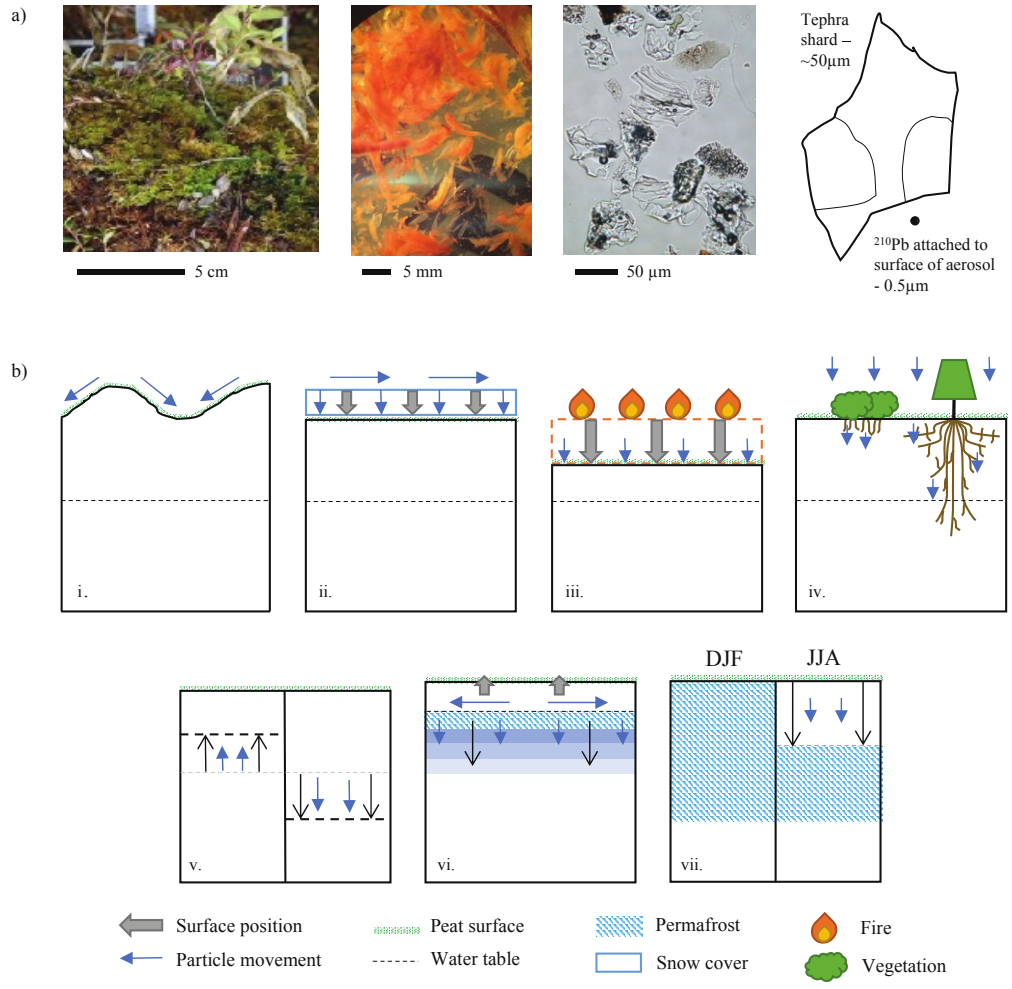

Figure 4.8: a) Relative size comparison of the peat macrofossil material, cryptotephra shards, and aerosols associated with ^{210}Pb and radioisotopes considered here.

b) Diagrams showing mechanisms for particle and surface movement in peatlands:

i. Variable microtopography; ii. Snow cover interception; iii. Local surface fire with removal of material; iv. Vegetation interception, root penetration; v. Water table movement; vi. Permafrost formation with raised surface, frozen substrate, and exclusion of aqueous ions; vii. Seasonal thaw of the active layer.

These processes can be considered for both the chronometer particles, and any organic matter or complexes they are bound to — the host material can also be redistributed mechanically by erosion and transport processes (e.g. mixing, bioturbation, infiltration, and decomposition) once the chronological signal has been retained. For example, ^{210}Pb demonstrates limited root absorption and uptake by plants, but has a strong affinity with the surface of soil particles and reports have shown a strong fixing to transported soil and sediment (van Hoof and Andren, 1989; He and Walling, 1996; Martínez and McBride, 1999; Novák et al., 2011). Peat itself is a highly complex porous substrate and particle movement within a peat sequence will relate to characteristics of the peat itself, including but not limited to: porosity, tortuosity, and hydraulic conductivity, related in turn to the bulk density and degree of decomposition, humification, and compaction. It is expected that these properties change over time with environmental and ecological variation, and 'anomalous' records may therefore reflect changes in processes unrelated to mobility of the signal particles. The presence of intact or degrading permafrost has been shown to affect trends in carbon accumulation and the nutrient status, organic matter accumulation, and chemistry of near surface peat (Turetsky et al., 2000; Robinson et al., 2003; Treat et al., 2016) which will also likely affect both particle retention and the ^{14}C signal.

At the sites shown here, the processes shown in Figure 8b may affect the peat deposits. However, the piecewise multi-chronometer approach is most appropriate to use when they are not occurring consistently and their influence on peat accumulation and/or signal preservation is variable or unknown. Here, local surface fires and hydrological changes in response to climatic variability, including depth of the water table and development/thaw of permafrost, are argued to be the most important processes affecting the peat deposits and their retained chronological signal. Leaching or downwash is possible with the movement and flow of water (Hansson et al., 2015). In the catotelm, the metabolism of organisms results in anaerobic conditions and many elements form organometallic complexes with organic matter. However, if the water table is lowered and oxidation takes place (through percolating surface waters or exposure to air) these complexes are disintegrated, and the previously fixed elements can be transported out of the system (Franzén, 2006). Work using pollen and spores (Clymo and Mackay, 1987) has also demonstrated their potential mobility, although for cryptotephra the higher density and angular morphology of shards means the process would likely be less effective for glass (Payne and Gehrels, 2010).

The study sites are located in areas with sporadic permafrost identified between 150-700 years BP (Zoltai, 1995) and evidence for permafrost formation and thaw are seen in macrofossil records at ANZ, McM, and UTK. There are no extensive studies of the mobility of similar-sized particles within permafrost peatlands although there is discussion of deposition and particle retention in Arctic areas (e.g. Bergman et al., 2004; Łokas et al., 2013). While it might be expected that post-depositional mobility in peats is diminished under cold environmental conditions due to the reduced decomposition of organic matter, and limited bioturbation, we argue here that the changes associated with periods of permafrost development and thaw can affect signal preservation negatively. Sites within the zone of continuous permafrost in western Canada have well-preserved tephrostratigraphies (e.g. Davies and Froese, 2015), but it has not been confirmed if the same is true for sites with either discontinuous syngenetic permafrost, formed with peat accumulation, or ephemeral epigenetic permafrost, formed after peat has been deposited (Zoltai, 1993).

The formation of either type of permafrost has implications for particle mobility. In the catotelm, bogs may typically be stagnant and water saturated but the base of the active layer provides a frozen substrate that can act as a surface for potential lateral movement and runoff. Additionally, the process of freezing will concentrate ions in aqueous solution by excluding them from the ice, and as syngenetic permafrost commonly freezes more rapidly from the top down, this process will potentially relocate any metal ions and low molecular weight humic substances as dissolved organic matter to deeper layers in the peat profile.

The six sites studied here show a range of environmental histories with varying impacts on their chronological records. We see this clearly with disturbance events — for example, the loss of organic material from burning by local fires at ANZ and McM, which have left hiatuses in the records, while other fire events at many of the sites have no such loss. Permafrost development and thaw, and percolation of chronometer particles (or particles hosting them) likely affected records at several sites, but UTK appears unaffected. All of the chronometers applied to the peat records presented here have identified complexities in their preservation, but this does not render them unusable — using multiple chronometers and having detailed environmental histories allows identification and incorporation of these variables on a site by site basis to provide robust chronological models.

4.5 Conclusions

This study compared multiple chronometers for the modern (post AD 1800) period at six peatlands in central and northern Alberta to evaluate variability in both the dating methods and individual site records. The resulting datasets are combined in robust, high-resolution Bayesian age models to allow accurate and precise chronologies and thorough subsequent interpretations of associated proxy data (e.g. trace metals, organic contaminants). While subtle differences in the chronometers occurred at five of the six sites, the use of multiple chronometers and supporting environmental histories allowed an informed assessment of the data that resulted in well constrained models.

These models varied in their complexity, but the largest differences in chronometers were in the pre-bomb period, coincident with the development of permafrost, drying of the peat surface and local fires. Hiatuses and significant changes in accumulation rates are common in these records, and may not be detected using only one dating technique. ^{210}Pb commonly underestimates the age of sediments in this area between AD 1875-1950, most likely due to changes in peat accumulation rates, particularly where permafrost has developed. Cryptotephra isochrons have the potential to help identify chronometer offsets where they occur, and here also helped narrow the broad error ranges associated with calibrated radiocarbon dates at and before the turn of the 20th century. New reports of glass from Novarupta-Katmai 1912, Mt. St. Helens ash bed Z and Mt. Churchill also demonstrate the potential for new additions to Alberta's regional tephrostratigraphy.

At most sites there is good agreement between dating methods for the post-bomb interval, but chronological signals from the decades to centuries before this are more challenging to reconcile. There is no recommended 'one size fits all' approach for constructing these age-depth models and, as stated by previous studies, specific local environmental histories can significantly impact records at the site scale. We argue here that for sites without 'uniform' peat accumulation, where there is significant variability over time in the processes affecting both peat accumulation rates and chronological signal retention, a piecewise approach combining multiple chronological techniques, environmental data and Bayesian modelling will produce the most reliable results.

4.6 References

Alaska Volcano Observatory, 2014. Alaska Volcano Observatory Online Library [WWW Document]. URL www.avo.alaska.edu/downloads/. (accessed 6.30.17).

Ali, A.A., Ghaleb, B., Garneau, M., Asnong, H., Loisel, J., 2008. Recent peat accumulation rates in minerotrophic peatlands of the Bay James region, Eastern Canada, inferred by 210Pb and 137Cs radiometric techniques. Appl. Radiat. Isot. 66, 1350–1358. doi:10.1016/j.apradiso.2008.02.091

Appleby, P.G., 2001. Chronostratigraphic Techniques in Recent Sediments, in: Last, W.M., Smol, J.P. (Eds.), Tracking Environmental Change Using Lake Sediments. Kluwer Academic Publishers, Dordrecht, pp. 171–203. doi:10.1007/0-306-47669-X_9

Appleby, P.G., Nolan, P.J., Oldfield, F., Richardson, N., Higgitt, S.R., 1988. 210Pb dating of lake sediments and ombrotrophic peats by gamma essay. Sci. Total Environ. 69, 157–177. doi:10.1016/0048-9697(88)90341-5

Appleby, P.G., Oldfield, F., 1983. The assessment of 210Pb data from sites with varying sediment accumulation rates. Hydrobiologia 103, 29–35. doi:10.1007/BF00028424

Appleby, P.G., Oldfield, F., 1978. The calculation of lead-210 dates assuming a constant rate of supply of unsupported 210Pb to the sediment. Catena 5, 1–8. doi:10.1016/S0341-8162(78)80002-2

Appleby, P.G., Shotyk, W., Fankhauser, A., 1997. Lead-210 age dating of three peat cores in the Jura Mountains, Switzerland. Water. Air. Soil Pollut. 100, 223–231. doi:10.1023/A:1018380922280

Baird, A.J., Belyea, L.R., Morris, P.J., 2009. Upscaling of peatland-atmosphere fluxes of methane: Small-scale heterogeneity in process rates and the pitfalls of "bucket-and-slab" models, in: Eichelberger, J.C., Gordeev, E., Izbekov, P., Kasahara, M., Lees, J. (Eds.), Carbon Cycling in Northern Peatlands. American Geophysical Union, Washington DC, pp. 37–53. doi:10.1029/2008GM000826

Bao, K.S., Shen, J., Zhang, Y., Wang, J., Wang, G.P., 2014. A 200-year record of polycyclic aromatic hydrocarbons contamination in an ombrotrophic peatland in Great Hinggan Mountain, northeast China. J. Mt. Sci. 11, 1085–1096. doi:10.1007/s11629-014-3167-1

Barber, K.E., 1993. Peatlands as scientific archives of past biodiversity. Biodivers. Conserv. 2, 474–489. doi:10.1007/BF00056743

Barber, K.E., Charman, D.J., 2014. Holocene palaeoclimate records from peatlands, in: Global Change in the Holocene. Routledge, pp. 210–226.

Barber, K.E., Dumayne-Peaty, L., Hughes, P.D.M., Mauquoy, D., Scaife, R., 1998. Replicability and variability of the recent macrofossil and proxy-climate record from raised bogs: Field stratigraphy and macrofossil data from Bolton Fell Moss and Walton Moss, Cumbria,

England. J. Quat. Sci. 13, 515–528. doi:10.1002/(SICI)1099-1417(1998110)13:6<515::AID-JQS393>3.0.CO;2-S

Bauer, I.E., Bhatti, J.S., Swanston, C., Wieder, R.K., Preston, C.M., 2009. Organic matter accumulation and community change at the peatland-upland interface: Inferences from 14C and 210Pb dated profiles. Ecosystems 12, 636–653. doi:10.1007/s10021-009-9248-2

Beierle, B., Bond, J., 2002. Density-induced settling of tephra through organic lake sediments. J. Paleolimnol. 28, 433–440. doi:10.1023/A:1021675501346

Beilman, D.W., Vitt, D.H., Halsey, L.A., 2001. Localized Permafrost Peatlands in Western Canada: Definition, Distributions, and Degradation. Arctic, Antarct. Alp. Res. 33, 70–77. doi:10.2307/1552279

Belyea, L.R., Clymo, R.S., 2001. Feedback control of the rate of peat formation. Proc. R. Soc. B Biol. Sci. 268, 1315–1321. doi:10.1098/rspb.2001.1665

Belyea, L.R., Warner, B.G., 1994. Dating of the near-surface layer of a peatland in northwestern Ontario, Canada. Boreas 23, 259–269. doi:10.1111/j.1502-3885.1994.tb00948.x

Bergman, J., Wastegård, S., Hammarlund, D., Wohlfarth, B., Roberts, S.J., 2004. Holocene tephra horizons at Klocka Bog, west-central Sweden: Aspects of reproducibility in subarctic peat deposits. J. Quat. Sci. 19, 241–249. doi:10.1002/jqs.833

Berset, J.D., Kuehne, P., Shotyk, W., 2001. Concentrations and distribution of some polychlorinated biphenyls (PCBs) and polycyclic aromatic hydrocarbons (PAHs) in an ombrotrophic peat bog profile of Switzerland. Sci. Total Environ. 267, 67–85. doi:10.1016/S0048-9697(00)00763-4

Blaauw, M., Christen, J.A., 2005. Radiocarbon peat chronologies and environmental change. J. R. Stat. Soc. Ser. C Appl. Stat. 54, 805–816. doi:10.1111/j.1467-9876.2005.00516.x

Blaauw, M., Heuvelink, G.B.M., Mauquoy, D., Van Der Plicht, J., Van Geel, B., 2003. A numerical approach to 14C wiggle-match dating of organic deposits: Best fits and confidence intervals. Quat. Sci. Rev. 22, 1485–1500. doi:10.1016/S0277-3791(03)00086-6

Blaauw, M., van Geel, B., Mauquoy, D., van der Plicht, J., 2004. Carbon-14 wiggle-match dating of peat deposits: Advantages and limitations. J. Quat. Sci. 19, 177–181. doi:10.1002/jqs.810

Blackford, J.J., 2000. Palaeoclimatic records from peat bogs. Trends Ecol. Evol. 15, 193–198. doi:10.1016/S0169-5347(00)01826-7

Blockley, S.P.E., Pyne-O'Donnell, S.D.F., Lowe, J.J., Matthews, I.P., Stone, A., Pollard, A.M., Turney, C.S.M., Molyneux, E.G., 2005. A new and less destructive laboratory procedure for the physical separation of distal glass tephra shards from sediments. Quat. Sci. Rev. 24, 1952–1960. doi:10.1016/j.quascirev.2004.12.008

Booth, R.K., Jackson, S.T., Notaro, M., 2010. Using peatland archives to test paleoclimate hypotheses. PAGES news 18, 1–5.

Bracewell, J.M., Hepburn, A., Thomson, C., 1993. Levels and distribution of polychlorinated biphenyls on the Scottish land mass. Chemosphere 27, 1657–1667. doi:10.1016/0045-6535(93)90147-W

Brock, F., Lee, S., Housley, R.A., Bronk Ramsey, C., 2011. Variation in the radiocarbon age of different fractions of peat: A case study from Ahrenshöft, northern Germany. Quat. Geochronol. 6, 550–555. doi:10.1016/j.quageo.2011.08.003

Bronk Ramsey, C., 2013. Recent and Planned Developments of the Program OxCal. Radiocarbon 55, 720–730. doi:10.2458/azu_js_rc.55.16215

Bronk Ramsey, C., 2009a. Bayesian Analysis of Radiocarbon Dates. Radiocarbon 51, 337–360. doi:10.1017/S0033822200033865

Bronk Ramsey, C., 2009b. Dealing with Outliers and Offsets in Radiocarbon Dating. Radiocarbon 51, 1023–1045. doi:10.1017/S0033822200034093

Bronk Ramsey, C., 2008. Deposition models for chronological records. Quat. Sci. Rev. 27, 42–60. doi:10.1016/j.quascirev.2007.01.019

Campbell, I.D., Campbell, C., Yu, Z., Vitt, D.H., Apps, M.J., 2000. Millennial-Scale Rhythms in Peatlands in the Western Interior of Canada and in the Global Carbon Cycle. Quat. Res. 54, 155–158. doi:10.1006/qres.2000.2134

Certini, G., 2005. Effects of fire on properties of forest soils: A review. Oecologia 143, 1–10. doi:10.1007/s00442-004-1788-8

Chambers, F.M., Dresser, P.Q., Smith, A.G., 1979. Radiocarbon dating evidence on the impact of atmospheric pollution on upland peats. Nature 282, 829–831. doi:10.1038/282829a0

Charman, D.J., Barber, K.E., Blaauw, M., Langdon, P.G., Mauquoy, D., Daley, T.J., Hughes, P.D.M., Karofeld, E., 2009. Climate drivers for peatland palaeoclimate records. Quat. Sci. Rev. 28, 1811–1819. doi:10.1016/j.quascirev.2009.05.013

Charman, D.J., Caseldine, C., Baker, A., Gearey, B., Hatton, J., Proctor, C., 2001. Paleohydrological Records from Peat Profiles and Speleothems in Sutherland, Northwest Scotland. Quat. Res. 55, 223–234. doi:10.1006/qres.2000.2190

Charman, D.J., Garnett, M.H., 2005. Chronologies for recent peat deposits using wiggle-matched radiocarbon ages: Problems with old carbon contamination. Radiocarbon 47, 135–145.

Christen, J.A., Clymo, R.S., Litton, C.D., 1995. A Bayesian Approach to the Use of 14C Dates in the Estimation of the Age of Peat. Radiocarbon 37, 431–441. doi:10.1017/S0033822200030915

Clague, J.J., Evans, S.G., Rampton, V.N., Woodsworth, G.J., 1995. Improved age estimates for the White River and Bridge River tephras, western Canada. Can. J. Earth Sci. 32, 1172–1179. doi:10.1139/e95-096

Clymo, R.S., Mackay, D., 1987. Upwash and Downwash of Pollen and Spores in the Unsaturated Surface Layer of Sphagnum Dominated Peat. New Phytol. 105, 175–183. doi:10.1111/j.1469-8137.1987.tb00120.x

Clymo, R.S., Oldfield, F., Appleby, P.G., Pearson, G.W., Ratnesar, P., Richardson, N., 1990. The Record of Atmospheric Deposition on a Rainwater-Dependent Peatland. Philos. Trans. R. Soc. B Biol. Sci. 327, 331–338. doi:10.1098/rstb.1990.0070

Coulter, S.E., Pilcher, J.R., Plunkett, G., Baillie, M., Hall, V.A., Steffensen, J.P., Vinther, B.M., Clausen, H.B., Johnsen, S.J., 2012. Holocene tephras highlight complexity of volcanic signals in Greenland ice cores. J. Geophys. Res. Atmos. 117, 1–11. doi:10.1029/2012JD017698

Damman, A.W.H., 1978. Distribution and Movement of Elements in Ombrotrophic Peat Bogs. Oikos 30, 480. doi:10.2307/3543344

Davies, L.J., Froese, D.G., 2015. Developing a cryptotephra framework for North America: A baseline chronostratigraphy for the Holocene from northwestern sources., in: XIX INQUA Congress. Nagoya, Japan.

Davies, L.J., Jensen, B.J.L., Froese, D.G., Wallace, K.L., 2016. Late Pleistocene and Holocene tephrostratigraphy of interior Alaska and Yukon: Key beds and chronologies over the past 30,000 years. Quat. Sci. Rev. 146, 28–53. doi:10.1016/j.quascirev.2016.05.026

Davies, S.M., Elmquist, M., Bergman, J., Wohlfarth, B., Hammarlund, D., 2007. Cryptotephra sedimentation processes within two lacustrine sequences from west central Sweden. The Holocene 17, 319–330. doi:10.1177/0959683607076443

de Vleeschouwer, F., Fagel, N., Cheburkin, A.K., Pazdur, A., Sikorski, J., Mattielli, N., Renson, V., Fiałkiewicz-Kozieł, B., Piotrowska, N., Le Roux, G., 2009. Anthropogenic impacts in North Poland over the last 1300 years - A record of Pb, Zn, Cu, Ni and S in an ombrotrophic peat bog. Sci. Total Environ. 407, 5674–5684. doi:10.1016/j.scitotenv.2009.07.020

Degryse, F., Smolders, E., Parker, D.R., 2009. Partitioning of metals (Cd, Co, Cu, Ni, Pb, Zn) in soils: concepts, methodologies, prediction and applications - a review. Eur. J. Soil Sci. 60, 590–612. doi:10.1111/j.1365-2389.2009.01142.x

Devito, K.J., Mendoza, C., Petrone, R.M., Kettridge, N., Waddington, J.M., 2016. Utikuma Region Study Area (URSA) - Part 1: Hydrogeological and ecohydrological studies (HEAD). For. Chron. 92, 57–61. doi:10.5558/tfc2016-017

Devito, K.J., Mendoza, C., Qualizza, C., 2012. Conceptualizing water movement in the Boreal Plains: Implications for watershed reconstruction, Canadian Oil Sands Network for Research and Development. Environmental and Reclamation Research Group.

Donovan, J., Kremser, D., Fournelle, J.H., Goemann, K., 2015. Probe for EPMA: Acquisition, automation and analysis.

Dörr, H., 1995. Application of 210Pb in soils. J. Paleolimnol. 13, 157–168. doi:10.1007/BF00678104

Dreyer, A., Blodau, C., Turunen, J., Radke, M., 2005. The spatial distribution of PAH depositions to peatlands of Eastern Canada. Atmos. Environ. 39, 3725–3733. doi:10.1016/j.atmosenv.2005.03.009

Dugmore, A.J., Larsen, G., Newton, A.J., 1995. Seven tephra isochrones in Scotland. The Holocene 5, 257–266. doi:10.1177/095968369500500301

Dugmore, A.J., Newton, A.J., Edwards, K.J., Larsen, G., Blackford, J.J., Cook, G.T., 1996. Long-distance marker horizons from small-scale eruptions: British tephra deposits from the AD 1510 eruption of Hekla, Iceland. J. Quat. Sci. 11, 511–516. doi:10.1002/(SICI)1099-1417(199611/12)11:6<511::AID-JQS284>3.0.CO;2-C

El-Daoushy, F., Tolonen, K., Rosenberg, R., 1982. 210 Pb and moss-increment dating of two Finnish Sphagnum hummocks. Nature 296, 429–431. doi:10.1038/296429a0

Environment and Climate Change Canada, n.d. Canadian Climate Normals. [WWW Document]. URL http://climate.weather.gc.ca/climate_normals/index_e.html (accessed 6.30.17).

Ferraz, M.C.M.A., Lourençlo, J.C.N., 2000. The influence of organic matter content of contaminated soils on the leaching rate of heavy metals. Environ. Prog. 19, 53–58. doi:10.1002/ep.670190118

Fiałkiewicz-Kozieł, B., Kołaczek, P., Michczyński, A., Piotrowska, N., 2015. The construction of a reliable absolute chronology for the last two millennia in an anthropogenically disturbed peat bog: Limitations and advantages of using a radio-isotopic proxy and age-depth modelling. Quat. Geochronol. 25, 83–95. doi:10.1016/j.quageo.2014.10.003

Fiałkiewicz-Kozieł, B., Smieja-Król, B., Frontasyeva, M., Słowiński, M., Marcisz, K., Lapshina, E., Gilbert, D., Buttler, A., Jassey, V.E.J., Kaliszan, K., Laggoun-Défarge, F., Kołaczek, P., Lamentowicz, M., 2016. Anthropogenic- and natural sources of dust in peatland during the Anthropocene. Sci. Rep. 6, 38731. doi:10.1038/srep38731

Franzén, L.G., 2006. Chapter 11 Mineral matter, major elements, and trace elements in raised bog peat: a case study from southern Sweden, Ireland and Tierra del Fuego, south Argentina. Dev. Earth Surf. Process. 9, 241–269. doi:10.1016/S0928-2025(06)09011-0

Gallagher, D., McGee, E.J., Mitchell, P.I., 2001. A Recent History of 14C, 137Cs, 210Pb, and 241Am Accumulation at Two Irish Peat Bog Sites: an East Versus West Coast Comparison. Radiocarbon 43, 517–525. doi:10.1017/S0033822200041175

Garnett, M.H., Stevenson, A.C., 2004. Testing the Use of Bomb Radiocarbon to Date the Surface Layers of Blanket Peat. Radiocarbon 46, 841–851. doi:10.1017/S0033822200035876

Goodsite, M.E., Rom, W., Heinemeier, J., Lange, T., Ooi, S., Appleby, P.G., Shotyk, W., van der Knaap, W.O., Lohse, C., Hansen, T.S., 2001. High-resolution AMS 14C dating of post-bomb peat archives of atmospheric pollutants. Radiocarbon 43, 495–515. doi:10.1017/S0033822200041163

Goslar, T., Knaap, W.O. Van Der, Hicks, S., Andric, M., Czernik, J., Goslar, E., Rasanen, S., Hyotyla, H., 2005. Radiocarbon dating of modern peat profiles: pre- and post-bomb 14C variations in the construction of age-depth models. Radiocarbon 47, 115–134.

Griggs, A.J., Davies, S.M., Abbott, P.M., Coleman, M., Palmer, A.P., Rasmussen, T.L., Johnston, R., 2015. Visualizing tephra deposits and sedimentary processes in the marine environment: The potential of X-ray microtomography. Geochemistry, Geophys. Geosystems 16, 4329–4343. doi:10.1002/2015GC006073

Grybos, M., Davranche, M., Gruau, G., Petitjean, P., 2007. Is trace metal release in wetland soils controlled by organic matter mobility or Fe-oxyhydroxides reduction? J. Colloid Interface Sci. 314, 490–501. doi:10.1016/j.jcis.2007.04.062

Halsey, L.A., Vitt, D.H., Zoltai, S.C., 1995. Disequilibrium response of permafrost in boreal continental western Canada to climate change. Clim. Change 30, 57–73. doi:10.1007/BF01093225

Hansson, S. V., Kaste, J.M., Olid, C., Bindler, R., 2014. Incorporation of radiometric tracers in peat and implications for estimating accumulation rates. Sci. Total Environ. 493, 170–177. doi:10.1016/j.scitotenv.2014.05.088

Hansson, S. V., Tolu, J., Bindler, R., 2015. Downwash of atmospherically deposited trace metals in peat and the influence of rainfall intensity: An experimental test. Sci. Total Environ. 506–507, 95–101. doi:10.1016/j.scitotenv.2014.10.083

He, Q., Walling, D.E., 1996. Interpreting particle size effects in the adsorption of 137Cs and unsupported 210Pb by mineral soils and sediments. J. Environ. Radioact. 30, 117–137. doi:10.1016/0265-931X(96)89275-7

Holmquist, J.R., Finkelstein, S.A., Garneau, M., Massa, C., Yu, Z., MacDonald, G.M., 2016. A comparison of radiocarbon ages derived from bulk peat and selected plant macrofossils in basal peat cores from circum-arctic peatlands. Quat. Geochronol. 31, 53–61. doi:10.1016/j.quageo.2015.10.003

Hua, Q., Barbetti, M., Rakowski, A.Z., 2013. Atmospheric radiocarbon for the period 1950-2010. Radiocarbon 55, 2059–2072. doi:10.2458/azu_js_rc.v55i2.16177

Ingram, H.A.P., 1978. Soil Layers in Mires: Function and Terminology. J. Soil Sci. 29, 224–227. doi:10.1111/j.1365-2389.1978.tb02053.x

Jensen, B.J.L., Beaudoin, A.B., 2016. Geochemical characterization of tephra deposits at archaeological and palaeoenvironmental sites across south-central Alberta and southwest Saskatchewan, in: Woywitka, R. (Ed.), Back on the Horse: Recent Developments in Archaeological and Palaeontological Research in Alberta. Archaeological Survey of Alberta, Edmonton, Alberta, pp. 154–160.

Jensen, B.J.L., Froese, D.G., Preece, S.J., Westgate, J.A., Stachel, T., 2008. An extensive middle to late Pleistocene tephrochronologic record from east-central Alaska. Quat. Sci. Rev. 27, 411–427. doi:10.1016/j.quascirev.2007.10.010

Jensen, B.J.L., Pyne-O'Donnell, S., Plunkett, G., Froese, D.G., Hughes, P.D.M., Sigl, M., McConnell, J.R., Amesbury, M.J., Blackwell, P.G., van den Bogaard, C., Buck, C.E., Charman, D.J., Clague, J.J., Hall, V.A., Koch, J., Mackay, H., Mallon, G., McColl, L., Pilcher, J.R., 2014. Transatlantic distribution of the Alaskan White River Ash. Geology 42, 875–878. doi:10.1130/G35945.1

Jones, J.M., Hao, J., 1993. Ombrotrophic peat as a medium for historical monitoring of heavy metal pollution. Environ. Geochem. Health 15, 67–74. doi:10.1007/BF02627824

Kilian, M.R., Van der Plicht, J., Van Geel, B., 1995. Dating raised bogs: New aspects of AMS 14C wiggle matching, a reservoir effect and climatic change. Quat. Sci. Rev. 14, 959–966. doi:10.1016/0277-3791(95)00081-X

Kuehn, S.C., Froese, D.G., Carrara, P.E., Foit, F.F., Pearce, N.J.G., Rotheisler, P., 2009. Major- and trace-element characterization, expanded distribution, and a new chronology for the latest Pleistocene Glacier Peak tephras in western North America. Quat. Res. 71, 201–216. doi:10.1016/j.yqres.2008.11.003

Kuehn, S.C., Froese, D.G., Shane, P.A.R., 2011. The INTAV intercomparison of electron-beam microanalysis of glass by tephrochronology laboratories: Results and recommendations. Quat. Int. 246, 19–47. doi:10.1016/j.quaint.2011.08.022

Lamborg, C.H., Fitzgerald, W.F., Damman, A.W.H., Benoit, J.M., Balcom, P.H., Engstrom, D.R., 2002. Modern and historic atmospheric mercury fluxes in both hemispheres: Global and regional mercury cycling implications. Global Biogeochem. Cycles 16, 51-1-51–11. doi:10.1029/2001GB001847

Le Roux, G., Aubert, D., Stille, P., Krachler, M., Kober, B., Cheburkin, A., Bonani, G., Shotyk, W., 2005. Recent atmospheric Pb deposition at a rural site in southern Germany assessed using a peat core and snowpack, and comparison with other archives. Atmos. Environ. 39, 6790–6801. doi:10.1016/j.atmosenv.2005.07.026

Le Roux, G., Fagel, N., de Vleeschouwer, F., Krachler, M., Debaille, V., Stille, P., Mattielli, N., van der Knaap, W.O., van Leeuwen, J.F.N., Shotyk, W., 2012. Volcano- and climate-driven changes in atmospheric dust sources and fluxes since the late glacial in Central Europe. Geology 40, 335–338. doi:10.1130/G32586.1

Le Roux, G., Marshall, W.A., 2011. Constructing recent peat accumulation chronologies using atmospheric fall-out radionuclides. Mires Peat 7, 1–14.

Litton, C.D., Buck, C.E., 1995. The Bayesian Approach To the Interpretation of Archaeological Data. Archaeometry 37, 1–24. doi:10.1111/j.1475-4754.1995.tb00723.x

Łokas, E., Mietelski, J.W., Ketterer, M.E., Kleszcz, K., Wachniew, P., Michalska, S., Miecznik, M., 2013. Sources and vertical distribution of 137Cs, 238Pu, 239+240Pu and 241Am in peat profiles from southwest Spitsbergen. Appl. Geochemistry 28, 100–108. doi:10.1016/j.apgeochem.2012.10.027

Lowe, D.J., Blaauw, M., Hogg, A.G., Newnham, R.M., 2013. Ages of 24 widespread tephras erupted since 30,000 years ago in New Zealand, with re-evaluation of the timing and palaeoclimatic implications of the Lateglacial cool episode recorded at Kaipo bog. Quat. Sci. Rev. 74, 170–194. doi:10.1016/j.quascirev.2012.11.022

Lusa, M., Bomberg, M., Virtanen, S., Lempinen, J., Aromaa, H., Knuutinen, J., Lehto, J., 2015. Factors affecting the sorption of cesium in a nutrient-poor boreal bog. J. Environ. Radioact. 147, 22–32. doi:10.1016/j.jenvrad.2015.05.005

Mackay, H., Hughes, P.D.M., Jensen, B.J.L., Langdon, P.G., Pyne-O'Donnell, S.D.F., Plunkett, G., Froese, D.G., Coulter, S.E., Gardner, J.E., 2016. A mid to late Holocene cryptotephra framework from eastern North America. Quat. Sci. Rev. 132, 101–113. doi:10.1016/j.quascirev.2015.11.011

MacKenzie, A.B., Farmer, J.G., Sugden, C.L., 1997. Isotopic evidence of the relative retention and mobility of lead and radiocaesium in Scottish ombrotrophic peats. Sci. Total Environ. 203, 115–127. doi:10.1016/S0048-9697(97)00139-3

Martínez, C.E., McBride, M.B., 1999. Dissolved and labile concentrations of Cd, Cu, Pb, and Zn in aged ferrihydrite - Organic matter systems. Environ. Sci. Technol. 33, 745–750. doi:10.1021/es980576c

Miller, T.P., McGimsey, R.G., Richter, D.H., Riehle, J.R., Nye, G.J., Yount, M.E., Dumoulin, J.A., 1998. Catalog of the historically active volcanoes of Alaska (No. 98–582), Open-File Report. U.S. Dept. of the Interior, U.S. Geological Survey.

Morgan, G.B., London, D., 2005. Effect of current density on the electron microprobe analysis of alkali aluminosilicate glasses. Am. Mineral. 90, 1131–1138. doi:10.2138/am.2005.1769

Mullan-Boudreau, G., Belland, R., Devito, K.J., Noernberg, T., Pelletier, R., Shotyk, W., 2017. Sphagnum Moss as an Indicator of Contemporary Rates of Atmospheric Dust Deposition in

the Athabasca Bituminous Sands Region. Environ. Sci. Technol. 51, 7422–7431. doi:10.1021/acs.est.6b06195

Mullineaux, D., 1996. Pre-1980 tephra-fall deposits erupted from Mount St. Helens, Washington. (No. 1563), Professional Paper.

Nielsen, C.H., Sigurdsson, H., 1981. Quantitative methods for electron microprobe analysis of sodium in natural and synthetic glasses. Am. Mineral. 66, 547–552.

Nilsson, M., Klarqvist, M., Possnert, G., 2001. Variation in 14C age of macrofossils and different fractions of minute peat samples dated by AMS. The Holocene 11, 579–586. doi:10.1191/095968301680223521

Novák, M., Zemanova, L., Voldrichova, P., Stepanova, M., Adamova, M., Pacherova, P., Komarek, A., Krachler, M., Prechova, E., 2011. Experimental evidence for mobility/immobility of metals in peat. Environ. Sci. Technol. 45, 7180–7187. doi:10.1021/es201086v

Oldfield, F., Appleby, P.G., Cambray, R.S., Eakins, J.D., Barber, K.E., Battarbee, R.W., Pearson, G.R., Williams, J.M., 1979. 210 Pb, 137 Cs and 239 Pu Profiles in Ombrotrophic Peat. Oikos 33, 40. doi:10.2307/3544509

Oldfield, F., Richardson, N., Appleby, P.G., 1995. Radiometric dating (210Pb, 137Cs, 241Am) of recent ombrotrophic peat accumulation and evidence for changes in mass balance. The Holocene 5, 141–148. doi:10.1177/095968369500500202

Oldfield, F., Thompson, R., Crooks, P.R.J., Gedye, S.J., Hall, V.A., Harkness, D.D., Housley, R. a., McCormac, F.G., Newton, A.J., Pilcher, J.R., Renberg, I., Richardson, N., 1997. Radiocarbon dating of a recent high latitude peat profile: Stor Åmyran, northern Sweden. The Holocene 7, 283–290. doi:10.1177/095968369700700304

Oldfield, F., Tolonen, K., Thompson, R., 1981. History of particulate atmospheric pollution from magnetic measurements in dated Finnish peat profiles. Ambio 10, 185–188.

Olid, C., Diego, D., Garcia-Orellana, J., Cortizas, A.M., Klaminder, J., 2016. Modeling the downward transport of 210Pb in Peatlands: Initial Penetration-Constant Rate of Supply (IP-CRS) model. Sci. Total Environ. 541, 1222–1231. doi:10.1016/j.scitotenv.2015.09.131

Osborn, G., 1985. Holocene tephrostratigraphy and glacial fluctuations in Waterton Lakes and Glacier national parks, Alberta and Montana. Can. J. Earth Sci. 22, 1093–1101. doi:10.1139/e85-111

Parry, L.E., Charman, D.J., Blake, W.H., 2013. Comparative dating of recent peat deposits using natural and anthropogenic fallout radionuclides and Spheroidal Carbonaceous Particles (SCPs) at a local and landscape scale. Quat. Geochronol. 15, 11–19. doi:10.1016/j.quageo.2013.01.002

Payne, R., Blackford, J., van der Plicht, J., 2008. Using cryptotephras to extend regional tephrochronologies: An example from southeast Alaska and implications for hazard assessment. Quat. Res. 69, 42–55. doi:10.1016/j.yqres.2007.10.007

Payne, R.J., Gehrels, M., 2010. The formation of tephra layers in peatlands: An experimental approach. Catena 81, 12–23. doi:10.1016/j.catena.2009.12.001

Payne, R.J., Kilfeather, A.A., van der Meer, J.J.M., Blackford, J.J., 2005. Experiments on the taphonomy of tephra in peat. Suo 56, 147–156.

Petrone, R.M., Devito, K.J., Mendoza, C., 2016. Utikuma Region Study Area (URSA) - Part 2: Aspen Harvest and Recovery Study. For. Chron. 92, 62–65. doi:10.5558/tfc2016-018

Péwé, T.L., 1975. Quaternary Geology of Alaska. U.S. Geol. Surv. Prof. Pap., Geological Survery Professional Paper 835.

Pilcher, J.R., Hall, V.A., McCormac, F.G., 1995. Dates of Holocene Icelandic volcanic eruptions from tephra layers in Irish peats. The Holocene 5, 103–110. doi:10.1177/095968369500500111

Piotrowska, N., Blaauw, M., Mauquoy, D., Chambers, F.M., 2011. Constructing deposition chronologies for peat deposits using radiocarbon dating. Mires Peat 7, 1–14.

Piotrowska, N., De Vleeschouwer, F., Sikorski, J., Pawlyta, J., Fagel, N., Le Roux, G., Pazdur, A., 2010. Intercomparison of radiocarbon bomb pulse and 210Pb age models. A study in a peat bog core from North Poland. Nucl. Instruments Methods Phys. Res. Sect. B Beam Interact. with Mater. Atoms 268, 1163–1166. doi:10.1016/j.nimb.2009.10.124

Plunkett, G., 2006. Tephra-linked peat humification records from Irish ombrotrophic bogs question nature of solar forcing at 850 cal. yr BC. J. Quat. Sci. 21, 9–16. doi:10.1002/jqs.951

Pratte, S., Mucci, A., Garneau, M., 2013. Historical records of atmospheric metal deposition along the St. Lawrence Valley (eastern Canada) based on peat bog cores. Atmos. Environ. 79, 831–840. doi:10.1016/j.atmosenv.2013.07.063

Pyne-O'Donnell, S.D.F., 2011. The taphonomy of Last Glacial-Interglacial Transition (LGIT) distal volcanic ash in small Scottish lakes. Boreas 40, 131–145. doi:10.1111/j.1502-3885.2010.00154.x

Pyne-O'Donnell, S.D.F., Hughes, P.D.M., Froese, D.G., Jensen, B.J.L., Kuehn, S.C., Mallon, G., Amesbury, M.J., Charman, D.J., Daley, T.J., Loader, N.J., Mauquoy, D., Street-Perrott, F.A., Woodman-Ralph, J., 2012. High-precision ultra-distal Holocene tephrochronology in North America. Quat. Sci. Rev. 52, 6–11. doi:10.1016/j.quascirev.2012.07.024

Rausch, N., Nieminen, T., Ukonmaanaho, L., Le Roux, G., Krachler, M., Cheburkin, A.K., Bonani, G., Shotyk, W., 2005. Comparison of atmospheric deposition of copper, nickel, cobalt, zinc, and cadmium recorded by Finnish peat cores with monitoring data and emission records. Environ. Sci. Technol. 39, 5989–5998. doi:10.1021/es050260m

Reimer, P.J., Bard, E., Bayliss, A., Beck, J.W., Blackwell, P.G., Bronk Ramsey, C., Buck, C.E., Cheng, H., Edwards, R.L., Friedrich, M., Grootes, P.M., Guilderson, T.P., Haflidason, H., Hajdas, I., Hatté, C., Heaton, T.J., Hoffmann, D.L., Hogg, A.G., Hughen, K.A., Kaiser, K.F., Kromer, B., Manning, S.W., Niu, M., Reimer, R.W., Richards, D.A., Scott, E.M., Southon, J.R., Staff, R.A., Turney, C.S.M., van der Plicht, J., 2013. IntCal13 and Marine13 Radiocarbon Age Calibration Curves 0–50,000 Years cal BP. Radiocarbon 55, 1869–1887. doi:10.2458/azu_js_rc.55.16947

Reyes, A. V., Jensen, B.J.L., Zazula, G.D., Ager, T.A., Kuzmina, S., La Farge, C., Froese, D.G., 2010. A late-Middle Pleistocene (Marine Isotope Stage 6) vegetated surface buried by Old Crow tephra at the Palisades, interior Alaska. Quat. Sci. Rev. 29, 801–811. doi:10.1016/j.quascirev.2009.12.003

Robinson, S.D., Turetsky, M.R., Kettles, I.M., Wieder, R.K., 2003. Permafrost and peatland carbon sink capacity with increasing latitude, in: Phillips, M., Springman, S., Arenson, L. (Eds.), Proceedings of the 8th International Conference on Permafrost. Balkema Publishers, Zurich, pp. 965–970.

Roland, T.P., Mackay, H., Hughes, P.D.M., 2015. Tephra analysis in ombrotrophic peatlands: A geochemical comparison of acid digestion and density separation techniques. J. Quat. Sci. 30, 3–8. doi:10.1002/jqs.2754

Roos-Barraclough, F., Martinez-Cortizas, A., Garcia-Rodeja, E., Shotyk, W., 2002. A 14 500 year record of the accumulation of atmospheric mercury in peat: Volcanic signals, anthropogenic influences and a correlation to bromine accumulation. Earth Planet. Sci. Lett. 202, 435–451. doi:10.1016/S0012-821X(02)00805-1

Roos-Barraclough, F., Shotyk, W., 2003. Millennial-scale records of atmospheric mercury deposition obtained from ombrotrophic and minerotrophic peatlands in the Swiss Jura mountains. Environ. Sci. Technol. 37, 235–244. doi:10.1021/es0201496

Sanchez-Cabeza, J.A., Ruiz-Fernández, A.C., 2012. 210Pb sediment radiochronology: An integrated formulation and classification of dating models. Geochim. Cosmochim. Acta 82, 183–200. doi:10.1016/j.gca.2010.12.024

Sanders, G., Jones, K.C., Hamilton-Taylor, J., Dorr, H., 1995. PCB and PAH fluxes to a dated UK peat core. Environ. Pollut. 89, 17–25. doi:10.1016/0269-7491(94)00048-I

Sapkota, A., Cheburkin, A.K., Bonani, G., Shotyk, W., 2007. Six millennia of atmospheric dust deposition in southern South America (Isla Navarino, Chile). The Holocene 17, 561–572. doi:10.1177/0959683607078981

Schell, W.R., Tobin, M.J., Massey, C.D., 1989. Evaluation of trace metal deposition history and potential element mobility in selected cores from peat and wetland ecosystems. Sci. Total Environ. 87–88, 19–42. doi:10.1016/0048-9697(89)90223-4

Schleich, N., Degering, D., Unterricker, S., 2000. Natural and artificial radionuclides in forest and bog soils: Tracers for migration processes and soil development. Radiochim. Acta 88, 803–808. doi:10.1524/ract.2000.88.9-11.803

Schoning, K., Charman, D.J., Wastegård, S., 2005. Reconstructed water tables from two ombrotrophic mires in eastern central Sweden compared with instrumental meteorological data. The Holocene 15, 111–118. doi:10.1191/0959683605hl772rp

Shore, J.S., Bartley, D.D., Harkness, D.D., 1995. Problems encountered with the 14C dating of peat. Quat. Sci. Rev. 14, 373–383. doi:10.1016/0277-3791(95)00031-3

Shotyk, W., 1996. Peat bog archives of atmospheric metal deposition: geochemical evaluation of peat profiles, natural variations in metal concentrations, and metal enrichment factors. Environ. Rev. 4, 149–183. doi:10.1139/a96-010

Shotyk, W., Appleby, P.G., Bicalho, B., Davies, L.J., Froese, D.G., Grant-Weaver, I., Krachler, M., Magnan, G., Mullan-Boudreau, G., Noernberg, T., Pelletier, R., Shannon, B., van Bellen, S., Zaccone, C., 2016a. Peat bogs in northern Alberta, Canada reveal decades of declining atmospheric Pb contamination. Geophys. Res. Lett. 43, 9964–9974. doi:10.1002/2016GL070952

Shotyk, W., Appleby, P.G., Bicalho, B., Davies, L.J., Froese, D.G., Grant-Weaver, I., Magnan, G., Mullan-Boudreau, G., Noernberg, T., Pelletier, R., Shannon, B., van Bellen, S., Zaccone, C., 2017. Peat Bogs Document Decades of Declining Atmospheric Contamination by Trace Metals in the Athabasca Bituminous Sands Region. Environ. Sci. Technol. 51, 6237–6249. doi:10.1021/acs.est.6b04909

Shotyk, W., Cheburkin, A.K., Appleby, P.G., Fankhauser, A., Kramers, J.D., 1997. Lead in three peat bog profiles, Jura Mountains, Switzerland: Enrichment factors, isotopic composition, and chronology of atmospheric deposition. Water. Air. Soil Pollut. 100, 297–310. doi:10.1023/A:1018384711802

Shotyk, W., Kempter, H., Krachler, M., Zaccone, C., 2015. Stable (206Pb, 207Pb, 208Pb) and radioactive (210Pb) lead isotopes in 1year of growth of Sphagnum moss from four ombrotrophic bogs in southern Germany: Geochemical significance and environmental implications. Geochim. Cosmochim. Acta 163, 101–125. doi:10.1016/j.gca.2015.04.026

Shotyk, W., Rausch, N., Outridge, P.M., Krachler, M., 2016b. Isotopic evolution of atmospheric Pb from metallurgical processing in Flin Flon, Manitoba: Retrospective analysis using peat cores from bogs. Environ. Pollut. 218, 338–348. doi:10.1016/j.envpol.2016.07.009

Shotyk, W., Wayne Nesbitt, H., Fyfe, W.S., 1992. Natural and antropogenic enrichments of trace metals in peat profiles. Int. J. Coal Geol. 20, 49–84. doi:10.1016/0166-5162(92)90004-G

Smith, J.T., Appleby, P.G., Hilton, J., Richardson, N., 1997. Inventories and fluxes of 210Pb, 137Cs and 241Am determined from the soils of three small catchments in Cumbria, UK. J. Environ. Radioact. 37, 127–142. doi:10.1016/S0265-931X(97)00003-9

Sokolik, G., Ovsiannikova, S., Kimlenko, I., 2002. Distribution and mobility of 137 Cs, 90 Sr, 239,240 Pu and 241 Am in solid phase-interstitial soil solution system. Radioprotection 37, C1-259-C1-264. doi:10.1051/radiopro/2002048

Spray, J.G., Rae, D.A., 1995. Quantitative electron-microprobe analysis of alkali silicate glasses: a review and user guide. Can. Mineral. 33, 323–332.

Strawn, D.G., Sparks, D.L., 2000. Effects of Soil Organic Matter on the Kinetics and Mechanisms of Pb(II) Sorption and Desorption in Soil. Soil Sci. Soc. Am. J. 64, 144. doi:10.2136/sssaj2000.641144x

Swindles, G.T., De Vleeschouwer, F., Plunkett, G., 2010. Dating peat profiles using tephra: stratigraphy, geochemistry and chronology. Mires Peat 7, 1–9.

Swindles, G.T., Galloway, J.M., Outram, Z., Turner, K., Schofield, J.E., Newton, A.J., Dugmore, A.J., Church, M.J., Watson, E.J., Batt, C., Bond, J., Edwards, K.J., Turner, V., Bashford, D., 2013. Re-deposited cryptotephra layers in Holocene peats linked to anthropogenic activity. The Holocene 23, 1493–1501. doi:10.1177/0959683613489586

Swindles, G.T., Patterson, R.T., Roe, H.M., Galloway, J.M., 2012. Evaluating periodicities in peat-based climate proxy records. Quat. Sci. Rev. 41, 94–103. doi:10.1016/j.quascirev.2012.03.003

Syrovetnik, K., Malmström, M.E., Neretnieks, I., 2007. Accumulation of heavy metals in the Oostriku peat bog, Estonia: Determination of binding processes by means of sequential leaching. Environ. Pollut. 147, 291–300. doi:10.1016/j.envpol.2005.10.048

Testa, C., Jia, G., Degetto, S., Desideri, D., Guerra, F., Meli, M.A., Roselli, C., 1999. Vertical profiles of 239,240Pu and 241Am in two sphagnum mosses of Italian peat. Sci. Total Environ. 232, 27–31. doi:10.1016/S0048-9697(99)00106-0

Toohey, M., Sigl, M., 2017. Volcanic stratospheric sulfur injections and aerosol optical depth from 500 BCE to 1900 CE. Earth Syst. Sci. Data 9, 809–831. doi:10.5194/essd-9-809-2017

Treat, C.C., Jones, M.C., Camill, P., Gallego-Sala, A., Garneau, M., Harden, J.W., Hugelius, G., Klein, E.S., Kokfelt, U., Kuhry, P., Loisel, J., Mathijssen, P.J.H., O'Donnell, J.A., Oksanen, P.O., Ronkainen, T.M., Sannel, A.B.K., Talbot, J., Tarnocai, C., Väliranta, M., 2016. Effects of permafrost aggradation on peat properties as determined from a pan-Arctic synthesis of plant macrofossils. J. Geophys. Res. G Biogeosciences 121, 78–94. doi:10.1002/2015JG003061

Trivedi, P., Dyer, J.A., Sparks, D.L., 2003. Lead sorption onto ferrihydrite. 1. A macroscopic and spectroscopic assessment. Environ. Sci. Technol. 37, 908–914. doi:10.1021/es0257927

Turetsky, M.R., Manning, S.W., Wieder, R.K., 2004. Dating recent peat deposits. Wetlands 24, 324–356. doi:10.1672/0277-5212(2004)024[0324:DRPD]2.0.CO;2

Turetsky, M.R., Wieder, R.K., Vitt, D.H., Evans, R.J., Scott, K.D., 2007. The disappearance of relict permafrost in boreal north America: Effects on peatland carbon storage and fluxes. Glob. Chang. Biol. 13, 1922–1934. doi:10.1111/j.1365-2486.2007.01381.x

Turetsky, M.R., Wieder, R.K., Williams, C.J., Vitt, D.H., 2000. Organic Matter Accumulation, Peat Chemistry, and Permafrost Melting in Peatlands of Boreal Alberta. Ecoscience 7, 379–392. doi:10.1080/11956860.2000.11682608

Tylmann, W., Bonk, A., Goslar, T., Wulf, S., Grosjean, M., 2016. Calibrating 210Pb dating results with varve chronology and independent chronostratigraphic markers: Problems and implications. Quat. Geochronol. 32, 1–10. doi:10.1016/j.quageo.2015.11.004

Urban, N.R., Eisenreich, S.J., Grigal, D.F., Schurr, K.T., 1990. Mobility and diagenesis of Pb and 210Pb in peat. Geochim. Cosmochim. Acta 54, 3329–3346. doi:10.1016/0016-7037(90)90288-V

van der Linden, M., Vickery, E., Charman, D.J., van Geel, B., 2008. Effects of human impact and climate change during the last 350 years recorded in a Swedish raised bog deposit. Palaeogeogr. Palaeoclimatol. Palaeoecol. 262, 1–31. doi:10.1016/j.palaeo.2008.01.018

van der Plicht, J., Yeloff, D., van der Linden, M., van Geel, B., Brain, S., Chambers, F.M., Webb, J., Toms, P., 2013. Dating recent peat accumulation in European ombrotrophic bogs. Radiocarbon 55, 1763–1778. doi:10.2458/azu_js_rc.55.16057

van Geel, B., Mook, W.G., 1989. High-resolution 14C dating of organic deposits using natural atmospheric 14C variations. Radiocarbon 31, 151–155. doi:10.1017/S0033822200044805

van Hoof, P.L., Andren, A.W., 1989. Partitioning and Transport of 210Pb in Lake Michigan. J. Great Lakes Res. 15, 498–509. doi:10.1016/S0380-1330(89)71505-7

Vile, M.A., Wieder, R.K., Novák, M., 1999. Mobility of Pb in Sphagnum-derived peat. Biogeochemistry 45, 35–52. doi:10.1023/A:1006085410886

Vitt, D.H., Halsey, L.A., Zoltai, S.C., 2000. The changing landscape of Canada's western boreal forest: the current dynamics of permafrost. Can. J. For. Res. 30, 283–287. doi:10.1139/x99-214

Vitt, D.H., Halsey, L.A., Zoltai, S.C., 1994. The bog landforms of continental Western Canada in relation to climate and permafrost patterns. Arct. Alp. Res. 26, 1–13. doi:10.2307/1551870

Watson, E.J., Swindles, G.T., Lawson, I.T., Savov, I., 2015. Spatial variability of tephra and carbon accumulation in a Holocene peatland. Quat. Sci. Rev. 124, 248–264. doi:10.1016/j.quascirev.2015.07.025

Watson, E.J., Swindles, G.T., Lawson, I.T., Savov, I.P., 2016. Do peatlands or lakes provide the most comprehensive distal tephra records? Quat. Sci. Rev. 139, 110–128. doi:10.1016/j.quascirev.2016.03.011

Weiss, D., Shotyk, W., Kramers, J.D., Gloor, M., 1999. Sphagnum mosses as archives of recent and past atmospheric lead deposition in Switzerland. Atmos. Environ. 33, 3751–3763. doi:10.1016/S1352-2310(99)00093-X

Westgate, J.A., Smith, D., Nichols, H., 1969. Late Quaternary pyroclastic layers in the Edmonton area, Alberta. (No. 464), Geology Department Contract.

Westgate, J.A., Smith, D., Tomlinson, M., 1970. Late Quaternary tephra layers in southwestern Canada, in: Smith, R.A., Smith, J.W. (Eds.), Early Man and Environments in Northwest North America. Calgary, Alberta, pp. 13–34.

Wieder, R.K., Novák, M., Schell, W.R., Rhodes, T., 1994. Rates of peat accumulation over the past 200 years in five Sphagnum-dominated peatlands in the United States. J. Paleolimnol. 12, 35–47. doi:10.1007/BF00677988

Wieder, R.K., Vile, M.A., Albright, C.M., Scott, K.D., Vitt, D.H., Quinn, J.C., Burke-Scoll, M., 2016. Effects of altered atmospheric nutrient deposition from Alberta oil sands development on Sphagnum fuscum growth and C, N and S accumulation in peat. Biogeochemistry 129, 1–19. doi:10.1007/s10533-016-0216-6

Yamaguchi, D.K., Hoblitt, R.P., 1995. Tree-ring dating of pre-1980 volcanic flowage deposits at Mount St. Helens, Washington. Geol. Soc. Am. Bull. 107, 1077–1093. doi:10.1130/0016-7606(1995)107<1077:TRDOPV>2.3.CO;2

Yang, H., Rose, N.L., Boyle, J.F., Battarbee, R.W., 2001. Storage and distribution of trace metals and spheroidal carbonaceous particles (SCPs) from atmospheric deposition in the catchment peats of Lochnagar, Scotland. Environ. Pollut. 115, 231–238. doi:10.1016/S0269-7491(01)00107-5

Yeloff, D., Bennett, K.D., Blaauw, M., Mauquoy, D., Sillasoo, Ü., van der Plicht, J., van Geel, B., 2006. High precision 14C dating of Holocene peat deposits: A comparison of Bayesian calibration and wiggle-matching approaches. Quat. Geochronol. 1, 222–235. doi:10.1016/j.quageo.2006.08.003

Yu, Z., Vitt, D.H., Campbell, I.D., Apps, M.J., 2003. Understanding Holocene peat accumulation pattern of continental fens in western Canada. Can. J. Bot. 81, 267–282. doi:10.1139/b03-016

Zaccone, C., Cocozza, C., Cheburkin, A.K., Shotyk, W., Miano, T.M., 2008. Distribution of As, Cr, Ni, Rb, Ti and Zr between peat and its humic fraction along an undisturbed ombrotrophic bog profile (NW Switzerland). Appl. Geochemistry 23, 25–33. doi:10.1016/j.apgeochem.2007.09.002

Zaccone, C., Cocozza, C., Cheburkin, A.K., Shotyk, W., Miano, T.M., 2007. Highly organic soils as “witnesses” of anthropogenic Pb, Cu, Zn, and 137Cs inputs during centuries. Water. Air. Soil Pollut. 186, 263–271. doi:10.1007/s11270-007-9482-1

Zaretskaia, N.E., Ponomareva, V. V, Sulerzhitsky, L.D., Zhilin, M.G., 2001. Radiocarbon Studies of Peat Bogs: an Investigation of South Kamchatka Volcanoes and Upper Volga Archeological Sites. Radiocarbon 43, 571–580. doi:10.1017/S0033822200041229

Zhang, Y., Shotyk, W., Zaccone, C., Noernberg, T., Pelletier, R., Bicalho, B., Froese, D.G., Davies, L.J., Martin, J.W., 2016. Airborne Petcoke Dust is a Major Source of Polycyclic Aromatic Hydrocarbons in the Athabasca Oil Sands Region. Environ. Sci. Technol. 50, 1711–1720. doi:10.1021/acs.est.5b05092

Zhao, Y., Hölzer, A., Yu, Z., 2007. Late Holocene Natural and Human-Induced Environmental Change Reconstructed from Peat Records in Eastern Central China. Radiocarbon 49, 789–798. doi:10.1017/S0033822200042661

Zoltai, S.C., 1995. Permafrost Distribution in Peatlands of West-Central Canada during the Holocene Warm Period 6000 Years BP. Geogr. Phys. Quat. 49, 45–54. doi:10.7202/033029ar

Zoltai, S.C., 1993. Cyclic Development of Permafrost in the Peatlands of Northwestern Canada. Arct. Alp. Res. 25, 240–246. doi:10.2307/1551820

Zoltai, S.C., 1989. Late Quaternary volcanic ash in the peatlands of central Alberta. Can. J. Earth Sci. 26, 207–214. doi:10.1139/e89-017

Zoltai, S.C., Tarnocai, C., 1975. Perennially Frozen Peatlands in the Western Arctic and Subarctic of Canada. Can. J. Earth Sci. 12, 28–43. doi:10.1139/e75-004

Zoltai, S.C., Vitt, D.H., 1990. Holocene climatic change and the distribution of peatlands in western interior Canada. Quat. Res. 33, 231–240. doi:10.1016/0033-5894(90)90021-C

CHAPTER 5: CONCLUSIONS

One apparent conclusion from the work presented here is that there is a *lot* of glass in northwestern Canada. More glass than we expected given the distal records in Alaska, and much more than the ultra-distal east coast cryptotephra records allude to. The main goal of this thesis was to test the potential for the development of a cryptotephra framework in northwestern Canada - I believe this has been fully demonstrated. This chapter will synthesise the data reported in previous chapters, address the original aims and objectives of the project, and provide an outlook for future research and uses of these data.

Aim 1: *Address geographical gaps for cryptotephra records in northwestern Canada*

Objectives: Review current knowledge; produce new records

The hypothesis presented was that a paucity of cryptotephra records exist for northern Canada, despite the high potential for records due to being positioned downwind from active volcanoes and the presence of accumulating sedimentary archives (e.g. lakes, peatlands). The first aim - addressing these geographical gaps- has been discussed in two ways.

Firstly, Chapter 2 reviews the existing literature on tephra deposits that are transported distally from their eruptive sources in Alaska and have potential distributions downwind of the topographic barrier imposed by the North American Cordillera. This confirms that there are nineteen well characterized tephra, some of which have already been found as ultra-distal cryptotephra (e.g. Aniakchak CFE II, the eastern lobe of the White River Ash, Novarupta-Katmai 1912), that may be found downwind in northwestern Canada.

Secondly, two new records for western Canada are produced here. Chapter 3 reports a continuous 10,400 cal yr BP record from northcentral Yukon Territory – a baseline chronostratigraphy for tephra transportation from western sources. This is the first of its kind in western Canada and represents a meso-distal location between volcanic sources in Alaska and previous cryptotephra records from Greenland and eastern North America. The cryptotephra preserved are correlated with sources in Alaska, the Aleutian Arc, and the Wrangells, with the exception of two early Holocene layers from Kamchatka (KO) and the Kurile Islands (TR(Zv)). The northern location of this site and the prevailing wind directions result in no identifiable glass from southern sources (e.g. the Cascades).

While this is a detailed, high frequency record of cryptotephra deposition for most of the Holocene, it is also only one site and it raises as many questions as it answers. There are frequent, high concentration tephra-fall events occurring in northwestern Canada, however the overwhelming majority of these are not preserved on the east coast. There is a great distance between these locations, but where are the limits of distribution and preservation between these two end points? Delimiting cryptotephra presence over this spatial scale may shed light on patterns in atmospheric circulation and large-scale changes over time.

For example, there are significant shifts in the glass concentrations preserved at DHP174 around 8,000 to 7,500 cal yr BP and after 4,500 cal yr BP. Early Holocene peaks are 10s to 100s of shards with ultra-distal glass present from the Kurile Islands, Kamchatka, and Fisher. Peaks likely sourced from Redoubt, Augustine, and the KO eruption of Kurile Lake-Iliinsky, have modelled ages between ~8,000 and 7,600 cal yr BP and are the first higher concentration peaks (10,000s). After this, glass concentrations (from non-Mt. Churchill correlated peaks) are relatively low until a rise to 100,000s at 4,600 cal yr BP that continues until the last millennium when concentrations are more similar to the mid-Holocene values (10,000s). The correlated cryptotephra in the early Holocene have sources further along (and beyond) the Aleutian Arc than we see in more recent time periods, although this could be due to a lack of available reference material to enable a correlation, or the ultra-distal signal being overwhelmed and hidden by higher concentration fallout from volcanoes located closer to DHP174.

These shifts in concentration can be explained most easily by a change in either ash production (i.e. frequency of explosive volcanic eruptions) or dispersal (i.e. atmospheric circulation). While large volcanic eruptions have been documented in Alaska, Kamchatka and further afield throughout the Holocene, there is some evidence for patterns in the occurrence of volcanic eruptions over time, particularly related to deglaciation (e.g. Castellano et al., 2004; Huybers and Langmuir, 2009; Watt et al., 2013; Praetorius et al., 2016). There are several large and caldera-forming eruptions that have not been identified at DHP174 and if they are not present (e.g. as unknowns that aren't identified/correlated here) there are a number of factors that could have affected transportation, deposition and the final preserved record. In western Canada specifically, the retreat of the Laurentide ice sheet likely impacted wind patterns and is an important consideration for this region.

The second set of cryptotephra records presented in Chapter 4 show far fewer peaks are preserved in central and northern Alberta than at DHP174. Over the six peatlands, five cores preserve the WRAe and four preserve Novarupta-Katmai 1912. While these records were targeted analyses for the purpose of applied chronological assessment, they show the presence of cryptotephra not previously reported in Alberta, and the potential influence of material from southern sources (e.g. Mt. St. Helens), more mafic eruptions, and currently unknown eruptions. They also show the inherent variability in sites even within 10s to 100s of km from each other and the importance of using multiple cores and, if possible, coring locations, to validate records for a region. This is in line with observations from elsewhere in Alberta (Zoltai, 1989) and in peatlands more broadly (Payne and Gehrels, 2010; Watson et al., 2015).

Aim 2: *Define regionally significant cryptotephra beds that can be used to improve local and regional scale chronologies*

Objectives: Summarise key characteristics – age modelling, major element glass geochemistry, geographical distributions

In order to be most easily utilised by other researchers, the tephra discussed in Chapters 2-4 have major element geochemical data (with single point analyses of both unknowns and reference material included in the appendices) and modelled ages where appropriate. This is particularly important given the number of cryptotephra in the area that are geochemically similar or identical (e.g. multiple eruptions of Mt. Churchill from DHP174).

In Chapter 3, the major element geochemical data produced from DHP174 samples show many peaks have multiple populations, and only those with >~10 points were discussed. It is difficult to fully assess smaller populations or individual analyses, and to interpret if they represent a muted background signal, reworking from peaks nearby, or genuine populations. Either more analyses are required (although realistically this would require a significant additional investment of time and money), or a higher resolution record - DHP174 averages ~25 years per 1 cm. Given the observed eruptive frequency over the past century, the mixed populations are not surprising, although even with the increased accumulation in the upper moss and peat samples (~10 years per cm) mixed signals are still preserved.

In Chapter 4 we also see some mixed geochemical populations within one sample but these are interpreted as the result of changes to peat accumulation and the preserved record. For example,

at ANZ there are multiple samples with mixed geochemical signals that occur when a local fire removed material from the peat surface and concentrated the glass from ~300 years. At McK there are multiple geochemical populations in a glass concentration peak that is significantly higher than seen at any other site for the time period. This sample occurs at a time where the surface mosses are much drier than previously seen, and there was also a different dominant species (*Polytrichum* instead of *Sphagnum*). This is interpreted as a significant decrease in accumulation or stagnation of the peat surface for an extended period of time, hence accumulating multiple eruptions at one depth. Accumulation rates over the six sites are, expectedly, ~5x higher than at DHP174 with average rates of 2 years per cm since AD 1900. The higher accumulation rates are biased towards the surficial, less compact moss and peat samples.

There are two unexpected trends in the geochemical data from DHP174 – the prevalence of dacitic material, and rhyolites with unusually low wt.% K_2O for the Aleutian Arc and Alaska Peninsula. Dacites are not a previously well explored area for cryptotephra and they are not found in the records of distal visible tephra summarised in Chapter 2 or ultra-distal records. However, seven of the thirty-five populations listed as important distal correlatives from DHP174 are dacitic, including three of the four tephra from >8,000 cal yr BP. It is possible some of these samples relate to caldera forming eruptions (e.g. Black Peak, Makushin) but without more complete reference data sets this cannot be confirmed. It seems likely, however, that there are many large dacitic eruptions sourced from the Aleutian Arc and Alaska Peninsula that will continue to be found further distally.

Rhyolites with wt.% K_2O values <2 are not common in current data reported from Aleutian sources and are typically correlated to either Augustine or Kaguyak volcanoes. Nine populations (excluding KO and TR(Zv) that have other distinct major element signals, including wt. TiO_2, Al_2O_3 and FeO) have these values and only one (Augustine C) has an identified correlation. While there are a small number of reports of distal visible tephra from around the Cook Inlet that are suggested Augustine correlatives, it is not generally thought to be active before ~2,000 cal yr BP. However, distal material similar to Augustine is reported here, in northern Alaska, and in Newfoundland – this glass represents at least two and up to five large eruptive events.

Bayesian modelled ages are produced for all pre-historic eruptions with multiple high-quality reported dates in Chapter 2 and using a ^{14}C chronology (using dates reported here for the first

time) for glass concentration peaks in Chapter 3. The modelled ages produced in Chapter 2 are mostly in agreement with previous estimates, although there are some apparent discrepancies between the terrestrial ^{14}C dates and layer counted ice-core chronology ages for Aniakchak CFE II. While a suggested adjustment of 19 years brings the ages into agreement at the edge of 2.S.D, there is an offset of 100 years from the 1.S.D. model age range. As Aniakchak is one of the two most widely dispersed tephra from this region identified to date it is frequently used as an isochron. It has a large number of radiocarbon dates, with several AMS dates from immediately above and below the tephra horizon so it is surprising the Bayesian modelled age would be so different from the ice-core age.

Nine of the correlated tephra at DHP174 have modelled ages that match previous age estimates (within 1.S.D.), but one tephra (KO) has a modelled age which is younger than previous reports but does overlap at 2.S.D. DHP174 samples correlated to known eruptions are a good independent test of the age model and this is particularly important when associating modelled ages to new unknown tephra. It is important, therefore, to consider the modelled range of ages and not just the mean or median value. Average standard deviations for important tephra peaks over the whole DHP174 record are ~285 years with maximum values of 480 years.

Geographical distributions are updated here for the eleven tephra over the Holocene that can be correlated with known eruptions. Aniakchak CFE II, WRAe and Novarupta-Katmai 1912 have been reported as ultra-distal cryptotephra and are confirmed here as cryptotephra in Yukon territory and in Alberta for the latter two. WRAn has a visible distribution falling close to DHP174 and is the highest glass concentration peak of the record. The seven remaining tephra – Redoubt 1989-90, Augustine C, Hayes set H unit F2, Tephra J127, KO, TR(Zv) and the Funk/Fisher ash – have not been previously reported within Canada, and KO and TR(Zv) have not been reported within North America. The remaining unknown tephra appear Aleutian in origin, with an increased number of suggested correlations to Augustine, Redoubt, Hayes and Mt. Churchill than have been reported. As both Mt. Churchill and Hayes volcanoes are the closest geographically to DHP174 it is unsurprising that they have multiple eruptions recorded there, but there are a number of know eruptions missing, for example the remaining set H tephra, which shows there are numerous complex influences on tephra transportation and preservation.

Aim 3: *Demonstrate the potential for cryptotephra as isochrons in the area*

Objectives: Key beds for distal correlations, applications of modern eruptions, comparison to pre-existing records

Chapters 2 and 3 document the large number of eruptive events that are recorded across Alaska and Yukon Territory, and have the potential to be found in interior Canada and North America more broadly. In Chapter 2 we have shown that nineteen visible and cryptotephra records from Alaska can be characterised over the past 30,000 cal yr BP. Recent cryptotephra records from eastern North America and correlations with records in Greenland and Europe have recognised multiple cryptotephra that are continental- and international-scale isochrons (Coulter et al., 2012; Pyne-O'Donnell et al., 2012; Jensen et al., 2014; Mackay et al., 2016). These are predominantly focused in the mid- to late-Holocene and include eight eruptions from North American volcanic regions and three from other regions (Mexico, Kamchatka and Japan; Mackay et al., 2016). In Chapter 3, however, we describe thirty-four cryptotephra, including two sourced from Kamchatka and the Kurile Islands, that are recorded throughout the Holocene – a significant increase in the number, frequency, and chronological coverage. Cryptotephra chronostratigraphies are compared for each of these locations (Alaska, DHP174, and eastern North America) in Figure 5.1.

As mentioned above, Aniakchak CFE II, WRAe and Novarupta-Katmai are the most widespread, regionally important cryptotephra horizons. Beyond these, we show Hayes set H unit F2, and eruptions likely correlated to Redoubt and Augustine may provide isochrons at different times in the Holocene. As material correlated to Augustine has been reported distally at two points between 3000 to 2000 cal yr BP it is likely there are at least 3 large eruptions (NDN 230, Ruppert, J127) dispersing ash eastwards - more than previously reported. However, subtle variations in major element geochemical data (particularly wt.% Na_2O) produced from different labs make these tephra tricky to correlate definitively. It is also possible that they correlate to volcanic sources that we do not currently have data for. Both Augustine and Redoubt have extensive reports on their proximal volcanic units and while additional eruptions may be missing from these areas (e.g. due to burial, subsequent erosion) there are many active Holocene volcanoes that have little to no published data available and could have similar geochemical characterization given their location, shared magma chambers, etc.

Overall, the records from North America shown in Figure 5.1 include a lot of variation in the number and frequency of eruptions identified. There are definite patterns in geographical distribution that need additional records to fully address. But there are also several common elements and an intriguing mix of volcanic sources represented – while North American eruptive centers dominate, the presence of glass from Kamchatka, Kurile Islands, Japan and Mexico provides a fantastic dataset for cross-referencing between systems and transferring data from this regional tephrostratigraphy to international applications.

The use of Novarupta-Katmai 1912 in Chapter 4 demonstrates a direct application of modern cryptotephra which has not been previously utilised in the area. Cryptotephra layers are valuable as independent checks for sediment archive chronologies and, where present, helped to identify and correct offsets in ^{14}C and ^{210}Pb data, reduce associated modelled age ranges, and bring the two methods in to better agreement at a tricky time when the ^{14}C calibration curve has a plateau and ^{210}Pb has a severely reduced signal. These sites do, however, show there is a complex range of taphonomic processes affecting the final record and full analyses (rather than targeted time periods) would produce a more complete record of cryptotephra in Alberta and likely highlight additional unknowns for regional correlation. As Alberta has records of visible tephra from northern, western and southern volcanic sources, it represents a key area that is likely the geographical limit for the overlap of these tephra.

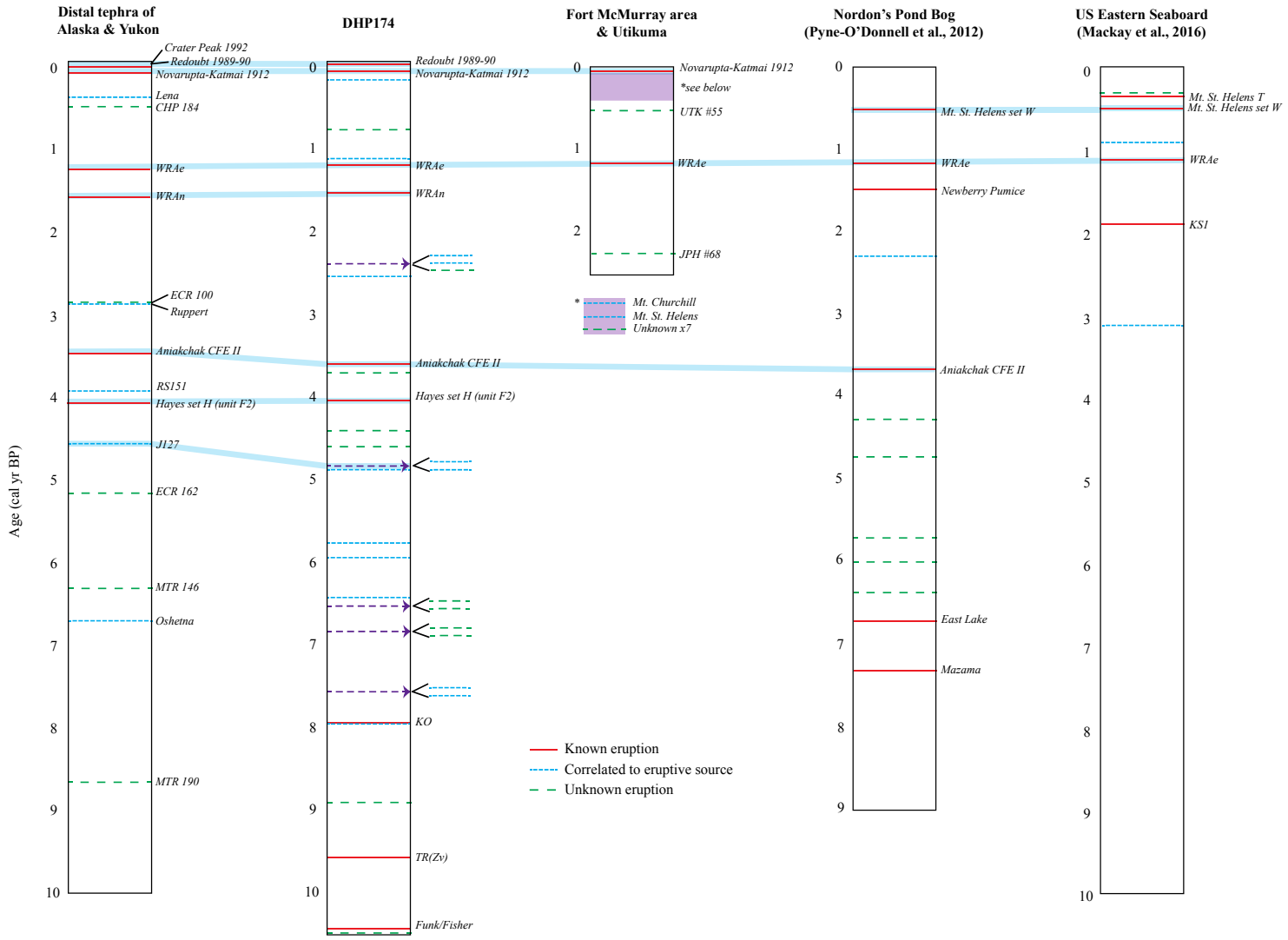

Figure 5.1: Comparative tephra chronostratigraphies across northern North America. Blue shading shows tephra links between records. Distal Alaska & Yukon records are compiled from Payne et al. (2008), Davies et al. (2016) and Monteath et al., (2017).

5.1 Future Outlook

The work summarised here significantly advances cryptotephra stratigraphy in northwestern North America and shows that there are many worthwhile possibilities still to be considered. The investigation of more sites will underlie any future advances in the area, and four major themes to address include: redefining the limits of the key tephra described here; tracking ultra-distal cryptotephra that are only recorded in the early Holocene in the Yukon but appear later in eastern Canada; delimiting any overlap between the main volcanic source areas in North America (e.g. Alaska, the Aleutian arc, the Wrangells, the Cascades) and also those from further afield (e.g. Kamchatka, the Kurile Islands, Japan, Mexico); and questioning the influence of changes in transportation and deposition (with suggested influence from air circulation and post-glacial ice presence).

Sites at key locations can act as tie-points between regions and overlap glass from different sources, or preserve more complete records covering a time period, but finding records of suitable length and resolution can be problematic. The complex interaction of local and more widescale issues of transportation, deposition and preservation mean there are no guarantees with site choice, even within an area with established records. Within northern Canada this is also complicated due to former ice cover and removal of surficial sediments. Soligenic peatlands in areas of continuous permafrost, however, are shown here to be reliable stratigraphic archives that are previously untapped but have the potential to contain long and undisturbed records.

In Canada, it would be beneficial to add new or more complete Holocene records where possible to continue addressing the paucity of records between the Yukon Territory and Newfoundland. Many regions across Canada have published palaeo-records covering anywhere from 4000 years to the whole Holocene, including lacustrine and peat deposits, and would enable a more precise demarcation of cryptotephra dispersal and the eastern and southern limits of preservation of ash from sources in Alaska. In the USA records from any central states would also help address geographic gaps while being distal from active sources. During the course of this dissertation several sites have been analysed for cryptotephra and shown to contain no glass, no discernible isochrons, or a background signal of geochemically identical or detrital glass. These include St. Paul Lake, AK; Silver Lake, OH; Appleman Lake, IN; and Ellesmere Island, NU. Hence, while

additional sites are suggested here in theory and the records included here show great potential, learning how useful other locations may actually be requires verification.

The data generated from new sites and cryptotephra described here have been formatted and provided in ways that are most deemed useful to their broad distribution and utilisation by other researchers. This relates to an issue that affects all researchers working in data-rich fields and has been raised and discussed by the tephra community specifically as a key requirement for co-operative work. Ongoing research requires comprehensive datasets (e.g. geochemical data, raw dates and age modelling) for thorough comparison. Chronological data is provided here as both the raw dates (including both the original whole datasets and the refined dates subjected to rigorous assessment) and the Bayesian modelled outputs. While the Bayesian ages are argued to be the most rigorous evaluation of tephra deposition where the eruption was not observed, the raw data are valuable for reassessment and future modelling work. Major element geochemical characterisation of tephra is now a commonly applied technique and there have been significant efforts to produce high quality, comparable data at labs around the world (e.g. Kuehn et al., 2011). Reporting of this data and how it is made available, however, is variable, particularly when dealing with older publications and datasets.

Chapter 2 addresses some of our concerns about alternative geochemical techniques, average EPMA data, and samples from grey literature. For comparisons with proximal material, there are many volcanic sources and/or eruptions with either no data or only whole rock analyses published. Re-analysis of this material, where possible, and concurrent analysis with unknowns can confirm correlations and reveal new research questions, providing inclusive datasets for future use. Defining individual cryptotephra for chronostratigraphic purposes without a known source cannot help to produce, for example, detailed eruptive histories, but where there is uncertainty in the data or a wide range of possibilities it is best not to pigeonhole data incorrectly.

Overall, my take-home message from the work outlined in this thesis is that when working with cryptotephra, you really never know what you might find until you've actually looked. What we see here scratches the surface of what is possible in North America, and provides a foundation from which cryptotephra can develop, as it has elsewhere in the world, into an important tool for palaeo-environmental science.

5.2 References

Alaska Volcano Observatory, 2014. Alaska Volcano Observatory Online Library [WWW Document]. URL www.avo.alaska.edu/downloads/. (accessed 6.30.17).

Castellano, E., Becagli, S., Jouzel, J., Migliori, A., Severi, M., Steffensen, J.P., Traversi, R., Udisti, R., 2004. Volcanic eruption frequency over the last 45 ky as recorded in Epica-Dome C ice core (East Antarctica) and its relationship with climatic changes. Glob. Planet. Change 42, 195–205. https://doi.org/10.1016/j.gloplacha.2003.11.007

Coulter, S.E., Pilcher, J.R., Plunkett, G., Baillie, M., Hall, V.A., Steffensen, J.P., Vinther, B.M., Clausen, H.B., Johnsen, S.J., 2012. Holocene tephras highlight complexity of volcanic signals in Greenland ice cores. J. Geophys. Res. Atmos. 117, 1–11. https://doi.org/10.1029/2012JD017698

Huybers, P., Langmuir, C., 2009. Feedback between deglaciation, volcanism, and atmospheric CO2. Earth Planet. Sci. Lett. 286, 479–491. https://doi.org/10.1016/j.epsl.2009.07.014

Jensen, B.J.L., Pyne-O'Donnell, S., Plunkett, G., Froese, D.G., Hughes, P.D.M., Sigl, M., McConnell, J.R., Amesbury, M.J., Blackwell, P.G., van den Bogaard, C., Buck, C.E., Charman, D.J., Clague, J.J., Hall, V.A., Koch, J., Mackay, H., Mallon, G., McColl, L., Pilcher, J.R., 2014. Transatlantic distribution of the Alaskan White River Ash. Geology 42, 875–878. https://doi.org/10.1130/G35945.1

Kuehn, S.C., Froese, D.G., Shane, P.A.R., 2011. The INTAV intercomparison of electron-beam microanalysis of glass by tephrochronology laboratories: Results and recommendations. Quat. Int. 246, 19–47. https://doi.org/10.1016/j.quaint.2011.08.022

Mackay, H., Hughes, P.D.M., Jensen, B.J.L., Langdon, P.G., Pyne-O'Donnell, S.D.F., Plunkett, G., Froese, D.G., Coulter, S.E., Gardner, J.E., 2016. A mid to late Holocene cryptotephra framework from eastern North America. Quat. Sci. Rev. 132, 101–113. https://doi.org/10.1016/j.quascirev.2015.11.011

Payne, R.J., Gehrels, M., 2010. The formation of tephra layers in peatlands: An experimental approach. Catena 81, 12–23. https://doi.org/10.1016/j.catena.2009.12.001

Praetorius, S., Mix, A., Jensen, B., Froese, D., Milne, G., Wolhowe, M., Addison, J., Prahl, F., 2016. Interaction between climate, volcanism, and isostatic rebound in Southeast Alaska during the last deglaciation. Earth Planet. Sci. Lett. 452, 79–89. https://doi.org/10.1016/j.epsl.2016.07.033

Pyne-O'Donnell, S.D.F., Hughes, P.D.M., Froese, D.G., Jensen, B.J.L., Kuehn, S.C., Mallon, G., Amesbury, M.J., Charman, D.J., Daley, T.J., Loader, N.J., Mauquoy, D., Street-Perrott, F.A., Woodman-Ralph, J., 2012. High-precision ultra-distal Holocene tephrochronology in North America. Quat. Sci. Rev. 52, 6–11. https://doi.org/10.1016/j.quascirev.2012.07.024

Watson, E.J., Swindles, G.T., Lawson, I.T., Savov, I., 2015. Spatial variability of tephra and carbon accumulation in a Holocene peatland. Quat. Sci. Rev. 124, 248–264. https://doi.org/10.1016/j.quascirev.2015.07.025

Watt, S.F.L., Pyle, D.M., Mather, T.A., 2013. The volcanic response to deglaciation: Evidence from glaciated arcs and a reassessment of global eruption records. Earth-Science Rev. 122, 77–102. https://doi.org/10.1016/j.earscirev.2013.03.007

Zoltai, S.C., 1989. Late Quaternary volcanic ash in the peatlands of central Alberta. Can. J. Earth Sci. 26, 207–214. https://doi.org/10.1139/e89-017

Bibliography

Abbott, M.B., Stafford, T.W., Jr., 1996. Radiocarbon Geochemistry of Modern and Ancient Arctic Lake Systems, Baffin Island, Canada. Quaternary Research 45, 300–311. doi:10.1006/qres.1996.0031

Abbott, P.M., Davies, S.M., 2012. Volcanism and the Greenland ice-cores: The tephra record. Earth-Science Rev. 115, 173–191. https://doi.org/10.1016/j.earscirev.2012.09.001

Addison, J.A., Begét, J.E., Ager, T.A., Finney, B.P., 2010. Marine tephrochronology of the Mt. Edgecumbe Volcanic Field, Southeast Alaska, USA. Quaternary Research 73, 277-292. doi:10.1016/j.yqres.2009.10.007

Adolphi, F., Muscheler, R., 2016. Synchronizing the Greenland ice core and radiocarbon timescales over the Holocene-Bayesian wiggle-matching of cosmogenic radionuclide records. Clim. Past 12, 15–30. https://doi.org/10.5194/cp-12-15-2016

Ager, T.A., 1982. Vegetational history of western Alaska during the Wisconsin glacial interval and the Holocene, in: Hopkins, D.M., Matthews, Jr. V.J., Schweger, C.E., Young, S.B. (Eds.), Paleoecology of Beringia. Academic Press, New York, pp. 75–93. doi:10.1016/B978-0-12-355860-2.50012-0

Ager, T.A., 2003. Late Quaternary vegetation and climate history of the central Bering land bridge from St. Michael Island, western Alaska. Quaternary Research 60, 19–32. doi:10.1016/S0033-5894(03)00068-1

Alaska Volcano Observatory, 2014. Alaska Volcano Observatory Online Library [WWW Document]. URL www.avo.alaska.edu/downloads/. (accessed 6.30.17).

Ali, A.A., Ghaleb, B., Garneau, M., Asnong, H., Loisel, J., 2008. Recent peat accumulation rates in minerotrophic peatlands of the Bay James region, Eastern Canada, inferred by 210Pb and 137Cs radiometric techniques. Appl. Radiat. Isot. 66, 1350–1358. https://doi.org/10.1016/j.apradiso.2008.02.091

Alloway, B.V., Larsen, G., Lowe, D.J., Shane, P.A.R., Westgate, J.A., 2007. Quaternary Stratigraphy - Tephrochronology, in: Elias, S.A. (Ed.), Encyclopedia of Quaternary Science. Elsevier, pp. 2869–2898. https://doi.org/10.1016/B0-44-452747-8/00075-2

Appleby, P.G., 2001. Chronostratigraphic Techniques in Recent Sediments, in: Last, W.M., Smol, J.P. (Eds.), Tracking Environmental Change Using Lake Sediments. Kluwer Academic Publishers, Dordrecht, pp. 171–203. https://doi.org/10.1007/0-306-47669-X_9

Appleby, P.G., Nolan, P.J., Oldfield, F., Richardson, N., Higgitt, S.R., 1988. 210Pb dating of lake sediments and ombrotrophic peats by gamma essay. Sci. Total Environ. 69, 157–177. https://doi.org/10.1016/0048-9697(88)90341-5

Appleby, P.G., Oldfield, F., 1983. The assessment of 210Pb data from sites with varying sediment accumulation rates. Hydrobiologia 103, 29–35. https://doi.org/10.1007/BF00028424

Appleby, P.G., Oldfield, F., 1978. The calculation of lead-210 dates assuming a constant rate of supply of unsupported 210Pb to the sediment. Catena 5, 1–8. https://doi.org/10.1016/S0341-8162(78)80002-2

Appleby, P.G., Shotyk, W., Fankhauser, A., 1997. Lead-210 age dating of three peat cores in the Jura Mountains, Switzerland. Water. Air. Soil Pollut. 100, 223–231. https://doi.org/10.1023/A:1018380922280

Bacon, C.R., Neal, C.A., Miller, T.P., McGimsey, R.G., Nye, C.J., 2014. Postglacial eruptive history, geochemistry, and recent seismicity of Aniakchak volcano, Alaska Peninsula, U.S. Geological Survey Professional Paper.

Baillie, M.G.L., McAneney, J., 2015. Tree ring effects and ice core acidities clarify the volcanic record of the first millennium. Clim. Past 11, 105–114. https://doi.org/10.5194/cp-11-105-2015

Baird, A.J., Belyea, L.R., Morris, P.J., 2009. Upscaling of peatland-atmosphere fluxes of methane: Small-scale heterogeneity in process rates and the pitfalls of "bucket-and-slab" models, in: Eichelberger, J.C., Gordeev, E., Izbekov, P., Kasahara, M., Lees, J. (Eds.), Carbon Cycling in Northern Peatlands. American Geophysical Union, Washington DC, pp. 37–53. https://doi.org/10.1029/2008GM000826

Balascio, N.L., Wickler, S., Narmo, L.E., Bradley, R.S., 2011. Distal cryptotephra found in a Viking boathouse: the potential for tephrochronology in reconstructing the Iron Age in Norway. Journal of Archaeological Science 38, 934–941. doi:10.1016/j.jas.2010.11.023

Bao, K.S., Shen, J., Zhang, Y., Wang, J., Wang, G.P., 2014. A 200-year record of polycyclic aromatic hydrocarbons contamination in an ombrotrophic peatland in Great Hinggan Mountain, northeast China. J. Mt. Sci. 11, 1085–1096. https://doi.org/10.1007/s11629-014-3167-1

Barber, K.E., 1993. Peatlands as scientific archives of past biodiversity. Biodivers. Conserv. 2, 474–489. https://doi.org/10.1007/BF00056743

Barber, K.E., Charman, D.J., 2014. Holocene palaeoclimate records from peatlands, in: Global Change in the Holocene. Routledge, pp. 210–226.

Barber, K.E., Dumayne-Peaty, L., Hughes, P.D.M., Mauquoy, D., Scaife, R., 1998. Replicability and variability of the recent macrofossil and proxy-climate record from raised bogs: Field stratigraphy and macrofossil data from Bolton Fell Moss and Walton Moss, Cumbria, England. J. Quat. Sci. 13, 515–528. https://doi.org/10.1002/(SICI)1099-1417(1998110)13:6<515::AID-JQS393>3.0.CO;2-S

Bauer, I.E., Bhatti, J.S., Swanston, C., Wieder, R.K., Preston, C.M., 2009. Organic matter accumulation and community change at the peatland-upland interface: Inferences from 14C and 210Pb dated profiles. Ecosystems 12, 636–653. https://doi.org/10.1007/s10021-009-9248-2

Begét, J.E., Reger, R.D., Pinney, D., Gillispie, T., Campbell, K., 1991. Correlation of the Holocene Jarvis Creek, Tangle Lakes, Cantwell, and Hayes Tephras in South-Central and Central Alaska. Quaternary Research 35, 174–189. doi:10.1016/0033-5894(91)90065-D

Begét, J.E., Mann, D., 1992. "Caldera" formation by unusually large phreatomagmatic eruptions through permafrost in arctic Alaska. Abstracts [Fall Meeting, 1992], Eos Trans. AGU, 73(43), 636, doi:10.1029/91EO10347.

Begét, J.E., Stihler, S.D., Stone, D.B., 1994. A 500-year-long record of tephra falls from Redoubt Volcano and other volcanoes in upper Cook Inlet, Alaska. Journal of Volcanology and Geothermal Research 62, 55–67. doi:10.1016/0377-0273(94)90028-0

Begét, J.E., Hopkins, D.M., Charron, S.D., 1996. The largest known maars on Earth, Seward Peninsula, northwest Alaska. Arctic 49, 62–69. doi:10.2307/40511986

Begét, J.E., Pedersen, T.F., Muhs, D., 2004. Terrestrial–marine correlation of the 24 kyr BP Dawson tephra: implications for dispersal and preservation of Alaskan tephra deposits. American Geophysical Union Annual Fall Meeting, San Francisco, CA, Fall Meeting Supplement 85, Abstract V21C-02.

Begét, J. E., Pederson, T., Muhs, D., 2005. Terrestrial-marine correlation of the Daswon tephra, in: Alloway, B.V., Froese, D.G., Westgate, J.A (Eds.), Proceedings of the International Field Conference and Workshop on Tephrochronology & Volcanism: Dawson City, Yukon Territory, Canada July 31st– August 8th, 2005. Institute of Geological & Nuclear Sciences science report 2005/22. 55.

Beierle, B., Bond, J., 2002. Density-induced settling of tephra through organic lake sediments. J. Paleolimnol. 28, 433–440. https://doi.org/10.1023/A:1021675501346

Beierle, B., Smith, D.G., 1998. Severe drought in the early Holocene (10,000-6800 BP) interpreted from lake sediment cores, southwestern Alberta, Canada. Palaeogeogr. Palaeoclimatol. Palaeoecol. 140, 75–83. https://doi.org/10.1016/S0031-0182(98)00044-3

Beilman, D.W., Vitt, D.H., Halsey, L.A., 2001. Localized Permafrost Peatlands in Western Canada: Definition, Distributions, and Degradation. Arctic, Antarct. Alp. Res. 33, 70–77. https://doi.org/10.2307/1552279

Belyea, L.R., Clymo, R.S., 2001. Feedback control of the rate of peat formation. Proc. R. Soc. B Biol. Sci. 268, 1315–1321. https://doi.org/10.1098/rspb.2001.1665

Belyea, L.R., Warner, B.G., 1994. Dating of the near-surface layer of a peatland in northwestern Ontario, Canada. Boreas 23, 259–269. https://doi.org/10.1111/j.1502-3885.1994.tb00948.x

Bergman, J., Wastegård, S., Hammarlund, D., Wohlfarth, B., Roberts, S.J., 2004. Holocene tephra horizons at Klocka Bog, west-central Sweden: Aspects of reproducibility in subarctic peat deposits. J. Quat. Sci. 19, 241–249. https://doi.org/10.1002/jqs.833

Berset, J.D., Kuehne, P., Shotyk, W., 2001. Concentrations and distribution of some polychlorinated biphenyls (PCBs) and polycyclic aromatic hydrocarbons (PAHs) in an ombrotrophic peat bog profile of Switzerland. Sci. Total Environ. 267, 67–85. https://doi.org/10.1016/S0048-9697(00)00763-4

Blaauw, M., Christen, J.A., 2005. Radiocarbon peat chronologies and environmental change. J. R. Stat. Soc. Ser. C Appl. Stat. 54, 805–816. https://doi.org/10.1111/j.1467-9876.2005.00516.x

Blaauw, M., Heuvelink, G.B.M., Mauquoy, D., Van Der Plicht, J., Van Geel, B., 2003. A numerical approach to 14C wiggle-match dating of organic deposits: Best fits and confidence intervals. Quat. Sci. Rev. 22, 1485–1500. https://doi.org/10.1016/S0277-3791(03)00086-6

Blaauw, M., van Geel, B., Mauquoy, D., van der Plicht, J., 2004. Carbon-14 wiggle-match dating of peat deposits: Advantages and limitations. J. Quat. Sci. 19, 177–181. https://doi.org/10.1002/jqs.810

Blackford, J.J., 2000. Palaeoclimatic records from peat bogs. Trends Ecol. Evol. 15, 193–198. https://doi.org/10.1016/S0169-5347(00)01826-7

Blackford, J.J., Payne, R.J., Heggen, M.P., de la Riva Caballero, A., van der Plicht, J., 2014. Age and impacts of the caldera-forming Aniakchak II eruption in western Alaska. Quat. Res. (United States) 82, 85–95. https://doi.org/10.1016/j.yqres.2014.04.013

Blockley, S.P.E., Pyne-O'Donnell, S.D.F., Lowe, J.J., Matthews, I.P., Stone, A., Pollard, A.M., Turney, C.S.M., Molyneux, E.G., 2005. A new and less destructive laboratory procedure for the physical separation of distal glass tephra shards from sediments. Quat. Sci. Rev. 24, 1952–1960. https://doi.org/10.1016/j.quascirev.2004.12.008

Blockley, S.P.E., Ramsey, C.B., Lane, C.S., Lotter, A.F., 2008. Improved age modelling approaches as exemplified by the revised chronology for the Central European varved lake Soppensee. Quaternary Science Reviews 27, 61–71. doi:10.1016/j.quascirev.2007.01.018

Blockley, S.P.E., Edwards, K.J., Schofield, J.E., Pyne-O'Donnell, S.D.F., Jensen, B.J.L., Matthews, I.P., Cook, G.T., Wallace, K.L., Froese, D.G., 2015. First evidence of cryptotephra in palaeoenvironmental records associated with Norse occupation sites in Greenland. Quaternary Geochronology 27, 145–157. doi:10.1016/j.quageo.2015.02.023

Booth, R.K., Jackson, S.T., Notaro, M., 2010. Using peatland archives to test paleoclimate hypotheses. PAGES news 18, 1–5.

Bowers, P.M., 1979. The Cantwell ash bed, a Holocene tephra in the central Alaska Range, in: Alaska Division of Geological & Geophysical Surveys, Short Notes on Alaskan Geology - 1978: Alaska Division of Geological & Geophysical Surveys Geologic Report 61E, p. 19-24. doi:10.14509/412

Bracewell, J.M., Hepburn, A., Thomson, C., 1993. Levels and distribution of polychlorinated biphenyls on the Scottish land mass. Chemosphere 27, 1657–1667. https://doi.org/10.1016/0045-6535(93)90147-W

Braitseva, O. a., Ponomareva, V. V., Sulerzhitsky, L.D., Melekestsev, I. V., Bailey, J., 1997. Holocene Key-Marker Tephra Layers in Kamchatka, Russia. Quat. Res. 47, 125–139. https://doi.org/10.1006/qres.1996.1876

Briner, J.P., McKay, N.P., Axford, Y., Bennike, O., Bradley, R.S., de Vernal, A., Fisher, D., Francus, P., Fréchette, B., Gajewski, K., Jennings, A., Kaufman, D.S., Miller, G., Rouston, C., Wagner, B., 2016. Holocene climate change in Arctic Canada and Greenland. Quat. Sci. Rev. 147, 340–364. https://doi.org/10.1016/j.quascirev.2016.02.010

Brock, F., Lee, S., Housley, R.A., Bronk Ramsey, C., 2011. Variation in the radiocarbon age of different fractions of peat: A case study from Ahrenshöft, northern Germany. Quat. Geochronol. 6, 550–555. https://doi.org/10.1016/j.quageo.2011.08.003

Bronk Ramsey, C., 2013. Recent and Planned Developments of the Program OxCal. Radiocarbon 55, 720–730. https://doi.org/10.2458/azu_js_rc.55.16215

Bronk Ramsey, C. 2005. OxCal program v.3.10. Oxford University.

Bronk Ramsey, C., 2009a. Bayesian Analysis of Radiocarbon Dates. Radiocarbon 51, 337–360. https://doi.org/10.1017/S0033822200033865

Bronk Ramsey, C., 2009b. Dealing with Outliers and Offsets in Radiocarbon Dating. Radiocarbon 51, 1023–1045. https://doi.org/10.1017/S0033822200034093

Bronk Ramsey, C., 2008. Deposition models for chronological records. Quat. Sci. Rev. 27, 42–60. https://doi.org/10.1016/j.quascirev.2007.01.019

Bronk Ramsey, C., Albert, P.G., Blockley, S.P.E., Hardiman, M., Housley, R.A., Lane, C.S., Lee, S., Matthews, I.P., Smith, V.C., Lowe, J.J., 2015. Improved age estimates for key Late Quaternary European tephra horizons in the RESET lattice. Quat. Sci. Rev. 118, 18–32. https://doi.org/10.1016/j.quascirev.2014.11.007

Browne, B.L., Gardner, J.E., Neal, C.A., Nicholson, R., 2003. The ~400 yr B.P. caldera-forming eruption Half Cone Volcano, Aniakchak Caldera, Alaska - Abstract, in: Alaska Geological Society 2003 Geology Symposium. p. 27.

Buck, C.E., Higham, T.F.G., Lowe, D.J., 2003. Bayesian tools for tephrochronology. The Holocene 13, 639–647. doi:10.1191/0959683603hl652ft

Bull, K.F., Cameron, C.E., Coombs, M.L., Diefenbach, A.K., Lopez, T., McNutt, S.R., Neal, C.A., Payne, A.L., Power, J.A., Schneider, D.J., Scott, W.E., Snedigar, S., Thompson, G., Wallace, K.L., Waythomas, C.F., Webley, P.W., Werner, C.A., 2011. The 2009 eruption of Redoubt Volcano, Alaska, Alaska Division of Geological and Geophysical Surveys Report of Investigation. doi:10.14509/23123

Calmels, F., Gagnon, O., Allard, M., 2005. A portable earth-drill system for permafrost studies. Permafr. Periglac. Process. 16, 311–315. https://doi.org/10.1002/ppp.529

Campbell, I.D., Campbell, C., Yu, Z., Vitt, D.H., Apps, M.J., 2000. Millennial-Scale Rhythms in Peatlands in the Western Interior of Canada and in the Global Carbon Cycle. Quat. Res. 54, 155–158. https://doi.org/10.1006/qres.2000.2134

Carson, E.C., Fournelle, J.H., Miller, T.P., Mickelson, D.M., 2002. Holocene tephrochronology of the Cold Bay area, southwest Alaska Peninsula. Quat. Sci. Rev. 21, 2213–2228. https://doi.org/10.1016/S0277-3791(02)00023-9

Casadevall, T.J., 1994. The 1989–1990 eruption of Redoubt Volcano, Alaska: impacts on aircraft operations. Journal of Volcanology and Geothermal Research 62, 301–316. doi:10.1016/0377-0273(94)90038-8

Castellano, E., Becagli, S., Jouzel, J., Migliori, A., Severi, M., Steffensen, J.P., Traversi, R., Udisti, R., 2004. Volcanic eruption frequency over the last 45 ky as recorded in Epica-Dome C ice core (East Antarctica) and its relationship with climatic changes. Glob. Planet. Change 42, 195–205. https://doi.org/10.1016/j.gloplacha.2003.11.007

Certini, G., 2005. Effects of fire on properties of forest soils: A review. Oecologia 143, 1–10. https://doi.org/10.1007/s00442-004-1788-8

Chambers, F.M., Dresser, P.Q., Smith, A.G., 1979. Radiocarbon dating evidence on the impact of atmospheric pollution on upland peats. Nature 282, 829–831. https://doi.org/10.1038/282829a0

Charman, D.J., Barber, K.E., Blaauw, M., Langdon, P.G., Mauquoy, D., Daley, T.J., Hughes, P.D.M., Karofeld, E., 2009. Climate drivers for peatland palaeoclimate records. Quat. Sci. Rev. 28, 1811–1819. https://doi.org/10.1016/j.quascirev.2009.05.013

Charman, D.J., Caseldine, C., Baker, A., Gearey, B., Hatton, J., Proctor, C., 2001. Paleohydrological Records from Peat Profiles and Speleothems in Sutherland, Northwest Scotland. Quat. Res. 55, 223–234. https://doi.org/10.1006/qres.2000.2190

Charman, D.J., Garnett, M.H., 2005. Chronologies for recent peat deposits using wiggle-matched radiocarbon ages: Problems with old carbon contamination. Radiocarbon 47, 135–145.

Child, J.K., Beget, J.E., Werner, A., 1998. Three Holocene Tephras Identified in Lacustrine Sediment Cores from the Wonder Lake Area, Denali National Park and Preserve, Alaska, U.S.A. Arctic and Alpine Research 30, 89–95. doi:10.2307/1551749

Christen, J.A., 1994. Bayesian interpretation of ^{14}C results. PhD thesis, University of Nottingham.

Christen, J.A., Clymo, R.S., Litton, C.D., 1995. A Bayesian Approach to the Use of 14C Dates in the Estimation of the Age of Peat. Radiocarbon 37, 431–441. https://doi.org/10.1017/S0033822200030915

Clague, J.J., Evans, S.G., Rampton, V.N., Woodsworth, G.J., 1995. Improved age estimates for the White River and Bridge River tephras, western Canada. Can. J. Earth Sci. 32, 1172–1179. https://doi.org/10.1139/e95-096

Clymo, R.S., Mackay, D., 1987. Upwash and Downwash of Pollen and Spores in the Unsaturated Surface Layer of Sphagnum Dominated Peat. New Phytol. 105, 175–183. https://doi.org/10.1111/j.1469-8137.1987.tb00120.x

Clymo, R.S., Oldfield, F., Appleby, P.G., Pearson, G.W., Ratnesar, P., Richardson, N., 1990. The Record of Atmospheric Deposition on a Rainwater-Dependent Peatland. Philos. Trans. R. Soc. B Biol. Sci. 327, 331–338. https://doi.org/10.1098/rstb.1990.0070

Combellick, R.A., Pinney, D.S., 1995. Radiocarbon age of probable Hayes tephra, Kenai Peninsula, Alaska, in: Combellick, R.A., Tannian, F. (Eds.), Short Notes on Alaskan Geology. Alaska Division of Geological and Geophysical Surveys, Professional Report 117. pp. 1–9.

Coulter, S.E., Pilcher, J.R., Plunkett, G., Baillie, M., Hall, V.A., Steffensen, J.P., Vinther, B.M., Clausen, H.B., Johnsen, S.J., 2012. Holocene tephras highlight complexity of volcanic signals in Greenland ice cores. J. Geophys. Res. Atmos. 117, 1–11. https://doi.org/10.1029/2012JD017698

Damman, A.W.H., 1978. Distribution and Movement of Elements in Ombrotrophic Peat Bogs. Oikos 30, 480. https://doi.org/10.2307/3543344

Davies, L.J., Froese, D.G., 2015. Developing a cryptotephra framework for North America: A baseline chronostratigraphy for the Holocene from north-western sources., in: XIX INQUA Congress. Nagoya, Japan.

Davies, L.J., Jensen, B.J.L., Froese, D.G., Wallace, K.L., 2016. Late Pleistocene and Holocene tephrostratigraphy of interior Alaska and Yukon: Key beds and chronologies over the past 30,000 years. Quat. Sci. Rev. 146, 28–53. https://doi.org/10.1016/j.quascirev.2016.05.026

Davies, S.M., 2015. Cryptotephras: The revolution in correlation and precision dating. J. Quat. Sci. 30, 114–130. https://doi.org/10.1002/jqs.2766

Davies, S.M., Turney, C.S.M., Lowe, J.J., 2001. Identification and significance of a visible, basalt-rich Vedde Ash layer in a Late-glacial sequence on the Isle of Skye, Inner Hebrides, Scotland. Journal of Quaternary Science 16, 99–104. doi:10.1002/jqs.611

Davies, S.M., Elmquist, M., Bergman, J., Wohlfarth, B., Hammarlund, D., 2007. Cryptotephra sedimentation processes within two lacustrine sequences from west central Sweden. The Holocene 17, 319–330. https://doi.org/10.1177/0959683607076443

Davies, S.M., Abbott, P.M., Pearce, N.J.G., Wastegård, S., Blockley, S.P.E., 2012. Integrating the INTIMATE records using tephrochronology: rising to the challenge. Quaternary Science Reviews 36, 11–27. doi:10.1016/j.quascirev.2011.04.005

Davies, S.M., Abbott, P.M., Meara, R.H., Pearce, N.J.G., Austin, W.E.N., Chapman, M.R., Svensson, A., Bigler, M., Rasmussen, T.L., Rasmussen, S.O., Farmer, E.J., 2014. A North Atlantic tephrostratigraphical framework for 130-60 ka b2k: New tephra discoveries, marine-based correlations, and future challenges. Quat. Sci. Rev. 106, 101–121. https://doi.org/10.1016/j.quascirev.2014.03.024

de Fontaine, C.S., Kaufman, D.S., Scott Anderson, R., Werner, A., Waythomas, C.F., Brown, T.A., 2007. Late Quaternary distal tephra-fall deposits in lacustrine sediments, Kenai Peninsula, Alaska. Quat. Res. 68, 64–78. https://doi.org/10.1016/j.yqres.2007.03.006

de Vleeschouwer, F., Fagel, N., Cheburkin, A.K., Pazdur, A., Sikorski, J., Mattielli, N., Renson, V., Fiałkiewicz-Kozieł, B., Piotrowska, N., Le Roux, G., 2009. Anthropogenic impacts in North Poland over the last 1300 years - A record of Pb, Zn, Cu, Ni and S in an ombrotrophic peat bog. Sci. Total Environ. 407, 5674–5684. https://doi.org/10.1016/j.scitotenv.2009.07.020

Degryse, F., Smolders, E., Parker, D.R., 2009. Partitioning of metals (Cd, Co, Cu, Ni, Pb, Zn) in soils: concepts, methodologies, prediction and applications - a review. Eur. J. Soil Sci. 60, 590–612. https://doi.org/10.1111/j.1365-2389.2009.01142.x

Demuro, M., Roberts, R.G., Froese, D.G., Arnold, L.J., Brock, F., Ramsey, C.B., 2008. Optically stimulated luminescence dating of single and multiple grains of quartz from perennially frozen loess in western Yukon Territory, Canada: Comparison with radiocarbon chronologies for the late Pleistocene Dawson tephra. Quaternary Geochronology 3, 346–364. doi:10.1016/j.quageo.2007.12.003

Denton, J.S., Pearce, N.J.G., 2008. Comment on "A synchronized dating of three Greenland ice cores throughout the Holocene" by B. M. Vinther et al.: No Minoan tephra in the 1642 B.C. layer of the GRIP ice core. J. Geophys. Res. Atmos. 113, 1–7. https://doi.org/10.1029/2007JD008970

Derkachev, A.N., Nikolaeva, N.A., Gorbarenko, S.A., Portnyagin, M. V., Ponomareva, V. V., Nürnberg, D., Sakamoto, T., Iijima, K., Liu, Y., Shi, X., Lv, H., Wang, K., 2016. Tephra layers of in the quaternary deposits of the Sea of Okhotsk: Distribution, composition, age and volcanic sources. Quat. Int. 425, 248–272. https://doi.org/10.1016/j.quaint.2016.07.004

Devito, K.J., Mendoza, C., Petrone, R.M., Kettridge, N., Waddington, J.M., 2016. Utikuma Region Study Area (URSA) - Part 1: Hydrogeological and ecohydrological studies (HEAD). For. Chron. 92, 57–61. https://doi.org/10.5558/tfc2016-017

Devito, K.J., Mendoza, C., Qualizza, C., 2012. Conceptualizing water movement in the Boreal Plains: Implications for watershed reconstruction, Canadian Oil Sands Network for Research and Development. Environmental and Reclamation Research Group.

Dilley, T.E., 1988. Holocene tephra stratigraphy and pedogenesis in the Middle Susitna River Valley, Alaska. University of Alaska, Fairbanks.

Dixon, E.J., 1985. Cultural chronology of central interior Alaska. Arctic Anthropology 22, 47-66. doi:10.2307/40316079

Dixon, E.J., Smith, G.S., 1990. A regional application of tephrochronology in Alaska, in: Lasca, M.P., Donahue, J. (Eds.), Archaeological Geology of North America, Centennial Special Volume 4. Geological Society of America, Boulder, Colorado, pp. 383–398.

Donovan, J., Kremser, D., Fournelle, J.H., Goemann, K., 2015. Probe for EPMA: Acquisition, automation and analysis.

Dörr, H., 1995. Application of 210Pb in soils. J. Paleolimnol. 13, 157–168. https://doi.org/10.1007/BF00678104

Dortch, J. M., Owen, L. A., Caffee, M. W., Li, D., Lowell, T. V., 2010. Beryllium-10 surface exposure dating of glacial successions in the Central Alaska Range. Journal of Quaternary Science 25, 1259–1269. doi:10.1002/jqs.1406

Dreyer, A., Blodau, C., Turunen, J., Radke, M., 2005. The spatial distribution of PAH depositions to peatlands of Eastern Canada. Atmos. Environ. 39, 3725–3733. https://doi.org/10.1016/j.atmosenv.2005.03.009

Dugmore, A.J., Larsen, G., Newton, A.J., 1995. Seven tephra isochrones in Scotland. The Holocene 5, 257–266. https://doi.org/10.1177/095968369500500301

Dugmore, A.J., Newton, A.J., Edwards, K.J., Larsen, G., Blackford, J.J., Cook, G.T., 1996. Long-distance marker horizons from small-scale eruptions: British tephra deposits from the AD 1510 eruption of Hekla, Iceland. J. Quat. Sci. 11, 511–516. https://doi.org/10.1002/(SICI)1099-1417(199611/12)11:6<511::AID-JQS284>3.0.CO;2-C

Duk-Rodkin, A., 1999. Glacial limits map of Yukon Territory; Geological Survey of Canada, Open File 3694, Indian and Northern Affairs Canada Geoscience Map 1999-2, scale 1:1 000 000. https://doi.org/10.4095/210739

Dunning, H.A., 2011. Extending the applications of tephrochronology in Northwestern North America. University of Alberta.

Egan, J., Staff, R., Blackford, J., 2015. A revised age estimate of the Holocene Plinian eruption of Mount Mazama, Oregon using Bayesian statistical modelling. The Holocene 25, 1054–1067. doi:10.1177/0959683615576230

El-Daoushy, F., Tolonen, K., Rosenberg, R., 1982. 210 Pb and moss-increment dating of two Finnish Sphagnum hummocks. Nature 296, 429–431. https://doi.org/10.1038/296429a0

Environment and Climate Change Canada, n.d. Canadian Climate Normals. [WWW Document]. URL http://climate.weather.gc.ca/climate_normals/index_e.html (accessed 6.30.17).

Evans, M.E., Jensen, B.J.L., Kravchinsky, V.A., Froese, D.G., 2011. The Kamikatsura event in the Gold Hill loess, Alaska. Geophysical Research Letters 38, L13302. doi:10.1029/2011GL047793

Ferraz, M.C.M.A., Lourençlo, J.C.N., 2000. The influence of organic matter content of contaminated soils on the leaching rate of heavy metals. Environ. Prog. 19, 53–58. https://doi.org/10.1002/ep.670190118

Fiałkiewicz-Kozieł, B., Kołaczek, P., Michczyński, A., Piotrowska, N., 2015. The construction of a reliable absolute chronology for the last two millennia in an anthropogenically disturbed peat bog: Limitations and advantages of using a radio-isotopic proxy and age-depth modelling. Quat. Geochronol. 25, 83–95. https://doi.org/10.1016/j.quageo.2014.10.003

Fiałkiewicz-Kozieł, B., Smieja-Król, B., Frontasyeva, M., Słowiński, M., Marcisz, K., Lapshina, E., Gilbert, D., Buttler, A., Jassey, V.E.J., Kaliszan, K., Laggoun-Défarge, F., Kołaczek, P., Lamentowicz, M., 2016. Anthropogenic- and natural sources of dust in peatland during the Anthropocene. Sci. Rep. 6, 38731. https://doi.org/10.1038/srep38731

Fierstein, J., 2007. Explosive eruptive record in the Katmai region, Alaska Peninsula: An overview. Bull. Volcanol. 69, 469–509. https://doi.org/10.1007/s00445-006-0097-y

Fierstein, J., Hildreth, W., 2008. Kaguyak dome field and its Holocene caldera, Alaska Peninsula. J. Volcanol. Geotherm. Res. 177, 340–366. https://doi.org/10.1016/j.jvolgeores.2008.05.016

Foit, F.F., Jr, Gavin, D.G., Hu, F.S., 2004. The tephra stratigraphy of two lakes in south-central British Columbia, Canada and its implications for mid-late Holocene volcanic activity at Glacier Peak and Mount St. Helens, Washington, USA. Canadian Journal of Earth Sciences 41, 1401–1410. doi:10.1139/e04-081

Franzén, L.G., 2006. Chapter 11 Mineral matter, major elements, and trace elements in raised bog peat: a case study from southern Sweden, Ireland and Tierra del Fuego, south Argentina. Dev. Earth Surf. Process. 9, 241–269. https://doi.org/10.1016/S0928-2025(06)09011-0

Fraser, T.A., Burn, C.R., 1997. On the nature and origin of "muck" deposits in the Klondike area, Yukon Territory. Can. J. Earth Sci. 34, 1333–1344. https://doi.org/10.1139/e17-106

Froese, D., Westgate, J., Preece, S., Storer, J., 2002. Age and significance of the Late Pleistocene Dawson tephra in eastern Beringia. Quat. Sci. Rev. 21, 2137–2142. https://doi.org/10.1016/S0277-3791(02)00038-0

Froese, D.G., Zazula, G.D., Reyes, A. V., 2006. Seasonality of the late Pleistocene Dawson tephra and exceptional preservation of a buried riparian surface in central Yukon Territory, Canada. Quat. Sci. Rev. 25, 1542–1551. https://doi.org/10.1016/j.quascirev.2006.01.028

Froggatt, P.C., 1992. Standardization of the chemical analysis of tephra deposits. Report of the ICCT Working Group. Quat. Int. 13–14, 93–96. https://doi.org/10.1016/1040-6182(92)90014-S

Fryxell, R., 1965. Mazama and Glacier Peak Volcanic Ash Layers: Relative Ages. Science (80-.). 147, 1288–1290. https://doi.org/10.1126/science.147.3663.1288

Gallagher, D., McGee, E.J., Mitchell, P.I., 2001. A Recent History of 14C, 137Cs, 210Pb, and 241Am Accumulation at Two Irish Peat Bog Sites: an East Versus West Coast Comparison. Radiocarbon 43, 517–525. https://doi.org/10.1017/S0033822200041175

Garnett, M.H., Stevenson, A.C., 2004. Testing the Use of Bomb Radiocarbon to Date the Surface Layers of Blanket Peat. Radiocarbon 46, 841–851. https://doi.org/10.1017/S0033822200035876

Goodsite, M.E., Rom, W., Heinemeier, J., Lange, T., Ooi, S., Appleby, P.G., Shotyk, W., van der Knaap, W.O., Lohse, C., Hansen, T.S., 2001. High-resolution AMS 14C dating of post-bomb peat archives of atmospheric pollutants. Radiocarbon 43, 495–515. https://doi.org/10.1017/S0033822200041163

Goetcheus, V.G., Birks, H.H., 2001. Full-glacial upland tundra vegetation preserved under tephra in the Beringia National Park, Seward Peninsula, Alaska. Quaternary Science Reviews 20, 135–147. doi:10.1016/S0277-3791(00)00127-X

Goslar, T., Knaap, W.O. Van Der, Hicks, S., Andric, M., Czernik, J., Goslar, E., Rasanen, S., Hyotyla, H., 2005. Radiocarbon dating of modern peat profiles: pre- and post-bomb 14C variations in the construction of age-depth models. Radiocarbon 47, 115–134.

Griggs, A.J., Davies, S.M., Abbott, P.M., Coleman, M., Palmer, A.P., Rasmussen, T.L., Johnston, R., 2015. Visualizing tephra deposits and sedimentary processes in the marine environment: The potential of X-ray microtomography. Geochemistry, Geophys. Geosystems 16, 4329–4343. https://doi.org/10.1002/2015GC006073

Grybos, M., Davranche, M., Gruau, G., Petitjean, P., 2007. Is trace metal release in wetland soils controlled by organic matter mobility or Fe-oxyhydroxides reduction? J. Colloid Interface Sci. 314, 490–501. https://doi.org/10.1016/j.jcis.2007.04.062

Haflidason, H., Eiriksson, J., Van Kreveld, S., 2000. The tephrochronology of Iceland and the North Atlantic region during the middle and Late Quaternary: A review. J. Quat. Sci. 15, 3–22. https://doi.org/10.1002/(SICI)1099-1417(200001)15:1<3::AID-JQS530>3.0.CO;2-W

Halsey, L.A., Vitt, D.H., Zoltai, S.C., 1995. Disequilibrium response of permafrost in boreal continental western Canada to climate change. Clim. Change 30, 57–73. https://doi.org/10.1007/BF01093225

Hansen, H.P., 1949. Postglacial Forests in South Central Alberta, Canada. Am. J. Bot. 36, 54–65.

Hansson, S. V., Kaste, J.M., Olid, C., Bindler, R., 2014. Incorporation of radiometric tracers in peat and implications for estimating accumulation rates. Sci. Total Environ. 493, 170–177. https://doi.org/10.1016/j.scitotenv.2014.05.088

Hansson, S. V., Tolu, J., Bindler, R., 2015. Downwash of atmospherically deposited trace metals in peat and the influence of rainfall intensity: An experimental test. Sci. Total Environ. 506–507, 95–101. https://doi.org/10.1016/j.scitotenv.2014.10.083

Hasegawa, T., Nakagawa, M., Yoshimoto, M., Ishizuka, Y., Hirose, W., Seki, S., Ponomareva, V., Alexander, R., 2011. Tephrostratigraphy and petrological study of Chikurachki and Fuss volcanoes, western Paramushir Island, northern Kurile Islands: Evaluation of Holocene eruptive activity and temporal change of magma system. Quat. Int. 246, 278–297. https://doi.org/10.1016/j.quaint.2011.06.047

He, Q., Walling, D.E., 1996. Interpreting particle size effects in the adsorption of 137Cs and unsupported 210Pb by mineral soils and sediments. J. Environ. Radioact. 30, 117–137. https://doi.org/10.1016/0265-931X(96)89275-7

Hildreth, W., Fierstein, J., 2012. The Novarupta-Katmai Eruption of 1912 — Largest Eruption of the Twentieth Century: Centennial Perspectives. US Geol. Surv. Prof. Pap. 259.

Hildreth, W., Fierstein, J., 2000. Katmai volcanic cluster and the great eruption of 1912. Bull. Geol. Soc. Am. 112, 1594–1620. https://doi.org/10.1130/0016-7606(2000)112<1594:KVCATG>2.0.CO;2

Höfle, C., Ping, C.L., 1996. Properties and soil development of late-Pleistocene paleosols from Seward Peninsula, northwest Alaska. Geoderma 71, 219–243. doi:10.1016/0016-7061(96)00007-9

Höfle, C., Edwards, M.E., Hopkins, D.M., Mann, D.H., Ping, C.-L., 2000. The Full-Glacial Environment of the Northern Seward Peninsula, Alaska, Reconstructed from the 21,500-Year-Old Kitluk Paleosol. Quaternary Research 53, 143–153. doi:10.1006/qres.1999.2097

Holmquist, J.R., Finkelstein, S.A., Garneau, M., Massa, C., Yu, Z., MacDonald, G.M., 2016. A comparison of radiocarbon ages derived from bulk peat and selected plant macrofossils in basal peat cores from circum-arctic peatlands. Quat. Geochronol. 31, 53–61. https://doi.org/10.1016/j.quageo.2015.10.003

Hopkins, D.M., 1988. The Espenberg maars: a record of explosive volcanic activity in the Devil Mountain-Cape Espenberg area, Seward Peninsula, Alaska, in: Schaaf, J. (Ed.), The Bering Land Bridge National Preserve: An Archeological Survey. National Park Service, Alaska Region Research/Management Report AR-14, Anchorage. p. 262-321.

Hua, Q., Barbetti, M., Rakowski, A.Z., 2013. Atmospheric radiocarbon for the period 1950-2010. Radiocarbon 55, 2059–2072. https://doi.org/10.2458/azu_js_rc.v55i2.16177

Hughen, K., Southon, J., Lehman, S., Bertrand, C., Turnbull, J., 2006. Marine-derived 14C calibration and activity record for the past 50,000 years updated from the Cariaco Basin. Quat. Sci. Rev. 25, 3216–3227. https://doi.org/10.1016/j.quascirev.2006.03.014

Hunt, J.B., Hill, P.G., 1996. An inter-laboratory comparison of the electron probe microanalysis of glass geochemistry. Quaternary International 34-36, 229–241. doi:10.1016/1040-6182(95)00088-7

Huybers, P., Langmuir, C., 2009. Feedback between deglaciation, volcanism, and atmospheric CO2. Earth Planet. Sci. Lett. 286, 479–491. https://doi.org/10.1016/j.epsl.2009.07.014

Ingram, H.A.P., 1978. Soil Layers in Mires: Function and Terminology. J. Soil Sci. 29, 224–227. https://doi.org/10.1111/j.1365-2389.1978.tb02053.x

Jensen, B.J.L., Froese, D.G., 2006. Characterization and revised distribution of the White River Ash in Yukon Territory and eastern Alaska, in: Program and Abstracts, 36th International Arctic Workshop, March 16–19, 2006: Boulder, Colorado. Institute of Arctic and Alpine Research, University of Colorado.

Jensen, B.J.L., Froese, D.G., Preece, S.J., Westgate, J.A., Stachel, T., 2008. An extensive middle to late Pleistocene tephrochronologic record from east-central Alaska. Quaternary Science Reviews 27, 411–427. doi:10.1016/j.quascirev.2007.10.010

Jensen, B.J.L., Preece, S.J., Lamothe, M., Pearce, N.J.G., Froese, D.G., Westgate, J.A., Schaefer, J., Beget, J.E., 2011. The variegated (VT) tephra: A new regional marker for middle to late marine isotope stage 5 across Yukon and Alaska. Quaternary International 1–12. doi:10.1016/j.quaint.2011.06.028

Jensen, B.J.L., Reyes, A.V., Froese, D.G., 2013. Marine tephrostratigraphy in the Gulf of Alaska and comparison to terrestrial records from eastern Beringia, in: Program and Abstracts, CANQUA-CGRG biannual meeting, August 18-21, 2013: University of Alberta, Edmonton.

Jensen, B.J.L., Pyne-O'Donnell, S.D.F., Plunkett, G., Froese, D.G., Hughes, P.D.M., Sigl, M., McConnell, J.R., Amesbury, M.J., Blackwell, P.G., van den Bogaard, C., Buck, C.E., Charman, D.J., Clague, J.J., Hall, V.A., Koch, J., Mackay, H., Mallon, G., McColl, L., Pilcher, J.R., 2014a. Transatlantic distribution of the Alaskan White River Ash. Geology 42, 875–878. doi:10.1130/G35945.1

Jensen, B.J.L., Mackay, H., Pyne-O'Donnell, S.D.F., Plunkett, G., Hughes, P.D.M., Froese, D.G., Booth, R., 2014b. Exceptionally Long Distance Transport of Volcanic Ash: Implications for Stratigraphy, Hazards and the Sourcing of Distal Tephra Deposits. American Geophysical Union Fall Meeting, Dec 15-19, San Francisco.

Jensen, B.J.L., Evans, M.E., Froese, D.G., Kravchinsky, V.A., 2016. 150,000 years of loess accumulation in central Alaska. Quaternary Science Reviews 135, 1–23. doi:10.1016/j.quascirev.2016.01.001

Jensen, B.J.L., Beaudoin, A.B., 2016. Geochemical characterization of tephra deposits at archaeological and palaeoenvironmental sites across south-central Alberta and southwest Saskatchewan, in: Woywitka, R. (Ed.), Back on the Horse: Recent Developments in Archaeological and Palaeontological Research in Alberta. Archaeological Survey of Alberta, Edmonton, Alberta, pp. 154–160.

Jones, J.M., Hao, J., 1993. Ombrotrophic peat as a medium for historical monitoring of heavy metal pollution. Environ. Geochem. Health 15, 67–74. https://doi.org/10.1007/BF02627824

Karrow, P.F., Anderson, T.W., 1975. Palynological study of lake sediment profiles from southwestern New Brunswick: Discussion. Canadian Journal of Earth Sciences 12, 1808–1812. doi:10.1139/e75-161

Kaufman, D.S., Ager, T.A., Anderson, N.J., Anderson, P.M., Andrews, J.T., Bartlein, P.J., Brubaker, L.B., Coats, L.L., Cwynar, L.C., Duvall, M.L., Dyke, A.S., Edwards, M.E., Eisner, W.R., Gajewski, K., Geirsdóttir, A., Hu, F.S., Jennings, A.E., Kaplan, M.R., Kerwin, M.W., Lozhkin, A. V., MacDonald, G.M., Miller, G.H., Mock, C.J., Oswald, W.W., Otto-Bliesner, B.L., Porinchu, D.F., Rühland, K., Smol, J.P., Steig, E.J., Wolfe, B.B., 2004. Holocene thermal maximum in the western Arctic (0-180°W). Quat. Sci. Rev. 23, 529–560. https://doi.org/10.1016/j.quascirev.2003.09.007

Kaufman, D.S., Jensen, B.J.L., Reyes, A. V., Schiff, C.J., Froese, D.G., Pearce, N.J.G., 2012. Late Quaternary tephrostratigraphy, Ahklun Mountains, SW Alaska. J. Quat. Sci. 27, 344–359. https://doi.org/10.1002/jqs.1552

Kennedy, K.E., Froese, D.G., Zazula, G.D., Lauriol, B., 2010. Last Glacial Maximum age for the northwest Laurentide maximum from the Eagle River spillway and delta complex, northern Yukon. Quaternary Science Reviews 29, 1288–1300. doi:10.1016/j.quascirev.2010.02.015

Kilian, M.R., Van der Plicht, J., Van Geel, B., 1995. Dating raised bogs: New aspects of AMS 14C wiggle matching, a reservoir effect and climatic change. Quat. Sci. Rev. 14, 959–966. https://doi.org/10.1016/0277-3791(95)00081-X

Kuehn, S.C., Froese, D.G., Carrara, P.E., Foit, F.F., Jr, Pearce, N.J.G., Rotheisler, P., 2009a. Major- and trace-element characterization, expanded distribution, and a new chronology for the latest Pleistocene Glacier Peak tephras in western North America. Quaternary Research 71, 201–216. doi:10.1016/j.yqres.2008.11.003

Kuehn, S.C., Froese, D.G., Pearce, N.J.G., Foit, F.F., 2009b. ID3506, a New/Old Lipari Obsidian Standard for Characterization of Natural Glasses and Tephrochronology: Eos Transactions of the AGU, Fall Meet. Suppl., Abstract V31E-2010.

Kuehn, S.C., Froese, D.G., Shane, P.A.R., INTAV Intercomparison Participants, 2011. The INTAV intercomparison of electron-beam microanalysis of glass by tephrochronology laboratories: Results and recommendations. Quaternary International 1–29. doi:10.1016/j.quaint.2011.08.022

Lakeman, T.R., Clague, J.J., Menounos, B., Osborn, G.D., Jensen, B.J.L., Froese, D.G., 2008. Holocene tephras in lake cores from northern British Columbia, Canada. Can. J. Earth Sci. 45, 935–947. https://doi.org/10.1139/E08-035

Lamborg, C.H., Fitzgerald, W.F., Damman, A.W.H., Benoit, J.M., Balcom, P.H., Engstrom, D.R., 2002. Modern and historic atmospheric mercury fluxes in both hemispheres: Global and regional mercury cycling implications. Global Biogeochem. Cycles 16, 51-1-51–11. https://doi.org/10.1029/2001GB001847

Lane, C.S., Blockley, S.P.E., Mangerud, J., Smith, V.C., Lohne, Ø.S., Tomlinson, E.L., Matthews, I.P., Lotter, A.F., 2012. Was the 12.1ka Icelandic Vedde Ash one of a kind? Quaternary Science Reviews 33, 87–99. doi:10.1016/j.quascirev.2011.11.011

Lane, C.S., Brauer, A., Blockley, S.P.E., Dulski, P., 2013. Volcanic ash reveals time-transgressive abrupt climate change during the Younger Dryas. Geology 41, 1251–1254. doi:10.1130/G34867.1

Lane, C.S., Lowe, D.J., Blockley, S.P.E., Suzuki, T., Smith, V.C., 2017. Advancing tephrochronology as a global dating tool: Applications in volcanology, archaeology, and palaeoclimatic research. Quat. Geochronol. 40, 1–7. https://doi.org/10.1016/j.quageo.2017.04.003

Larsen, J.F., Neal, C., Schaefer, J., Beget, J.E., Nye, C.J., 2007. Late Pleistocene and Holocene Caldera-Forming Eruptions of Okmok Caldera, Aleutian Islands, Alaska, in: Eichelberger, J., Gordeev, E., Izbekov, P., Kasahara, M., Lees, J., (Eds.), Volcanism and Subduction: The Kamchatka Region, Geophysical Monograph Series 172. American Geophysical Union, Washington, D. C. doi:10.1029/172GM24

Lawson, I.T., Swindles, G.T., Plunkett, G., Greenberg, D., 2012. The spatial distribution of Holocene cryptotephras in north-west Europe since 7 ka: Implications for understanding ash fall events from Icelandic eruptions. Quat. Sci. Rev. 41, 57–66. https://doi.org/10.1016/j.quascirev.2012.02.018

Le Roux, G., Aubert, D., Stille, P., Krachler, M., Kober, B., Cheburkin, A., Bonani, G., Shotyk, W., 2005. Recent atmospheric Pb deposition at a rural site in southern Germany assessed using a peat core and snowpack, and comparison with other archives. Atmos. Environ. 39, 6790–6801. https://doi.org/10.1016/j.atmosenv.2005.07.026

Le Roux, G., Fagel, N., de Vleeschouwer, F., Krachler, M., Debaille, V., Stille, P., Mattielli, N., van der Knaap, W.O., van Leeuwen, J.F.N., Shotyk, W., 2012. Volcano- and climate-driven changes in atmospheric dust sources and fluxes since the late glacial in Central Europe. Geology 40, 335–338. https://doi.org/10.1130/G32586.1

Le Roux, G., Marshall, W.A., 2011. Constructing recent peat accumulation chronologies using atmospheric fall-out radionuclides. Mires Peat 7, 1–14.

Lerbekmo, J.F., 2008. The White River Ash: Largest Holocene Plinian tephra. Canadian Journal of Earth Sciences 45, 693–700, doi:10.1139/E08-023.

Lerbekmo, J.F., Campbell, F.A., 1969. Distribution, composition, and the source of the White River Ash, Yukon Territory. Canadian Journal of Earth Sciences 6, 109–116. doi:10.1139/e69 -011 .

Leberkmo, J.F., Westgate, J.A., Smith, D.G., Denton, G.H., 1975. New data on the character and history of the White River volcanic eruption, Alaska, in: Suggate, R.P., Cresswell, M.M. (Eds.), Quaternary Studies. Royal Society of New Zealand, Wellington, pp. 203–209.

Litton, C.D., Buck, C.E., 1995. The Bayesian Approach To the Interpretation of Archaeological Data. Archaeometry 37, 1–24. https://doi.org/10.1111/j.1475-4754.1995.tb00723.x

Livingston, J.M., Smith, D.G., Froese, D.G., Hugenholtz, C.H., 2009. Floodplain stratigraphy of the ice jam dominated middle Yukon River: a new approach to long-term flood frequency. Hydrol. Process. 23, 357–371. https://doi.org/10.1002/hyp.7106

Lohne, O.S., Mangerud, J., Birks, H.H., 2013. Precise 14C ages of the Vedde and Saksunarvatn ashes and the Younger Dryas boundaries from western Norway and their comparison with the Greenland Ice Core (GICC05) chronology. J. Quat. Sci. 28, 490–500. https://doi.org/10.1002/jqs.2640

Łokas, E., Mietelski, J.W., Ketterer, M.E., Kleszcz, K., Wachniew, P., Michalska, S., Miecznik, M., 2013. Sources and vertical distribution of 137Cs, 238Pu, 239+240Pu and 241Am in peat profiles from southwest Spitsbergen. Appl. Geochemistry 28, 100–108. https://doi.org/10.1016/j.apgeochem.2012.10.027

Lowe, D.J., 2011. Tephrochronology and its application: A review. Quat. Geochronol. 6, 107–153. https://doi.org/10.1016/j.quageo.2010.08.003

Lowe, D.J., Alloway, B., 2014. Tephrochronology, in: Rink, W.J., Thompson, J. (Eds.), Encyclopedia of Scientific Dating Methods. Springer Netherlands, Dordrecht, p. 26. https://doi.org/10.1007/978-94-007-6326-5_19-2

Lowe, D.J., McFadgen, B.G., Higham, T.F.G., Hogg, A.G., Froggatt, P.C., Nairn, I.A., 1998. Radiocarbon age of the Kaharoa Tephra, a key marker for late- Holocene stratigraphy and archaeology in New Zealand. The Holocene 8, 487–495. doi:10.1191/095968398667037879

Lowe, D.J., Blaauw, M., Hogg, A.G., Newnham, R.M., 2013. Ages of 24 widespread tephras erupted since 30,000 years ago in New Zealand, with re-evaluation of the timing and palaeoclimatic implications of the Lateglacial cool episode recorded at Kaipo bog. Quat. Sci. Rev. 74, 170–194. https://doi.org/10.1016/j.quascirev.2012.11.022

Lowe, D.J., Shane, P.A.R., Alloway, B. V., Newnham, R.M., 2008. Fingerprints and age models for widespread New Zealand tephra marker beds erupted since 30,000 years ago: a framework for NZ-INTIMATE. Quat. Sci. Rev. 27, 95–126. https://doi.org/10.1016/j.quascirev.2007.01.013

Lowe, J.J., Walker, M.J.C., 2000. Radiocarbon dating the last glacial-interglacial transition (ca. 14-9 ^{14}C ka BP) in terrestrial and marine records: The need for new quality assurance protocols. Radiocarbon 42, 53–68.

Lowe, J.J., Blockley, S., Trincardi, F., Asioli, A., Cattaneo, A., Matthews, I.P., Pollard, M., Wulf, S., 2007. Age modelling of late Quaternary marine sequences in the Adriatic: Towards improved precision and accuracy using volcanic event stratigraphy. Continental Shelf Research 27, 560–582. doi:10.1016/j.csr.2005.12.017

Lowe, J.J., Barton, N., Blockley, S., Ramsey, C.B., Cullen, V.L., Davies, W., Gamble, C., Grant, K., Hardiman, M., Housley, R., Lane, C.S., Lee, S., Lewis, M., MacLeod, A., Menzies, M., Müller, W., Pollard, M., Price, C., Roberts, A.P., Rohling, E.J., Satow, C., Smith, V.C., Stringer, C.B., Tomlinson, E.L., White, D., Albert, P., Arienzo, I., Barker, G., Borić, D., Carandente, A., Civetta, L., Ferrier, C., Guadelli, J.-L., Karkanas, P., Koumouzelis, M., Müller, U.C., Orsi, G., Pross, J., Rosi, M., Shalamanov-Korobar, L., Sirakov, N., Tzedakis, P.C., 2012. Volcanic ash layers illuminate the resilience of Neanderthals and early modern humans to natural hazards. Proceedings of the National Academy of Sciences 109, 13532–13537. doi:10.1073/pnas.1204579109

Lowe, J.J., Ramsey, C.B., Housley, R.A., Lane, C.S., Tomlinson, E.L., Stringer, C., Davies, W., Barton, N., Pollard, M., Gamble, C., Menzies, M., Rohling, E., Roberts, A., Blockley, S., Cullen, V., Grant, K., Lewis, M., MacLeod, A., White, D., Albert, P., Hardiman, M., Lee, S., Oh, A., Satow, C., Cross, J.K., Law, C.B., Todman, A., Bourne, A., Matthews, I., Müller, W., Smith, V., Wulf, S., Anghelinu, M., Antl-Weiser, W., Bar-Yosef, O., Boric, D., Boscato, P., Ronchitelli, A., Chabai, V., Veselsky, A., Uthmeier, T., Farrand, W., Gjipali, I., Ruka, R., Güleç, E., Karavanic, I., Karkanas, P., King, T., Komšo, D., Koumouzelis, M., Kyparissi, N., Lengyel, G., Mester, Z., Neruda, P., Panagopoulou, E., Shalamanov-Korobar, L., Tolevski, I., Sirakov, N., Guadelli, A., Guadelli, J.L., Ferrier, C., Skrdla, P., Slimak, L., Soler, N., Soler, J., Soressi, M., Tushabramishvilii, N., Zilhão, J., Angelucci, D., Albert, P., Bramham Law, C., Cullen, V.L., Lincoln, P., Staff, R., Flower, K., Aouadi-Abdeljaouad, N., Belhouchet, L., Barker, G., Bouzouggar, A., Van Peer, P., Kindermann, K., Gerken, K., Niemann, H., Tipping, R., Saville, A., Ward, T., Clausen, I., Weber, M.J., Kaiser, K., Torksdorf, J.F., Turner, F., Veil, S., Nygaard, N., Pyne-O'Donnell, S.D.F., Masojc, M., Nalepka, D., Jurochnik, A., Kabacinski, J., Antoine, P., Olive, M., Christensen, M., Bodu, P., Debout, G., Orliac, M., De Bie, M., Van Gils, M., Paulissen, E., Brou, L., Leesch, D., Hadorn, P., Thew, N., Riede, F., Heinen, M., Joris, O., Richter, J., Uthmeier, T., Knipping, M., Stika, H.P., Friedrich, M., Conard, N., Malina, M., Kind, C.J., Beutelspacher, T., Mortensen, M.F., Burdukiewicz, J.M., Szynkiewicz, A., Poltowicz-Bobak, M., Bobak, D., Wisniewski, A., Przezdziecki, M., Valde-Nowak, P., Muzyczuk, A., Bramham Law, C., Cullen, V.L., Davies, L., Lincoln, P., MacLeod, A., Morgan, P., Aydar, E., çubukçu, E., Brown, R., Coltelli, M., Castro, D. Lo, Cioni, R., DeRosa, R., Donato, P., Roberto, A. Di, Gertisser, R., Giordano, G., Branney, M., Jordan, N., Keller, J., Kinvig, H., Gottsman, J., Blundy, J., Marani, M., Orsi, G., Civetta, L., Arienzo, I., Carandente, A., Rosi, M., Zanchetta, G., Seghedi, I., Szakacs, A., Sulpizio, R., Thordarson, T., Trincardi, F., Vigliotti, L., Asioli, A., Piva, A., Andric, M., Brauer, A., de Klerk, P., Filippi, M.L., Finsinger, W., Galovic, L., Jones, T., Lotter, A., Müller, U., Pross, J., Mangerud, J., Lohne, Pyne-O'Donnell, S., Markovic, S., Pini, R., Ravazzi, C., Riede, F., TheuerKauf, M., Tzedakis, C., Margari, V., Veres, D., Wastegård, S., Ortiz, J.E., Torres, T., Díaz-Bautista, A., Moreno, A., Valero-Garcés, B., Lowick, S., Ottolini, L., 2015. The RESET project: Constructing a European tephra lattice for refined synchronisation of environmental and archaeological events during the last c. 100 ka. Quat. Sci. Rev. 118, 1–17. https://doi.org/10.1016/j.quascirev.2015.04.006

Lusa, M., Bomberg, M., Virtanen, S., Lempinen, J., Aromaa, H., Knuutinen, J., Lehto, J., 2015. Factors affecting the sorption of cesium in a nutrient-poor boreal bog. J. Environ. Radioact. 147, 22–32. https://doi.org/10.1016/j.jenvrad.2015.05.005

Lynch, J.A., Clark, J.S., Bigelow, N.H., Edwards, M.E., Finney, B.P., 2002. Geographic and temporal variations in fire history in boreal ecosystems of Alaska. Journal of Geophysical Research 108, 8152–17. doi:10.1029/2001JD000332

Macáas, J.L., Sheridan, M.F., 1995. Products of the 1907 eruption of Shtyubel' Volcano, Ksudach Caldera, Kamchatka, Russia. Geological Society of America Bulletin 107, 969–0986. doi:10.1130/0016-7606(1995)107<0969:POTEOS>2.3.CO;2

Mackay, H., Hughes, P.D.M., Jensen, B.J.L., Langdon, P.G., Pyne-O'Donnell, S.D.F., Plunkett, G., Froese, D.G., Coulter, S.E., Gardner, J.E., 2016. A mid to late Holocene cryptotephra framework from eastern North America. Quat. Sci. Rev. 132, 101–113. https://doi.org/10.1016/j.quascirev.2015.11.011

MacKenzie, A.B., Farmer, J.G., Sugden, C.L., 1997. Isotopic evidence of the relative retention and mobility of lead and radiocaesium in Scottish ombrotrophic peats. Sci. Total Environ. 203, 115–127. https://doi.org/10.1016/S0048-9697(97)00139-3

MacLeod, A., Matthews, I.P., Lowe, J.J., Palmer, A.P., Albert, P.G., 2015. A second tephra isochron for the Younger Dryas period in northern Europe: The Abernethy Tephra. Quaternary Geochronology 28, 1–11. doi:10.1016/j.quageo.2015.03.010

Magnan, G., van Bellen, S., Davies, L., Froese, D., Garneau, M., Mullan-Boudreau, G., Zaccone, C., Shotyk, W., 2018. Impact of the Little Ice Age cooling and 20th century climate change on peatland vegetation dynamics in central and northern Alberta using a multi-proxy approach and high-resolution peat chronologies. Quat. Sci. Rev. 185, 230–243. https://doi.org/10.1016/j.quascirev.2018.01.015

Mangan, M.T., Waythomas, C.F., Miller, T.P., Trusdell, F.A., 2003. Emmons Lake Volcanic Center, Alaska Peninsula: source of the Late Wisconsin Dawson tephra, Yukon Territory, Canada. Can. J. Earth Sci. 40, 925–936. doi:10.1139/e03-026

Martínez, C.E., McBride, M.B., 1999. Dissolved and labile concentrations of Cd, Cu, Pb, and Zn in aged ferrihydrite - Organic matter systems. Environ. Sci. Technol. 33, 745–750. https://doi.org/10.1021/es980576c

Matthews, I.P., Birks, H.H., Bourne, A.J., Brooks, S.J., Lowe, J.J., MacLeod, A., Pyne-O'Donnell, S.D.F., 2011. New age estimates and climatostratigraphic correlations for the Borrobol and Penifiler Tephras: evidence from Abernethy Forest, Scotland. Journal of Quaternary Science 26, 247–252. doi:10.1002/jqs.1498

McGimsey, R.G., Richter, D.H., duBois, G.D., Miller, T.P., 1992. A Postulated New Source for the White River Ash, Alaska, in: Bradley, D.C., Ford, A.B., (Eds.), U.S. Geological Survey Bulletin B 1999, 212-218.

McGimsey, RG, Neal, CA, Riley, CM (2001) Areal Distribution, Thickness, Mass, Volume, and Grain Size of Tephra-Fall Deposits from the 1992 Eruptions of Crater Peak Vent, Mt. Spurr Volcano, Alaska. USGS Open-File Report 01–370, p. 32.

McKay, N.P., Kaufman, D.S., 2014. An extended Arctic proxy temperature database for the past 2,000 years. Sci. Data 1, 1–10. https://doi.org/10.1038/sdata.2014.26

Miller, T.P., McGimsey, R.G., Richter, D.H., Riehle, J.R., Nye, G.J., Yount, M.E., Dumoulin, J.A., 1998. Catalog of the historically active volcanoes of Alaska (No. 98–582), Open-File Report. U.S. Dept. of the Interior, U.S. Geological Survey.

Miller, T.P., Smith, R.L., 1987. Late Quaternary caldera-forming eruptions in the eastern Aleutian arc, Alaska. Geology 15, 434–438. https://doi.org/10.1130/0091-7613(1987)15<434:LQCEIT>2.0.CO;2

Miller, T.P., Smith, R.L., 1977. Spectacular mobility of ash flows around Aniakchak and Fisher calderas, Alaska. Geology 5, 173. https://doi.org/10.1130/0091-7613(1977)5<173:SMOAFA>2.0.CO;2

Miller, T.P., McGimsey, R.G., Richter, D.H., Riehle, J.R., Nye, C.J., Yount, M.E., Dumoulin, J.A., 1998. Catalog of the historically active volcanoes of Alaska, U.S. Geological Survey Open-File Report OF 98-0582, p. 104.

Monteath, A.J., van Hardenbroek, M., Davies, L.J., Froese, D.G., Langdon, P.G., Xu, X., Edwards, M.E., 2017. Chronology and glass chemistry of tephra and cryptotephra horizons from lake sediments in northern Alaska, USA. Quat. Res. 88, 169–178. https://doi.org/10.1017/qua.2017.38

Moodie, D.W., Catchpole, A.J.W., Abel, K., 1992. Northern Athapaskan Oral Traditions and the White River Volcano. Ethnohistory 39, 148. doi:10.2307/482391

Morgan, G.B., London, D., 2005. Effect of current density on the electron microprobe analysis of alkali aluminosilicate glasses. Am. Mineral. 90, 1131–1138. https://doi.org/10.2138/am.2005.1769

Moriwaki, H., Nakamura, N., Nagasako, T., Lowe, D.J., Sangawa, T., 2016. The role of tephras in developing a high-precision chronostratigraphy for palaeoenvironmental reconstruction and archaeology in southern Kyushu, Japan, since 30,000 cal. BP: An integration. Quaternary International 397, 79–92. doi:10.1016/j.quaint.2015.05.069

Muhs, D.R., Ager, T.A., Been, J., Bradbury, J.P., Dean, W.E., 2003. A late quaternary record of eolian silt deposition in a maar lake, St. Michael Island, western Alaska. Quat. Res. 60, 110–122. https://doi.org/10.1016/S0033-5894(03)00062-0

Mullen, P.O., 2012. An archaeological test of the effects of the White River Ash eruptions: Arctic Anthropology 49, 35–44, doi:10.1353 /arc.2012.0013.

Mullan-Boudreau, G., Belland, R., Devito, K.J., Noernberg, T., Pelletier, R., Shotyk, W., 2017. Sphagnum Moss as an Indicator of Contemporary Rates of Atmospheric Dust Deposition in the Athabasca Bituminous Sands Region. Environ. Sci. Technol. 51, 7422–7431. https://doi.org/10.1021/acs.est.6b06195

Mulliken, K., 2016. Holocene Volcanism and Human Occupation in the Middle Susitna River Valley, Alaska. University of Alaska, Fairbanks.

Mullineaux, D., 1996. Pre-1980 tephra-fall deposits erupted from Mount St. Helens, Washington. (No. 1563), Professional Paper.

Muscheler, R., Adolphi, F., Knudsen, M.F., 2014. Assessing the differences between the IntCal and Greenland ice-core time scales for the last 14,000 years via the common cosmogenic radionuclide variations. Quat. Sci. Rev. 106, 81–87. https://doi.org/10.1016/j.quascirev.2014.08.017

Naeser, N.D., Westgate, J.A., Hughes, O.L., Péwé, T.L., 1982. Fission-track ages of late Cenozoic distal tephra beds in the Yukon Territory and Alaska. Canadian Journal of Earth Sciences 19, 2167–2178. doi:10.1139/e82-191

Nakagawa, M., Ishizuka, Y., Hasegawa, T., Baba, A., Kosugi, A., 2008. Preliminary Report on Volcanological Research of KBP 2007-08 Cruise by Japanese Volcanology group. Sapporo. https://doi.org/10.6067/XCV8668F2H

Narcisi, B., Petit, J.R., Delmonte, B., Scarchilli, C., Stenni, B., 2012. A 16,000-yr tephra framework for the Antarctic ice sheet: A contribution from the new Talos Dome core. Quat. Sci. Rev. 49, 52–63. https://doi.org/10.1016/j.quascirev.2012.06.011

Neal, C. a., McGimsey, R.G., Miller, T.P., Riehle, J.R., Waythomas, C.F., 2001. Preliminary Volcano-Hazard Assessment for Aniakchak Volcano , Alaska. USGS Open-File Rep. 00–519, 1–35.

Nelson, R.E., Carter, L.D., Robinson, S.W., 1988. Anomalous radiocarbon ages from a Holocene detrital organic lens in Alaska and their implications for radiocarbon dating and paleoenvironmental reconstructions in the arctic. Quaternary Research 29, 66–71. doi:10.1016/0033-5894(88)90072-5

Nielsen, C.H., Sigurdsson, H., 1981. Quantitative methods for electron microprobe analysis of sodium in natural and synthetic glasses. Am. Mineral. 66, 547–552.

Nilsson, M., Klarqvist, M., Possnert, G., 2001. Variation in 14C age of macrofossils and different fractions of minute peat samples dated by AMS. The Holocene 11, 579–586. https://doi.org/10.1191/095968301680223521

Novák, M., Zemanova, L., Voldrichova, P., Stepanova, M., Adamova, M., Pacherova, P., Komarek, A., Krachler, M., Prechova, E., 2011. Experimental evidence for mobility/immobility of metals in peat. Environ. Sci. Technol. 45, 7180–7187. https://doi.org/10.1021/es201086v

Oldfield, F., Appleby, P.G., Cambray, R.S., Eakins, J.D., Barber, K.E., Battarbee, R.W., Pearson, G.R., Williams, J.M., 1979. 210 Pb, 137 Cs and 239 Pu Profiles in Ombrotrophic Peat. Oikos 33, 40. https://doi.org/10.2307/3544509

Oldfield, F., Richardson, N., Appleby, P.G., 1995. Radiometric dating (210Pb, 137Cs, 241Am) of recent ombrotrophic peat accumulation and evidence for changes in mass balance. The Holocene 5, 141–148. https://doi.org/10.1177/095968369500500202

Oldfield, F., Thompson, R., Crooks, P.R.J., Gedye, S.J., Hall, V.A., Harkness, D.D., Housley, R. a., McCormac, F.G., Newton, A.J., Pilcher, J.R., Renberg, I., Richardson, N., 1997. Radiocarbon dating of a recent high latitude peat profile: Stor Åmyran, northern Sweden. The Holocene 7, 283–290. https://doi.org/10.1177/095968369700700304

Oldfield, F., Tolonen, K., Thompson, R., 1981. History of particulate atmospheric pollution from magnetic measurements in dated Finnish peat profiles. Ambio 10, 185–188.

Olid, C., Diego, D., Garcia-Orellana, J., Cortizas, A.M., Klaminder, J., 2016. Modeling the downward transport of 210Pb in Peatlands: Initial Penetration-Constant Rate of Supply (IP-CRS) model. Sci. Total Environ. 541, 1222–1231. https://doi.org/10.1016/j.scitotenv.2015.09.131

Olsson, I.U., 1974. Some problems in connection with the evaluation of C 14dates. Geologiska Föreningen i Stockholm Förhandlingar 96, 311–320. doi:10.1080/11035897409454285

Olsson, I., 1986. Radiometric Methods, in: Berglund B (Ed) Handbook of Holocene palaeoecolgy and palaeohydrology. John Wiley and Sons, Chichester, 273-312.

Osborn, G., 1985. Holocene tephrostratigraphy and glacial fluctuations in Waterton Lakes and Glacier national parks, Alberta and Montana. Can. J. Earth Sci. 22, 1093–1101. https://doi.org/10.1139/e85-111

Oswald, W.W., Anderson, P.M., Brown, T.A., Brubaker, L.B., Hu, F.S., Lozhkin, A.V., Tinner, W., Kaltenrieder, P., 2005. Effects of sample mass and macrofossil type on radiocarbon dating of arctic and boreal lake sediments. The Holocene 15, 758–767. doi:10.1191/0959683605hl849rr

Parry, L.E., Charman, D.J., Blake, W.H., 2013. Comparative dating of recent peat deposits using natural and anthropogenic fallout radionuclides and Spheroidal Carbonaceous Particles (SCPs) at a local and landscape scale. Quat. Geochronol. 15, 11–19. https://doi.org/10.1016/j.quageo.2013.01.002

Patterson, R.T., Crann, C.A., Cutts, J.A., Courtney Mustaphi, C.J., Nasser, N.A., Macumber, A.L., Galloway, J.M., Swindles, G.T., Falck, H., 2017. New occurrences of the White River Ash (east lobe) in Subarctic Canada and utility for estimating freshwater reservoir effect in lake sediment archives. Palaeogeogr. Palaeoclimatol. Palaeoecol. 477, 1–9. https://doi.org/10.1016/j.palaeo.2017.03.031

Payne, R., Blackford, J., van der Plicht, J., 2008. Using cryptotephras to extend regional tephrochronologies: An example from southeast Alaska and implications for hazard assessment. Quat. Res. 69, 42–55. https://doi.org/10.1016/j.yqres.2007.10.007

Payne, R.J., Blackford, J.J., 2008. Extending the late holocene tephrochronology of the central Kenai Peninsula, Alaska. Arctic 61, 243–254.

Payne, R.J., Gehrels, M., 2010. The formation of tephra layers in peatlands: An experimental approach. Catena 81, 12–23. https://doi.org/10.1016/j.catena.2009.12.001

Payne, R.J., Kilfeather, A.A., van der Meer, J.J.M., Blackford, J.J., 2005. Experiments on the taphonomy of tephra in peat. Suo 56, 147–156.

Pearce, C., Varhelyi, A., Wastegärd, S., Muschitiello, F., Barrientos, N., O'Regan, M., Cronin, T.M., Gemery, L., Semiletov, I., Backman, J., Jakobsson, M., 2017. The 3.6ka Aniakchak tephra in the Arctic Ocean: A constraint on the Holocene radiocarbon reservoir age in the Chukchi Sea. Clim. Past 13, 303–316. https://doi.org/10.5194/cp-13-303-2017

Pearce, N.J.G., Westgate, J.A., Preece, S.J., Eastwood, W.J., Perkins, W.T., 2004. Identification of Aniakchak (Alaska) tephra in Greenland ice core challenges the 1645 BC date for Minoan eruption of Santorini. Geochemistry, Geophys. Geosystems 5. https://doi.org/10.1029/2003GC000672

Petrone, R.M., Devito, K.J., Mendoza, C., 2016. Utikuma Region Study Area (URSA) - Part 2: Aspen Harvest and Recovery Study. For. Chron. 92, 62–65. https://doi.org/10.5558/tfc2016-018

Péwé, T.L., 1975a. Quaternary stratigraphic nomenclature in unglaciated Central Alaska. U.S. Geol. Surv. Prof. Pap. 862, 1.

Péwé, T.L., 1975b. Quaternary Geology of Alaska. U.S. Geol. Surv. Prof. Pap., Geological Survery Professional Paper 835.

Péwé, T.L., Westgate, J.A., Preece, S.J., Brown, P.M., Leavitt, S.W., 2009. Late pliocene dawson cut forest bed and new tephrochronological findings in the Gold Hill Loess, east-central Alaska. Bull. Geol. Soc. Am. 121, 294–320. https://doi.org/10.1130/B26323.1

Pilcher, J.R., Hall, V.A., McCormac, F.G., 1995. Dates of Holocene Icelandic volcanic eruptions from tephra layers in Irish peats. The Holocene 5, 103–110. https://doi.org/10.1177/095968369500500111

Pilcher, J.R., Hall, V.A., McCormac, F.G., 1996. An outline tephrochronology for the Holocene of the north of Ireland. Journal of Quaternary Science 11, 485–494. doi:10.1002/(SICI)1099-1417(199611/12)11:6<485::AID-JQS266>3.3.CO;2-K

Piotrowska, N., Blaauw, M., Mauquoy, D., Chambers, F.M., 2011. Constructing deposition chronologies for peat deposits using radiocarbon dating. Mires Peat 7, 1–14.

Piotrowska, N., De Vleeschouwer, F., Sikorski, J., Pawlyta, J., Fagel, N., Le Roux, G., Pazdur, A., 2010. Intercomparison of radiocarbon bomb pulse and 210Pb age models. A study in a peat bog core from North Poland. Nucl. Instruments Methods Phys. Res. Sect. B Beam Interact. with Mater. Atoms 268, 1163–1166. https://doi.org/10.1016/j.nimb.2009.10.124

Plunkett, G., 2006. Tephra-linked peat humification records from Irish ombrotrophic bogs question nature of solar forcing at 850 cal. yr BC. J. Quat. Sci. 21, 9–16. https://doi.org/10.1002/jqs.951

Plunkett, G., Coulter, S.E., Ponomareva, V. V., Blaauw, M., Klimaschewski, A., Hammarlund, D., 2015. Distal tephrochronology in volcanic regions: Challenges and insights from Kamchatkan lake sediments. Glob. Planet. Change 134, 26–40. https://doi.org/10.1016/j.gloplacha.2015.04.006

Ponomareva, V., Polyak, L., Portnyagin, M., Abbott, P.M., Zelenin, E., Vakhrameeva, P., Garbe-Schönberg, D., 2018. Holocene tephra from the Chukchi-Alaskan margin, Arctic Ocean: Implications for sediment chronostratigraphy and volcanic history. Quat. Geochronol. 45, 85–97. https://doi.org/10.1016/j.quageo.2017.11.001

Ponomareva, V., Polyak, L., Portnyagin, M., Abbott, P.M., Zelenin, E., Vakhrameeva, P., Garbe-Schönberg, D., 2017a. Holocene tephra from the Chukchi-Alaskan margin, Arctic Ocean: Implications for sediment chronostratigraphy and volcanic history. Quat. Geochronol. https://doi.org/10.1016/j.quageo.2017.11.001

Ponomareva, V., Portnyagin, M., Pendea, I.F., Zelenin, E., Bourgeois, J., Pinegina, T., Kozhurin, A., 2017b. A full holocene tephrochronology for the Kamchatsky Peninsula region: Applications from Kamchatka to North America. Quat. Sci. Rev. 168, 101–122. https://doi.org/10.1016/j.quascirev.2017.04.031

Ponomareva, V. V., Polyak, L., Portnyagin, M. V., Abbott, P.M., Davies, S., 2014. A Holocene cryptotephra record from the Chukchi margin: the first tephrostratigraphic study in the Arctic Ocean., in: PAST Gateways International Conference and Workshop. Trieste, Italy.

Praetorius, S., Mix, A., Jensen, B., Froese, D., Milne, G., Wolhowe, M., Addison, J., Prahl, F., 2016. Interaction between climate, volcanism, and isostatic rebound in Southeast Alaska during the last deglaciation. Earth Planet. Sci. Lett. 452, 79–89. https://doi.org/10.1016/j.epsl.2016.07.033

Pratte, S., Mucci, A., Garneau, M., 2013. Historical records of atmospheric metal deposition along the St. Lawrence Valley (eastern Canada) based on peat bog cores. Atmos. Environ. 79, 831–840. https://doi.org/10.1016/j.atmosenv.2013.07.063

Preece, S.J., McGimsey, R.G., Westgate, J.A., Pearce, N.J.G., Hart, W.K., Perkins, W.T., 2014. Chemical complexity and source of the White River Ash, Alaska and Yukon. Geosphere 10, 1020–1042. https://doi.org/10.1130/GES00953.1

Preece, S.J., Pearce, N.J.G., Westgate, J.A., Froese, D.G., Jensen, B.J.L., Perkins, W.T., 2011a. Old Crow tephra across eastern Beringia: A single cataclysmic eruption at the close of Marine Isotope Stage 6. Quat. Sci.Rev. 30, 2069–2090. https://doi.org/10.1016/j.quascirev.2010.04.020

Preece, S.J., Westgate, J.A., Froese, D.G., Pearce, N.J.G., Perkins, W.T., Fisher, T., 2011b. A catalogue of late Cenozoic tephra beds in the Klondike goldfields and adjacent areas, Yukon Territory [1 1] Yukon Geological Survey Contribution 010. Can. J. Earth Sci. 48, 1386–1418. https://doi.org/10.1139/e10-110

Preece, S.J., Westgate, J.A., Stemper, B.A., Péwé, T.L., 1999. Tephrochronology of late Cenozoic loess at Fairbanks, central Alaska. Bull. Geol. Soc. Am. 111, 71–90. https://doi.org/10.1130/0016-7606(1999)111<0071:TOLCLA>2.3.CO;2

Pyne-O'Donnell, S.D.F., 2007. Three new distal tephras in sediments spanning the Last Glacial–Interglacial Transition in Scotland. Journal of Quaternary Science 22, 559–570. doi:10.1002/jqs.1066

Pyne-O'Donnell, S.D.F., 2011. The taphonomy of Last Glacial-Interglacial Transition (LGIT) distal volcanic ash in small Scottish lakes. Boreas 40, 131–145. https://doi.org/10.1111/j.1502-3885.2010.00154.x

Pyne-O'Donnell, S.D.F., Cwynar, L.C., Jensen, B.J.L., Vincent, J.H., Kuehn, S.C., Spear, R., Froese, D.G., 2016. West Coast volcanic ashes provide a new continental-scale Lateglacial isochron. Quat. Sci. Rev. 142, 16–25. https://doi.org/10.1016/j.quascirev.2016.04.014

Pyne-O'Donnell, S.D.F., Hughes, P.D.M., Froese, D.G., Jensen, B.J.L., Kuehn, S.C., Mallon, G., Amesbury, M.J., Charman, D.J., Daley, T.J., Loader, N.J., Mauquoy, D., Street-Perrott, F.A., Woodman-Ralph, J., 2012. High-precision ultra-distal Holocene tephrochronology in North America. Quat. Sci. Rev. 52, 6–11. https://doi.org/10.1016/j.quascirev.2012.07.024

Rausch, N., Nieminen, T., Ukonmaanaho, L., Le Roux, G., Krachler, M., Cheburkin, A.K., Bonani, G., Shotyk, W., 2005. Comparison of atmospheric deposition of copper, nickel, cobalt, zinc, and cadmium recorded by Finnish peat cores with monitoring data and emission records. Environ. Sci. Technol. 39, 5989–5998. https://doi.org/10.1021/es050260m

Reger, R.D., Pinney, D.S., Burke, R.M., Wiltse, M.A., 1995. Catalog and initial analyses of geologic data related to middle to late Quaternary deposits, Cook Inlet region, Alaska. Report of Investigations 95-6.

Reimer, P.J., Baillie, M.G.L., Bard, E., Bayliss, A., Beck, J.W., Blackwell, P.G., Bronk Ramsey, C., Buck, C.E., Burr, G.S., Edwards, R.L., Friedrich, M., Grootes, P.M., Guilderson, T.P., Hajdas, I., Heaton, T.J., Hogg, A.G., Hughen, K.A., Kaiser, K.F., Kromer, B., McCormac, F.G., Manning, S.W., Reimer, R.W., Richards, D.A., Southon, J.R., Talamo, S., Turney, C.S.M., van der Plicht, J., Weyhenmeyer, C.E., 2009. IntCal09 and Marine09 Radiocarbon Age Calibration Curves, 0–50,000 Years cal BP. Radiocarbon 51, 1111–1150. https://doi.org/10.1017/S0033822200034202

Reimer, P.J., Bard, E., Bayliss, A., Beck, J.W., Blackwell, P.G., Bronk Ramsey, C., Buck, C.E., Cheng, H., Edwards, R.L., Friedrich, M., Grootes, P.M., Guilderson, T.P., Haflidason, H., Hajdas, I., Hatté, C., Heaton, T.J., Hoffmann, D.L., Hogg, A.G., Hughen, K.A., Kaiser, K.F., Kromer, B., Manning, S.W., Niu, M., Reimer, R.W., Richards, D.A., Scott, E.M., Southon, J.R., Staff, R.A., Turney, C.S.M., van der Plicht, J., 2013. IntCal13 and Marine13 Radiocarbon Age Calibration Curves 0–50,000 Years cal BP. Radiocarbon 55, 1869–1887. https://doi.org/10.2458/azu_js_rc.55.16947

Reyes, A.V., Cooke, C.A., 2011. Northern peatland initiation lagged abrupt increases in deglacial atmospheric CH4. Proceedings of the National Academy of Sciences 108, 4748–4753. doi:10.1073/pnas.1013270108

Reyes, A. V., Jensen, B.J.L., Zazula, G.D., Ager, T.A., Kuzmina, S., La Farge, C., Froese, D.G., 2010. A late-Middle Pleistocene (Marine Isotope Stage 6) vegetated surface buried by Old Crow tephra at the Palisades, interior Alaska. Quat. Sci. Rev. 29, 801–811. https://doi.org/10.1016/j.quascirev.2009.12.003

Richter, D.H., Preece, S.J., McGimsey, R.G., Westgate, J.A., 1995. Mount Churchill, Alaska: source of the late Holocene White River Ash. Canadian Journal of Earth Sciences 32, 741–748. doi:10.1139/e95-063

Riehle, J.R., 1985. A reconnaissance of the major Holocene tephra deposits in the upper Cook Inlet region, Alaska. Journal of Volcanology and Geothermal Research 26, 37–74. doi:10.1016/0377-0273(85)90046-0

Riehle, J.R., 1994. Heterogeneity, Correlatives, and Proposed Stratigraphic Nomenclature of Hayes Tephra Set H, Alaska. Quaternary Research 41, 285–288. doi:10.1006/qres.1994.1032

Riehle, J.R., Brew, D.A., 1984. Explosive latest Pleistocene(?) and Holocene activity of the Mount Edgecumbe volcanic field, Alaska. In: Reed, K.M., Bartsch-Winkler, S. (Eds.), The United States Geological Survey in Alaska: accomplishments during 1982, 111–115.

Riehle, J.R., Meyer, C.E., Ager, T.A., Kaufman, D.S., Ackerman, R.E., 1987. The Aniakchak tephra deposit, a late Holocene marker horizon in western Alaska, in: Hamilton, T.D., Galloway, J.P. (Eds.) Geologic Studies in Alaska by the U.S. Geological Survey during 1986. U.S. Geological Survey Circular 998.

Riehle, J.R., Bowers, P.M., Ager, T.A., 1990. The Hayes tephra deposits, and upper Holocene marker horizon in south-central Alaska. Quaternary Research 33, 276–290. doi:10.1016/0033-5894(90)90056-Q

Riehle, J. R., Meyer, C. E., Miyaoka, R. T., 1999. Data on Holocene tephra (volcanic ash) deposits in the Alaska Peninsula and lower Cook Inlet region of the Aleutian volcanic arc, Alaska: U.S. Geological Survey Open-File Report OF 99-0135.

Robinson, S.D., 2001. Extending the late Holocene White River ash distribution, northwestern Canada. Arctic 54, 157–161.

Robinson, S.D., Turetsky, M.R., Kettles, I.M., Wieder, R.K., 2003. Permafrost and peatland carbon sink capacity with increasing latitude, in: Phillips, M., Springman, S., Arenson, L. (Eds.), Proceedings of the 8th International Conference on Permafrost. Balkema Publishers, Zurich, pp. 965–970.

Roland, T.P., Mackay, H., Hughes, P.D.M., 2015. Tephra analysis in ombrotrophic peatlands: A geochemical comparison of acid digestion and density separation techniques. J. Quat. Sci. 30, 3–8. https://doi.org/10.1002/jqs.2754

Roos-Barraclough, F., Martinez-Cortizas, A., Garcia-Rodeja, E., Shotyk, W., 2002. A 14 500 year record of the accumulation of atmospheric mercury in peat: Volcanic signals, anthropogenic influences and a correlation to bromine accumulation. Earth Planet. Sci. Lett. 202, 435–451. https://doi.org/10.1016/S0012-821X(02)00805-1

Roos-Barraclough, F., Shotyk, W., 2003. Millennial-scale records of atmospheric mercury deposition obtained from ombrotrophic and minerotrophic peatlands in the Swiss Jura mountains. Environ. Sci. Technol. 37, 235–244. https://doi.org/10.1021/es0201496

Sanborn, P.T., Smith, C.A.S., Froese, D.G., Zazula, G.D., Westgate, J.A., 2006. Full-glacial paleosols in perennially frozen loess sequences, Klondike goldfields, Yukon Territory, Canada. Quaternary Research 66, 147–157. doi:10.1016/j.yqres.2006.02.008

Sanchez-Cabeza, J.A., Ruiz-Fernández, A.C., 2012. 210Pb sediment radiochronology: An integrated formulation and classification of dating models. Geochim. Cosmochim. Acta 82, 183–200. https://doi.org/10.1016/j.gca.2010.12.024

Sanders, G., Jones, K.C., Hamilton-Taylor, J., Dorr, H., 1995. PCB and PAH fluxes to a dated UK peat core. Environ. Pollut. 89, 17–25. https://doi.org/10.1016/0269-7491(94)00048-I

Sapkota, A., Cheburkin, A.K., Bonani, G., Shotyk, W., 2007. Six millennia of atmospheric dust deposition in southern South America (Isla Navarino, Chile). The Holocene 17, 561–572. https://doi.org/10.1177/0959683607078981

Sarna-Wojcicki, A., 2000. Tephrochronology, in: Noller, J.S., Sowers, J.M., Lettis, W.R. (Eds.), Quaternary Geochronology; Methods and Applications. American Geophysical Union, Washington, DC, pp. 357–377. https://doi.org/10.1029/RF004p0357

Schell, W.R., Tobin, M.J., Massey, C.D., 1989. Evaluation of trace metal deposition history and potential element mobility in selected cores from peat and wetland ecosystems. Sci. Total Environ. 87–88, 19–42. https://doi.org/10.1016/0048-9697(89)90223-4

Schiff, C.J., Kaufman, D.S., Wallace, K.L., Ketterer, M.E., 2010. An improved proximal tephrochronology for Redoubt Volcano, Alaska. J. Volcanol. Geotherm. Res. 193, 203–214. https://doi.org/10.1016/j.jvolgeores.2010.03.015

Schiff, C.J., Kaufman, D.S., Wallace, K.L., Werner, A., Ku, T.L., Brown, T.A., 2008. Modeled tephra ages from lake sediments, base of Redoubt Volcano, Alaska. Quat. Geochronol. 3, 56–67. https://doi.org/10.1016/j.quageo.2007.05.001

Schleich, N., Degering, D., Unterricker, S., 2000. Natural and artificial radionuclides in forest and bog soils: Tracers for migration processes and soil development. Radiochim. Acta 88, 803–808. https://doi.org/10.1524/ract.2000.88.9-11.803

Schoning, K., Charman, D.J., Wastegård, S., 2005. Reconstructed water tables from two ombrotrophic mires in eastern central Sweden compared with instrumental meteorological data. The Holocene 15, 111–118. https://doi.org/10.1191/0959683605hl772rp

Scott, W.E., McGimsey, R.G., 1994. Character, mass, distribution, and origin of tephra-fall deposits of the 1989-1990 eruption of redoubt volcano, south-central Alaska. J. Volcanol. Geotherm. Res. 62, 251–272. https://doi.org/10.1016/0377-0273(94)90036-1

Shore, J.S., Bartley, D.D., Harkness, D.D., 1995. Problems encountered with the 14C dating of peat. Quat. Sci. Rev. 14, 373–383. https://doi.org/10.1016/0277-3791(95)00031-3

Shotyk, W., 1996. Peat bog archives of atmospheric metal deposition: geochemical evaluation of peat profiles, natural variations in metal concentrations, and metal enrichment factors. Environ. Rev. 4, 149–183. https://doi.org/10.1139/a96-010

Shotyk, W., Appleby, P.G., Bicalho, B., Davies, L.J., Froese, D.G., Grant-Weaver, I., Krachler, M., Magnan, G., Mullan-Boudreau, G., Noernberg, T., Pelletier, R., Shannon, B., van Bellen, S., Zaccone, C., 2016a. Peat bogs in northern Alberta, Canada reveal decades of declining atmospheric Pb contamination. Geophys. Res. Lett. 43, 9964–9974. https://doi.org/10.1002/2016GL070952

Shotyk, W., Appleby, P.G., Bicalho, B., Davies, L.J., Froese, D.G., Grant-Weaver, I., Magnan, G., Mullan-Boudreau, G., Noernberg, T., Pelletier, R., Shannon, B., van Bellen, S., Zaccone, C., 2017. Peat Bogs Document Decades of Declining Atmospheric Contamination by Trace Metals in the Athabasca Bituminous Sands Region. Environ. Sci. Technol. 51, 6237–6249. https://doi.org/10.1021/acs.est.6b04909

Shotyk, W., Cheburkin, A.K., Appleby, P.G., Fankhauser, A., Kramers, J.D., 1997. Lead in three peat bog profiles, Jura Mountains, Switzerland: Enrichment factors, isotopic composition, and chronology of atmospheric deposition. Water. Air. Soil Pollut. 100, 297–310. https://doi.org/10.1023/A:1018384711802

Shotyk, W., Kempter, H., Krachler, M., Zaccone, C., 2015. Stable (^{206}Pb, ^{207}Pb, ^{208}Pb) and radioactive (^{210}Pb) lead isotopes in 1year of growth of Sphagnum moss from four ombrotrophic bogs in southern Germany: Geochemical significance and environmental implications. Geochim. Cosmochim. Acta 163, 101–125. https://doi.org/10.1016/j.gca.2015.04.026

Shotyk, W., Rausch, N., Outridge, P.M., Krachler, M., 2016b. Isotopic evolution of atmospheric Pb from metallurgical processing in Flin Flon, Manitoba: Retrospective analysis using peat cores from bogs. Environ. Pollut. 218, 338–348. https://doi.org/10.1016/j.envpol.2016.07.009

Shotyk, W., Wayne Nesbitt, H., Fyfe, W.S., 1992. Natural and antropogenic enrichments of trace metals in peat profiles. Int. J. Coal Geol. 20, 49–84. https://doi.org/10.1016/0166-5162(92)90004-G

Smith, D.G.W., Westgate, J.A., 1968. Electron probe technique for characterising pyroclastic deposits. Earth and Planetary Science Letters 5, 313–319. doi:10.1016/S0012-821X(68)80058-5

Smith, J.T., Appleby, P.G., Hilton, J., Richardson, N., 1997. Inventories and fluxes of 210Pb, 137Cs and 241Am determined from the soils of three small catchments in Cumbria, UK. J. Environ. Radioact. 37, 127–142. https://doi.org/10.1016/S0265-931X(97)00003-9

Smith, V.C., Pearce, N.J.G., Matthews, N.E., Westgate, J.A., Petraglia, M.D., Haslam, M., Lane, C.S., Korisettar, R., Pal, J.N., 2011. Geochemical fingerprinting of the widespread Toba tephra using biotite compositions. Quaternary International 246, 97–104. doi:10.1016/j.quaint.2011.05.012

Smith, V.C., Staff, R.A., Blockley, S.P.E., Bronk Ramsey, C., Nakagawa, T., Mark, D.F., Takemura, K., Danhara, T., Suigetsu 2006 project members, 2013. Identification and correlation of visible tephras in the Lake Suigetsu SG06 sedimentary archive, Japan: chronostratigraphic markers for synchronising of east Asian/west Pacific palaeoclimatic records across the last 150 ka. Quaternary Science Reviews 67, 121–137. doi:10.1016/j.quascirev.2013.01.026

Sokolik, G., Ovsiannikova, S., Kimlenko, I., 2002. Distribution and mobility of 137 Cs, 90 Sr, 239,240 Pu and 241 Am in solid phase-interstitial soil solution system. Radioprotection 37, C1-259-C1-264. https://doi.org/10.1051/radiopro/2002048

Spray, J.G., Rae, D.A., 1995. Quantitative electron-microprobe analysis of alkali silicate glasses: a review and user guide. Can. Mineral. 33, 323–332.

Spiker, E., Kelley, L., Rubin, M., 1978. US Geological Survey radiocarbon dates XIII. Radiocarbon 20, 139-156.

Stelling, P., Gardner, J.E., Beget, J.E., 2005. Eruptive history of Fisher Caldera, Alaska, USA. Journal of Volcanology and Geothermal Research 139, 163–183. doi:10.1016/j.jvolgeores.2004.08.006

Strawn, D.G., Sparks, D.L., 2000. Effects of Soil Organic Matter on the Kinetics and Mechanisms of Pb(II) Sorption and Desorption in Soil. Soil Sci. Soc. Am. J. 64, 144. https://doi.org/10.2136/sssaj2000.641144x

Streeter, R., Dugmore, A., 2014. Late-Holocene land surface change in a coupled social-ecological system, southern Iceland: a cross-scale tephrochronology approach. Quaternary Science Reviews 86, 99–114. doi:10.1016/j.quascirev.2013.12.016

Sundqvist, H.S., Kaufman, D.S., McKay, N.P., Balascio, N.L., Briner, J.P., Cwynar, L.C., Sejrup, H.P., Seppä, H., Subetto, D.A., Andrews, J.T., Axford, Y., Bakke, J., Birks, H.J.B., Brooks, S.J., De Vernal, A., Jennings, A.E., Ljungqvist, F.C., Rühland, K.M., Saenger, C., Smol, J.P., Viau, A.E., 2014. Arctic Holocene proxy climate database - New approaches to assessing geochronological accuracy and encoding climate variables. Clim. Past 10, 1605–1631. https://doi.org/10.5194/cp-10-1605-2014

Swindles, G.T., De Vleeschouwer, F., Plunkett, G., 2010. Dating peat profiles using tephra: stratigraphy, geochemistry and chronology. Mires Peat 7, 1–9.

Swindles, G.T., Galloway, J.M., Outram, Z., Turner, K., Schofield, J.E., Newton, A.J., Dugmore, A.J., Church, M.J., Watson, E.J., Batt, C., Bond, J., Edwards, K.J., Turner, V., Bashford, D., 2013. Re-deposited cryptotephra layers in Holocene peats linked to anthropogenic activity. The Holocene 23, 1493–1501. https://doi.org/10.1177/0959683613489586

Swindles, G.T., Lawson, I.T., Savov, I.P., Connor, C.B., Plunkett, G., 2011. A 7000 yr perspective on volcanic ash clouds affecting northern Europe. Geology 39, 887–890. https://doi.org/10.1130/G32146.1

Swindles, G.T., Patterson, R.T., Roe, H.M., Galloway, J.M., 2012. Evaluating periodicities in peat-based climate proxy records. Quat. Sci. Rev. 41, 94–103. https://doi.org/10.1016/j.quascirev.2012.03.003

Syrovetnik, K., Malmström, M.E., Neretnieks, I., 2007. Accumulation of heavy metals in the Oostriku peat bog, Estonia: Determination of binding processes by means of sequential leaching. Environ. Pollut. 147, 291–300. https://doi.org/10.1016/j.envpol.2005.10.048

Tappen, C.M., Webster, J.D., Mandeville, C.W., Roderick, D., 2009. Petrology and geochemistry of ca. 2100-1000 a.B.P. magmas of Augustine volcano, Alaska, based on analysis of prehistoric pumiceous tephra. J. Volcanol. Geotherm. Res. 183, 42–62. https://doi.org/10.1016/j.jvolgeores.2009.03.007

Testa, C., Jia, G., Degetto, S., Desideri, D., Guerra, F., Meli, M.A., Roselli, C., 1999. Vertical profiles of 239,240Pu and 241Am in two sphagnum mosses of Italian peat. Sci. Total Environ. 232, 27–31. https://doi.org/10.1016/S0048-9697(99)00106-0

Thorarinsson, S., (1954) The tephra-fall from Hekla on March 29, 1947, in: The Eruption of Hekla 1947– 48, part 2. Soc. Sci. Islandica, Reykjavik, 1-68.

Toohey, M., Sigl, M., 2017. Volcanic stratospheric sulfur injections and aerosol optical depth from 500 BCE to 1900 CE. Earth Syst. Sci. Data 9, 809–831. https://doi.org/10.5194/essd-9-809-2017

Torbenson, M.C.A., Plunkett, G., Brown, D.M., Pilcher, J.R., Leuschner, H.H., 2015. Asynchrony in key Holocene chronologies: Evidence from Irish bog pines. Geology 43, 799–802. https://doi.org/10.1130/G36914.1

Treat, C.C., Jones, M.C., Camill, P., Gallego-Sala, A., Garneau, M., Harden, J.W., Hugelius, G., Klein, E.S., Kokfelt, U., Kuhry, P., Loisel, J., Mathijssen, P.J.H., O'Donnell, J.A., Oksanen, P.O., Ronkainen, T.M., Sannel, A.B.K., Talbot, J., Tarnocai, C., Väliranta, M., 2016. Effects of permafrost aggradation on peat properties as determined from a pan-Arctic synthesis of plant macrofossils. J. Geophys. Res. G Biogeosciences 121, 78–94. https://doi.org/10.1002/2015JG003061

Trivedi, P., Dyer, J.A., Sparks, D.L., 2003. Lead sorption onto ferrihydrite. 1. A macroscopic and spectroscopic assessment. Environ. Sci. Technol. 37, 908–914. https://doi.org/10.1021/es0257927

Turetsky, M.R., Manning, S.W., Wieder, R.K., 2004. Dating recent peat deposits. Wetlands 24, 324–356. https://doi.org/10.1672/0277-5212(2004)024[0324:DRPD]2.0.CO;2

Turetsky, M.R., Wieder, R.K., Vitt, D.H., Evans, R.J., Scott, K.D., 2007. The disappearance of relict permafrost in boreal north America: Effects on peatland carbon storage and fluxes. Glob. Chang. Biol. 13, 1922–1934. https://doi.org/10.1111/j.1365-2486.2007.01381.x

Turetsky, M.R., Wieder, R.K., Williams, C.J., Vitt, D.H., 2000. Organic Matter Accumulation, Peat Chemistry, and Permafrost Melting in Peatlands of Boreal Alberta. Ecoscience 7, 379–392. https://doi.org/10.1080/11956860.2000.11682608

Turner, R., Hurst, T., 2001. Factors influencing volcanic ash dispersal from the 1995 and 1996 eruptions of Mount Ruapehu, New Zealand. Journal of Applied Meteorology 40, 56–69. doi:10.1175/1520-0450(2001)040<0056:FIVADF>2.0.CO;2

Turney, C., Harkness, D.D., Lowe, J.J., 1997. The use of microtephra horizons to correlate Late-glacial lake sediment successions in Scotland. Journal of Quaternary Science 525–531. doi:10.1002/(SICI)1099-1417(199711/12)12:63.3.CO;2-D

Turney, C.S.M., Lowe, J.J., Davies, S.M., Hall, V., Lowe, D.J., Wastegård, S., Hoek, W.Z., Alloway, B., 2004. Tephrochronology of Last Termination sequences in Europe: A protocol for improved analytical precision and robust correlation procedures (a joint SCOTAV-INTIMATE proposal). J. Quat. Sci. 19, 111–120. https://doi.org/10.1002/jqs.822

Tylmann, W., Bonk, A., Goslar, T., Wulf, S., Grosjean, M., 2016. Calibrating 210Pb dating results with varve chronology and independent chronostratigraphic markers: Problems and implications. Quat. Geochronol. 32, 1–10. https://doi.org/10.1016/j.quageo.2015.11.004

Urban, N.R., Eisenreich, S.J., Grigal, D.F., Schurr, K.T., 1990. Mobility and diagenesis of Pb and 210Pb in peat. Geochim. Cosmochim. Acta 54, 3329–3346. https://doi.org/10.1016/0016-7037(90)90288-V

van der Hoek, R., Myron, R., 2004. An archaeological overview and assessment of Aniakchak National Monument and Preserve. U.S. National Park Service Research/Resources Management Report AR/CRR-2004-47.

van der Linden, M., Vickery, E., Charman, D.J., van Geel, B., 2008. Effects of human impact and climate change during the last 350 years recorded in a Swedish raised bog deposit. Palaeogeogr. Palaeoclimatol. Palaeoecol. 262, 1–31. https://doi.org/10.1016/j.palaeo.2008.01.018

van der Plicht, J., Yeloff, D., van der Linden, M., van Geel, B., Brain, S., Chambers, F.M., Webb, J., Toms, P., 2013. Dating recent peat accumulation in European ombrotrophic bogs. Radiocarbon 55, 1763–1778. https://doi.org/10.2458/azu_js_rc.55.16057

van Geel, B., Mook, W.G., 1989. High-resolution 14C dating of organic deposits using natural atmospheric 14C variations. Radiocarbon 31, 151–155. https://doi.org/10.1017/S0033822200044805

van Hoof, P.L., Andren, A.W., 1989. Partitioning and Transport of 210Pb in Lake Michigan. J. Great Lakes Res. 15, 498–509. https://doi.org/10.1016/S0380-1330(89)71505-7

Vile, M.A., Wieder, R.K., Novák, M., 1999. Mobility of Pb in Sphagnum-derived peat. Biogeochemistry 45, 35–52. https://doi.org/10.1023/A:1006085410886

Vinther, B.M., Clausen, H.B., Johnsen, S.J., Rasmussen, S.O., Andersen, K.K., Buchardt, S.L., Dahl-Jensen, D., Seierstad, I.K., Siggaard-Andersen, M.L., Steffensen, J.P., Svensson, A., Olsen, J., Heinemeier, J., 2006. A synchronized dating of three Greenland ice cores throughout the Holocene. J. Geophys. Res. Atmos. 111. https://doi.org/10.1029/2005JD006921

Vitt, D.H., Halsey, L.A., Zoltai, S.C., 2000. The changing landscape of Canada's western boreal forest: the current dynamics of permafrost. Can. J. For. Res. 30, 283–287. https://doi.org/10.1139/x99-214

Vitt, D.H., Halsey, L.A., Zoltai, S.C., 1994. The bog landforms of continental Western Canada in relation to climate and permafrost patterns. Arct. Alp. Res. 26, 1–13. https://doi.org/10.2307/1551870

Waitt, R.B., Begét, J.E., 2009. Volcanic processes and geology of augustine volcano, Alaska. US Geol. Surv. Prof. Pap. 1–78.

Wallace, K.L., Coombs, M.L., Hayden, L.A., Waythomas, C.F., 2014. Significance of a near-source tephra-stratigraphic sequence to the eruptive history of Hayes Volcano, south-central Alaska. U.S. Geological Survey Scientific Investigations Report 2014-5133.

Wastegård, S., 2002. Early to middle Holocene silicic tephra horizons from the Katla volcanic system, Iceland: new results from the Faroe Islands. Journal of Quaternary Science 17, 723–730. doi:10.1002/jqs.724

Watson, E.J., Swindles, G.T., Lawson, I.T., Savov, I., 2015. Spatial variability of tephra and carbon accumulation in a Holocene peatland. Quat. Sci. Rev. 124, 248–264. https://doi.org/10.1016/j.quascirev.2015.07.025

Watson, E.J., Swindles, G.T., Lawson, I.T., Savov, I.P., 2016. Do peatlands or lakes provide the most comprehensive distal tephra records? Quat. Sci. Rev. 139, 110–128. https://doi.org/10.1016/j.quascirev.2016.03.011

Watt, S.F.L., Pyle, D.M., Mather, T.A., Martin, R.S., Matthews, N.E., 2009. Fallout and distribution of volcanic ash over Argentina following the May 2008 explosive eruption of Chaitén, Chile. Journal of Geophysical Research 114, B04207–11. doi:10.1029/2008JB006219

Watt, S.F.L., Pyle, D.M., Mather, T.A., 2013. The volcanic response to deglaciation: Evidence from glaciated arcs and a reassessment of global eruption records. Earth-Science Rev. 122, 77–102. https://doi.org/10.1016/j.earscirev.2013.03.007

Weiss, D., Shotyk, W., Kramers, J.D., Gloor, M., 1999. Sphagnum mosses as archives of recent and past atmospheric lead deposition in Switzerland. Atmos. Environ. 33, 3751–3763. https://doi.org/10.1016/S1352-2310(99)00093-X

Westgate, J.A., Smith, D., Nichols, H., 1969. Late Quaternary pyroclastic layers in the Edmonton area, Alberta. Geology Department Contract 464, 179-86, University of Alberta.

Westgate, J.A., Smith, D., Tomlinson, M., 1970. Late Quaternary tephra layers in southwestern Canada, in: Smith, R.A., Smith, J.W. (Eds.), Early Man and Environments in Northwest North America. Proceedings of the Second Annual Palaeo-environmental Workshop, University of Calgary Archaeological Association, The Students' Press, Calgary, Alberta, 13–34.

Westgate, J.A., Gorton, M.P., 1981. Correlation techniques in tephra studies, in: Self, S., Sparks, R.S.J., (Eds.), Tephra Studies. Reidel, Dordrecht, pp. 73-94.

Westgate, J.A., Preece, S.J., Kotler, E., Hall, S., 2000. Dawson tephra: a prominent stratigraphic marker of Late Wisconsinan age in west-central Yukon, Canada. Canadian Journal of Earth Sciences 37, 621–627. doi:10.1139/cjes-37-4-621

Westgate, J.A., Preece, S.J., Froese, D.G., Walter, R.C., Sandhu, A.S., Schweger, C.E., 2001. Dating Early and Middle (Reid) Pleistocene Glaciations in Central Yukon by Tephrochronology. Quat. Res. 56, 335–348. https://doi.org/10.1006/qres.2001.2274

Westgate, J.A., Preece, S.J., Froese, D.G., Pearce, N.J.G., Roberts, R.G., Demuro, M., Hart, W.K., Perkins, W., 2008. Changing ideas on the identity and stratigraphic significance of the Sheep Creek tephra beds in Alaska and the Yukon Territory, northwestern North America. Quaternary International 178, 183–209. doi:10.1016/j.quaint.2007.03.009

Westgate, J.A., Pearce, N.J.G., Perkins, W.T., Preece, S.J., Chesner, C.A., Muhammad, R.F., 2013. Tephrochronology of the Toba tuffs: four primary glass populations define the 75-ka Youngest Toba Tuff, northern Sumatra, Indonesia. Journal of Quaternary Science 28, 772–776. doi:10.1002/jqs.2672

Wieder, R.K., Novák, M., Schell, W.R., Rhodes, T., 1994. Rates of peat accumulation over the past 200 years in five Sphagnum-dominated peatlands in the United States. J. Paleolimnol. 12, 35–47. https://doi.org/10.1007/BF00677988

Wieder, R.K., Vile, M.A., Albright, C.M., Scott, K.D., Vitt, D.H., Quinn, J.C., Burke-Scoll, M., 2016. Effects of altered atmospheric nutrient deposition from Alberta oil sands development on Sphagnum fuscum growth and C, N and S accumulation in peat. Biogeochemistry 129, 1–19. https://doi.org/10.1007/s10533-016-0216-6

Wilson, S.R., Ward, G.K., 1981. Evaluation and clustering of radiocarbon age determinations: procedures and paradigms. Archaeometry 23, 19–39. doi:10.1111/j.1475-4754.1981.tb00952.x

Wohlfarth, B., Blaauw, M., Davies, S.M., Andersson, M., Wastegård, S., Hormes, A., Possnert, G., 2006. Constraining the age of Lateglacial and early Holocene pollen zones and tephra horizons in southern Sweden with Bayesian probability methods. Journal of Quaternary Science 21, 321–334. doi:10.1002/jqs.996

Yalcin, K., Wake, C.P., Germani, M.S., 2003. A 100-year record of North Pacific volcanism in an ice core from Eclipse Icefield, Yukon Territory, Canada. J. Geophys. Res. 108, 4012. https://doi.org/10.1029/2002JD002449

Yamaguchi, D.K., Hoblitt, R.P., 1995. Tree-ring dating of pre-1980 volcanic flowage deposits at Mount St. Helens, Washington. Geol. Soc. Am. Bull. 107, 1077–1093. https://doi.org/10.1130/0016-7606(1995)107<1077:TRDOPV>2.3.CO;2

Yang, H., Rose, N.L., Boyle, J.F., Battarbee, R.W., 2001. Storage and distribution of trace metals and spheroidal carbonaceous particles (SCPs) from atmospheric deposition in the catchment peats of Lochnagar, Scotland. Environ. Pollut. 115, 231–238. https://doi.org/10.1016/S0269-7491(01)00107-5

Yeloff, D., Bennett, K.D., Blaauw, M., Mauquoy, D., Sillasoo, Ü., van der Plicht, J., van Geel, B., 2006. High precision 14C dating of Holocene peat deposits: A comparison of Bayesian calibration and wiggle-matching approaches. Quat. Geochronol. 1, 222–235. https://doi.org/10.1016/j.quageo.2006.08.003

Yu, Z., Vitt, D.H., Campbell, I.D., Apps, M.J., 2003. Understanding Holocene peat accumulation pattern of continental fens in western Canada. Can. J. Bot. 81, 267–282. https://doi.org/10.1139/b03-016

Zaccone, C., Cocozza, C., Cheburkin, A.K., Shotyk, W., Miano, T.M., 2008. Distribution of As, Cr, Ni, Rb, Ti and Zr between peat and its humic fraction along an undisturbed ombrotrophic bog profile (NW Switzerland). Appl. Geochemistry 23, 25–33. https://doi.org/10.1016/j.apgeochem.2007.09.002

Zaccone, C., Cocozza, C., Cheburkin, A.K., Shotyk, W., Miano, T.M., 2007. Highly organic soils as "witnesses" of anthropogenic Pb, Cu, Zn, and 137Cs inputs during centuries. Water. Air. Soil Pollut. 186, 263–271. https://doi.org/10.1007/s11270-007-9482-1

Zaretskaia, N.E., Ponomareva, V. V, Sulerzhitsky, L.D., Zhilin, M.G., 2001. Radiocarbon Studies of Peat Bogs: an Investigation of South Kamchatka Volcanoes and Upper Volga Archeological Sites. Radiocarbon 43, 571–580. https://doi.org/10.1017/S0033822200041229

Zdanowicz, C., Fisher, D., Bourgeois, J., Demuth, M., Zheng, J., Mayewski, P., Kreutz, K., Osterberg, E., Yalcin, K., Wake, C., Steig, E.J., Froese, D., Goto-Azuma, K., 2014. Ice Cores from the St. Elias Mountains, Yukon, Canada: Their Significance for Climate, Atmospheric Composition and Volcanism in the North Pacific Region. Arctic 67, 35. https://doi.org/10.14430/arctic4352

Zhang, Y., Shotyk, W., Zaccone, C., Noernberg, T., Pelletier, R., Bicalho, B., Froese, D.G., Davies, L.J., Martin, J.W., 2016. Airborne Petcoke Dust is a Major Source of Polycyclic Aromatic Hydrocarbons in the Athabasca Oil Sands Region. Environ. Sci. Technol. 50, 1711–1720. https://doi.org/10.1021/acs.est.5b05092

Zhao, Y., Hölzer, A., Yu, Z., 2007. Late Holocene Natural and Human-Induced Environmental Change Reconstructed from Peat Records in Eastern Central China. Radiocarbon 49, 789–798. https://doi.org/10.1017/S0033822200042661

Zimov, S.A., Voropaev, Y.V., Semiletov, I.P., Davidov, S.P., Prosiannikov, S.F., Chapin, F.S., Chapin, M.C., Trumbore, S., Tyler, S., 1997. North Siberian Lakes: A Methane Source Fueled by Pleistocene Carbon. Science 277, 800–802. doi:10.1126/science.277.5327.800

Zoltai, S.C., 1995. Permafrost Distribution in Peatlands of West-Central Canada during the Holocene Warm Period 6000 Years BP. Geogr. Phys. Quat. 49, 45–54. https://doi.org/10.7202/033029ar

Zoltai, S.C., 1993. Cyclic Development of Permafrost in the Peatlands of Northwestern Canada. Arct. Alp. Res. 25, 240–246. https://doi.org/10.2307/1551820

Zoltai, S.C., 1989. Late Quaternary volcanic ash in the peatlands of central Alberta. Can. J. Earth Sci. 26, 207–214. https://doi.org/10.1139/e89-017

Zoltai, S.C., Tarnocai, C., 1975. Perennially Frozen Peatlands in the Western Arctic and Subarctic of Canada. Can. J. Earth Sci. 12, 28–43. https://doi.org/10.1139/e75-004

Zoltai, S.C., Vitt, D.H., 1990. Holocene climatic change and the distribution of peatlands in western interior Canada. Quat. Res. 33, 231–240. https://doi.org/10.1016/0033-5894(90)90021-C

Index of Appendices and Supplementary Data

Appendices are included here; supplementary Tables and Figures are deposited as digital files through Dataverse (doi available after June 15th).

Chapter 2: Late Pleistocene and Holocene tephrostratigraphy of interior Alaska and Yukon: Key beds and chronologies over the past 30,000 years

Table S2.1: Summary of glass morphology and mineralogy for tephra of interest. Information is unavailable in some cases where no samples of the tephra were accessible and characteristics were not reported in publications.

Table S2.2: Individual major element EPMA glass shard analyses from this study.

Table S2.3: Secondary standard data accompanying EPMA glass analyses.

Table S2.4: Average major-element geochemical data included in this study.

Table S2.5: Radiocarbon dates reviewed within this study listed by associated tephra.

Table S2.6: Non-radiocarbon dates reviewed within this study.

Table S2.7: Summary statistics for dates associated with tephra layers from this paper.

Chapter 3: A Holocene cryptotephra record from northwestern Canada with more than 34 distal tephra falls since 10,400 cal yr BP

Table S3.1: Radiocarbon standard data

Table S3.2: Average major-element EPMA glass shard analyses from this study.

Table S3.3: Individual major element EPMA glass shard analyses from this study.

Chapter 4: High-resolution age modelling of ombrotrophie peat bog profiles from northern Alberta, using pre- and post-bomb ^{14}C, ^{210}Pb and historical cryptotephra

Appendix A: Peat sub-sampling protocol.

Appendix B: ^{210}Pb sample analysis.

Figure S4.1-4.6: Evolution of age-depth models for each site. a) Raw dates, with no event boundaries or adjustments; b) Raw dates with event boundaries; c) Final models with outliers removed and tephra dates and corrected ^{210}Pb included where relevant.

Table S4.1: Individual major element EPMA glass shard analyses from this study.

Table S4.2: Radiocarbon standard data.

Table S4.3: Radiometric data for each core including the total and unsupported ^{210}Pb, ^{226}Ra, ^{137}Cs and ^{241}Am concentrations versus depth.

Table S4.4: Resulting ^{210}Pb dates, including corrections from reference dates (AD 1963, 1912) where relevant.

Table S4.5: Final age model output.

Chapter 4, Appendix A: Peat sub-sampling protocol

Three peat cores were collected from each bog, ca. 3 m apart, using a modified Wardenaar monolith sampler. The custom built Ti-Al-Mn alloy corer has serrated cutting edges and removes a monolith of 15 x 15 x 100 cm. The top of the corer is reinforced to allow it to be driven into the bog surface using a nylon sledgehammer: this minimizes compression of the peat core. The peat cores were extracted, photographed, wrapped in polyethylene cling film, then packed into wooden boxes in the field. In the lab, the cores were frozen at -18^{o}C. The living (green) layer at the top of the peat core is removed first: although this material represents the first sample in each peat bog profile, this is living plant material and not peat. The remainder of each core was then cut in to 1 cm slices, while frozen, using a stainless steel band saw.

Each 1cm slice was subsampled as shown in Figure A.1. The edges (1 cm) were trimmed away from each slice and the porewaters extracted for pH and electrical conductivity; these pieces were then dried and combusted to determine ash content and initial tephra counts. A 3 cm slice of each remaining sample was reserved for a separate study of organic contaminants, and a 2 cm wide slice was cut and split for archive material, as well as mercury and macrofossil analyses. Material for ^{14}C analyses was taken from the macrofossil portion, and material tephra geochemical analyses was taken from the archive material. The remaining sample was dried at 105^{o}C for 36 h in polypropylene jars before being ground using a Retsch agate ball mill (PM 400, Haan, Germany) with 250 mL jars containing three 30 mm balls at 300 rpm for four x 2.3 minutes (first forward, then reverse, then forward, then reverse). This portion was used for ^{210}Pb and radioisotope (^{137}Cs, ^{241}Am) analyses.

Figure A.1: Peat subsampling protocol. Tephra counts used material from the trimmed edges; material for tephra geochemical analyses was taken from the archive portion; ^{14}C samples were taken from the macrofossil subsample; ^{210}Pb and radioisotopes were measured on the central oven-dried and milled peat.

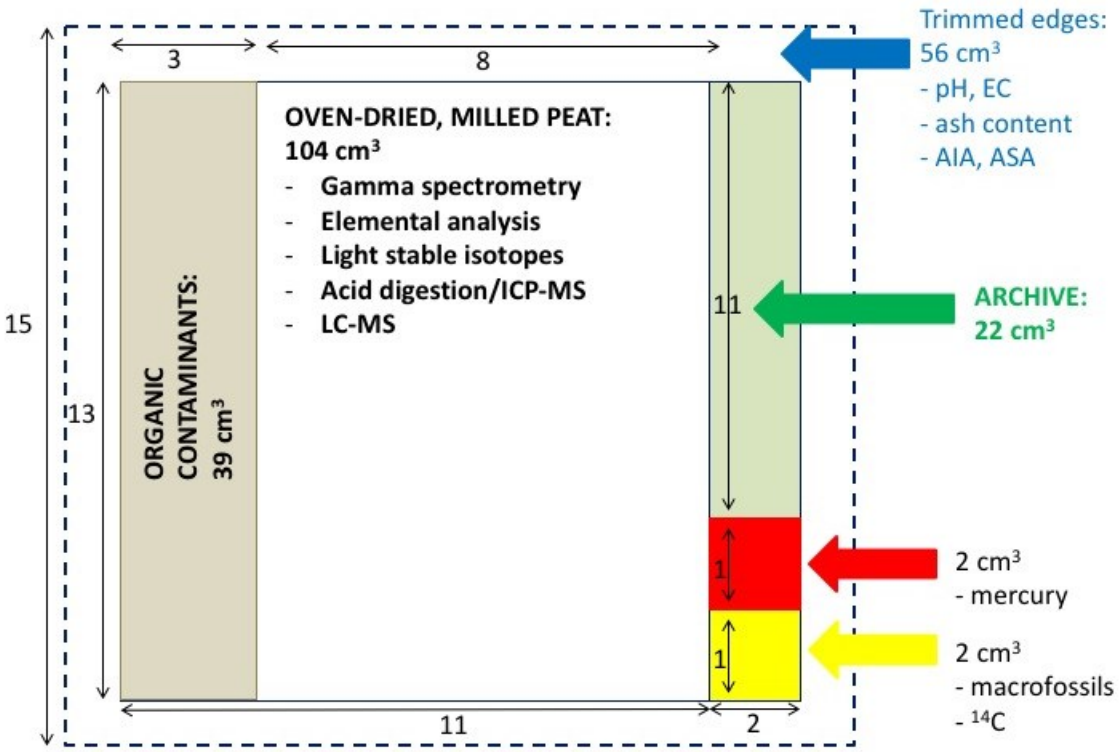

Chapter 4, Appendix B: ^{210}Pb sample analysis

The sample mass of the dried, milled peat samples used ranged from 1.6-3.5 g (average 2.2 g), depending on peat density. After a 30-day period for equilibration of ^{222}Rn and decay progeny, ^{210}Pb was determined using its gamma-ray emission at 46.5 keV line; ^{226}Ra was determined based on gamma emissions of ingrown decay progeny at 352 (^{214}Pb) and 609 (^{214}Bi) keV; ^{137}Cs and ^{241}Am were determined simultaneously based on their respective photopeaks at 662 and 59.5 keV.

The spectrometers were calibrated for measurement of ^{210}Pb, ^{226}Ra, ^{241}Am, and ^{137}Cs in peat using six, custom-made calibration standards (Eckert and Ziegler Analytics, Atlanta, GA, USA): two low-density (gas-equivalent) standards containing either a nine-nuclide mixture (including ^{137}Cs, ^{241}Am, and ^{210}Pb), or a mixture of ^{210}Pb and ^{226}Ra; and four with the same two radionuclide mixtures homogenously distributed in ancient peat from a Swiss bog spanning the range of densities of the calibration standards (0.02 to 0.41 g/cm^3) All calibration standards are traceable to the National Institute of Standards and Technology (NIST).

Spectra were processed using ORTEC DSPEC Jr. 2.0 Digital Gamma Spectrometer with GammaVision 7 software. Acquisition times of 24, 48, or 72 hours varied depending on the ^{210}Pb activity of the sample. For quality assurance, a check standard of known nuclide activity was measured on each detector between each peat sample. Each successive 1 cm peat slice was measured until ^{210}Pb was observed in equilibrium with its decay-chain parent ^{226}Ra.